

19th International Conference on  
Ion Beam Modification of Materials

# IBMM LEUVEN 2014

September 14 – 19, 2014



**PROGRAM  
&  
ABSTRACTS**

[www.ibmm2014.be](http://www.ibmm2014.be)

**KU LEUVEN**

Online version dd. 08 october 2014

# **19th International Conference on Ion Beam Modification of Materials**

**IBMM2014**

Leuven, September 14 – 19, 2014

Program and Abstracts

Online version d.d. October 08, 2014

Edited by Kristiaan Temst, Wilfried Vandervorst, and André Vantomme

© Instituut voor Kern- en Stralingsfysica, KU Leuven, Celestijnenlaan 200 D – bus 2418,  
B-3001 Leuven, Belgium

ISBN: 9789082271805

NUR: 910

All rights reserved. No part of this publication may be reproduced in any form by print, photoprint, microfilm, electronic or any other means without written permission of the publisher.

## Welcome to IBMM 2014

On behalf of the local organizing committee, the KU Leuven and the city of Leuven, it is our pleasure to welcome you to the 19<sup>th</sup> edition of the international conference on Ion Beam Modification of Materials, which takes place from September 14<sup>th</sup> until September 19<sup>th</sup>, 2014.

This conference, which started in 1978 in Budapest, Hungary, remains the major international forum for discussing interdisciplinary, novel scientific results and practical implementations of ion beam induced modification, synthesis and patterning of hard and soft materials. As illustrated by the 440 abstracts that were submitted to this conference, the field is very lively. As of 2014, new ion beam developments keep on popping up, ultimate dimensions, ultimate time scales and harsh environmental conditions are challenged, thereby crossing the borders of different domains where the use of ion beams was so far unknown.



Along the tradition of this conference, there are no parallel sessions and the poster sessions constitute an important part of the scientific program. To this end, the posters will be presented in three sessions, providing sufficient time for in-depth discussion.

This book of abstracts compiles the scientific contributions presented at IBMM 2014. An author list is provided at the end of the book. The presentations include invited talks, oral contributions and poster presentations, reflecting the width and breadth of the scientific topics and underlining that the field and scientific community of ion beam modification of materials is thriving, exciting, and vibrant.

We wish you a very interesting conference with exciting new results and discussions, and a pleasant stay in the historic city of Leuven, where centuries-old culture meets with frontier science and technology.

André Vantomme  
Kristiaan Temst  
Wilfried Vandervorst

*Instituut voor Kern- en Stralingsfysica*

*KU Leuven*

*Celestijnenlaan 200 D*

*B-3001 Leuven*

*Belgium*

<http://fys.kuleuven.be/iks/nvsf/home>

## Committees

### Local Organizing Committee

André Vantomme (KU Leuven), Chair  
Wilfried Vandervorst (KU Leuven and imec), Co-chair  
Kristiaan Temst (KU Leuven), Co-chair  
Fabienne Vanalphen (KU Leuven), conference secretary  
Bert Keyaerts (KU Leuven)  
Diederik Depla (UGent)  
Guy Terwagne (UNamur)  
Arnaud Delcorte (UCL)  
Sébastien Couet (KU Leuven)  
Enric Menéndez (KU Leuven)  
Lino M.C. Pereira (KU Leuven)

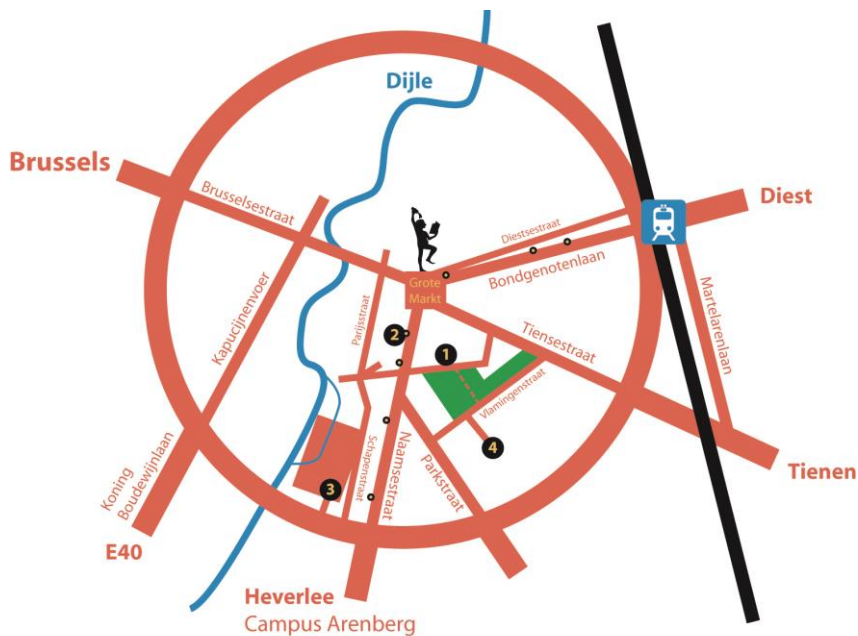
### Program Committee

Flyura Djurabekova (Helsinki, Finland)  
Robert G. Elliman (Canberra, Australia)  
Stefan Facsko (Dresden, Germany)  
Maria-Grazia Grimaldi (Catania, Italy)  
Karen Kirkby (Guildford, U.K.)  
Jiro Matsuo (Kyoto, Japan)  
François Schiettekatte (Montréal, Canada)  
Christina Trautmann (Darmstadt, Germany)  
André Vantomme (Leuven, Belgium)  
William J. Weber (Knoxville, U.S.A.)

### International Advisory Committee

Eduardo Alves (Lisbon, Portugal)  
Robert G. Elliman (Canberra, Australia)  
Jürgen Fassbender (Dresden, Germany)  
Paulo Fichtner (Porto Alegre, Brazil)  
Kenji Gamo (Osaka, Japan)  
Frederico Garrido (Paris-Sud, France)  
Maria-Grazia Grimaldi (Catania, Italy)  
Russell Gwilliam (Guildford, United Kingdom)  
Mike A. Nastasi (Lincoln, USA)  
Kai Nordlund (Helsinki, Finland)  
Sjoerd Roorda (Montréal, Canada)  
Bernd Stritzker (Augsburg, Germany)  
André Vantomme (Leuven, Belgium)  
Xi Wang (Shanghai, China)  
William J. Weber, (Knoxville, U.S.A.)  
Isao Yamada (Kyoto, Japan)

## IBMM Venue in Leuven



- 1 Pieter De Somer Auditorium**  
Conference lectures and poster sessions  
(Charles Deberiotstraat 24)
- 2 Jubilee Hall of the University Halls**  
Registration and welcome reception  
(Naamsestraat 22)
- 3 Faculty Club**  
Conference dinner  
(Groot Begijnhof 14)

- 4 Alma 2**  
Lunch breaks  
(Monnikenstraat)
- Bus stop**

Sun. 14 Sept. 2014

Mon. 15 Sept. 2014

Tue. 16 Sept. 2014

8:00				8:00
		Registration		
9:00		Conference opening	P. GRANDE – Characterization of ion-implanted films with high-energy electron scattering	9:00
			H. KARL	
10:00		T. MICHELY - New phenomena in 2D-layer irradiation with low energy ions	F. CHEN	10:00
		D. PRIMETZHOFFER	R. ELLIMAN	
11:00		Coffee	Coffee	11:00
		H. JOHNSON	R.M. BRADLEY – Producing nanodot arrays, virtually defect-free ripples and exotic new patterns by ion bombardment of binary metals	
		M. RADEK	R. CUERNO	
12:00		L. THOME	X. OU	12:00
		W. WEBER	T. SKEREN	
13:00		Lunch	W.-K. CHU	13:00
			Lunch	
14:00		S. RAUSCHENBACH – Active control of protein conformation on surfaces by hyperthermal ion-surface interaction	H. HOFSAESS – Doping of graphene by ultra low energy mass selected ion implantation	14:00
		R. BOETTGER		
15:00		B. RAUSCHENBACH	U. WAHL	15:00
		D. REPETTO	J. WILLIAMS	
		G. RIZZA – Plasmonic properties of ion-shaped nanoparticles	N. COWERN	
16:00		T. KOBAYASHI	R. MILAZZO	16:00
		I. BOGDANOVIC RADOVIC	R. GIULIAN	
17:00	Registration	Poster session A	J. ENGLAND	17:00
			Poster session B	
18:00				18:00
19:00	Welcome reception			19:00
20:00				20:00

Wed. 17 Sept. 2014

Thur. 18 Sept. 2014

Fri. 19 Sept. 2014

8:00

8:00

B. APPLETON – Selective synthesis of nanostructure graphene by ion-solid interactions and pulsed laser annealing

W. MOELLER

G. GREAVES

K. NORDLUND

*Coffee*

S. FACSKO

J. MATSUO

V. POPOK

H.-S. TSAI

D. KING – Test simulation of neutron damage to electronic components using accelerator facilities

D. GOSSET

F. GARRIDO

S. AGARWAL

*Coffee*

J. LEVENEUR – Enhancement of the magnetic properties of iron nanoparticles upon incorporation of Samarium

N. SHUKLA

T. MATSUI

S. MAYR

*Lunch*

F. SCHIETTEKATTE– Defect complex evolution in semiconductors: long-range elastic interactions matter

O. PÉNA-RODRIGUEZ

M.-L. DAVID

S. ROORDA

F. MAZEN – In-situ characterization of silicon layer separation by light ions implantation

**IBMM prize  
Announcement and invited talk**

Poster session C

*Conference dinner  
19:00 – 22:00*

M. MERCHANT – Applications and development of ion beams in radiobiology

W. ENSINGER

A. BENYAGOUB

P. KLUTH

N. SELLAMI

*Coffee*

C. RONNING – Ion beam doping of semiconductor nanowires

D. MATHIOT

S. PRUCNAL

**IBMM2016 and Conference closing**

9:00

9:00

10:00

10:00

11:00

11:00

12:00

12:00

13:00

13:00

14:00

14:00

15:00

15:00

16:00

16:00

17:00

17:00

18:00

18:00

19:00

19:00

20:00

20:00

*Excursion  
11:50 – 22:00*



## Timetable

### Sunday, September 14, 2014

15.30-18.00 Registration

18.00-20.30 Welcome reception

### Monday, September 15, 2014

08.00-09.00 Registration

09.00-09.30 Conference opening

#### 09.30-10.40 Fundamentals of ion-solid interaction 1

**Chair: André Vantomme**

- |       |   |                     |
|-------|---|---------------------|
| 09.50 | New phenomena in 2D-layer irradiation with low energy ions<br>(INV)                           | Thomas Michely      |
| 10.20 | Characterization of the electronic energy loss of keV ions by<br>Medium-Energy Ion Scattering | Daniel Primetzhofer |

10.40-11.10 Coffee

#### 11.10-12.30 Fundamentals of ion-solid interaction 1

**Chair: Kai Nordlund**

- |       |   |                |
|-------|---|----------------|
| 11.10 | Large scale parallel molecular dynamics modeling of focused ion<br>beam processing: observation of explosive boiling and Marangoni<br>effects | Harley Johnson |
| 11.30 | Temperature and flux dependence of ion-beam mixing in<br>crystalline and amorphous germanium isotope multilayers                              | Manuel Radek   |
| 11.50 | Similarities and differences between SHIBIEC and SNEEL in<br>ion-irradiated solids  | Lionel Thomé   |
| 12.10 | A unique synergistic damage effect due to electronic and nuclear<br>energy loss in SrTiO <sub>3</sub>   | William Weber  |

12.30-14.00 Lunch

#### 14.00-15.30 Ion-driven self-organization and nanopatterning 1

**Chair: Rodolfo Cuerno**

- |       |   |                         |
|-------|---|-------------------------|
| 14.00 | Active control of protein conformation on surfaces by<br>hyperthermal ion-surface interaction (INV)   | Stephan<br>Rauschenbach |
| 14.30 | Extremely high energy density deposition by heavy polyatomic ion<br>impacts – surface nanopatterning and frozen phase diagram<br>pathways     | Roman Böttger           |
| 14.50 | Ion beam ultra-precision smoothing of surfaces  | Bernd Rauschenbach      |
| 15.10 | Transparent aluminium nanowires electrodes with optical and<br>electrical anisotropic response fabricated by defocused ion beam<br>sputtering | Diego Repetto           |

## **15.30-16.40 Nanostructure synthesis and modification 1**

**Chair: Paulo F.P. Fichtner**

- |       |   |                        |
|-------|---|------------------------|
| 15.30 | Plasmonic properties of ion-shaped nanoparticles <b>(INV)</b>                                     | Giancarlo Rizza        |
| 16.00 | Catalytic nanoparticle formation by ion irradiation at solid-liquid interface                     | Tomohiro Kobayashi     |
| 16.20 | Formation and tailoring of metal and semiconductor quantum dots in amorphous matrices by MeV ions | Iva Bogdanovic Radovic |

16.40-18.40 Poster session A

## **Tuesday, September 16, 2014**

### **09.00-10.30 Modification of insulators**

**Chair: Eduardo Alves**

- |       |  |                |
|-------|--|----------------|
| 09.00 | Characterization of ion-implanted films with high-energy electron scattering <b>(INV)</b>                          | Pedro Grande   |
| 09.30 | Tailoring of the thermomechanical performance of VO <sub>2</sub> nanowire bimorph actuators by ion implantation    | Helmut Karl    |
| 09.50 | Ion beam micro-structuring and fluorescence modification of dielectric crystals applied to waveguide laser devices | Feng Chen      |
| 10.10 | Ion-beam synthesis of transition-metal oxide/suboxide heterostructures for non-volatile memory applications        | Robert Elliman |

10.30-11.00 Coffee

### **11.00-12.50 Ion-driven self-organization and nanopatterning 2**

**Chair: Hans Hofsäss**

- |       |   |                 |
|-------|---|-----------------|
| 11.00 | Producing nanodot arrays, virtually defect-free ripples and exotic new patterns by ion bombardment of binary materials <b>(INV)</b> | R. Mark Bradley |
| 11.30 | Nonuniform stress as a key to surface nanopatterning by ion beam irradiation  | Rodolfo Cuerno  |
| 11.50 | Reverse epitaxy on semiconductor surfaces   | Xin Ou          |
| 12.10 | Ion-induced pattern formation: the origin of perpendicular mode ripples   | Tomas Skeren    |
| 12.30 | Self-assembled metal structures by cluster ion beam bombardment and applications in plasmonic bio sensing                           | Wei-Kan Chu     |

12.50-14.20 Lunch

### **14.20-16.50 Modification of semiconductors**

**Chair: Elke Wendler and Maria Grazia Grimaldi**

- |       |  |              |
|-------|--|--------------|
| 14.20 | Doping of graphene by ultra low energy mass selected ion implantation <b>(INV)</b>   | Hans Hofsäss |
| 14.50 | Lattice sites of implanted Mg in GaN   | Ulrich Wahl  |
| 15.10 | Supersaturation of implanted gold in silicon by pulsed laser melting and rapid thermal annealing for enhanced infrared photoresponse at room temperature | Jim Williams |
| 15.30 | Shedding light on the complex physics of self-interstitials in   | Nick Cowern  |

	germanium	
15.50	Ge doping by ion implantation and melting laser thermal annealing	Ruggero Milazzo
16.10	Structural, electrical and optical properties of InSb and AlSb modified by ion irradiation	Raquel Giulian
16.30	Industrial challenges in ion beam processing and metrology in the 3D era	Jonathan England
16.50-19.00 Poster session B		

## Wednesday, September 17, 2014

### 08.30-10.00 Fundamentals of ion-solid interaction 2

**Chair: Sibylle Gemming**

08.30	Selective synthesis of nanostructure graphene by ion-solid interactions and pulsed laser annealing <b>(INV)</b>	Bill Appleton
09.00	Sputtering of nanospheres – a computer simulation study	Wolfgang Möller
09.20	In-situ TEM irradiation of gold nanorods with heavy ions	Graeme Greaves
09.40	Corrections to the Kinchin-Pease damage equation to account for athermal defect recombination and ion beam mixing: arc-dpa and rpa	Kai Nordlund

10.00-10.30 Coffee

### 10.30-11.50 Cluster ions, single ion, highly charged ions, plasma immersion

**Chair: Isao Yamada**

10.30	Energy loss and charge exchange of highly charged ions in carbon nanomembranes	Stefan Facsko
10.50	Recent progress in cluster beam – from semiconductor to soft materials	Jiro Matsuo
11.10	Modification of graphite and diamond on the nanoscale by energetic ion clusters	Vladimir Popok
11.30	Direct formation of large-scale germanene from SiGe thin film assisted by plasma immersion	Hsu-Sheng Tsai

11.50-22.00 Excursion to Bruges

## Thursday, September 18, 2014

### 09.00-10.30 Irradiation effects in nuclear materials

**Chair: Yong Wang**

09.00	Test simulation of neutron damage to electronic components using accelerator facilities <b>(INV)</b>	Donald King
09.30	Evidence of amorphisation of boron carbide B <sub>4</sub> C under slow, heavy ion irradiation	Dominique Gosset
09.50	Radiation damage in nuclear oxides bombarded with low-energy ions – an advanced description of the crystal evolution via ion	Frederico Garrido

- |       |   |                 |
|-------|---|-----------------|
|       | channeling and MC simulations   |                 |
| 10.10 | Comparison of helium mobility in transition metal carbides and nitrides | Shradha Agarwal |

10.30-11.00 Coffee

### 11.00-12.30 Modification of magnetic materials

**Chair: John Kennedy**

- |       |   |                  |
|-------|---|------------------|
| 11.00 | Enhancement of the magnetic properties of iron nanoparticles upon incorporation of Samarium <b>(INV)</b>                    | Jérôme Leveneur  |
| 11.30 | Emergence of ferromagnetic order in pulsed laser deposited ZnO thin film on Si by 600 keV $^{12}\text{C}^+$ ion irradiation | Neeraj Shukla    |
| 11.50 | Process of three-dimensional magnetic patterning of FeRh alloys by using low and high energy ion beam irradiation           | Toshiyuki Matsui |
| 12.10 | Recent progress in ion beam assisted synthesis of ferromagnetic shape memory alloys: fundamentals and applications          | Stefan Mayr      |

12.30-14.00 Lunch

### 14.00-16.00 Defects in materials – defect engineering

**Chair: Michael Nastasi**

- |       |   |                        |
|-------|---|------------------------|
| 14.00 | Defect complex evolution in semiconductors: long-range elastic interactions matter <b>(INV)</b>   | François Schiettekatte |
| 14.30 | Comparative study of high energy ion beam-irradiation effects on alpha-quartz and silica based on in-situ optical measurements and MD simulations | Ovidio Peña-Rodriguez  |
| 14.50 | Multiscale study of implantation-induced helium bubbles in elemental semiconductors   | Marie-Laure David      |
| 15.10 | Pure amorphous silicon made by ion implantation is a disordered but hyperuniform solid  | Sjoerd Roorda          |
| 15.30 | In-situ characterization of silicon layer separation by light ions implantation <b>(INV)</b>  | Frederic Mazen         |

### 16.00-16.10 IBMM Prize

**Chair: Robert Elliman**

### 16.10-16.40 Invited talk IBMM Prize

**Chair: Robert Elliman**

16.40-18.40 Poster session C

19.00-22.00 Conference dinner in the Faculty Club

**Friday, September 19, 2014**

**09.30-10.20 Modification of polymers, biomaterials and biomedical applications**

**Chair: Karen Kirkby**

- |       |  |                   |
|-------|--|-------------------|
| 09.30 | Applications and development of ion beams in radiobiology (INV)  | Michael Merchant  |
| 10.00 | High energy heavy ion tracks for creation of polymeric nanochannels as a base for highly sensitive molecular sensors | Wolfgang Ensinger |

**10.20-11.20 Ultra-low energy implantation, swift heavy ions**

**Chair: Lionel Thomé**

- |       |  |                     |
|-------|--|---------------------|
| 10.20 | Quantitative analysis of the epitaxial recrystallization effect induced by swift heavy ions in silicon carbide | Abdenacer Benyagoub |
| 10.40 | Swift heavy ion irradiation induced porosity in GaSb   | Patrick Kluth       |
| 11.00 | Modifications of structural and physical properties induced by swift heavy ions in pyrochlore oxides           | Neila Sellami       |

11.20-11.50 Coffee

**11.50-13.00 Nanostructure synthesis and modification 2**

**Chair: Iva Bogdanovic Radovic**

- |       |  |                  |
|-------|--|------------------|
| 11.50 | Ion beam doping of semiconductor nanowires (INV)                     | Carsten Ronning  |
| 12.20 | Ion beam synthesis: a simple method to dope Si nanocrystals          | Daniel Mathiot   |
| 12.40 | Ion beam synthesis for hybrid nanoelectronics: beyond silicon limits | Slawomir Prucnal |

13.00-13.20 IBMM2016 / Closing

## **Invited and oral presentations**

## New phenomena in 2D-layer irradiation with low energy ions

Thomas Michely

*II. Physikalisches Institut, Universität zu Köln, Germany*

With the rise of atomically thin 2D-layers as new class of materials in nanotechnology, the interaction of ion beams with them has become an emerging subject.

Here we focus on low energy ion beam effects in graphene supported by Ir(111), a metal substrate to which it only weakly couples, and investigate radiation damage and annealing by scanning tunneling microscopy combined with ab initio calculations as well as molecular dynamics simulations. We address four phenomena, not observable for 3D materials.

First, at grazing incidence single ions may penetrate graphene and are then guided in between the substrate and the graphene layer. The resulting axial and planar interface channeling is visible through a bead chain of vacancy clusters in graphene.

Second, the annealing of ion beam induced graphene vacancies displays distinct temperature stages. Around 900 K the vacancies created randomly within the graphene layer arrange through thermal diffusion to a rather regular mesh of vacancy clusters. The formation of the nanomesh relies on the moiré formed through graphene and the Ir(111) surface lattice.

Thirdly, while for a 3D material the sputtering yield fully characterizes the amount of material detached by ions, for a supported 2D-layer atoms are not only sputtered in backward direction, but also in detached in forward direction, trapped in the space between the 2D-layer and the substrate or mixed into the substrate. For the case of graphene on Ir (111) we demonstrate that by proper annealing the C-atoms detached in forward direction all assemble underneath the 2D-layer and form platelets of second layer graphene. By measuring the area of these platelets the trapping yield can be quantitatively determined. Its dependence on ion energy, ion mass and the angle of incidence is discussed.

Lastly, a 2D-layer may protect the underlying substrate material from ion erosion. This sputter protection effect is quantitatively demonstrated for graphene on Ir(111).

## Characterization of the electronic energy loss of keV ions by Medium-Energy Ion Scattering

Daniel Primetzhofer<sup>1</sup>, Margareta K. Linnarsson<sup>2</sup>, Hallen Anders<sup>2</sup>

<sup>1</sup>*Uppsala University, Division of Applied Nuclear Physics, Department of Physics and Astronomy, P.O. Box 534, SE-751 21 Uppsala, Sweden*

<sup>2</sup>*KTH Royal Institute of Technology, School of Information and Communication Technology, Integrated Circuits and Devices, P. O. Box E229, SE-16440 Kista-Stockholm, Sweden*

The electronic energy loss of ions at keV energies is of great relevance in the field of ion-beam modification of materials, e.g. ion implantation. Whereas at MeV energies, as employed in conventional ion beam analysis, the interactions of ions with the electronic system of different target materials has been investigated extensively both experimentally and in theory data at lower ion energies is found much less complete with reference data being absent for some highly relevant compounds (for an extensive data collection see [1]).

In this contribution we show why time-of-flight medium-energy ion scattering (TOF-MEIS) [2] is a particularly suitable tool to deduce electronic stopping power data from sensitive thin film targets. It will be explained how accurate data analysis can be performed with the help of Monte-Carlo simulations. We will present recent results obtained by TOF-MEIS for the energy loss of H, He and Ne ions at energies ranging from 5 - 150 keV. A part of the deduced data show unexpected non-linear velocity scaling, as in the case of He ions in Au, Pt and HfO<sub>2</sub> (hafnium dioxide) [3], [4], or comparatively high electronic stopping power, as observed for Ne ions in Au and Pt.

It will be discussed how details of the electronic structure of material and intruding ion can complicate the description of the energy loss. The experimental observations will be put in context with other recent studies showing complex energy dependence of electronic energy losses. This includes a discussion of possible trajectory dependent effects for ions other than H.

[1] H. Paul, Stopping power graphs, available from <http://www.exphys.jku.at/stopping/>

[2] M.K. Linnarsson, A. Hallén, J. Aström, D. Primetzhofer, S. Legendre, and G. Possnert, Rev. Sci. Instrum. 83, 095107 (2012).

[3] D. Primetzhofer, Phys. Rev. B 86, 094102 (2012).

[4] D. Primetzhofer, Phys. Rev. A 89, 032711 (2014).



## **Large scale parallel molecular dynamics modeling of focused ion beam processing: observation of explosive boiling and Marangoni effects**

Harley Johnson, Jonathan Freund, Kallol Das

*University of Illinois at Urbana-Champaign, USA*

Despite the widespread use of focused ion beam (FIB) processing as a microscopic material processing method, the basic material removal mechanisms are not well understood. Here we report the first complete atomistic computational studies of high-flux FIB. We carry out molecular dynamics simulations with up to 5.1 million atoms over millions of time steps, to study nanopore fabrication in freestanding thin film targets. We report two key results that emerge from the simulations: the observation of explosive boiling as a material removal mechanism, and the role of Marangoni effects in the mass transport that occur at the atomic scale.

Nanopore fabrication using FIB is typically understood to occur via sputter erosion, whereby each ion impact sputters several target atoms, thinning the target until a through-thickness nanopore is formed. While this may describe low-flux behavior, our detailed molecular dynamics simulations suggest that for ion beam fluxes above a threshold level, the primary mechanism of material removal changes to a significantly accelerated, thermally dominated process. In this case the target is heated faster than it cools via thermal conduction, leading to melting, and eventually explosive boiling, with local temperatures approaching the critical temperature. Atomic mass is rapidly rearranged via bubble growth and coalescence, leading to material removal that is orders of magnitude faster than would occur by sputter erosion.

The results also show a large temperature gradient where the beam impacts the surface, giving rise to a circulating flow of liquid silicon due to steep surface tension gradients, or a Marangoni flow. This drives mass transport inside the target and along the nanopore surfaces, from high temperature to low temperature. For films of a particular thickness, two counter-circulating flow regions form in the target, thus promoting material rearrangement at the free surfaces and modifying the surface morphology.

## Temperature and flux dependence of ion-beam mixing in crystalline and amorphous germanium isotope multilayers

Manuel Radek<sup>1</sup>, Matthias Posselt<sup>2</sup>, Bartosz Liedke<sup>2</sup>, Bernd Schmidt<sup>2</sup>, Lothar Bischoff<sup>2</sup>,  
Slawomir Prucnal<sup>2</sup>, Dominique Bougeard<sup>3</sup>, Hartmut Bracht<sup>1</sup>

<sup>1</sup>*Institute of Materials Science, WWU Münster, Germany*

<sup>2</sup>*Helmholtz-Zentrum Dresden-Rossendorf, Germany*

<sup>3</sup>*University of Regensburg, Germany*

The availability of highly enriched stable isotopes enables the preparation of isotopically controlled semiconductors. By means of crystalline (c-Ge) and preamorphized (a-Ge) germanium isotope multilayer structures we investigated the temperature and flux dependence of ion-beam induced self-atom mixing. Low, intermediate, and high temperature regions with different mixing behavior are identified after Ga implantation at 310 keV and various temperatures. In the first region (0K - 470K) the amount of mixing in c-Ge and a-Ge is very similar, an increasing mixing with increasing temperature is observed. Region 2 (470K - 540K) reveals a strong drop of mixing in c-Ge whereas the mixing in a-Ge still increases with temperature. In region 3 (570K and above) the mixing in a-Ge drops to the level of c-Ge. Within region 2 no significant structural change occurs during implantation suggesting an efficient annealing of the radiation damage. In addition we performed Focused-Ion-Beam (FIB) implantations with 60 keV Si ions into Ge using two different fluxes at two different temperatures. The experimental results indicate that the annealing of radiation damage is not only temperature but also flux dependent.

Molecular dynamics simulations with a Stillinger-Weber type potential are used to study the self-atom mixing observed in the experiment. It is found that the dominant mechanisms of mixing are thermal spikes formed by transferring kinetic energy of the incident ion to the lattice. If the transferred energy is high enough, locally molten regions are created in which the atoms can move more freely compared to the lattice atoms. With increasing temperature the thermal spikes last longer and the mixing increases. This is in accord with the experimentally observed mixing behavior in region 1. Differences between the mixing in a-Ge and c-Ge in region 2 are related to the initial crystal structure. Qualitative agreement is achieved with molecular dynamics simulations.

## Similarities and differences between SHIBIEC and SNEEL in ion-irradiated solids

Lionel Thomé<sup>1</sup>, Gihan Velisa<sup>2</sup>, Sandrine Miro<sup>2</sup>, Aurélien Debelle<sup>1</sup>, Frédérico Garrido<sup>1</sup>, Patrick Troceller<sup>2</sup>, Yves Serruys<sup>2</sup>

<sup>1</sup>CSNSM, CNRS-IN2P3-Université Paris-Sud, F-91405 Orsay, France

<sup>2</sup>CEA, DMN/SRMP/Laboratoire JANNUS, F-91191 Gif/Yvette Cedex, France

A few years ago, a new phenomenon called SHIBIEC (Swift Heavy Ion Induced Epitaxial Crystallization) was discovered to take place in some solids irradiated with swift ions [1-2]. This phenomenon consists in the recrystallization induced by the intense electronic excitation (Se) occurring in the wake of swift heavy ions of an amorphous layer formed by low energy ion irradiation (Sn). Very recently, SNEEL (Synergy between Nuclear and Electronic Energy Losses) effects were put forward in SiC and MgO irradiated with a dual ion beam [3]. It is worth mentioning that SHIBIEC requires the use of sequential two-step (low and high energy) ion irradiations, whereas SNEEL occurs during concomitant single-step (low and high energy) ion irradiations.

This paper presents studies performed in order to make strides in the understanding of the relationship between Sn and Se by pointing out similarities and differences between SHIBIEC and SNEEL in ion-irradiated oxides (ZrO<sub>2</sub>, MgO, Gd<sub>2</sub>Ti<sub>2</sub>O<sub>7</sub>) and carbides (SiC). Advanced techniques (RBS/C, XRD, TEM and Raman) were used to characterize the damage accumulated during the various irradiation steps. Results show that synergistic effects between Sn and Se, leading to a strong decrease of the accumulated damage, were observed in SiC and MgO, whereas the damage resulting from dual-beam irradiation is a simple addition of the damage created by Sn and Se alone in ZrO<sub>2</sub> and Gd<sub>2</sub>Ti<sub>2</sub>O<sub>7</sub>.

The results presented in this paper present a crucial interest for both fundamental studies and industrial applications. Concerning the operating cycle of future nuclear reactors, expected synergistic Sn/Se effects may lead to a strong reduction of the damage production allowing the preservation of the physical integrity of materials submitted to severe irradiations.

[1]A. Benyagoub et al., Appl. Phys. Lett. 89, 241914 (2006).

[2]A. Debelle et al., Phys. Rev. B 86, 100102R (2012).

[3]L. Thomé et al., Appl. Phys. Lett. 102, 141906 (2013).

## A unique synergistic damage effect due to electronic and nuclear energy loss in SrTiO<sub>3</sub>

William Weber<sup>1</sup>, Eva Zarkadoula<sup>2</sup>, Ritesh Sachan<sup>2</sup>, Peng Liu<sup>1</sup>, Haizhou Xue<sup>1</sup>, Ke Jin<sup>1</sup>, Yanwen Zhang<sup>2</sup>

<sup>1</sup>*University of Tennessee, USA*

<sup>2</sup>*Oak Ridge National Laboratory, USA*

The interaction of ions with solids results in energy loss to both electrons and atomic nuclei in the solid. The simple additive [1,2] and competitive [3-5] effects of electronic and nuclear energy loss have been demonstrated over a wide energy range. In our recent work, a highly synergistic effect of electronic and nuclear energy loss has been identified in SrTiO<sub>3</sub> in a separate effects study, in which single crystals of SrTiO<sub>3</sub> are pre-damaged with 900 keV Au<sup>+</sup> ions at 300 K to produce four intermediate levels of disorder. Both virgin and the pre-damaged single crystals were subsequently irradiated with 21 MeV Ni<sup>+</sup> ions (9.9 and 0.92 keV/nm for electronic and nuclear stopping, respectively, within pre-damaged region) and characterized by Rutherford backscattering spectrometry/channeling and transmission electron microscopy. While the virgin crystal was insensitive to any damage production from the 21 MeV Ni<sup>+</sup> ions, the pre-damaged states were highly sensitized to electronic energy deposition, with full amorphization being achieved at ion fluences as low as 0.02 Ni<sup>+</sup> ions/nm<sup>2</sup> (<0.0001 dpa). Based on a fit of the direct-impact model to the data, the effective damage track diameter increases from 4 nm to a saturation value of 15 nm with increasing level of initial disorder. Molecular dynamics simulations confirm that the introduction of cascade-like damage sensitizes SrTiO<sub>3</sub> to amorphous track formation at relative low values of electronic energy loss.

This work was supported by the U.S. Department of Energy, Office of Basic Energy Sciences, Materials Sciences and Engineering Division.

[1] M. Toulemonde et al., Phys. Rev. B 83, 054106 (2011).

[2] L. Thomé et al., Appl. Phys. Lett. 102, 141906 (2013).

[3] A. Debelle et al., Phys. Rev. B 86, 100102 (2012).

[4] W. J. Weber et al., RSC Advances 2, 595-604 (2012).

[5] Y. Zhang et al., Nucl. Instr. Meth. B 327, 33-43 (2014).

## Active control of protein conformation on surfaces by hyperthermal ion-surface interaction

Stephan Rauschenbach<sup>1</sup>, Gordon Rinke<sup>1</sup>, Ludger Harnau<sup>2</sup>, Alyanzan Albarghash<sup>1</sup>, Matthias Pauly<sup>1</sup>, Klaus Kern<sup>1</sup>

<sup>1</sup>*Max-Planck-Institute for Solid State Research, Germany*

<sup>2</sup>*Max-Planck-Institute for Intelligent Systems, Germany*

The physical, chemical, and biological properties of macromolecules like proteins are strongly dependent on their conformation. The degrees of freedom of their chemical bonds inflate a huge conformational space, of which however only a small fraction is accessible in thermal equilibrium. The conformation of a protein can be influenced by choosing a solvent, or in electrospray ionization, by the charge state and mode of transfer into the gas phase.

We show that soft-landing electrospray ion beam deposition (ES-IBD) of unfolded proteins on a surface allows to choose their conformation from of a wide range spanning from fully extended to completely compact, evidenced on the single molecule level by scanning tunneling microscopy (STM) at sub-nanometer resolution. Our experiments are supported by molecular dynamics simulations of the landing process.

We image proteins at the surface as extended strands for low charge states or as compact patches for low charge states. Upon increasing the deposition energy, we find that the high charge state proteins adopt more compact conformations.

The final conformation of the protein on the surface is reached through a mechanical deformation of the gas phase conformation during the ion-surface-collision. This process can be actively steered by controlling either the charge state to change the stiffness or the deposition energy in the hyperthermal energy regime to have a more intense collision. Therewith a new dimension to the processing of macromolecular materials is added to the existing coating technology, with the potential to reach otherwise inaccessible conformational states with potentially important functionalities.

## Extremely high energy density deposition by heavy polyatomic ion impacts – surface nanopatterning and frozen phase diagram pathways

Roman Böttger<sup>1</sup>, Karl-Heinz Heinig<sup>1</sup>, Lothar Bischoff<sup>1</sup>, Christian Anders<sup>2</sup>, Herbert M. Urbassek<sup>2</sup>, Renè Hübner<sup>1</sup>, Bartosz Liedke<sup>1</sup>

<sup>1</sup>*Helmholtz-Zentrum Dresden-Rossendorf, Germany*

<sup>2</sup>*University Kaiserslautern & Research Center OPTIMAS, Germany*

Au and Bi ions of a few tens of keV deposit a high energy density into the collision cascade volume due to (i) their high mass and (ii) their low projected range. At higher energies this density becomes diluted as the cascade volume increases super-linearly with ion energy.

Compared to monatomic ions, polyatomic ions deposit a much higher energy density. This is sufficient to form a pool of a localized, almost classical melt in a semiconductor surface lasting up to half of a nanosecond. Local melting and resolidification by single polyatomic ion impacts is proven by molecular dynamics calculations.

Well-ordered, self-organized dot patterns have been found after heavy polyatomic ion irradiation, which can be attributed to the impact-induced local transient melting. The kinetics of localized melt pools leads to a generic, Bradley-Harper-type partial differential equation for the surface evolution. Whereas so far the mechanisms of ion-induced surface pattern evolution are assumed to be surface curvature dependent ion erosion or ion-momentum-induced mass drift of surface atoms, for heavy polyatomic ions we have identified a completely different mechanism.

The local melting and quenching process is so far from equilibrium that particularities of phase diagrams like the Bi state in Si or Ge are frozen into the nanostructure of the resolidified volume. This opens the possibility to study extremely fast solid-liquid phase transitions.

Financial support by the German Research Foundation via the research unit 845 is acknowledged.

[1] L. Bischoff, K.-H. Heinig, B. Schmidt, S. Facsko, W. Pilz, Nucl. Instr. Meth. Phys. B 272, 198 (2012).

[1] R. Böttger, L. Bischoff, K.-H. Heinig, B. Schmidt, J. Vac. Sci. Technol. B 30, 06FF12 (2012).

[2] R. Böttger, K.-H. Heinig, L. Bischoff, B. Liedke, R. Hübner, W. Pilz, Phys. Status Soli RRL7, 501 (2013).

[3] C. Anders, K.-H. Heinig, H.M. Urbassek, Phys. Rev. B 87, 245434 (2013).

[4] L. Bischoff, R. Böttger, K.-H. Heinig, S. Facsko, W. Pilz, Appl. Surf. Sci. doi: 10.1016/j.apsusc.2014.03.166 (2014).

## **Ion beam ultra-precision smoothing of surfaces**

Bernd Rauschenbach, Frank Frost, Thomas Arnold

*Leibniz Institute of Surface Modification, Germany*

Ion beam erosion can be used as an alternative process for surface smoothing at microscopic length scales and for the preparation of ultra-smooth surfaces. This requires that in the evolution of the surface topography different relaxation mechanisms dominate over roughening, i.e. smoothing of initially rough surfaces can occur. This contribution focus on the basic mechanisms as well as potential application of surface smoothing by ion beams.

The topography evolution of surfaces with respect to different process parameters (ion energy, ion incidence angle, erosion time, sample rotation) has been investigated. Based on the time evolution of different roughness parameters the relevant surface relaxation mechanisms responsible for surface smoothing are discussed. In this context also physical constraints with regard to the effectiveness of surface smoothing by ion bombardment will be addressed.

In the application-oriented part of this presentation recent technological developments related to ion beam assisted smoothing of optically relevant surfaces are summarized. It will be demonstrated that smoothing by direct ion bombardment of various technologically important material surfaces down to 0.1 nm rms roughness level showing a great promise for large-area surface processing. Specific examples are given for ion beam smoothing, especially for substrates used for advanced optical applications (e.g. x-ray optics, components for the extreme ultraviolet lithography, spheres for new definition of the kilogram).

Finally it is demonstrated several modular machine systems for the ultra-precision smoothing of surfaces up to 1000 mm in diameter. Such machines are used in the optical and semiconductor industry. Typical examples for the ultra-precision smoothing under industrial conditions are discussed.

## Transparent aluminium nanowires electrodes with optical and electrical anisotropic response fabricated by defocused ion beam sputtering

Diego Repetto, Marina Giordano, Christian Martella, Francesco Buatier De Mongeot

*Physics Department, University of Genoa, Italy*

Self-organised Ion Beam Sputtering (IBS) can lead to the formation of ordered metallic nanowire (NW) arrays by direct IBS patterning of a metal film supported on a flat low cost glass substrate. For increasing ion dose, the rippled metal film decomposed into a disconnected NW array which exhibits tunable anisotropic optical properties as well as anisotropic electrical conductivity. So far, for the metal sacrificial layer, noble metals as Au [1,2] or Ag [3] were chosen since, beyond having a very low resistivity, they support localised plasmon resonances in the VIS-NIR spectral range [1,2].

In this work, we have explored the possibility to find an alternative to transparent conductive oxides in optoelectronic devices. In this view, self-organised Al NWs electrodes have been obtained by defocused IBS of polycrystalline Al films grown by sputter deposition, adopting experimental conditions which are compatible with industrial processes, in view of the fabrication of low cost transparent electrodes.

The electrical characteristics have been acquired in situ during the morphological evolution of the samples, evidencing an increase of the electronic transport anisotropy as a function of ion dose between the two directions parallel and orthogonal to the NWs axis.

Optical spectra in transmission also show a large dichroism between the two directions, suggesting the role of localised plasmons in the UV spectral range. After a fluence of  $1,2 \times 10^{18}$  ions/cm<sup>2</sup>, the Al NWs electrodes showed transparencies of about 40% and sheet resistances, longitudinal and transverse, of 18  $\Omega$ sq and 4,5  $\Omega$ sq. At higher fluencies, higher transparencies are obtained at the expense of conductivity.

[1] D. Chiappe, A. Toma, and F. Buatier de Mongeot, Phys. Rev. B 86, 045414 (2012).

[2] D. Chiappe, A. Toma, and F. Buatier de Mongeot, Small 9, 913-919 (2013).

[3] A. Toma et al., Journal of Applied Physics 104, 104313 (2008).



## Plasmonic properties of ion-shaped nanoparticles

Giancarlo Rizza

*Ecole Polytechnique, Paliseau, France*

In the last years, ion-shaping has been proposed as an innovative and powerful tool to sculpt the matter at the nanometer scale. Its importance relies in its unique capability to control both the morphology and the spatial orientation of metallic nanoparticles embedded within an amorphous host matrix. Consequently, the ion-shaping technique can be seen as a novel route for downscaling the engineering of embedded NPs with a precision that is barely reachable with standard techniques.

In the first part of this talk the fabrication of a model system and the potentialities offered by the ion-shaping technique will be reviewed. I show that the ion-shaping is not limited to the transformation of spherical NPs into prolate rod-like nanostructures. Indeed, depending on the initial NP size and irradiation fluence, several other classes of ion-shaped NPs can be obtained: i) faceted-like NPs, ii) nanowires growing from a faceted core, iii) chromosome-like NPs and iv) hollow nanorods.

Besides, a rational description of the ion-beam shaping is given by coupling the experimental results to the evolution of the temperature profile obtained with a 3D version of the thermal-spike model adapted for anisotropic and composite media.

Finally, maps of the plasmon modes of the ion-shaped NPs are obtained using Electron Energy Loss Spectroscopy (EELS). Optical spectra are simulated using a specifically developed Auxiliary Differential Equations-Finite Difference Time Domain (ADE-FTDT) code whereas plasmon maps are simulated using the MNPBEM toolbox.

This work demonstrates the possibility to use ion irradiation as tool for the controllable fabrication of a whole family of plasmonic nanostructures with topologically tunable optical properties. These ion-shaped composite media have potential applications spanning from plasmonic photovoltaics, to bio-sensing, SERS and SEIRA spectroscopies.

## Catalytic nanoparticle formation by ion irradiation at solid-liquid interface

Tomohiro Kobayashi<sup>1</sup>, Tetsuya Yamaki<sup>2</sup>, Teruyuki Hakoda<sup>2</sup>, Yasunori Yamazaki<sup>1</sup>

<sup>1</sup>*RIKEN, Japan*

<sup>2</sup>*JAEA, Japan*

Energetic ions ejected into liquid promote a regional chemical reaction such as reduction of metallic ions. In this paper, we report deposition of platinum nanoparticles on carbonaceous substrates by MeV H<sup>+</sup> ion irradiation in liquid. Uniformly supported platinum nanoparticles with appropriate size on substrates can be applied to electrodes for electrochemical gas sensors and fuel cells.

By using a tapered glass capillary with a thin lid at the tip, we have developed irradiation system in liquid with MeV ions. Previously, we reported a polymerization of monomers at a target surface using this system [1]. The inlet diameter of the capillary was 1.8 mm and outlet diameter was 100 – 200  $\mu\text{m}$ . 3MeV H<sup>+</sup> ion beam of a tandem accelerator is focused and guided by small angle scatterings with inner wall of tapered glass capillaries with inserted in a liquid container. The substrate of glassy carbon or carbon cloth was set at the distance of 100  $\mu\text{m}$  from the tip. The irradiation was performed at a beam current of 2 nA in hexachloroplatinic (IV) acid (H<sub>2</sub>[PtCl<sub>6</sub>]) with ethanol as a reducing agent. The particles were observed using microscopes (TEM/SEM).

The nanoparticles of 5-10 nm were observed by TEM in filtered products. The EDX analysis showed the particles consist of platinum with little contamination of chlorine. Some of the particles formed in the liquid adhered on the target materials and grew up. The SEM observation of substrates showed the numbers and the density of particles on the surface depended on the metal ion concentration and the beam scanning speed. The particles attached on the substrate can be grown up by additional irradiation and finally we could make a dense platinum coating on substrates. The electrochemical property of supported particles has also been measured.

[1] T. Kobayashi, T. Ikeda, K. Ogiwara and Y. Yamazaki., NIMB 272, 405-408 (2012).

## Formation and tailoring of metal and semiconductor quantum dots in amorphous matrices by MeV ions

Iva Bogdanovic Radovic<sup>1</sup>, Nikola Radic<sup>1</sup>, Milko Jaksic<sup>1</sup>, Goran Drazic<sup>2</sup>, Sigrid Bernstorff<sup>3</sup>, Maja Buljan<sup>1</sup>, Marko Karlusic<sup>1</sup>

<sup>1</sup>*Rudjer Boskovic Institute, Croatia*

<sup>2</sup>*National Institute of Chemistry, Hajdrihova 19, 1000 Ljubljana, Slovenia*

<sup>3</sup>*Elettra-Sincrotrone Trieste, S.S. 14 – km 163,5, 34149 Basovizza, Italy*

Materials based on metal or semiconductor quantum dots (QDs) are very interesting for many applications, especially in the field of photonics (lasers, sensors, photovoltaic devices, imaging, data storage, etc.) and also as materials with enhanced thermoelectric efficiency. Due to the fact that their properties strongly depend on QD size and arrangement it is important to achieve a controllable production of such materials. Recently we have demonstrated that if (Ge+SiO<sub>2</sub>)/SiO<sub>2</sub> multilayers are irradiated by MeV ions, the sizes, distances, and arrangement type of the QDs follow simple equations dependent on the irradiation and the multilayer properties [1]. Self-ordering can be explained by two ion properties: ion electronic stopping and efficiency to transfer deposited energy from the electron to the phonon system [2]. The most effective formation and ordering of Ge QDs were achieved by 3 MeV oxygen ions. In the present work we investigate further the influence of MeV ions on the formation and arrangement quality of QDs in several other multilayer types. Multilayers containing metal (Ni) or semiconductor (Ge, Si or SiGe) atoms uniformly mixed with the matrix or already formed QDs in different types of amorphous matrices (ITO, silica or alumina) have been irradiated with MeV oxygen and silicon ions at several ion energies and under different incident angles. Ion beam parameters leading to QD formation and ordering, as well as induced changes in the already formed QDs in different multilayer types have been compared and discussed.

[1] M. Buljan, I. Bogdanovic Radovic, M. Karlusic, U.V. Desnica, N. Radic, M. Jaksic, K. Salamon, G. Drazic, S. Bernstorff, V. Holy, Phys. Rev. B 84, 155312 (2011).

[2] I. Bogdanovic Radovic, M. Buljan, M. Karlusic, N. Skukan, I. Bozicevic, M. Jaksic, N. Radic, G. Drazic, S. Bernstorff, Phys. Rev. B 86, 165316 (2012).

## Characterization of ion-implanted films with high-energy electron scattering

Pedro Grande<sup>1</sup>, Robert Elliman<sup>2</sup>, Maarten Vos<sup>2</sup>, Dinesh Venkatachalam<sup>2</sup>, Sanjoy Nandi<sup>2</sup>

<sup>1</sup>*Instituto de Física, UFRGS, Brazil*

<sup>2</sup>*Australian National University, Australia*

Determining the composition and structure of the near-surface of solids is essential for understanding their physical and chemical properties. As a consequence, many experimental techniques have been developed to characterize such layers, each having their specific advantages and limitations. Here we introduce a new technique for probing the composition and electronic structure of the near-surface region of solids, namely: high-energy electron backscattering spectrometry (or Electron Rutherford backscattering spectrometry (ERBS)).

Measurements are performed by irradiating samples with mono-energetic (5-40 keV) electrons and detecting the backscattered electrons with high-energy resolution ( $\sim 0.3$  eV FWHM). This energy resolution is sufficient to distinguish electrons scattered elastically from different mass atoms, as well as those that undergo additional inelastic scattering events (e.g. plasmon excitation, or band-gap transitions).

The use of the ERBS technique is illustrated for the case of ion-beam synthesised transition metal oxides that are of interest for non-volatile memory applications. Results include oxide synthesis in Ta and Hf films implanted with low energy O ions to high fluences. ERBS analysis is shown to provide quantitative compositional analysis of the implanted surface and to identify the formation of stoichiometric insulating phases (e.g.  $\text{Ta}_2\text{O}_5$ ) via their characteristic band gaps (e.g. 4.5 eV for  $\text{Ta}_2\text{O}_5$ ). Such analysis is shown to provide a fairly detailed picture of the elemental composition and electronic properties of the films. Results are compared with predictions from the dynamic Monte Carlo simulator, TriDyn, x-ray photoelectron spectroscopy (XPS) and transmission electron microscopy (TEM). We also show that the ERBS technique is capable of distinguishing  $^{16}\text{O}$  and  $^{18}\text{O}$  isotopes and that this can be used to investigate other properties of thin-film oxides, including oxygen self-diffusion coefficients.

## **Tailoring of the thermomechanical performance of VO<sub>2</sub> nanowire bimorph actuators by ion implantation**

Helmut Karl

*Physics Department, University of Augsburg, Germany*

The strongly correlated electron material vanadium dioxide (VO<sub>2</sub>) undergoes a metal-insulator phase transition (MIT) at 68°C which is marked by a tremendous decrease of its electrical resistivity and change in optical transmittance and reflectance in the near infrared spectral region. In addition the MIT is accompanied by a structural phase transition with a large anisotropic and abrupt length change of 1% and 2% when the materials transforms from either the insulating monoclinic M1 or mechanically stress stabilized monoclinic M2 to the tetragonal rutile phase R. This allows fabrication of VO<sub>2</sub> nanowire based bimorph actuators with an extreme change of bending curvature from 0 to up to 100000m<sup>-1</sup> over the small MIT temperature interval. A key parameter for improved of thermomechanical actuator efficiency and performance is the temperature hysteresis of the MIT which is inherently large for single domain VO<sub>2</sub> nanowires coated along one side by iridium. In this work we demonstrate for the first time the fabrication of a novel type all oxide VO<sub>2</sub> nanowire bimorph actuator by ion implantation along one side into free standing single-clamped VO<sub>2</sub> nanowires. The temperature hysteresis of the mechanical bending is nearly completely suppressed in these bimorphs. This is explained by ion induced lattice defects at the end of ion implantation range seeding the MIT along the defect free side of the VO<sub>2</sub> bimorph. Moreover we demonstrate that mechanical strain intentionally built-in during bimorph fabrication or side ion implantation of dopands changing the MIT transition temperature directs the phase transition from M1 via M2 to the R phase. This allows realizing complex bimorph bending schemes, e.g. positive followed by negative bending curvature change of the bimorph during a unidirectional temperature sweep.

## **Ion beam micro-structuring and fluorescence modification of dielectric crystals applied to waveguide laser devices**

Feng Chen<sup>1</sup>, Yang Tan<sup>1</sup>, Shengqiang Zhou<sup>2</sup>

<sup>1</sup>*Shandong University, P.R. China*

<sup>2</sup>*Helmholtz-Zentrum Dresden-Rossendorf, Germany*

Techniques of energetic ion beams, such as ion implantation, swift heavy ion irradiation, and proton beam writing, have been applied to achieve micro-structuring of dielectrics, constructing optical waveguides with diverse configurations via refractive index engineering. In active crystals, the fluorescence features were modified as well through the interaction of incident ions and bulk lattices. The induced disorders in the optically microstructured materials by electronic and nuclear energy deposition were responsible for the luminescence modification. However, it has been confirmed that in the waveguiding cores of the irradiated crystals, the fluorescence properties were well preserved with respect to the bulks, whilst the considerable changes mainly happen at the boundary of waveguide and bulk. This paves a way for further applications of ion beam irradiated active dielectric waveguides as miniature laser devices. Efficient lasing at both continuous-wave (cw) and pulsed regimes has been realized in ion beam processed dielectric waveguides. The maximum output power of cw waveguide lasers was as high as 0.3 W, and high slope efficiencies close to the quantum defect limit were obtained in some systems. Recently, we have fabricated the graphene based passive Q-switched lasers in ion beam irradiated waveguides. With ion beam processed graphene layer, the evanescent-field interaction with graphene became more efficient than that without ion beam processing. In this work, we report on some of the most recently obtained results in our research. The excellent performances of the ion irradiated waveguide lasers have shown strong potential in applications of future integrated photonic devices.

## **Ion-beam synthesis of transition-metal oxide/suboxide heterostructures for non-volatile memory applications**

Robert Elliman<sup>1</sup>, Dinesh Venkatachalam<sup>1</sup>, Sanjoy Nandi<sup>1</sup>, Xinjun Liu<sup>1</sup>, Shuai Li<sup>1</sup>, Kidane Belay<sup>1</sup>, Pedro Grande<sup>2</sup>, Maarten Vos<sup>3</sup>, Simon Ruffell<sup>4</sup>, Jonathan England<sup>4</sup>

<sup>1</sup>*Department of Electronic Materials Engineering, Research School of Physics and Engineering, Australian National University, Canberra ACT 0200, Australia*

<sup>2</sup>*Institute of Physics, Universidade Federal do Rio Grande do Sul, Porto Alegre, Brazil*

<sup>3</sup>*Atomic and Molecular Physics Laboratory, Research School of Physics and Engineering, Australian National University, Canberra ACT 0200, Australia*

<sup>4</sup>*Varian Semiconductor Equipment, Silicon Systems Group, Applied Materials Inc, USA*

As thin films, transition-metal oxides (TMOs) can be subjected to high electric fields and exhibit characteristic resistance changes that are of interest for future non-volatile memory applications, such as resistance random access memory (ReRAM). The resistance changes in a ReRAM are sensitive to film stoichiometry and can often be better controlled by using stoichiometric (oxide)/sub-stoichiometric (suboxide) heterostructures. In this study, we show that ion-implantation provides an effective means of fabricating such heterostructures at room temperature, and that these exhibit resistance changes that are suitable for ReRAM applications.

Specifically, oxide/suboxide heterostructures are fabricated by oxygen implantation of Ta, Hf and Nb films using either directed beam implantation or plasma-immersion implantation. Detailed compositional, structural and electrical characterisation is reported, including analysis using a newly developed electron backscattering technique that is analogous to Rutherford backscattering spectrometry (e-RBS). The e-RBS technique provides important insight into the electronic structure of the films and shows that ion-beam synthesised films are indistinguishable from their bulk counterparts, despite being formed at room temperature. Standard electrical characterisation of ion-beam synthesised ReRAM devices show sub-100 ns switching speeds with switching currents <100  $\mu$ A, and endurance >10<sup>6</sup> cycles for particular structures.

Oxide/suboxide composition profiles are compared with predictions from the dynamic Monte Carlo simulator, TriDyn, and electrical characteristics are compared with finite elements models based on defect drift and diffusion.

## Producing nanodot arrays, virtually defect-free ripples and exotic new patterns by ion bombardment of binary materials

R. Mark Bradley<sup>1</sup>, Patrick D. Shipman<sup>2</sup>, Francis C. Motta<sup>2</sup>

<sup>1</sup>*Department of Physics, Colorado State University, USA*

<sup>2</sup>*Department of Mathematics, Colorado State University, USA*

We have developed a theory that explains the genesis of the strikingly regular hexagonal arrays of nanodots that can form when the surface of a binary compound is subjected to normal-incidence ion bombardment [1]. In our theory, the coupling between the topography of the surface and a thin surface layer of altered composition is the key to the observed pattern formation.

For oblique-incidence bombardment of a binary material, we find that remarkably defect-free ripples can be produced if the ion species, energy and angle of incidence are appropriately chosen [2]. In addition, a "dots-on-ripples" topography can emerge for a different range of parameter values. Nanodots arranged in a hexagonal array sit atop a ripple topography in this novel type of pattern.

A closely related theory yields insight into the results of recent experiments in which silicon was bombarded with a beam of gold ions, yielding patches of ripples with two distinct wave vectors that were oblique to the beam [3]. We have advanced a theory that accounts for the emergence of this fascinating type of order --- in our theory, it is the result of (i) an anisotropic fourth order term in the equations of motion and (ii) the coupling between the surface height and a thin surface layer in which implanted gold is present.

[1] R. M. Bradley and P. D. Shipman, Phys. Rev. Lett. 105, 145501 (2010).

[2] F. C. Motta, P. D. Shipman and R. M. Bradley, J. Phys. D 45, 122001 (2012).

[3] S. A. Mollick, D. Ghose, P. D. Shipman and R. M. Bradley, Appl.Phys. Lett. 104, 043103 (2014).



## Nonuniform stress as a key to surface nanopatterning by ion beam irradiation

Rodolfo Cuerno<sup>1</sup>, Ana Moreno Barrado<sup>2</sup>, Mario Castro<sup>2</sup>, Raul Gago<sup>3</sup>, Luis Vazquez<sup>3</sup>, Javier Munoz Garcia<sup>1</sup>, Beatriz Galiana<sup>1</sup>, Carmen Ballesteros<sup>1</sup>

<sup>1</sup>*Universidad Carlos III de Madrid, Leganes, Spain*

<sup>2</sup>*Universidad Pontificia Comillas, Madrid, Spain*

<sup>3</sup>*Instituto de Ciencia de Materiales de Madrid, Consejo Superior de Investigaciones Cientificas, Madrid, Spain*

Irradiation by low- to medium-energy ions has proven as a highly efficient technique to nanostructure surfaces of many materials [1]. For systems that become amorphous under this type of processing, like semiconductors, recent developments are changing the classic physical description [2] of the ensuing pattern-formation process. E.g., it has been established that the ion incidence angle has to go beyond a non-zero critical value in order to produce structured (rippled) morphologies [3]. Such a threshold has been theoretically explained on the basis of viscous flow [4] or mass redistribution [5]. However, recent experimental results further indicate a (non-classic) lack of universality with respect to ion species [6], which affects basic process characteristics, like the very same value of the critical angle. To date, this variability has remained unaccounted for. Here we show [7] that the key factor behind the range of experimental observations is the non-uniform generation of stress across the damaged amorphous layer induced by the irradiation. In turn, it is the ion/target combination which controls the inhomogeneity of this stress field, leading to different values of the critical angle for each particular case. We reach these conclusions by contrasting a multiscale theoretical approach, which combines Molecular Dynamics and a continuum viscous flow model, with experiments on silicon using Ar+ and Xe+ ions. Our general approach can apply to a variety of systems and conditions.

[1] J. Munoz-Garcia et al., in ‘Toward Functional Nanomaterials’, ed. Z. M. Wang (Springer, New York, 2009), 323-398.

[2] R. Bradley and J. Harper, J. Vac. Sci. Technol. A 6, 2390 (1988).

[3] C. S. Madi et al., Phys. Rev. Lett. 101, 246102 (2008).

[4] M. Castro and R. Cuerno, Appl. Surf. Sci. 258, 4171 (2012).

[5] S. A. Norris et al., Nat. Commun. 2, 276 (2011).

[6] For Si, see e.g. S. Macko et al., Nanotechnol. 21, 085301 (2010).

[7] A. Moreno-Barrado et al., submitted (2014).

## Reverse epitaxy on semiconductor surfaces

Xin Ou, Rene Hübner, Manfred Helm, Jürgen Fassbender, Stefan Facsko

*Helmholtz-Zentrum Dresden-Rossendorf, Germany*

Arrays of semiconductor nanostructures are emerging as building blocks for the next generation of electronic and optoelectronic nanodevices. Besides the conventional low efficiency lithographic techniques broad ion beam irradiation is a simple and mass productive technique to fabricate nanostructure patterns on semiconductor surfaces [1,2]. The main drawback of this technique is, however, that the irradiated semiconductor surfaces are amorphized [1,2]. For device fabrication, a crystalline surface of high quality is indispensable. In this talk, we demonstrate single crystal elemental and compound semiconductor nanostructure pattern formation based on a “reverse epitaxy” process [3]. The formation of these patterns is interpreted as the result of a surface instability due to an Ehrlich-Schwoebel barrier for vacancies created during ion beam irradiation at elevated temperature. Moreover, these vacancies distribute according to the crystallographic anisotropy, which results in an orientation-dependent pattern formation on single crystal semiconductor surfaces. The formation of “inverse structures” in this process shows nicely the equivalence of epitaxy with deposited adatoms and “reverse epitaxy” with ion induced surface vacancies. The simulation of the pattern formation is performed by a continuum equation which includes anisotropic effective surface currents due to the Ehrlich-Schwoeble barrier.

Our work establishes an entirely new and complementary epitaxial method for the fabrication of high-quality faceted semiconductor nanostructures. The potential application of reverse epitaxy for the fabrication of quantum devices and optical components will be discussed.

[1] S. Facsko et al., Science 285, 1551 (1999).

[2] X. Ou et al., AIP Advances 1, 042174 (2011).

[3] X. Ou et al., Physical Review Letters 111, 016101 (2013).

**Ion-induced pattern formation: the origin of perpendicular mode ripples**

Tomas Skeren<sup>1</sup>, Kristiaan Temst<sup>2</sup>, Wilfried Vandervorst<sup>3</sup>, André Vantomme<sup>2</sup>

<sup>1</sup>*Czech Technical University in Prague, Czech Republic*

<sup>2</sup>*Instituut voor Kern- en Stralingsfysica, KU Leuven, Belgium*

<sup>3</sup>*imec, Leuven, Belgium*

Irradiation of surfaces with low energy ions often leads to the formation of well-defined periodic nanostructures. This phenomenon attracts a lot of attention as a potential nanofabrication tool but despite significant effort its physical origin remains puzzling.

A typical example of ion-induced morphologies are so-called ripples – 1 dimensional periodic corrugations with periodicities ranging from a few nanometers up to micrometers. They typically form at off-normal ion bombardment and, intriguingly, the orientation of the wavevector of the ripple structure can be both perpendicular or parallel to the ion beam depending on the conditions. The existence of these two ripple modes (PeMR and PaMR) has been explained by the classical Bradley-Harper (BH) theory based on a single linear instability – PaMR should form at lower angles of incidence while at grazing incidence the orientation of the ripples should change to PeMR. Although this scenario has been reported in certain publications, there are numerous reports which deviate from this behavior.

In the recent past, the validity of the BH theory has been challenged and several alternatives have been proposed (hydrodynamic instability, mass redistribution...) Interestingly, these mechanisms do not predict PeMR formation at all.

One class of materials where only PeMR is typically observed are metals. We formulated a model which explains the PeMR formation on the metallic surfaces based on an interplay of a general roughening mechanism (which promotes formation of isotropic roughness) and non-linearities which are universally active at grazing incidence. By computer simulations we were able to excellently reproduce the patterning behavior of metals including PeMR formation.

In this contribution, we review the general phenomenology of the PeMR formation on both metallic and non-metallic surfaces and we show that the non-linear PeMR formation mechanism can be relevant for a broader group of materials than just metals.

## **Self-assembled metal structures by cluster ion beam bombardment and applications in plasmonic biosensing**

Dharshana Wijesundera, Buddhi Tilakaratne, [Wei-Kan Chu](#)

*Department of Physics & Texas Center for Superconductivity at University of Houston, USA*

Oblique angle cluster ion beam irradiation of metal (gold) surfaces induces self-assembly of arrays of periodic nano-sized ripple structures. The surface morphology of these ripple structures closely resembles Aeolian sand ripples, however, in contrast, they have partially open cavities in them. Optical scattering from the rippled surfaces shows a sharp resonance in the visible range indicative of LSPR in the ripples. The resonance frequency of LSPR and the high cross-section of scattering indicates that plasmon resonance is coupled with cavity resonance in the hollows of the ripple structures. Simulations further show that the electromagnetic power density is dramatically enhanced in the cavities at the resonance frequency. Substrates with such properties are ideal for plasmonic bio-sensing applications such as SPR based immunoassays and surface Raman enhancement. In this talk we will discuss the formation process of gold ripple arrays by 30 keV oblique angle Ar gas cluster ion beam bombardment, their plasmonic optical properties and their shift when perturbed by organic molecular adsorption resembling bio-molecular adhesion.

## Doping of graphene by ultra low energy mass selected ion implantation

Hans Hofsäss

*2nd Institute of Physics, University Göttingen, Germany*

Ultra low energy implantation of mass selected ions is a versatile method for doping of graphene. It allows doping of even monolayer graphene with different dopant atoms and control of the dopant concentration.

We use a low energy mass selected ion beam system with UHV ion irradiation and implantation chamber. A 30 keV mass selected ion beam is decelerated in a UHV-chamber down to energies of as low as 10 eV. An area of about 1 cm<sup>2</sup> can be uniformly irradiated with a beam current up to several  $\mu$ A. The energy distribution of the beam starts at the maximum ion energy given by the deceleration bias voltage and has a tail towards lower energies.

I will discuss results for (i) doping of free-standing monolayer graphene with  $^{11}\text{B}^+$  and  $^{14}\text{N}^+$  ions using atomic resolution high-angle dark field imaging (HAADF) combined with single-atom electron energy loss (EEL)[1] and (ii) doping of graphene monolayers grown on SiC(0001) with 25 eV  $\text{N}^+$  ions and characterization using scanning tunneling microscopy. Nitrogen atoms are incorporated almost exclusively as graphitic substitution in the graphene honeycomb lattice and generate an electronic contrast with three-fold symmetry [2].

Before implantation, the graphene samples have to be cleaned in order to remove surface contaminants and adsorbates. This usually requires vacuum annealing to temperatures above 700 K. Another option is ion beam cleaning with ultra low energy noble gas ions and energies below a certain threshold for defect generation. This is demonstrated using X-ray photoelectron spectroscopy of successively irradiated graphene. Ultra-low energy ion irradiation of graphene with  $^{12}\text{C}^+$  ions also allows the controlled generation of point defects.

[1]U. Bangert, W. Pierce, D. Kepaptsoglou, Q. Ramasse, R. Zan, M. Gass, J. A. Van den Berg, C. Boothroyd, J. Amani, and H. Hofsäss, Nano Letters 13, 4902 (2013).

[2]P. Willke, J. A. Amani, S. Thakur, S. Weikert, T. Druga, K. Maiti, H. Hofsäss, and M. Wenderoth, Appl. Phys. Lett., submitted

### Lattice sites of implanted Mg in GaN

Ulrich Wahl<sup>1</sup>, Lígia Amorim<sup>2</sup>, Lino Pereira<sup>2</sup>, Stefan Decoster<sup>2</sup>, Daniel Silva<sup>3</sup>, João Guilherme Correia<sup>4</sup>, Manuel Ribeiro Da Silva<sup>5</sup>, Kristiaan Temst<sup>2</sup>, André Vantomme<sup>2</sup>

<sup>1</sup>*Instituto Tecnológico e Nuclear, Sacavém, Portugal*

<sup>2</sup>*Instituut voor Kern- en Stralingsfysica, KU Leuven, Belgium*

<sup>3</sup>*Departamento de Física e Astronomia da Faculdade de Ciências da Universidade do Porto, Portugal*

<sup>4</sup>*Centro de Ciências e Tecnologias Nucleares, Instituto Superior Técnico, Universidade de Lisboa, Portugal*

<sup>5</sup>*Centro de Física Nuclear, Universidade de Lisboa, Portugal*

The wide band gap semiconductor GaN is the base material for a great variety of optoelectronic devices including white LEDs and blue lasers. Its only relevant p-type dopant is Mg, usually introduced during epitaxial growth. Ion implantation doping of GaN with Mg was investigated in the 1990s but concluded not feasible since the implantation damage could not be sufficiently removed. However, recently efficient electrical activation of implanted Mg in GaN by means of a multicycle RTA process up to 1400°C has been claimed [1], motivating further investigations of the basic processes of Mg implantation into GaN. Following our previous work on Mg in AlN [2], in this contribution we focus on the lattice sites of Mg following low fluence ( $6 \times 10^{10} \text{ cm}^{-2}$  at 50 keV) implantation into thin GaN films. Using the electron emission channeling technique from radioactive <sup>27</sup>Mg ( $t_{1/2}=9.5 \text{ min}$ ) at the CERN-ISOLDE facility, we have directly and unambiguously determined its lattice location for implantation temperatures up to 800°C.

As expected, the majority of <sup>27</sup>Mg was always found on the Ga site, however for RT and 300°C implantation also ~25% of Mg occupies interstitial octahedral sites. Annealing or implanting at 600°C converts interstitial Mg to substitutional Ga sites, a process which is complete at 800°C. The activation energy for migration of interstitial Mg is estimated to be ~1.6-2.6 eV. According to a recent theoretical model [3], Mg in GaN forms a so-called “polaronic acceptor” which traps a hole on a nearby N atom, inducing considerable lattice distortions for Mg, however, we found no evidence of substitutional Mg being displaced  $>0.1 \text{ Å}$  from the ideal Ga site.

[1] T.J. Anderson et al, Electron. Lett. 50, 197 (2014); Pat US 2012068188-A1.

[2] L.M. Amorim, U. Wahl, L.M.C. Pereira, S. Decoster, D.J. Silva, M.R. da Silva, A. Gottberg, J.G. Correia, K. Temst, A. Vantomme, Appl. Phys. Lett. 103, 262102 (2013).

[3] J.L. Lyons, A. Janotti, C.G. Van de Walle, J. Appl. Phys. 115, 012014 (2014).

## **Supersaturation of implanted gold in silicon by pulsed laser melting and rapid thermal annealing for enhanced infrared photoresponse at room temperature**

Jim Williams<sup>1</sup>, Wenjie Yang<sup>1</sup>, S.Q. Lim<sup>1</sup>, T.T. Tran<sup>1</sup>, A.J. Akey<sup>2</sup>, J.P. Mailoa<sup>2</sup>, D. Recht<sup>3</sup>, T. Buonassisi<sup>2</sup>, M.J. Aziz<sup>3</sup>

<sup>1</sup>*Australian National University, Australia*

<sup>2</sup>*MIT, Cambridge MA, USA*

<sup>3</sup>*Harvard University, Cambridge MA, USA*

Recently we have demonstrated a working infrared photodetector from silicon hyperdoped with gold using ion-implantation followed by pulsed laser melting (PLM) [1]. It was shown that the optical absorption in the infrared increases with gold concentration but saturates at high implant doses due to the effect of gold on the recrystallization of the molten silicon layer during PLM. Furthermore, it has been assumed that supersaturated gold in substitutional lattice positions introduces discrete mid-gap defect levels in silicon that allows direct sub-band gap absorption in the infrared.

In this study we employ Rutherford backscattering spectroscopy and channeling to measure the precise atom location of the supersaturated gold for comparison with optical absorption measurements. Detailed angular scans from both axial ( $\langle 100 \rangle$ ,  $\langle 110 \rangle$  and  $\langle 111 \rangle$ ) and planar directions ( $\{100\}$  and  $\{110\}$ ) were performed along with simulations to locate gold sites in silicon. We show that the observed non-linear increase in optical absorption is partly attributed to the segregation of gold atoms towards the silicon surface during pulsed laser melting, but lattice strain as a result of gold supersaturation may also play an important role. We have also undertaken double crystal x-ray diffraction to measure the residual strain in hyperdoped silicon as a function of gold concentration to compare with atom location and optical absorption results. In addition, attempts to form supersaturated gold of similar concentrations by ion-implantation followed by rapid thermal annealing have been made. While it is not possible to achieve high supersaturations by this method, we have been able to measure the achievable gold solubility in silicon at low implant doses.

[1] J. P. Mailoa et al., Nature Communications 5, 3011 (2014).

**Shedding light on the complex physics of self-interstitials in germanium**

Nick Cowern<sup>1</sup>, Elena Bruno<sup>2</sup>, Salvatore Mirabella<sup>2</sup>, Chihak Ahn<sup>3</sup>, Nick Bennett<sup>4</sup>, Sergei Simdyankin<sup>1</sup>, Jonathan Goss<sup>1</sup>, Enrico Napolitani<sup>5</sup>, Davide De Salvador<sup>5</sup>

<sup>1</sup>Newcastle University, UK

<sup>2</sup>Universita di Catania, Italy

<sup>3</sup>Samsung Semiconductor Inc., San Jose, USA

<sup>4</sup>Edinburgh University, UK

<sup>5</sup>Universita di Padova, Italy

Recent experiments on self- and B diffusion during irradiation and post-implant annealing reveal a dual contribution of compact self-interstitials (dominating self-diffusion at temperatures  $T < 475$  C with entropy 4 k and enthalpy 4.55 eV) and extended self-interstitials (dominating at  $T > 475$  C with entropy 30k and enthalpy 6.1 eV) [1]. Atomistic modelling shows that the extended form has many properties of the amorphous phase, including formation energies approximately equal to the number of atoms in the defect multiplied by the energy difference between the crystalline and amorphous phases, prompting the name ‘morphs’ [1,2]. Since publication of Ref. [1] the contribution of morphs to interstitial mediated self-diffusion has been vigorously disputed by one group [3,4]. We will show that their objection is based on an erroneous analysis of their own experiments [4,5], and that a correct analysis confirms our results. Moreover, the interstitial migration energy of 1.87 eV reported in Ref. [5] in the range  $T > 550$  C is perfectly characteristic of morph migration and essentially excludes a compact interstitial mechanism. In general morphs are much slower diffusing than compact interstitials but have vastly higher concentrations at elevated temperature and can be formed easily by non-equilibrium processes at low temperature. Thus morphs will be the dominant defects in many aspects of germanium processing, including defect engineering for control of n-type dopant diffusion and activation.

[1] N.E.B. Cowern et al., Phys. Rev. Lett. 110, 155501 (2013).

[2] S. Simdyankin et al., submitted to Nature Materials.

[3] H. Bracht et al., Solid State Phenomena 205-206, 151 (2014).

[4] A. Chroneos and H. Bracht, Appl. Phys. Rev. 1, 011301 (2014).

[5] S. Schneider et al., Phys. Rev. B 87, 115202 (2013).



## Ge doping by ion implantation and melting laser thermal annealing

Ruggiero Milazzo<sup>1</sup>, Enrico Napolitani<sup>1</sup>, Massimo Mastromatteo<sup>1</sup>, Antonino La Magna<sup>2</sup>, Guglielmo Fortunato<sup>3</sup>, Francesco Priolo<sup>4</sup>, Vittorio Privitera<sup>4</sup>, Alberto Carnera<sup>1</sup>, Giuliana Impellizzeri<sup>4</sup>, Giuseppe Fisicaro<sup>2</sup>, Simona Boninelli<sup>2</sup>, Massimo Cuscunà<sup>3</sup>, Davide De Salvador<sup>1</sup>

<sup>1</sup>*CNR-IMM MATIS and Dipartimento di Fisica Astronomia, Università di Padova, Via Marzolo 8, 35131 Padova, Italy*

<sup>2</sup>*CNR-IMM, Z.I. VIII Strada 5, 95121 Catania, Italy*

<sup>3</sup>*CNR-IMM, Via del Fosso del Cavaliere 100, 00133 Roma, Italy*

<sup>4</sup>*CNR-IMM MATIS and Dipartimento di Fisica e Astronomia, Università di Catania, Via S. Sofia 64, 95123 Catania, Italy*

The interest in Ge doping by laser thermal annealing (LTA) in the melting regime following ion implantation is recently renewed with the aim of replacing Si in future CMOS devices due to the LTA capability of activating dopants beyond the solid solubility while reducing diffusion paths and controlling the defect formation.

Ge samples implanted with B or As and subjected to LTA using a pulsed XeCl laser (308 nm, 30 ns), with different energy densities and multiple pulses, were characterized by secondary ion mass spectrometry (SIMS), spreading resist profiling (SRP), cross-section transmission electron microscope (X-TEM) and high resolution x-ray diffraction (HR-XRD).

An anomalous dopant redistribution was observed in both cases, and it has been simulated assuming two diffusivity states of liquid Ge [1] and non-equilibrium segregation at the liquid/solid interface. Interaction and formation of defects with oxygen atoms diffusing from the surface native oxide is found to limit the activation of B [2]. On the contrary, a new record of activation ( $1 \times 10^{20} \text{ cm}^{-2}$ ) has been established for As [3]. The B junctions show a good thermal stability up to 600 °C, whereas As tends to deactivate at lower temperatures due to its tendency to form clusters with vacancies.

These results are crucial in perspective of implementing LTA in advanced Ge-based CMOS.

[1]G. Fisicaro, K. Huet, R. Negru, M. Hackenberg, P. Pichler, N. Taleb, and A. La Magna, Phys. Rev. Lett. 110, 117801 (2013).

[2]G. Impellizzeri, E. Napolitani, S. Boninelli, G. Fisicaro, M. Cuscunà, R. Milazzo, A. La Magna, G. Fortunato, F. Priolo and V. Privitera, J. Appl. Phys. 113, 113505 (2013).

[3]R. Milazzo, E. Napolitani, G. Impellizzeri, G. Fisicaro, S. Boninelli, M. Cuscunà, D. De Salvador, M. Mastromatteo, M. Italia, A. La Magna, G. Fortunato, F. Priolo, V. Privitera and A. Carnera, J. Appl. Phys. 115, 053501 (2014).

## Structural, electrical and optical properties of InSb and AlSb modified by ion irradiation

Raquel Giulian, Josiane B. Salazar, Daniel L. Baptista, Paulo F. P. Fichtner, William Just, Danay Manzo Jaime, Rafael S. Japur, Carlo R. Da Cunha, Antônio Marcos H. De Andrade, Julio R. Schoffen, Paulo Franzen

*Universidade Federal do Rio Grande do Sul, Brazil*

Semiconductors are commonly implanted or irradiated with heavy ions to increase the number of defects in the matrix and enhance specific electrical and optical properties. For high energy irradiations, the formation of ion tracks is well known and can be observed for a variety of materials, while ion energies around hundreds of keV can yield amorphisation of crystalline substrates. A very peculiar effect is observed upon ion irradiation of antimonides, in the nuclear or electronic stopping power regime: the formation of a porous, sponge-like structure, forming a network of interconnected nanowires. The effective surface area of the material is greatly increased, producing structures suitable for gas sensing or bolometry.

Here we show the effects of ion irradiation on InSb and AlSb films grown by molecular beam epitaxy and magnetron sputtering, respectively. The first stages of porosity in InSb irradiated with 18 MeV Au ions were investigated by transmission electron microscopy, revealing the formation of pores before amorphysation. The electrical and optical properties of porous InSb were also probed as a function of irradiation fluence and measurement temperature. The growth of AlSb by co-sputtering of Al and Sb is also presented, as well as the ion irradiation effects on the film, which were characterized by Rutherford backscattering spectrometry, scanning electron microscopy and x-ray diffraction analysis.

## Industrial challenges in ion beam processing and metrology in the 3D era

Jonathan England<sup>1</sup>, Wolfhard Moeller<sup>2</sup>

<sup>1</sup>*Applied Materials, UK*

<sup>2</sup>*Helmholtz-Zentrum Dresden-Rossendorf, Germany*

Moore's Law has been historically maintained by progressively reducing the widths of planar semiconductor devices. As the ability to scale laterally reaches its limits, the semiconductor industry is moving from planar to 3D devices. In logic, planar transistors are being replaced by FINFETs, and nano-wires are on the horizon. In memory, horizontal planar FLASH is transitioning to 3D NAND architectures in which the cells are stacked vertically. This talk will illustrate the major challenges of conformal implantation into logic structures of low width-to-height aspect ratios, the sidewall doping of memory vias that have depth-to-diameter aspect ratios of ~100:1, and the as yet unfulfilled requirements for metrology to measure the outcome of such processes.

Other scaling approaches involve new materials, such as Ge and III-V compounds for logic channels and transition metal oxides for ReRAM memories. Both of these trends set challenges that implantation must overcome if it is to continue its traditional doping roles. At the same time they suggest opportunities for new implant processes that precisely modify material properties, often requiring new implant species, high fluences and low energies. Modelling such implant processes requires codes that account for ion beam mixing and sputtering during the implantation. The modification of the sample by the metrology technique must also be considered. The dynamic ion implantation code TRIDYN will be used to illustrate high fluence implant processes into planar structures and show how the as-implanted profiles are distorted by ion beams used to sputter profile during SIMS and dynamic XPS measurements.

## Selective synthesis of nanostructure graphene by ion–solid interactions and pulsed laser annealing

Bill Appleton<sup>1</sup>, Arthur Hebard<sup>1</sup>, Robert Elliman<sup>2</sup>, Fan Ren<sup>1</sup>, Nick Rudawski<sup>1</sup>, Xiaotie Wang<sup>1</sup>,  
Dinesh Venkatachalam<sup>2</sup>, Joel Fridmann<sup>3</sup>, Kara Berke<sup>1</sup>

<sup>1</sup>*University of Florida, USA*

<sup>2</sup>*Australian National University, Australia*

<sup>3</sup>*Raith, Inc., USA*

Conventional ion implantation (II) and multi-ion beam nano-lithography (MIBL) have been combined with pulsed laser annealing (PLA) to selectively synthesize graphene (G), few-layer graphene (FLG), and multi-layer graphene (MLG) on crystalline SiC. Graphene is produced only where ions are implanted, and in a variety of environments (air, Ar, N<sub>2</sub>, vacuum, etc.). The II and PLA processing parameters can also be manipulated to synthesize a wide variety of other carbon nano-structures (CNS) such as carbon onions. When II is performed using the University of Florida MIBL system, ArF PLA can produce G nano-ribbons and other device features with nanometer to micron dimensions over 100x100 cm<sup>2</sup> areas with nanometer precision, and at much lower surface temperatures than current methods. Since these processing methods are compatible with current manufacturing techniques this approach may improve the chances of integrating graphene into future device structures.

Both the ion-solid interactions and implanted ion species are factors in the selective synthesis. Similarly, the non-equilibrium nature of PLA as well of the laser fluence, number and frequency of pulses, and the annealing environment, are important determinants in controlling G, FLG, MLG, and CNS production.

To identify the fundamental ion-solid and-laser-solid interactions responsible for particular graphene nanostructures, samples were prepared under a range of II and PLA conditions. Samples were characterized using Raman spectroscopy, SEM, AFM, AES, cross-sectional transmission electron microscopy, thermal diffusion and heat-flow calculations, Rutherford backscattering spectrometry and ion channeling. We will discuss the current understanding of our graphene synthesis approach and how II and PLA parameters can be optimized to selectively produce G and control its quality. The possible use of this approach for the synthesis of graphene on materials other than SiC will also be discussed.

## Sputtering of nanospheres – a computer simulation study

Wolfhard Moeller<sup>1</sup>, Maureen L. Nietadi<sup>2</sup>, Luis Sandoval<sup>3</sup>, Herbert M. Urbassek<sup>2</sup>

<sup>1</sup>*Helmholtz-Zentrum Dresden-Rossendorf, Germany*

<sup>2</sup>*Physics Department, University of Kaiserslautern, Germany*

<sup>3</sup>*Theoretical Division, Los Alamos National Laboratory, USA*

The sputtering of spherical objects – such as clusters, nanoparticles or aerosol particles – being exposed to energetic ion irradiation has been studied using both Monte Carlo simulation in the binary collisions approximation (MC) and molecular dynamics simulation (MD). 20 keV Ar impact on a-Si has been chosen as a typical example. With  $a$  denoting the mean depth of energy deposition in a planar target, inverse scaled cluster radii  $a/R$  ranging from 0 to 20 have been investigated, both addressing the impact parameter dependence and the average sputtering yield. For large radii ( $a/R < 0.2$ ) sphere sputtering follows closely the sputtering of planar targets, if the variation of the incidence angle on the sphere surface is taken into account. For smaller radii, the yield increases due to the influence of sphere curvature. For  $a/R > 1$ , pronounced forward sputtering leads to a maximum in the sputter yield. In the limit of small radii, sputter emission becomes largely isotropic, but decreases in yield since the projectile energy is only partly deposited in the sphere and the surface area shrinks. However, for all spheres studied, the average sputter yield is larger than for the planar surface. Within the uncertainties of the modelling, there is an excellent agreement between the planar surface sputtering yields as obtained by MC and MD. For small spheres, however, the MD yields are significantly larger which is attributed to the influence of collisional spikes.

## In-situ TEM irradiation of gold nanorods with heavy ions

Graeme Greaves, Jonathan Hinks, Stephen Donnelly

*University of Huddersfield, UK*

The irradiation of gold nanorods with heavy ions has led to the measurement of large sputtering yields, enhanced by more than an order of magnitude compared to that of a flat surface. Gold nanowires ~20 nm in diameter, have been irradiated at room temperature with 80 keV Xe ions, whilst under constant observation with a transmission electron microscope, using the Microscope and Ion Accelerator for Materials Investigations (MIAMI) facility, at the University of Huddersfield. Under irradiation, the wires were observed initially to “neck” at grain boundaries and then to segment into single crystal nanorods of length 50-100 nm, enabling dimensional measurements to be made. Single ion impacts were observed to create craters in the surface that were subsequently filled by flow processes, maintaining the cylindrical symmetry of the nanorod. Sputtering yields in the range 100-1900 atoms per ion have been measured with considerable variation between individual nanorods. Whilst the nanowire geometry will lead to an increase in sputtering, MD modelling shows that the enhanced sputtering yields can be explained by the ejection of clusters of atoms as a result of the thermal and pressure spikes due to ion impacts. The variation in measured yields can be explained by varying degrees of alignment of the ion beam with channelling directions in the single-crystal nanorods. The MD modelling indicates that the acceptance angle for channelling for 80 keV Xe on Au is large leading to a high probability of having some degree of alignment with planar or axial channels. Recent experiments have been aimed at exploring further the link between channelling and sputter yield by carrying out in-situ experiments on commercial single crystal gold nanorods.

## **Corrections to the Kinchin-Pease damage equation to account for athermal defect recombination and ion beam mixing: arc-dpa and rpa**

Kai Nordlund

*University of Helsinki, Finland*

The most common way to estimate analytically or with binary collision approximation simulations the amount of damage produced by ion and neutron irradiation relies on the Kinchin-Pease (KP) and NRT displacements-per-atom (dpa) equations. These simple equations tell that the damage produced above the threshold displacement energy is linearly proportional to the nuclear damage energy deposited to the material, and are used for instance in the SRIM quick damage calculation. They are also widely used to compare damage production by different kinds of irradiation. However, in the case of metals, it is well known that the KP and NRT equations are wrong. Both overestimate the damage production by a factor of 3 for most common keV and MeV ion and neutron energies. Moreover, with respect to ion beam mixing, they underestimate the amount of replaced atoms by an order of magnitude. Thus, in metals the standard NRT-dpa calculation leads to a number that does in most cases not correspond to any experimentally measurable quantity.

Even though this serious overestimation has been known and the reasons understood since the 1980's, the KP and NRT equations continue to be used, and there have until recently been no systematic attempts to improve on the situation.

I will report on the work of the OECD Nuclear Energy Agency primary radiation damage expert group, which recognized the problem and devised two new extensions of the KP and NRT-dpa equations, namely the athermal-recombination corrected dpa (arc-dpa) and the replacements-per-atom (rpa) equations. I will show that these equations give, with only two additional adjustable parameters, predictions for the amount of Frenkel pairs and replaced atoms that agree with the experimental and MD results within the experimental or systematic MD uncertainties. I will finally discuss the physical limitations that also the improved equations have in damage prediction calculations.

## Energy loss and charge exchange of highly charged ions in carbon nanomembranes

Stefan Facsko<sup>1</sup>, Richard Arthur Wilhelm<sup>1</sup>, Elisabeth Gruber<sup>2</sup>, Robert Ritter<sup>2</sup>, René Heller<sup>1</sup>, Fritz Aumayr<sup>2</sup>

<sup>1</sup>*Helmholtz-Zentrum Dresden-Rossendorf, Institute of Ion Beam Physics and Materials Research, Bautzner Landstr. 400, 01328 Dresden, Germany*

<sup>2</sup>*TU Wien - Vienna University of Technology, Institute of Applied Physics, Wiedner Hauptstr. 8-10/E134, 1040 Wien, Austria*

During the interaction of highly charged ions with solids the ions potential energy, i.e. the stored ionization energy, is released via multiple charge exchanges on a fs time scale. Thus, HCIs reach charge equilibrium after passing only a few nanometers of the solid. The dependence of the charge state on the stopping force of the ions is therefore not accessible in irradiation experiments with bulk material. In order to investigate this pre-equilibrium regime films of just a few nanometers have to be used.

We examined the charge state and the energy loss of highly charged Xe ions after their passage through 1 nm thick carbon nanomembranes. Surprisingly, two distinct exit charge distributions were observed [1]. Part of the ions are passing the membrane with almost no charge loss, whereas the other part loses most of their charge. Apparently, the measured charge distribution reflects two different impact parameter regimes. Ions with trajectories far away of any C atom of the membrane can stabilize only few electrons and exit therefore in a high charge state, whereas ions with trajectories close to a C atom can capture enough electrons and exit the membrane in a low charge state. The different impact parameter regimes are also connected to different energy losses: ions with large impact parameters are practically not stopped, whereas ions in close collisions exhibit high stopping force which is strongly dependent on the incident charge state.

The charge distribution and energy loss of Xe<sup>q+</sup> ions of different incident charge states up to q=30 will be presented and the implication for the formation of holes in these nanomembranes by the HCIs [2] will be discussed.

[1] R.A. Wilhelm, E. Gruber, R. Ritter, R. Heller, S. Facsko, F. Aumayr, Phys. Rev. Lett. 112, 153201 (2014).

[2] R. Ritter, R.A. Wilhelm, M. Stöger-Pollach, R. Heller, A. Mücklich, U. Werner, H. Vieker, A. Beyer, S. Facsko, A. Götzhäuser, F. Aumayr, Appl. Phys. Lett. 102, 063112 (2013).



**Recent progress in cluster beam - from semiconductor to soft materials**

Jiro Matsuo, Makiko Fujii, Toshio Seki, Takaaki Aoki

*Kyoto University, Japan*

Much attention is devoted to studying gas cluster ion beams (GCIB) not only for fundamental research but also for practical applications. When many atoms in a cluster bombard, high-density collision, non-linear effects and lateral sputtering are realized [1]. Cluster beams have been utilized for advanced nanofabrication and characterization techniques, because of the unique interactions of energetic cluster ions with solid surfaces. As each atom in a cluster shares the total kinetic energy, an ultra-low energy ion beam with less than several eV/atom can be easily realized. Due the low energy effect, no serious damage is accumulated on surfaces during irradiation. Therefore, sputtering of fragile materials, such as polymers, organic semiconductor and biological materials, is realized, and compact Ar cluster ion sources are now commercially available to measure depth profiling with both XPS and SIMS instruments. Fine focused cluster beam with 1  $\mu\text{m}$  has been reported recently [2].

Clusters are generated with not only Ar but also other molecules, such as  $\text{SF}_6$ ,  $\text{O}_2$ ,  $\text{NH}_4$  and  $\text{ClF}_3$ . Surface chemical reactions are initiated by collision of reactive molecules and lead to enhancement of sputtering, even when the kinetic energy of cluster beam is extremely low ( $<1\text{eV/atom}$ ). Very high etching rates above 40  $\mu\text{m/min}$ . and highly anisotropic etching of Si are demonstrated with non-ionized cluster beam generated with  $\text{ClF}_3$  [3].

This result opens up new possibly of cluster beam for TSV (through-silicon via) or MEMS (micro-electro-mechanical system) processing.

Recent progress and prospects of cluster beams will be discussed in conjunction with the atomistic mechanism of energetic cluster impacts and possible applications

This work is partially supported by JST CREST and A-STEP.

[1] I. Yamada, et al., Mater. Sci. Eng. R.34, 231 (2001).

[2] J. Matsuo, et al., Appl. Phys. Express 7, 056602 (2014).

[3] K. Koike, et al., Appl. Phys. Express 3, 126501 (2010).

## Modification of graphite and diamond on the nanoscale by energetic argon clusters

Vladimir Popok<sup>1</sup>, Muhammad Hanif<sup>1</sup>, Juha Samela<sup>2</sup>, Kai Nordlund<sup>2</sup>, Vladimir Popov<sup>3</sup>

<sup>1</sup>*Aalborg University, Denmark*

<sup>2</sup>*University of Helsinki, Finland*

<sup>3</sup>*Institute of Semiconductor Physics, Novosibirsk, Russia*

Cluster ion implantation is a powerful tool for engineering of surfaces and thin layers on the nanoscale [1, 2]. Cluster consisting of many atoms generates multiple collisions, thus, transferring locally a significant amount of energy causing a number of specific phenomena. In the current work, keV-energy argon cluster ions of a few tens of atoms in size were implanted in graphite and diamond [3, 4]. Radiation damage areas formed by individual clusters were studied experimentally using atomic force and scanning tunneling microscopy for as implanted samples and after thermal and chemical treatments. The experimental part was corroborated by molecular dynamics simulations that allowed grounding several conclusions relevant for the development of cluster stopping theory and practical applications of cluster beams.

It is found that (i) cluster implantation shows a clear presence of size effect, larger clusters have lower stopping power and produce deeper damage; (ii) there is no crater formation on graphite due to elastic response of graphene planes to cluster impact while craters on diamond are formed by direct sputtering, there is no liquid flow effect found; (iii) threshold displacement energy for cluster impact on diamond is estimated; (iv) stopping of clusters in diamond shows a strong similarity to the stopping in graphite, thus, demonstrating the same scaling law in which both depth of radiation damage and projected range of cluster constituents linearly depend on cluster momentum.

### References

1. V.N. Popok, Mater. Sci. Eng. R: Rep 72, 137 (2011).
2. N. Toyoda and I. Yamada, IEEE Trans. Plasma Sci. 36, 1471 (2008).
3. V.N. Popok, J. Samela, K. Nordlund, E.E.B. Campbell, Phys. Rev. B 82, 201403R (2010).
4. V.N. Popok, J. Samela, K. Nordlund, V.P. Popov, Phys. Rev. B 85, 033405 (2012).

## Direct formation of large-scale germanene from SiGe thin film assisted by plasma immersion

Hsu-Sheng Tsai<sup>1</sup>, Yu-Lun Chueh<sup>1</sup>, Jenq-Horng Liang<sup>2</sup>

<sup>1</sup>*Department of Material Science and Engineering, National Tsing Hua University, Hsinchu 30013, Taiwan, ROC*

<sup>2</sup>*Institute of Nuclear Engineering and Science, National Tsing Hua University, Hsinchu 30013, Taiwan, ROC*

Beyond graphene, other two dimensional materials of group IV such as silicene and germanene become more important recently due to the present silicon complementary metal-oxide-semiconductor (CMOS) technology. So far, the researches concerning silicene and germanene only announced the computation results in addition to epitaxial silicene in ultra-high vacuum (UHV) system. In our investigation, the plasma treatment followed by annealing process is utilized in order to obtain large-scale germanene films from SiGe layer via selective reaction. After N<sub>2</sub> plasma immersion, the annealing process, which promotes nitrogen ions to react with Si and simultaneously squeeze Ge out onto the surface, is implemented. A thin silicon nitride layer formed during annealing may exclude Ge atoms from the SiGe layer. Eventually, a uniform large-scale germanene film on SiGe/Si wafer will be achieved. The Raman analysis shows typical spectra of germanene and the XPS results indicate that the formation of silicon nitride layer. Furthermore, the TEM images verify that there are several layers of germanene on the top of SiGe layer. In this research, we create a simple method for synthesizing large-scale germanene.

## Test simulation of neutron damage to electronic components using accelerator facilities

Donald King, Edward Bielejec, Kyle McDonald, Robert Fleming, George Vizkelethy

*Sandia National Laboratories, USA*

Historically, reactors have been used to test the transient response of electronic systems to displacement damage and ionization. With the diminishing availability of reactor facilities, an ongoing effort exists to use alternative facilities and radiation types, such as light and heavy ions as well as electrons, to simulate the displacement damage of neutrons. The concept of “equivalent” damage between these types of irradiation is a topic of much interest. This paper examines the relations between several measured damage metrics of electronic components after irradiation by reactor neutrons and by ions and electrons generated by particle accelerators. Metrics considered include measured early- and late-time gain degradation in III-V Npn heterojunction bipolar transistors and the type and number of defects as measured in GaAs diodes using deep level transient spectroscopy (DLTS). Reactor facilities used to test electronics include the White Sands Missile Range Fast Burst Reactor (WSMR FBR) and the Sandia National Laboratories Annular Core Research Reactor (SNL ACRR). The ion facility used in this work is the SNL Ion Beam Laboratory (IBL). A 6 MV tandem Van de Graaff and numerous ion sources allow the IBL to provide a wide variety ions and energies. The electron facility addressed is the Little Mountain Test Facility linear accelerator (LMTF LINAC), located at Hill AFB in Utah, operated in electron beam mode. Electron energy levels ranging from 3 to 20 MeV were investigated. Little Mountain has a unique capability among LINACs in that pulse widths can be tailored from 25 nsec to 50  $\mu$ sec settings with beam currents ranging from 0.1 to 2 Amps. In summary, we will demonstrate that alternate accelerator facilities have great utility in replacing the use of reactors to test discrete GaAs diodes and transistors when the appropriate damage metrics are selected. We intend to expand the approach of using alternate facilities to circuit applications.

## Evidence of amorphisation of boron carbide B<sub>4</sub>C under slow, heavy ion irradiation

Dominique Gosset<sup>1</sup>, Sandrine Miro<sup>1</sup>, Sylvie Doriot<sup>1</sup>, Guillaume Victor<sup>2</sup>, Vianney Motte<sup>1</sup>

<sup>1</sup>CEA, France

<sup>2</sup>CNRS/IN2P3, France

Boron carbide is widely used either as armor-plate or neutron absorber. In both cases, a good structural stability is required. However, a few studies have shown amorphisation may occur in severe conditions. Hard impacts lead to the formation of amorphous bands. Some irradiations in electronic regime with H or He ions have also shown amorphisation of the material. Most authors however consider the structure is not drastically affected by irradiations in the ballistic regime.

Here, we have irradiated at room temperature dense boron carbide pellets with Au 4 MeV ions, for which most of the damage is ballistic. This study is part of a program devoted to the behavior of boron carbide under irradiation. Complementary results are reported in the communication of G. Victor et al. In-situ and ex-situ Raman observations have been performed together with transmission electron microscope (TEM) observations. Raman observations show a strong structural damage at moderate fluences ( $10^{14}/\text{cm}^2$ ), in agreement with previous studies. On the other hand, TEM shows the structure remains crystalline up to  $10^{15}/\text{cm}^2$  (i.e. a few dpas) then amorphises. The amorphisation is heterogeneous, with the formation of nanometric amorphous zones with increasing density. It then appears short range and long range disorder occurs at quite different damage levels. Further experiments are in progress aiming at studying the structural stability of boron carbide and isostructural materials ( $\alpha$ -B, B<sub>6</sub>Si,...).

## **Radiation damage in nuclear oxides bombarded with low-energy ions – An advanced description of the crystal evolution via ion channelling and MC simulations**

Tien Hien Nguyen<sup>1</sup>, Frederico Garrido<sup>2</sup>, Cyril Bachelet<sup>2</sup>, Jérôme Bourçois<sup>2</sup>, Aurélien Debelle<sup>2</sup>,  
Stamatis Mylonas<sup>2</sup>, Lech Nowicki<sup>3</sup>, Lionel Thomé<sup>2</sup>

<sup>1</sup>*Hanoi University of Agriculture, Department of Physics, Hanoi, Vietnam*

<sup>2</sup>*CSNSM, CNRS-Université Paris-Sud, Orsay Campus, France*

<sup>3</sup>*Soltan Institute for Nuclear Studies, Warsaw, Poland*

Quantifying the evolution of the radiation damage inflicted on bombarded materials as a function of key parameters (ions, energy, fluence, concentration, temperature) is of prime importance. Although ion channelling performed on single crystals was extensively applied to monitor defects and their depth-distribution, most of the analyses implicitly assume the sole presence of randomly displaced atoms, a feature at clear variance with the formation of extended defects at large fluence. In fact, radiation defects are very complex and consist of various types with their distinct scattering factors. Such a complex configuration may be simulated by MC assuming a simplified model where the two dominant types, corresponding to conditions of pure obstruction-type (Randomly Displaced Atoms) and pure distortion-type (Bent Channels) channelling, are considered. Every complex mixture of defects can be reproduced by a distribution of defects of both types (RDA and BC). This model was successfully applied to the description of urania single crystals bombarded with various ions (fission products Xe, La, Ce, with similar Z and A, either fully soluble or insoluble into the matrix) over a very large fluence range, i.e. from the formation of isolated defects up a complete overlapping of damage cascades (from 1E14 to 1E17 cm<sup>-2</sup>). The evolution of RDA with increasing ion fluence leads to two (one step, respectively) steps in the damage kinetics for crystals bombarded with insoluble atoms (soluble atoms, respectively), separated by constant plateaus. The difference between soluble versus insoluble atoms is mostly due to the size of the implanted species. Conversely, the accumulation of BC leads to a very similar evolution, irrespective of the nature of ion. This smooth increase reveals a dramatic and continuous structural modification that was totally hidden according to the sole evolution of RDA. These evolutions are compared to results coming from complementary techniques, XRD and TEM.

## Comparison of helium mobility in transition metal carbides and nitrides

Shradha Agarwal<sup>1</sup>, Patrick Trocellier<sup>1</sup>, Sylvain Vaubailon<sup>2</sup>, Daniel Brimbal<sup>1</sup>, Sandrine Miro<sup>1</sup>

<sup>1</sup>CEA, DEN, Service de Recherches de Métallurgie Physique, Laboratoire JANNUS, F-91191 Gif-sur-Yvette, France

<sup>2</sup>CEA, INSTN, UEPTN, Laboratoire JANNUS, F-91191 Gif sur Yvette, France

Metal transition ceramics are excellent candidate materials for fuel applications in Generation IV nuclear reactors. The consequences of helium accumulation in this type of material need to be clearly understood to obtain better predictions about their ageing processes. The study of helium mobility includes various challenges a) to accurately determine the He depth profile and calculate activation energies of He migration b) to understand the trapping of He atoms into point defects resulting in the formation of He-Vacancy cluster or bubbles c) to determine the role of grain boundaries which acts as effective short circuits for He release d) to know the role of He implantation concentration and presence of native vacancies on He mobility. To solve above challenges our approach includes following steps: 1) 3 MeV  $^3\text{He}^+$  ion implantation with fluence of  $5 \times 10^{16}$  at/cm<sup>2</sup> into polycrystalline samples of TiC, TiN and ZrC. 2) Thermal annealing of helium implanted samples at T= 1000 to 1600 °C. 3) He depth profiling of as-implanted and annealed samples using the  $^3\text{He}$  (d,p)  $^4\text{He}$  nuclear reaction and the use of models like AGEING and SIMNRA to calculate migration parameters. 4) 3-D elemental distribution image of He atom from micro-NRA to study the role of grain boundaries. 5) TEM to observe nucleation and growth mechanisms of He bubbles in as-implanted and annealed samples. 6) Raman micro-spectroscopy to study the defect created during He implantation and subsequent changes in defects after thermal annealing. We have developed diffusion models to calculate activation energies of helium diffusion and release from experimentally obtained helium depth profiles. A detailed approach was followed to understand helium bubble growth mechanisms under thermal annealing. An approach was also established to apply theoretical models on experimental data to calculate pressure inside the helium bubbles and to find the limit of the He gas pressure, which can plastify the material.

## Enhancement of the magnetic properties of iron nanoparticles upon incorporation of Samarium

Jérôme Leveueur<sup>1</sup>, Felipe Kremer<sup>2</sup>, John Kennedy<sup>1</sup>, Mark Ridgway<sup>2</sup>, Grant Williams<sup>3</sup>, James Metson<sup>4</sup>, Andreas Markwitz<sup>1</sup>

<sup>1</sup>*GNS Science, New Zealand*

<sup>2</sup>*The Australian National University, Australia*

<sup>3</sup>*The MacDiarmid Institute for Advanced Materials and Nanotechnology, SCPS, Victoria University, New Zealand*

<sup>4</sup>*The University of Auckland, New Zealand*

Ion implantation is a promising technique to modify the magnetic properties of nanomaterials at through composition changes and defect engineering. For instance, high Curie temperature diluted magnetic semiconductors were recently produced through ion implantation from semiconductors that, by default, would not display magnetic ordering. High energy ion irradiation of multilayered thin film was shown to induce changes in the magnetic anisotropy as a function of the ion incidence. The damage-induced ferromagnetism from Ga focused ion beam implantation on a FeAl substrate allowed the formation of magnetic nanodots.

In this work, ion implantation of a rare-earth element is shown to dramatically enhance the magnetic properties of Fe nanostructures. Low energy Sm<sup>+</sup> ion implantation was used to modify the properties of superparamagnetic Fe nanoparticles on the surface of a SiO<sub>2</sub> film on Si. Ion beam analysis and transmission electron microscopy measurements showed this resulted in the formation of a Sm<sub>x</sub>Fe<sub>1-x</sub>O<sub>y</sub> layer on the nanoparticles and significant sputtering. An anomalously large moment per implanted atom is found which is above the values expected for Fe or any known Sm<sub>x</sub>Fe<sub>1-x</sub>O<sub>y</sub> compound. This leads to a greater than 14-fold improvement of the permeability of the materials. High Sm fluences result in complete ablation of the Fe nanoparticles and the magnetic order disappears. Detailed results and discussion will be provided in the presentation.



## Emergence of ferromagnetic order in pulsed laser deposited ZnO thin film on Si by 600 keV $12\text{C}^+$ ion irradiation

Neeraj Shukla<sup>1</sup>, Sujoy Chakravarty<sup>1</sup>, Ramjanay Chaudhary<sup>2</sup>, Binay Kumar Panigrahi<sup>3</sup>, K.G.M. Nair<sup>3</sup>, G. Amarendra<sup>4</sup>

<sup>1</sup>UGC DAE CSR Kalpakkam Node, Kokilamedu 603104, TN, India

<sup>2</sup>UGC DAE CSR Indore 452017, MP, India

<sup>3</sup>Material Science Group, IGCAR, Kalpakkam 603102, TN, India

<sup>4</sup>Material Science Group, IGCAR, Kalpakkam 603102, TN, India & UGC DAE CSR Kalpakkam Node, Kokilamedu 603104, TN, India

We report the emergence of ferromagnetic ordering in 840 nm ZnO thin film deposited by pulsed laser deposition, by 600 KeV  $12\text{C}^+$  ion irradiation. It has been reported that carbon doping in ZnO crystal by pulsed laser deposition can lead to ferromagnetic ordering [1]. Ion irradiation induced ferromagnetic ordering has been established to provide consistent ferromagnetic ordering in HOPG, Fullerene etc. [2-3]. The key to the ion beam induced ferromagnetism, is tuning the defect density [2, 3] so that the crystalline sample is not completely amorphized and the distance between defects does not get close to the lattice parameter. In the present experiment, the carbon ion fluence has been varied from 1-10 pico-Coloumb/ $\mu\text{m}^2$ . It has been observed that with optimum fluence, 600 keV  $12\text{C}^+$  ion irradiation upon ZnO thin film sample develops ferromagnetic ordering of about  $\sim 4\text{E}-6$  emu, confirmed by 7 T Superconducting Quantum Interference Device (SQUID) Vibration sample magnetometer (VSM). It is noteworthy that beyond optimum fluence, sample's ferromagnetism is diminished due to excessive damage. XRD data analysis shows, that the thin film is highly crystalline, which makes the sample an ideal candidate for ion beam induced ferromagnetism. Post-Ion-beam-irradiation XRD data also, shows that sample's crystalline behavior is intact. Elemental analysis data of virgin sample and of Ion beam irradiated sample will also be presented to concur that the induced ferromagnetic order is intrinsic in nature. Thus a novel approach to inducing inherent ferromagnetic ordering has been achieved in ZnO thin film by carbon ion irradiation.

### References:

- [1] H. Pan et al., Phys Rev Lett. 99, 127201 (2007).
- [2] P. Esquinazi et al., Phys Rev Lett. 91, 227201 (2003).
- [3] N. Shukla et al., Carbon 50, 1817 (2012).

## Process of three-dimensional magnetic patterning of FeRh alloys by using low and high energy ion beam irradiation

Toshiyuki Matsui<sup>1</sup>, Tetsuya Koide<sup>1</sup>, Masako Sakamaki<sup>2</sup>, Kenta Amemiya<sup>2</sup>, Satoh Takahiro<sup>3</sup>,  
Masashi Koka<sup>3</sup>, Yuichi Saitoh<sup>3</sup>, Hiroyuki Uno<sup>4</sup>, Hitoshi Sakane<sup>4</sup>, Akihiro Iwase<sup>1</sup>

<sup>1</sup>*Osaka Prefecture University, Japan*

<sup>2</sup>*High Energy Acceleration Research Organization, KEK, Japan*

<sup>3</sup>*Japan Atomic Energy Agency, Takasaki, Japan*

<sup>4</sup>*S.H.I.Examination & Inspection, Ltd., Japan*

Iron-rhodium ordered alloy with B2 (CsCl-type) crystal structure has a first-order phase transition from low-temperature antiferromagnetic (AF) phase to high-temperature ferromagnetic (FM) phase near room temperature. We previously reported that the ion beam irradiation with various energies ranging from GeV to keV orders can induce the ferromagnetic state in FeRh bulk and film samples without any structural changes below room temperature at which they are originally in the antiferromagnetic state. By using this nature, we have attempted to fabricate micro scale magnetic patterns using the ion microbeam and focused ion beam techniques that enable us to control the ion beam scanning. In the course of these studies, we realized that the magnetic modified regions in the depth can be also controlled, because the beam energy solely determines the regions where the elastic energy deposited. In the present paper we discuss the possibilities three dimensional micro-scale magnetic patterns for FeRh alloys by high and low energy ion beam irradiation, such as 1 keV Ar, 30 keV Ga, 2-6MeV H and He ion beams.

Bulk and thin film FeRh samples were irradiated at various ion beam facilities, and were characterized by SQUID, MFM, XMCD and PEEM. Various shapes of magnetic patterns were successfully produced in lateral direction of the FeRh alloys which could be confirmed by MFM and XMCD-PEEM. In addition, in-situ XMCD measurement revealed that the magnetic state at the most outer surface of the FeRh alloys could be modified by 1 keV Ar ion-beam irradiation. In contrast to this, the samples irradiated with energetic ion beam induced the ferromagnetic state in the deep region rather than in the surface region. These facts suggest that the three-dimensional magnetic modification can be practical technology if the ion beam irradiations with various energies are suitably designed to be combined.

## Recent progress in ion beam assisted synthesis of ferromagnetic shape memory alloys: fundamentals and applications

Stefan Mayr<sup>1</sup>, Mareike Zink<sup>2</sup>, Uta Allenstein<sup>1</sup>, Ariyan Arabi-Hashemi<sup>1</sup>

<sup>1</sup>*Leibniz-Institute for Surface Modification (IOM), Translational Center for Regenerative Medicine and Faculty of Physics and Earth Sciences, University of Leipzig, Germany*

<sup>2</sup>*Division of Soft Matter Physics, University of Leipzig, Germany*

Yielding magnetically switchable strains of several percent, ferromagnetic shape memory alloys have attracted tremendous interest during the past years for use in contact-less actuators in engineering and biomedical applications. Vice versa, they can also be applied as strain sensors, yielding magnetization changes upon straining. Yet, miniaturization as functional thin films and foils has been hampered by several unresolved issues during synthesis, including i) selection of the desirable phase, ii) single crystalline growth and iii) a martensite temperature located sufficiently above body temperature.

For the example of the Fe-Pd ferromagnetic shape memory alloy we demonstrate, how irradiation with heavy MeV ions allows to precisely select the phase at room / body temperature and modify the properties of the martensite-austenite transition. The physics underlying these scenarios are explored with classical molecular dynamics computer simulations employing a newly constructed embedded atom method potential for the martensite - austenite transition in Fe-Pd, fitted to recent ab-initio calculations. According to these simulations, ion irradiation affects martensite-austenite transition in Fe-Pd in a two-fold way, by modifying short range order within the alloy and insertion of point defects. Both result in a shift of the martensite temperature, as can understood by a newly-proposed Clausius-Clapyron type of equation, involving generalized stresses created due to disorder and radiation defects.

The present contribution will also review properties and applications of the resulting films and foils, including magnetic and mechanical response as well as functionalization for biomedical applications.

[1] A. Arabi-Hashemi and S.G. Mayr, Phys. Rev. Lett. 109, 195704 (2012).

[2] S.G. Mayr and A. Arabi-Hashemi, New J. Phys. 14, 103006 (2012).

[3] M. Zink, F. Szillat, U. Allenstein and S. G. Mayr, Adv. Func. Mat. 23, 1383 (2013).

## Defect complex evolution in semiconductors: long-range elastic interactions matter

Laurent K. Béland, Yonathan Anahory, Matthieu Guihard, Normand Mousseau, François Schiettekatte

*Université de Montréal, Canada*

Current models of implantation damage annealing consider either point defect diffusion or damage complexes that anneal by processes internal to the complexes. However, neither of these models explains the broad shape of the heat release observed by nanocalorimetry. Here, we compare the heat release of 10 or 80 keV Si ions implanted at low-fluence ( $0.02\text{-}0.1\text{ Si/nm}^2$ ) in monocrystalline Si at 110 K or 300 K, to a new atomistic simulation method that runs over time scales reaching seconds. The kinetic Activation-Relaxation Technique (k-ART), an off-lattice kinetic Monte-Carlo method with on-the-fly catalogue construction. This method takes fully into account all elastic effects both for energy minima and barriers. Here, k-ART is applied to a 27000-atom cell of Stillinger-Weber silicon self-implanted with a single ion at 3 keV. The simulation results reveal a logarithmic time dependence of defect annealing and closely reproduce the heat-release experiments. It is found that annealing occurs in a process where the system needs to unlock metastable states, which requires crossing ever-higher barriers with time. These unlocking steps do not generally decrease the potential energy; they only allow relaxation to eventually take place. Interestingly, relaxation does not affect significantly the energy landscape, the system still seeing evolving through a similar, uniform distribution of barrier. The picture that emerges is that self-implantation or keV-recoil-induced damage in c-Si consists of a collection of relatively simple structures that, rather than only relaxing by interacting with the crystal surrounding them, overcome reconfiguration barriers in order to interact with each other and undergo relaxation, resulting in a logarithmic time-dependent evolution. Given that long-range elastic effects are a general feature found in most materials, we estimate that these conclusions apply at least to many covalently bond crystals, but probably also to many other materials.

## Comparative study of high energy ion beam-irradiation effects on alpha-quartz and silica based on in-situ optical measurements and MD

José Olivares<sup>1</sup>, Ovidio Peña-Rodriguez<sup>2</sup>, Alejandro Prada<sup>2</sup>, Antonio Rivera<sup>2</sup>, Javier Manzano-Santamaría<sup>3</sup>, Miguel Luis Crespillo<sup>3</sup>, María Jose Caturla<sup>4</sup>, Eduardo Bringa<sup>5</sup>

<sup>1</sup>*Instituto de Optica, Consejo Superior de Investigaciones Científicas, Madrid, Spain*

<sup>2</sup>*Instituto de Fusión Nuclear, Universidad Politécnica de Madrid, E-28006 Madrid, Spain*

<sup>3</sup>*Centro de Microanálisis de Materiales (CMAM), Universidad Autónoma de Madrid, Spain*

<sup>4</sup>*Departamento de Física, Universidad de Alicante, Spain*

<sup>5</sup>*CONICET and Instituto de Ciencias Básicas, U. Nacional de Cuyo, Mendoza 5500, Argentina.*

In this work we review our recent and extensive work, experimental and theoretical, made on the high energy ion irradiations effects on both kind of SiO<sub>2</sub>, amorphous and crystalline. We have performed several in-situ optical measurements: the optical reflectance (to obtain the refractive index), the transmittance (to obtain the absorption spectra), the Raman and the ionoluminescence spectra. Extremely detailed (in terms of fluence step) kinetics curves have been efficiently obtained for a wide range of ions and energies in order to change the values of the electronic stopping power (Se) from about 2 keV/nm (near the threshold) to 10 keV/nm, well above the threshold. This extensive dataset has also been compared in quartz with the damage obtained, at a few particular fluencies irradiated in the corresponding samples, by standard RBS/C.

Both type of substrates have been irradiated under the same conditions with several ions and energies covering a broad range of electronic stopping powers from 1 keV/nm to 7 keV/nm. The growth of the main color center bands, NBOHC (4.8 eV and 6.8 eV), OCDI (7.6 eV), OCDII (5 eV) and E' (5.8 eV) has been measured as a function of irradiation fluence. The growth kinetics for all centers approximately obeys a Poisson-type law in both materials. On the other hand, for silica, the initial coloring rates depend linearly on energy and roughly on electronic stopping power. For quartz the dependences are clearly nonlinear at low stopping powers, and a very low coloring rates is observed below Se < 4 keV/nm (inhibition stage).

We will discuss the experiments with the aid of phenomenological models as well as atomistic simulations to depict the underlying physical phenomena in terms of defect generation and annihilation. The combined use of sophisticated complementary experiments and the detailed simulations allow us to correlate the changes in the optical properties with the microscopic changes in the structures.

## Multiscale study of implantation-induced helium bubbles in elemental semiconductors

Marie-Laure David<sup>1</sup>, Kévin Alix<sup>1</sup>, Gianluigi A. Botton<sup>2</sup>, Laurent Pizzagalli<sup>1</sup>, Erwan Oliviero<sup>3</sup>, Frédéric Pailloux<sup>1</sup>, Vincent Mauchamp<sup>1</sup>, Guillaume Lucas<sup>4</sup>, Duncan T.L. Alexander<sup>4</sup>, Cécile Hébert<sup>4</sup>, Martin Couillard<sup>2</sup>

<sup>1</sup>*Institut Pprime-CNRS - Université de Poitiers, France*

<sup>2</sup>*CCEM, Mc Master University, Canada*

<sup>3</sup>*CSNSM-CNRS-IN2P3-Université Paris Sud, France*

<sup>4</sup>*Centre Interdisciplinaire de Microscopie Électronique (CIME), EPFL, Switzerland*

In many materials, high fluence He implantation or transmutation reactions in nuclear reactors lead to the formation of nanometric He bubbles. These defects are of major interest in several domains, from materials for microelectronics and energy, to more fundamental fields (study of plasmon excitations, nanofuidics).

In this work, a multiscale picture of the formation of He bubbles and their evolution under external stimuli is derived from the combination of numerical simulations and Electron Energy Loss Spectroscopy (EELS) in the Transmission Electron Microscope (TEM).

First, numerical simulations were performed to study the elementary mechanisms of formation of the bubbles [1]. Aggregation mechanisms were investigated using first principles calculations; in particular, the optimal He fillings in small vacancy clusters was determined. For larger clusters, classical molecular dynamics simulations showed a clear separation of time between the aggregation of vacancies and the slower incremental filling of the cavities by single He atoms. Migration and coalescence mechanisms were also observed.

In a second part, ion beam was used to synthesize nanometric He bubbles. Their physical properties (morphology, He density and pressure) were determined using spatially-resolved EELS [2] or Energy-filtered TEM. In situ thermal annealing experiments clearly show He detrapping, movement and shape alteration between room temperature and 800°C. Acquisitions were performed with various annealing temperatures and time steps, allowing for the detailed study of the bubble behavior. Moreover, in situ ion irradiation was used to induce He detrapping from bubbles. The conditions under which detrapping occurs were studied in details and compared with the results obtained by in situ electron irradiation [3].

[1] L. Pizzagalli et al., *Mod. Simul. Mat. Sci. Eng.* 21, 065002 (2013).

[2] M.L. David et al., *Appl. Phys. Lett.* 98, 171903 (2011).

[3] M.L. David et al., *J. Appl. Phys.* 115, 123508 (2014).

**Pure amorphous silicon made by ion implantation is a disordered but hyperuniform solid**

Sjoerd Roorda

*Université de Montréal, Canada*

Hyperuniform point patterns are characterized by a local variance that grows only as the surface area (rather than the volume) as the system gets larger and therefore do not possess infinite-wavelength fluctuations [1]. Equivalently, it can be stated that for hyperuniform materials, the structure factor tends to zero for very small scattering vectors :  $S(q \rightarrow 0) = 0$ . It has been conjectured that pure amorphous silicon, a fully disordered and nearly-four fold coordinated solid, is nearly fully hyperuniform [2]. However this suggestion has been contested, based on a large structure factor at small scattering vectors deduced from a computer model of amorphous silicon [3]. We have undertaken measurements of the structure factor of pure amorphous silicon, made by ion implantation, at the Argonne Advanced Photon Source. The experimentally determined structure factor is much smaller than the value deduced from the model, and thus we conclude that pure amorphous silicon is nearly hyperuniform [4].

[1] F. Torquato and F.H. Stillinger, Phys. Rev. E 68, 041113 (2003)

[1] M. Florescu et al., PNAS 106, 20658 (2009).

[2] A.M.R. de Graff and M.F. Thorpe, Acta Crystallogr. A 66, 22–31 (2010).

[3] R. Xie et al., PNAS 110, 13250 (2013).

## **In-situ characterization of silicon layer separation by light ions implantation.**

Frederic Mazen<sup>1</sup>, François Rieutord<sup>2</sup>, Didier Landru<sup>3</sup>, Damien Massy<sup>2</sup>, Shay Reboh<sup>1</sup>, Florence Madeira<sup>1</sup>

<sup>1</sup>*CEA-LETI, France*

<sup>2</sup>*CEA-INAC, France*

<sup>3</sup>*SOITEC, France*

The implantation of relatively high doses of light ions (H, He) in Si substrates leads to the formation of a buried damaged layer, characterized by punctual and extended defects combining vacancies and gas atoms. Under annealing, these defects evolve to cracks lying parallel to the surface, and a controlled fracture process occurs along the implanted layer. The thin overlayer which splits above the fracture line can then be transferred onto a host substrate using direct wafer bonding. By the beginning of the 1990's, this concept gave rise to the Smart-cut<sup>TM</sup> technology, allowing an industrial scale production of Silicon-On-Insulator (SOI) substrates. However, the complete scenario describing of the underlying mechanisms, from the atomic defects to the macroscopic fracture is still challenging. In this paper, we present advances, concerning the fundamentals of Smart-cut<sup>TM</sup>, based on in-situ direct observation of growth and propagation of hydrogen related extended defects up to the micro and mesoscale.

New results, based on infra-red in-situ imaging, show that micron-scale cracks evolve by pure coalescence. This contrasts with the Ostwald Ripening process that controls the evolution of nano-scale cracks population. The correlation between the evolution of the microcracks and the amount of gas released during the fracture, suggest that the hydrogen supply which sustain microcracks growth during annealing, is continuously collected from the surrounding matrix. To study the fracture at the sample scale, we have developed an experimental setup to measure in-situ the final and catastrophic fracture of the implanted material. The speed of the cracking interface is determined to be in the Km/s range. The evolution of the fracture speed with experimental parameters (implantation conditions, annealing temperature...) was measured and modeled. We point out that the interaction between the fracture tip and microcracks influence the surface state of the transferred film.



## **Applications and Development of Ion Beams in Radiobiology**

Michael Merchant

*Ion Beam Centre, University of Surrey, UK*

The unique properties of particle beams, in that they deposit dose primarily within a “Bragg peak” was first exploited for cancer therapy by Robert Wilson in 1946 [1]. However adoption of particle therapy for treatment was not widespread, with limitations in imaging preventing accurate delivery of dose to the tumour. Today, advances in accelerator and imaging technology have overcome these limitations, and there are many facilities worldwide for particle therapy.

However, despite progress in this field, many questions remain related to the fundamental mechanisms of radiation induced DNA damage. “Micro” ion beams were first used to irradiate cells in the 1950s by Zirkle and Bloom [2], and this technique has led to several advanced research beamlines worldwide, capable of targeting single cells with precise doses. Such facilities are critical to discovering the mechanisms of the single cell response to ion beam damage. However, this approach has only had modest impact on clinical practice thus far.

Nevertheless, this is an exciting time for radiobiology research using focused beams given the recent advances enabling beam-spot dimensions of 20 nm to be achieved [3] and advances in optical microscopy providing the capability for visualisation of single fluorescent proteins. These developments enable investigation of DNA damage on a sub-cellular level never before possible. Here we present an overview of several key areas where the use of focused ions beams can inform clinical practise, and what technical advances are required to achieve these aims.

[1] R. R. Wilson, Radiology 47, 487-491 (1946).

[2] R.E. Zirkle and W. Bloom, Science 117, 487-493 (1953).

[3] F. Watt et al., Nucl. Instr. and Methods B 269 (2011).

## High energy heavy ion tracks for creation of polymeric nanochannels as a base for highly sensitive molecular sensors

Wolfgang Ensinger

*Darmstadt University of Technology, Germany*

Polymer foils of polyethylene terephthalate PET and polycarbonate PC are through-irradiated with GeV heavy ions at the GSI linear accelerator single ion facility. The projected ion range is larger than the foil thickness of 20  $\mu\text{m}$ , leading to a straight track with a very large transferred electronic energy, typically several keV/nm, which leads to large amount of bond scission. As a consequence, the damage track is a zone of lower density and weakened chemical bonds. Thus, the generated single ion track can asymmetrically chemically be etched up to a conical nanochannel with a diameter of the small tip side of several nanometers. The nanochannel walls are chemically modified by attaching biorecognition molecules by appropriate coupling chemistry. The foil with the conditioned nanochannel then acts as a separation membrane between the two compartments of an electrochemical cell. The electrolyte current, consisting of K and Cl ions, is measured. When molecules to be analyzed are present, they specifically interact with the nanochannel walls (key-lock-principle) and change the electrical current. Thus, a highly sensitive and selective nanosensor can be obtained.

The paper discusses as a survey all aspects of this technology, from ion mass end energy dependent threshold radiation damage and the damage mechanisms of different polymers, to polymer etching and nanochannel chemistry up to the principles of the sensor, with the examples of sensing small molecules such as hydrogen peroxide up to larger biomolecules, such as carbohydrates and peptides. Eventually, the application potential of the sensors for biomedical applications is discussed.

## **Quantitative analysis of the epitaxial recrystallization effect induced by swift heavy ions in silicon carbide**

Abdenacer Benyagoub

*CIMAP-GANIL, France*

The irradiation of crystalline materials with swift heavy ions (SHI) often leads to the formation of highly defective or amorphous tracks. It was also found that crystalline-to-crystalline phase transitions may occur [1]. These results were supplemented by recent studies which showed that amorphous-to-crystalline phase transformations can also take place. The latter phenomenon is well illustrated with the case of SiC where the damage formed by low energy ion irradiation can be removed at room temperature by the electronic excitations generated by swift heavy ions [2].

This contribution describes recent results on the recrystallization effect induced by swift heavy ions in pre-damaged SiC. The recrystallization kinetics was followed by using increasing SHI fluences and by starting from different levels of initial damage within the SiC samples. This quantitative analysis showed that the recrystallization rate depends drastically on the local amount of crystalline material: it is nil in fully amorphous regions and becomes more and more significant with increasing amount of crystalline material. For instance, in samples initially nearly half-disordered, the recrystallization rate per incident ion is found to be 3 orders of magnitude higher than what it is observed with the well-known IBIEC process using low energy ions. This high rate can therefore not be explained by the existing IBIEC models. A comprehensive quantitative analysis of all the experimental data shows that the SHI induced recrystallization effect can be accounted for by a mechanism based on the melting of the amorphous zones through a thermal spike process [3,4] followed by an epitaxial recrystallization initiated from the neighboring crystalline regions if the size of the latter exceeds a certain critical value.

- [1] A. Benyagoub, Phys. Rev. B 72, 094114 (2005).
- [2] A. Benyagoub et al., Appl. Phys. Lett. 89, 241914 (2006).
- [3] A. Benyagoub, Nucl. Instr. Meth. B 266, 2766 (2008).
- [4] A. Benyagoub and A. Audren, J. Appl. Phys. 106, 083516 (2009).

## Swift heavy ion irradiation induced porosity in GaSb

Patrick Kluth, Saliha Muradoglu, Mark Ridgway, James Sullivan, Matias Rodriguez, Boshra Afra

*The Australian National University, Australia*

We report on the formation of nano-porous networks in GaSb induced by swift heavy ion irradiation, i.e. where the energy transfer is virtually entirely due to electronic interactions [1]. For this study we have irradiated 2  $\mu\text{m}$  thin crystalline GaSb layers, grown on InP by metal organic chemical vapor deposition, with 185 MeV and 89 MeV Au ions. We have investigated the resulting structure and morphology of the material using synchrotron x-ray absorption spectroscopy (XAS), scanning electron microscopy (SEM), and positron annihilation lifetime spectroscopy (PALS) as a function of irradiation fluence and angle of irradiation with respect to the surface normal. The irradiation renders the GaSb porous and induces structural disorder. Initially, spherical voids form which elongate along the ion beam direction and evolve into irregularly shaped hollow pockets with thin sidewalls. This structure is significantly different from that observed previously for irradiation in the nuclear energy loss regime [2]. When irradiation is performed under an angle of 45° with respect to the surface normal, plastic flow of the material is observed in the direction of the projection of the ion beam. The latter has previously only been observed for amorphous materials, however, XAS measurements reveal residual crystallinity after irradiation albeit with enhanced local disorder. The porous layer thickness and the related porous micro-structure is critically dependent on the angle of irradiation. We will present a systematical investigation of the morphology of GaSb as a function of irradiation fluence and angle and discuss the possible underlying mechanisms for the transformation.

[1]P. Kluth, J. Sullivan, W. Li, R. Weed, C. S. Schnohr, R. Giulian, L. L. Araujo, W. Lei, M. D. Rodriguez, B. Afra, T. Bierschenk, R. C. Ewing, and M. C. Ridgway, Appl. Phys. Lett. 104, 023105 (2014).

[2]S. M. Kluth, J. D. Fitz Gerald, and M. C. Ridgway, Appl. Phys. Lett. 86, 131920 (2005).

## Modifications of structural and physical properties induced by swift heavy ions in pyrochlore oxides

Gaël Sattonnay<sup>1</sup>, Neila Sellami<sup>1</sup>, Lionel Thomé<sup>2</sup>, Clara Grygiel<sup>3</sup>, Isabelle Monnet<sup>3</sup>, Corinne Legros<sup>1</sup>, Sandrine Miro<sup>4</sup>, Denis Menut<sup>5</sup>, Jean Luc Bechade<sup>5</sup>, Sébastiano Cammelli<sup>6</sup>

<sup>1</sup>*University of Paris Sud, France*

<sup>2</sup>*CSNSM-Orsay, France*

<sup>3</sup>*CIMAP, France*

<sup>4</sup>*CEA Saclay-SRMP-JANNUS*

<sup>5</sup>*CEA Saclay SRMA*

<sup>6</sup>*SOLEIL synchrotron, France*

Complex oxides such as  $A_2B_2O_7$  pyrochlores exhibit a variety of properties which make them suitable for potential applications in different fields from electrolytes in solid oxide fuel cells to inert matrices for actinide transmutation. Swift heavy ion irradiations have been used to investigate the effects of high electronic excitations on the structural (phase transformations, amorphization) and thermal (thermal diffusivities) properties of pyrochlores with different compositions, namely  $Gd_2Ti_2O_7$ ,  $Y_2Ti_2O_7$ ,  $Gd_2Zr_2O_7$  and  $Nd_2Zr_2O_7$ . Modifications in the structural properties of pyrochlores upon ion irradiations performed at GANIL in Caen were investigated by using complementary tools at different scale observations. X-ray diffraction measurements revealed phase transitions induced by irradiation that include crystalline-to-amorphous and order-disorder structural transformations depending on the pyrochlore composition. Raman spectroscopy, performed on cross-section samples, allowed the investigation of the amorphous phase distribution as a function of depth, correlated with the variation of ion energy losses (both nuclear and electronic). X-ray absorption spectroscopy (XANES and EXAFS) performed at synchrotron facility SOLEIL were used to characterize the local order in the amorphous phase induced by irradiation in titanates.

Changes in the thermal diffusivities of irradiated pyrochlores were studied by laser-flash experiments. Phase transformations induced by swift heavy ion irradiations lead to modifications of the thermal conductivity. Finally, a specific study concerning the thermal recovery of irradiated pyrochlores was performed by using in situ high temperature X-ray diffraction in order to determine the thermal stability of the phases produced by irradiation. The results suggest that the recrystallization temperature is related to the amorphization sensitivity observed under irradiation.

## Ion beam doping of semiconductor nanowires

Carsten Ronning

*Friedrich-Schiller-Universität Jena, Germany*

Semiconductor nanowires are of major importance within the area of nanotechnology, and are usually synthesized using the so-called vapor-liquid-solid (VLS) growth mechanism. Controlled doping, a necessary issue in order to realize advanced devices, is an unsolved problem and an extremely difficult task if using such a growth mechanism. We use an alternative route for modifying either the electrical, optical or magnetic properties of semiconductor nanowires: ion implantation [1]. However, one cannot simply adapt bulk implantation parameters when the ion range is comparable to the size of the nanostructures. Therefore, we developed a new simulation tool in order to account for this. I will present the program *iradina* [2], as well as several recent studies on the modification of semiconductor nanowires by ion beam doping [3,4,5].

- [1] C. Ronning, C. Borschel, R. Niepelt, S. Geburt, *Materials Science and Engineering R* 70, 30 (2010).
- [2] C. Borschel, C. Ronning, *Nuclear Instruments & Methods B* 269, 2133 (2011).
- [3] S. Kumar et al., *Nano Letters* 13, 5079 (2013).
- [4] J. Segura-Ruiz et al., *Nano Letters* 11, 5322 (2011).
- [5] A. Colli et al., *Nano Letters* 8, 2188 (2008).

**Ion beam synthesis : a simple method to dope Si nanocrystals.**

Rim Khelifi<sup>1</sup>, Mathieu Fregnaux<sup>1</sup>, Dominique Muller<sup>1</sup>, Sebastien Duguay<sup>2</sup>, Jérôme Tribollet<sup>3</sup>,  
Daniel Mathiot<sup>1</sup>

<sup>1</sup>*ICube, Université de Strasbourg and CNRS, Strasbourg, France*

<sup>2</sup>*GPM, Université de Rouen and CNRS, Saint Etienne de Rouvray, France*

<sup>3</sup>*Institut de Chimie, Université de Strasbourg and CNRS, Strasbourg, France*

Silicon nanocrystals (Si-nc's) have been attracting a great deal of attention because of their remarkable electronic and optical properties. Several fabrication methods, and among them, those based on ion beams, permit to control the size, the shape and the density of the nc. The possibility to dope such nanostructures can open new prospects in optoelectronics or photovoltaics.

Thanks to the versatility of the ion beam synthesis, we propose to fabricate well-defined pure and doped Si-nc's, embedded in thermal SiO<sub>2</sub>, with various dopant concentrations (P, As and B). Co-implantation, with overlapping implantation projected ranges, of Si and of the doping species followed by a single thermal anneal step, is proved to be a viable route to form doped Si-nc's embedded in SiO<sub>2</sub>, with diameters of a few nanometers.

Atom Probe Tomography (APT) is used to image directly the spatial distribution of the various species at the atomic scale. As a first result, we show that the Si-nc's are formed by a mixture of implanted and matrix related silicon. The 3D APT data demonstrate that n-type dopant atoms (P and As) are efficiently introduced inside the Si-nc's, whereas B atoms are preferentially located at their periphery, at the Si/SiO<sub>2</sub> interface. Raman spectroscopy confirms the presence of crystalline Si particles. Photoluminescence results, which present a gradual quenching effect with the increasing dopant doses, will be discussed and related to the incorporation or not of the dopants in the Si-nc's. This behaviour is confirmed by Electron Paramagnetic Resonance (EPR) spectroscopy in the case of P doping, through the observation of the EPR signal of exchange coupled clusters of phosphorous shallow donors in Si-nc's.

**Ion beam synthesis for hybrid nanoelectronics: beyond silicon limits**

Slawomir Prucnal<sup>1</sup>, M. Glaser<sup>2</sup>, A. Lugstein<sup>2</sup>, M. Helm<sup>1</sup>, S. Zhou<sup>1</sup>, W. Skorupa<sup>1</sup>

<sup>1</sup>*Institute of Ion Beam Physics and Materials Research, Helmholtz-Zentrum  
Dresden-Rossendorf, Germany*

<sup>2</sup>*Institute of Solid State Electronics, Vienna University of Technology, Floragasse 7, 1040  
Vienna, Austria*

A key milestone for the next generation of high-performance nanoelectronic devices is the monolithic integration of III-V compound semiconductor materials with silicon technology. The incorporation of different functional III-V nano- and optoelectronic elements on a single chip enables performance progress, which can overcome the downsizing limit in silicon technology. Conventionally, the integration of III-V semiconductors with Si is based on the heteroepitaxial growth of multi-layered structures on Si or a variety of wafer bonding techniques. Devices based on such structures combine the high carrier mobility and high luminescence efficiency of III-V semiconductors with the advantages of well-developed silicon technology.

We have shown that the ion beam implantation technique (fluences of  $1 \times 10^{16}$  ion/cm<sup>2</sup> to  $4 \times 10^{16}$  ion/cm<sup>2</sup>) followed by millisecond-range flash lamp annealing can be successfully utilised for the fabrication of different Si/III-V heterojunctions on bulk Si and SOI substrates [1-3]. Recently, we have extended the application of ion beam implantation followed by ms liquid-phase processing into the fabrication of hybrid 1D materials. We have demonstrated axial heteronanowires consisting of III-V compound semiconductor and Si using advanced processing steps of silicon technology [4]. The clou of this approach is the phase formation within milliseconds via the liquid phase leading to excellent crystalline properties in the volume and at the interface of the nanocrystals. This paves the way for a hybrid 1D nano-/optoelectronics with high-mobility and optically active materials, compatible to standard Si technology. Moreover, this kind of processing on the nanoscale could lead to a renewed interest in the field of ion beam synthesis.

[1] S. Prucnal et al., Nano Lett. 11, 2814 (2011).

[2] S. Prucnal et al., Nanotechnology 23, 485204 (2012).

[3] S. Prucnal et al., J. Appl. Phys. 115, 074306 (2014).

[4] S. Prucnal et al., Nano Research, submitted (2014).





**Poster session A**  
**Monday, September 15, 2014**  
**16.40 – 18.40**

## Experimental simulation of radiation damage of polymers in space applications by cosmic-ray-type high energy heavy ions

Wolfgang Ensinger<sup>1</sup>, Umme Habiba Hossain<sup>1,2</sup>, Vincent Lima<sup>1</sup>

<sup>1</sup>*Darmstadt University of Technology, Germany*

<sup>2</sup>*GSI Helmholtz-Center of Heavy Ion Research, Germany*

Devices operating in space, e.g. in satellites or space-based telescopes, are being hit by cosmic rays. Apart from electromagnetic waves and small particles, these include so-called HZE-ions, with High mass (Z) and energy (E). They consist of elements of the first row of the transition metals of the periodic system of elements, such as Fe. These ions are able to pass the space vehicles hull, penetrate deeply into the materials and deposit a large amount of energy, typically several keV per nm range. No chemical bond can stand such energies: as a consequence, serious damage is created. In electronic devices, polymers such as polyimide are used for electrical insulation. When they are hit by HZE-ions, their polymeric network is degraded and they transform to compounds closer to graphite with progressively losing their insulating character. HZE ion irradiation can experimentally be simulated in large scale accelerators. In the present study, the radiation damage of polyimide and polyvinylacetate by heavy ions in the energy range from 500 to 1000 MeV, created in the GSI linear accelerator, is described. The results are based on FT infrared absorption, UV-Vis transmission, thermogravimetric analysis, mass spectroscopy and electrical conductivity measurements. Polymer structural degradation, fragmentation with outgassing of molecules, and loss of macroscopic properties are shown as a function of ion fluence/radiation dose. Molecular degradation mechanisms are proposed. Such investigations are important for estimating service life-times in long-term space missions.

## **Ion beam-induced luminescence as method of characterization of radiation damage in polycrystalline materials**

Iwona Jozwik-Biala<sup>1</sup>, Jacek Jagielski<sup>1</sup>, Grzegorz Gawlik<sup>1</sup>, Gerard Panczer<sup>2</sup>, Nathalie Moncoffre<sup>3</sup>, Renata Ratajczak<sup>4</sup>, Przemyslaw Jozwik<sup>1</sup>, Anna Wajler<sup>1</sup>, Agata Sidorowicz<sup>1</sup>

<sup>1</sup>*Institute of Electronic Materials Technology, Poland*

<sup>2</sup>*Institut Lumière Matière ILM, UMR5306 Université Lyon 1-CNRS, France*

<sup>3</sup>*Institut de Physique Nucléaire de Lyon IPNL, Université de Lyon, France*

<sup>4</sup>*National Centre for Nuclear Research, Poland*

Magnesium aluminate spinel is one of the oxides envisaged to be used in manufacturing of inert matrix fuel. Although the material is recognized for its radiation resistance, most of the experiments were performed on single crystals mainly by the use of RBS/C method and not much is known about the effects of irradiation of this material in polycrystalline form. The very recent concept is to use luminescence techniques as an experimental method able to measure the level of disorder in polycrystals, as it may be applied to both single and polycrystalline solids, is non-destructive, fast and can be easily implemented in-situ. The ion beam-induced luminescence (IBIL or IL) technique has been chosen to analyze the level of damage formation in ion-irradiated single and polycrystals of magnesium aluminate spinel. Samples were irradiated with 320 keV Ar<sup>+</sup> ions at fluences ranging from 1e12 to 2e16 cm<sup>-2</sup> in order to create various levels of radiation damage. The ionoluminescence (IL) was measured using a homemade system based on the use of Hamamatsu spectrometer collecting the light from a sample installed inside a target chamber of an ion implanter (Balzers MPB 202RP). The IL spectra of single and polycrystalline samples were analyzed in terms of the variation of peaks intensities with the irradiation fluence. Additionally, for single crystals, the damage-build up as a function of accumulated ion fluence was established through RBS/c. The results of IL and RBS/c analysis were then processed using Multi-Step Damage Accumulation (MSDA) model. That allowed for the determination of damage build-up kinetics, and finally cross-section for radiation damage build-up. Complementary information has been extracted from RBS/C and IL measurements in the case of single crystals.

This work was partially sponsored by the National Science Centre (Poland) under the contract number DEC-2011/03/D/ST8/04490 and by 09-133 French – Polish collaboration program.

## Role of implanted atoms on dynamic defect annealing in ZnO

Alexander Azarov<sup>1</sup>, Elke Wendler<sup>2</sup>, Andrej Kuznetsov<sup>1</sup>, Bengt Svensson<sup>1</sup>

<sup>1</sup>*Department of Physics, Centre for Materials Science and Nanotechnology, University of Oslo, Oslo, Norway*

<sup>2</sup>*Friedrich-Schiller-Universität Jena, Institut für Festkörperphysik, Jena, Germany*

Processes of dynamic annealing, i.e. defect evolution after thermalization of collision cascades, are exceptionally efficient in radiation hard materials resulting in non-amorphizable behavior even for high fluences of heavy ions. However, the mechanisms of defect formation/evolution in these materials are quite different from those in amorphizable ones and still far from being fully understood [1].

In the present work, we investigate the structural disorder in mono-crystalline wurtzite ZnO samples implanted at 15 K, room and elevated temperatures with different ions over a wide fluence range. The structural analysis was undertaken by RBS/C spectrometry. The results show that the bulk disorder exhibits the so-called IV-stage evolution with ion fluence, where the high fluence regime is characterized by both a strong influence of the damage build-up by the ion type and a reverse temperature effect [2]. In particular, Ag implantation results in an enhanced formation of extended defects, while for B a pronounced dopant-induced stabilization of defects leads to a dramatic enhancement of the damage production for the same value of DPA compared to that for N, Ar and Ag ions. Moreover, a strong dependence of the damage accumulation on implantation temperature was observed for N in the range of 300-923 K which is correlated with the recently found reverse annealing in N implanted ZnO [3].

The obtained results are interpreted in terms of formation and stability of different dopant-defect complexes and dopant agglomerations. In addition, a straight-forward methodology is demonstrated to differentiate between the contributions of pure ballistic and ion-defect reaction processes in the damage formation [2].

[1] W. Wesch, E. Wendler and C. S. Schnohr, Nucl. Instr. Meth. B 277, 58 (2012).

[2] A. Yu. Azarov, E. Wendler, A. Yu. Kuznetsov and B. G. Svensson, Appl. Phys. Lett. 104, 052101 (2014).

[3] A. Yu. Azarov et al., J. Appl. Phys. 115, 073512 (2014).

## Silicon defects characterization for low temperature ion implantation and RTP anneal

Giovanni Margutti<sup>1</sup>, Massimo Bersani<sup>2</sup>, Damiano Giubertoni<sup>2</sup>, Mario Barozzi<sup>2</sup>, Claudio Spaggiari<sup>3</sup>, Diego Martirani Paolillo<sup>1</sup>, Marco De Biase<sup>1</sup>

<sup>1</sup>*LFoundry S.r.l., Avezzano, Italy*

<sup>2</sup>*Fondazione Bruno Kessler, Trento, Italy*

<sup>3</sup>*Axcelis Technologies Srl, Agrate Brianza, Italy*

In the last years a lot of effort has been directed in order to reduce silicon defects eventually formed during the ion implantation/anneal sequence used in the fabrication of CMOS devices. In this work we explored the effect of ion implant dose rate and temperature on the formation of silicon defects for high dose BF<sub>2</sub> implantations. The considered processes (implantation and annealing conditions) are the one typically used to form the source/drain region of P Channel X-tors in the submicron technology node and will be detailed in the document. Characterization of implant damage, dopant distribution, dopant activation and extended silicon defects, left after anneal, has been performed by TEM (planar view and X-section). SIMS and SRA (Spreading Resistance Analysis) analysis were performed looking for Boron and Fluorine profiles and to determine the amount of activated dopant. We have verified that it's possible to reduce the formation of silicon defects modulating the ion implant process conditions. In particular, implant dose rate and temperature modulate the thickness of the amorphous silicon observed after implant, as well as the amount of silicon defect observed after thermal budget. Effect of low temperature implantation on product device was also performed, showing a reduction of leakage current on small p-channel x-tors. Experimental set up, results and possible explanation will be reported and discussed in the paper.

## **Imaging of hydrogen in zirconium alloy with secondary ion mass spectrometry (SIMS) : time of flight and quadrupole sims methods**

Nicolas Mine, Stéphane Portier, Matthias Martin

*Hot Laboratory Division, Paul Scherrer Institute, 5232 Villigen, Switzerland*

Although hydrogen can be detected easily in Secondary Ion Mass Spectrometry (SIMS), its source must be well identified and the contamination carefully limited. Characterization of hydrogen in metals requires local information, which motivates the development of imaging methods. In this work, we investigated Zirconium alloy cladding specimens (used for nuclear fuel cladding) hydrogenated in a Sievert apparatus. The hydrogen content varies from 130 to 600 wppm locally (heterogeneously distributed).

Processes were developed on a Quadrupole SIMS with gallium depth profiling (Atomika 4000) and a dual beam ToF-SIMS (IONTOF GmbH). Cesium sputtering is used to improve the secondary ion yield of  $H^+$ , coupled to a high brightness source for analysis (gallium or bismuth cluster source on the Quadrupole and Time of Flight SIMS respectively). The hydrides have been clearly identified and confirmed in Secondary Electron Microscopy (back scattering electron images). Precipitates are monitored with sub-micrometer spatial resolution (about 500 nm). We discuss the resolution limiting factors for hydrogen imaging using both SIMS methods. The correlation between the Secondary Phase Particles (Ni, Cr, Fe,...), monitored with a better lateral resolution, and the hydrides will be investigated in ToF-SIMS.

From XRD experiments, we know that the major hydride phase at room temperature is the  $\delta$ -phase ( $ZrH_{1.66}$ ) for slowly cooled hydrogenated Zr alloys. Using the latter assumption, the hydrogen content can be approximated with the quadrupole SIMS imaging process and compared to values measured with different techniques (BSE, hot gas extraction). The improved  $H^+$  useful yield that comes specifically from the cesium effect can be integrated by following the disappearance cross-section as a function of the primary ion fluence. The  $H^+$  useful yield in a wide precipitate serves as a reference/standard of stoichiometry ( $\delta$ -phase).

**Point defects in helium ion microscopy: an ionoluminescence study**

Gregor Hlawacek<sup>1</sup>, Vasilisa Veligura<sup>2</sup>, Raoul Van Gastel<sup>2</sup>, Harold J. W. Zandvliet<sup>2</sup>, Bene Poelsema<sup>2</sup>

<sup>1</sup> *Helmholtz-Zentrum Dresden-Rossendorf, Institute of Ion Beam Physics and Materials Research, Bautzner Landstr. 400, 01328 Dresden, Germany*

<sup>2</sup> *Physics of Interfaces and Nanomaterials, University of Twente, The Netherlands*

In Helium Ion Microscopy (HIM) [1] several signals are available to form an image and obtain information on sample properties. Besides secondary electrons and backscattered helium atoms also photons can be utilized. The latter phenomenon is referred to as ionoluminescence (IL). We show how the ion beam can be used to create sub surface luminescence patterns, that can be made visible using optical techniques [2]. The patterned areas are not visible in the obtained images of the sample surface.

Here, we use IL together with HIM to understand the creation of defects and their behaviour in ionic crystals. The emission of the created point defects has been analyzed in dependence of scanning parameters (pixel spacing and primary current). The fluence dependent results can be understood when the different diffusion behaviour of the identified defects is taken into account [3].

In a second step, single pixel exposures have been used to directly measure the surface projected interaction volume of the beam with sodium chloride. The results are compared to different theoretical calculations. We find that in the presented case a minimum density of 3 emission centers per nm<sup>2</sup> is needed for a detectable IL signal [2].

This research is supported by the Dutch Technology Foundation STW, which is the applied science division of NWO, and the Technology Programme of the Ministry of Economic Affairs.

[1] G. Hlawacek et al., J. Vac. Sci. Technol. B Microelectron. Nanom. Struct., 32, 020801 (2014).

[2] V. Veligura, G. Hlawacek, U. Jahn, R. van Gastel, H. J. W. Zandvliet, and B. Poelsema. J. Appl. Phys. 115, 183502 (2014).

[3] V. Veligura, G. Hlawacek, R. van Gastel, H. J. W. Zandvliet, and B. Poelsema. J. Phys. Condens. Matter 26, 165401 (2014).



## **Novel ion beam modifications of gemological and biological materials using an economic compact ion implanter**

Somsorn Singkarat, [Liangdeng Yu](#)

*Chiang Mai University, Chiang Mai 50200, Thailand*

In our efforts in developing ion beam technology for novel applications in biology and gemology, an economic compact ion implanter specially for the purpose was constructed. The designing of the machine was aimed at providing our users with a simple, economic, user friendly, convenient and easy operateable accelerator for ion implantation of biological living materials and gemstones for biotechnological applications and modification of gemstones. For convenient holding irregularly sized and shaped biological and gemological samples which were hard to hold vertically, the machine was in a vertical setup so that the samples could be placed horizontally and even without fixing. For a high beam current and intensity and a simple structure, the machine was a non-mass-analyzing ion implanter using mixed molecular and atomic nitrogen (N) ions so that material modifications could be more effective. For a homogeneous ion implantation, the machine was equipped with a focusing/defocusing lens and an X-Y beam scanner. For fast evacuation and short vacuum exposure to better maintain biological living samples surviving, the target chamber was made relatively small while supported by a powerful pump. To save equipment materials and costs, most of the components of the machine were taken from our abandoned ion beam facilities. The total maximum accelerating voltage of the accelerator could be up to 100 kV, which was ideally necessary for crop mutation induction and gem modification by ion beams from our experience. N-ion implantation of local rice seeds and cut gemstones was carried out. Various phenotype changes of grown rice from the ion-implanted seeds and improvements in gemological quality of the ion-bombarded gemstones were observed. The success in development of such a low-cost and simple-structured ion accelerator/implanter provides developing countries with a model of utilizing our limited resources to develop novel accelerator-based technologies and applications.

## **Radiation induced deep level defects in PNP bipolar junction transistors under various bias conditions**

Xingji Li<sup>1</sup>, Liyi Xiao<sup>1</sup>, Joachim Bollmann<sup>2</sup>, Chaoming Liu<sup>1</sup>, Jianqun Yang<sup>1</sup>, Guoliang Ma<sup>1</sup>

<sup>1</sup>*Harbin Institute of Technology, P.R. China*

<sup>2</sup>*TU Bergakademie Freiberg, Germany*

Bipolar junction transistor (BJT) is sensitive to ionization and displacement radiation effects in space. In this paper, 35 MeV Si ions were used as an irradiation source to research the radiation damage on PNP bipolar transistors. Changes in electrical parameters of transistors were in situ measured with increasing irradiation fluence of 35 MeV Si ions. Defects in the bipolar junction transistors under various bias conditions are measured after irradiation using deep level transient spectroscopy (DLTS). Results show that the bias conditions affect the concentration of deep level defects, and the degradation of current gain of BJTs induced by heavy ions irradiation.

**Radiation defects studies on silicon bipolar junction transistor irradiated by br ions and electrons**

Chaoming Liu<sup>1</sup>, Xingji Li<sup>1</sup>, Jianqun Yang<sup>1</sup>, Guoliang Ma<sup>1</sup>, Liyi Xiao<sup>1</sup>, Joachim Bollmann<sup>2</sup>

<sup>1</sup>*Harbin Institute of Technology, P.R. China*

<sup>2</sup>*TU Bergakademie Freiberg, Germany*

BJTs have important applications in analog or mixed-signal integrated circuits and BiCMOS circuits, some of which are still employed for space application. BJTs are sensitive to both ionization and displacement damage. Charged particles in space could be incident upon the semiconductor devices, producing displacement and ionization damage respectively. The silicon bipolar junction transistors (BJT) are sensitive to both ionization damage (oxide layer) and displacement damage (Si bulk). Heavy ions can induce displacement damage in Si bulk, while lower energy electrons can cause ionization damage to the oxide layer in BJTs. Therefore, based on the heavy ion and lower energy electron combined irradiation, it is valuable to research the interaction between the ionization and displacement damage in the BJTs. This paper researches the interaction between the ionization and displacement damage in NPN BJTs induced by combined irradiation of 20MeV Br ions and 110keV electrons, employing the electrical parameter measurement and DLTS analysis. Based on the results, the interaction between ionization and displacement damage in NPN BJTs is revealed clearly, which is useful to the radiation damage mechanism and hardness.

## Helium ion beam charging of an oxide layer on a silicon substrate: a comparison between observed and Monte Carlo-simulated results

Kaoru Ohya<sup>1</sup>, Emile Van Veldhoven<sup>2</sup>, Paul F.A. Alkemade<sup>3</sup>, Diederik J. Maas<sup>2</sup>

<sup>1</sup>*Institute of Technology and Science, The University of Tokushima, Japan*

<sup>2</sup>*Van Leeuwenhoek Laboratory, TNO Science and Industry, The Netherlands*

<sup>3</sup>*Kavli Institute of Nanoscience, Delft University of Technology, The Netherlands*

Charging of an insulating material is an important issue in applying an ion beam for imaging, inspection, metrology and lithography in integrated circuit device manufacture. In spite of the increasing importance, no systematic study of the ion beam charging has been carried out to understand the mechanism. This paper presents experiments with a helium ion microscope (HIM) of both charging of a SiO<sub>2</sub> layer with the thickness of several hundreds of nanometer and imaging of the charged surface on a Si substrate.

In order to compare with the observation in a low-dose irradiation, a Monte Carlo calculation was performed to simulate the ion beam charging of the SiO<sub>2</sub> layer on Si. It models the transport of impinging ions and secondary electrons (SEs) and the charge accumulation in the layer, and the resultant electric field in the layer and in the vacuum [1]. Trajectories of the SEs emitted in the vacuum are simulated where some SEs turn towards the positively charged area on the layer; these SEs are unable to produce a net emission. To model the observed charging distributions, a small part of the SiO<sub>2</sub> surface (1×1, 30×30 and 100×100 nm<sup>3</sup>) was cumulatively irradiated with 10000 ions. After the irradiation, the net SE yield was calculated with noncumulative irradiation at each point of the charged SiO<sub>2</sub> surface and uncharged surroundings.

The calculated charging voltage and SE yield of the charged area were increased and decreased, respectively, with increasing thickness of the layer, as found in the observed images. The charged area distributed more for thicker layers, whereas it was less influenced by the irradiation areas. The calculated area was in good agreement with the observation for 100 nm- and 310 nm-thick SiO<sub>2</sub> layers in the low-dose irradiation. Further comparison between the experiment and the calculation is presented along with detailed discussion on the ion beam charging.

[1] K. Ohya, T. Yamanaka, Nucl. Instr. Meth. Phys. Res. B 315, 295 (2013).

## Modelling and observation of a trench pattern on a silicon substrate in helium ion microscope

Takuya Yamanaka<sup>1</sup>, Kaoru Ohya<sup>1</sup>, Emile Van Veldhoven<sup>2</sup>, Paul F.A. Alkemade<sup>3</sup>, Diederik J. Maas<sup>2</sup>

<sup>1</sup>*Institute of Technology and Science, The University of Tokushima, Japan*

<sup>2</sup>*Van Leeuwenhoek Laboratory, TNO Science and Industry, The Netherlands*

<sup>3</sup>*Kavli Institute of Nanoscience, Delft University of Technology, The Netherlands*

As the dimensions of integrated circuit devices continue to shrink, controlling the size and shape of the structure has become important. Although the scanning electron microscope (SEM) has been a powerful tool to measure the sizes of patterns, SEM may have limitations when moving nanometer-scale patterns. The scanning ion microscope (SIM) constructs a secondary-electron (SE) image of a specimen surface scanned by an ion beam, similarly to the conventional SEM. A SIM with a He gas field ion source (HIM) has attracted interest as a new option for such metrology applications. We performed a model calculation of a 100 nm-wide and 100 nm-deep trench formed on a Si substrate, the surface of which was irradiated with He ions at energies relevant to the HIM. The calculated SE profile across the pattern was compared with HIM images of the trench at different tilt angles of the ion beam.

The SE emission was modeled by simulating trajectories of ions penetrating into the specimen and SEs produced by the ions using a Monte Carlo technique. The details of the model are presented in a previous paper [1]. The present calculation takes into consideration re-entering ions and SEs escaping from the sidewall and the bottom to other positions of the trench. The calculated SE profiles showed a sharp peak at the edge of the trench, due to additional SE emission from the side wall, and a gradual decrease at the bottom of the trench due to re-entrance of SEs into the sidewall. The peak and decrease in the SE yield reproduced the bright band and dark region, respectively, found in the HIM image. The calculation showed the largest increase in the SE peak when the tilt angle of the ion beam agrees with the sidewall angle of the trench. It can explain the reason for a very sharp bright band observed at the tilt angle of  $\sim 20^\circ$ . Further comparisons between the observed and calculated results are presented.

[1] K. Ohya. T. Yamanaka et al., Nucl. Instr. Meth. Phys. Res. B 267, 584 (2009).

## **Light Ion and Heavy Cluster Focused Ion Beam Nanofabrication**

Paul Mazarov, Sven Bauerdick, Lars Bruchhaus, Ralf Jede

*Raith GmbH, Germany*

Focused Ion Beam (FIB) processing is nearly exclusively based on gallium Liquid Metal Ion Sources (LMIS). With the appreciation that the ion type has dramatic consequences on the physical and chemical nature of the resulting nanostructures, we have extended the Gallium ion column and source technology towards the long-term stable delivery of multiple species for a nanometer-scale focused ion beam employing a liquid metal alloy ion source (LMAIS). The advantage of having different species of different mass or charge can be beneficial for various nanofabrication applications given the interaction volume in the sample as well as specifically reducing the contamination due to unwanted ion implantation. Nearly half of the elements of the Periodic Table are in principle available in LMAIS based FIB technology. Key features of a LMAIS are long life-time, high brightness and stable ion current. We present the capabilities and applications of the multiple-species FIB nanofabrication instrument including excellent long term current stability and sub-10 nm beam resolution for various ions and clusters from  $\text{Be}^{++}$  to  $\text{Au}^{5+}$ . Employing the multi-species system nanostructures with dimensions below 15 nm can be achieved with light ion species. Heavy ions like  $\text{Au}^{+,++}$  or  $\text{Au}_n^+$  clusters have a sputter yield much larger than  $\text{Ga}^+$ , which enable to reduce the working time. This difference can be consistently explained by the Sigmund theory of sputtering by bombardment with heavier ions in comparison to light ions. The non-linear sputter effects induced by cluster bombardment give additional milling enhancement. Additionally it is shown that sputter erosion under bombardment with clusters ions provides much better depth resolution enabling new applications based on functionalization or true surface milling.

## **Comparison of patterning silicon and silicon carbide using focused ion beams**

Savita Kaliya Perumal Veerapandian<sup>1</sup>, Susanne Beuer<sup>2</sup>, Maximilian Rumler<sup>2</sup>, Florian Stumpf<sup>2</sup>, Mathias Rommel<sup>2</sup>, Lothar Frey<sup>1,2</sup>, Keith Thomas<sup>3</sup>, Lex Pillatsch<sup>3</sup>, Johann Michler<sup>3</sup>

<sup>1</sup>*Chair of Electron Devices, Friedrich-Alexander-University Erlangen-Nuremberg, Cauerstrasse 6, 91058 Erlangen, Germany*

<sup>2</sup>*Fraunhofer Institute of Integrated Systems and Device Technology (IISB), Schottkystrasse 10, 91058 Erlangen, Germany*

<sup>3</sup>*Empa Materials Science and Technology, Feuerwerkerstrasse 39, 3602 Thun, Switzerland*

Focused ion beam (FIB) milling of micro- and nano-structures has been widely used in various fields of applications. However, it is difficult to achieve complex 2D and 3D structures as many effects have to be considered. But even the fabrication of simple holes and trenches is not trivial when flat bottom and perpendicular side walls are targeted. In this work, FIB milling of different structures is studied and compared for two important electronic materials, i.e., silicon and silicon carbide (SiC). It is shown that significantly different trench cross-sections are achieved for silicon and SiC using the same processing parameters even when accounting for the different material removal rates for both materials. It will be shown that this is mainly due to the significant difference in the angle dependent sputter yield for both materials. To investigate more complex structures, fabrication of nanocone arrays by simply milling vertical and horizontal lines separated by a particular periodicity [1] has been repeated in SiC. The difference will be critically discussed and explained. Apart from the differences in the angle dependent sputter yield for both materials, other secondary effects during FIB irradiation are compared for both materials. Such effects include the swelling as observed for irradiation of silicon at low doses or the influence of the non-ideal beam shape. The effects will be studied by scanning probe microscopy techniques, e.g. sample topography will be measured by atomic force microscopy (AFM) immediately after irradiation by an in-built AFM. In addition, the influence of FIB irradiation on the electrical material properties will be very sensitively studied by scanning spreading resistance microscopy (SSRM) for SiC and compared to the results observed in silicon [2].

[1] M. Rommel et al., Microelectron. Eng. 98, 242-245 (2012).

[2] M. Rommel et al., J. Vac. Sci. Tech. B 28, 595-607 (2010).

## **Focused ion beam developments for nano prototyping**

Hans Mulders, Daniela Sudfeld

*FEI, The Netherlands*

Focused ion beam systems have been available since almost 25 years and are applied by many scientists for a variety of applications. Although one of the major applications is related to the creation of a TEM lamella, the FIB is also used to create other micro- and nano-scale structures. The FIB can be used for material removal (milling) and for material addition (deposition) and both techniques, use a variety of beam chemistry components. With the growing application space for FIB, the technology demand also has increased and the most relevant instrumentation trends for nano-prototyping are discussed below:

- 1) Reduction of the minimum spot size, particularly at lower energy to reduce beam penetration and residual damage. This is achieved by improvement of ion beam optical elements, but also by reduction of beam scattering, due to residual gas in the chamber.
- 2) Development of new and improved beam chemistry processes for deposition. New materials have been enabled such as for the deposition of magnetic materials (Fe, Co), plasmonic materials (Au) and contacting materials (Pt, Pd).
- 3) Use of non-Ga based FIB such as He ions or Xe ions. Especially the noble gas ions are of interest because they are chemically inert for the sample and hence there is no additional dopant implanted during milling.
- 4) Sample clean up after milling: this refers to the removal of Ga over the full implantation depth and by minimizing or removal of re-deposition. Reduction of the amorphization layer and the implanted Ga can be achieved by exposure to a new in-situ broad ion beam of for example 50 to 500 V Ar<sup>+</sup>.
- 5) Addition of a Raman system to the tool to study sensitive samples such as graphene, during processing with the ion beam or with the electron beam.



## Printing nearly-discrete magnetic patterns using ion beams

Rantej Bali<sup>1</sup>, Sebastian Wintz<sup>1</sup>, Sergio Valencia<sup>2</sup>, Andreas Neudert<sup>1</sup>, Kay Potzger<sup>1</sup>, Jürgen Bauch<sup>3</sup>, Florian Kronast<sup>2</sup>, Stefan Facsko<sup>1</sup>, Jürgen Lindner<sup>1</sup>, Jürgen Fassbender<sup>1</sup>, Falk Meutzner<sup>1</sup>, René Hübner<sup>1</sup>, Richard Boucher<sup>3</sup>, Ahmet Akin Ünal<sup>2</sup>

<sup>1</sup>*Helmholtz-Zentrum Dresden-Rossendorf, Germany*

<sup>2</sup>*Helmholtz-Zentrum Berlin für Materialien und Energie, Germany*

<sup>3</sup>*TU Dresden, Germany*

We show that sub-50 nm resolution lateral patterning of magnetic structures can be enabled by disorder induced ferromagnetism. [1] Disorder is induced through exposure of a chemically ordered alloy to energetic ions; collision cascades formed by the ions knock atoms from their ordered sites and the concomitant vacancies are filled randomly via thermal diffusion of atoms at room temperature. Here we consider the case of  $\text{Fe}_{60}\text{Al}_{40}$  wherein the chemically ordered B2 structure is paramagnetic, and chemical disordering leads to the formation of the A2 structure which is ferromagnetic. [2] Thin films of chemically ordered  $\text{Fe}_{60}\text{Al}_{40}$  were irradiated with  $\text{Ne}^+$  ions with energies up to 30 keV and fluence of  $6 \times 10^{14}$  ions  $\text{cm}^{-2}$ . Magnetometry showed that 40 nm thick  $\text{Fe}_{60}\text{Al}_{40}$  films can be fully magnetized using  $\text{Ne}^+$  at 20 keV, and a semi-empirical estimation shows that lateral penetration of the magnetic phase is restricted to within 25 nm of a mask edge. This ion-induced transition can be exploited to induce ferromagnetism in localized regions by ion-irradiation through lithographed shadow masks. We show that this technique may be useful for fabricating novel spin-transport devices.

[1] R. Bali et al., Nano Letters 14, 435–441 (2014).

[2] J. Fassbender et al., Phys. Rev. B 77, 174430 (2008).

## Creation of double tilted pillar structures for microfluidic applications

Istvan Rajta<sup>1</sup>, Attila Szabo<sup>1</sup>, Gabor Jarvas<sup>2</sup>, Marton Szigeti<sup>2</sup>, Laszlo Hajba<sup>2</sup>, Judit Bodnar<sup>2</sup>, Szabolcs Szilasi<sup>1,3</sup>, Andras Guttman<sup>2</sup>, Gyula Nagy<sup>1</sup>, Robert Huszank<sup>1</sup>, Eszter Baradacs<sup>4</sup>, Peter Furjes<sup>5</sup>, Zoltan Fekete<sup>5</sup>

<sup>1</sup>MTA Atomki, H-4026 Debrecen, Bem tér 18/c, Hungary

<sup>2</sup>MTA-PE Translational Glycomics Group, MUKKI, University of Pannonia, H-8200 Veszprém, Egyetem u. 10, Hungary

<sup>3</sup>University of North Texas, TX, USA

<sup>4</sup>DE TTK - ATOMKI Joint Department of Environmental Physics, Debrecen, Hungary

<sup>5</sup>Research Centre for Natural Sciences, Institute for Technical Physics and Materials Science, Hungarian Academy of Sciences, H-1525 Budapest, P.O. Box 49, Hungary

Exploiting the advantages of P-beam writing lithographic method to make irradiations into tilted samples, doubly tilted pillar microstructures are created for microfluidic applications.

SU-8 negative tone resist spin-coated on glass substrate was irradiated with 2 MeV proton microbeam. The created structures consisted of pillars standing in rows inside an appropriate frame. The fluid (water, blood, etc.) can be coupled through an inlet into the chip and extracted through an outlet. The goniometer feature of the Atomki microbeam facility enabled us to tilt the pillars relative to the surface normal (in this case odd rows were tilted by +20° and even rows by -20° degrees).

The aim of tilting the pillars is to increase the functional surface of the pillars with which the fluid can interact with the stationary phase, and to improve the fluid dynamics properties. With the help of this promising method we are able to create microfluidic chips that can be used for an improved efficiency cell capture device.

## Photon emission from solid surfaces irradiated by cluster ion beams

Gikan Takaoka<sup>1</sup>, Hiromichi Ryuto<sup>1</sup>, Francesco Musumeci<sup>2</sup>, Mitsuaki Takeuchi<sup>1</sup>, Akira Sakata<sup>1</sup>

<sup>1</sup>*Kyoto University, Japan*

<sup>2</sup>*Catania University, Italy*

The impact of an energetic cluster ion on substrate surface represented unique properties. Extremely high temperature and pressure could be obtained in the impact area by accelerating the cluster ion beams. In this work, water cluster ions and Ar cluster ions were irradiated on Si, SiO<sub>2</sub> and Au surfaces at different acceleration voltages, and photon emission was investigated by the photon counting instrument developed. The intensity of luminescence induced by the water and Ar cluster ion irradiation increased with increase of the acceleration voltage. The temperature of clusters irradiated on the Au surface was estimated to be approximately 13,000 K at an acceleration voltage of 9 kV. For Ar cluster ion irradiation on Si, SiO<sub>2</sub> and Au surfaces, the number of photons emitted was approximately 100 cps/nA/cm<sup>2</sup> at an acceleration voltage of 9 kV, and the intensity was similar for all the substrate surfaces. On the other hand, for water cluster ion irradiation, the intensity was approximately 60 cps/nA/cm<sup>2</sup> at an acceleration voltage of 9 kV for Au surface, and it was stronger by five times than that for Si and SiO<sub>2</sub> surfaces. Furthermore, the luminescence spectra for the Au surfaces were measured, although the wavelength resolution was not fine. For the Ar cluster ion irradiation, the peak appeared around the wavelength of 450 nm corresponding to the emissions from Ar ion. For the water cluster ion irradiation, a few peaks appeared at higher wavelengths between 500 nm and 650 nm. They might be related to the emissions from water molecules excited. Thus, the photon emission from solid surfaces could be performed by water cluster ion irradiation as well as Ar cluster ion irradiation.

## Damage evolution in LiNbO<sub>3</sub> crystals under ionizing irradiation using MeV Si ions

Liu Peng<sup>1</sup>, Yanwen Zhang<sup>2</sup>, Haizhou Xue<sup>1</sup>, Xuelin Wang<sup>3</sup>, W. J. Weber<sup>1</sup>

<sup>1</sup>*Department of Materials Science and Engineering, University of Tennessee, Knoxville, TN 37996, USA*

<sup>2</sup>*Materials Science and Technology Division, Oak Ridge National Laboratory, Oak Ridge, TN 37831, USA*

<sup>3</sup>*School of Physics, State Key Laboratory of Crystal Materials and Key Laboratory of Particle Physics and Particle Irradiation (MOE), Shandong University, Jinan 250100, P.R. China*

LiNbO<sub>3</sub> crystal, as one of the most attractive functional materials due to its outstanding acousto-optic, electro-optic and nonlinear properties, has been widely used in the optical communication, laser technique and other optics applications. Recent studies have revealed that this material is very sensitive to ionizing radiation and can be readily damaged due to extreme electronic excitation resulting from ion irradiation. In this work, based on the Rutherford backscattering spectrometry and channeling technique, the damage behavior in z-cut LiNbO<sub>3</sub> crystals under MeV to tens of MeV Si-ion irradiation are studied at room temperature. The work focuses on the relationship between the pre-existing damage and the irradiation conditions in the surface region, with variables of the stopping power and the ion fluence.

Under 0.9 MeV Si<sup>+</sup> irradiation with the electronic stopping power of ~1.4 keV/nm, the damage induced by the electronic excitation can be detected at an ion fluence at  $5 \times 10^{14}$  cm<sup>-2</sup>, and the damage mechanism can be reasonably explained utilizing the thermal spike model suggested by F. Agulló-López et al. Under 21 MeV Si<sup>7+</sup> irradiation, the surface region of LiNbO<sub>3</sub> becomes completely amorphous under non-channeling ion irradiation at a fluence of  $2 \times 10^{13}$  cm<sup>-2</sup>. The damage level, however, reduces to 81% under the same irradiation condition if the irradiations are carried out along the main axial channeling direction perpendicular to the surface. Our experimental results also indicate that, for the same electronic stopping power on both sides of the Bragg peak, the radius of the ion-track produced by ions at a lower velocity is larger. This observation is consistent with the prediction of velocity dependent damage cross-section based on the thermal spike model by A. Meftah et al.

## The effect of charge-cycling in various materials by medium speed ions from an experimental and theoretical perspective

Jennifer Schofield<sup>1</sup>, Jay Laverne<sup>2</sup>, Simon Pimblott<sup>1</sup>

<sup>1</sup>*The University of Manchester, UK*

<sup>2</sup>*The University of Notre Dame, USA*

Charge cycling, that is the gain and loss of electrons by energetic ions, plays a significant role in the energy transfer from, and attenuation of, ions in materials, especially in the medium energy range of heavy ions. Most treatments of electronic stopping power avoid the issue and employ an empirical energy dependent effective charge derived from experimental stopping powers [1]. Detailed information on charge exchange cross-sections is required to understanding the effects of charged particle radiation on solid materials.

The results of experiments examining the charge cycling of  $\text{Li}^{2+}$  and  $\text{Li}^{3+}$  ions in Ti and Zr thin films will be presented. These studies were performed using the 10MV tandem accelerator at the Nuclear Structure Laboratory, University of Notre Dame, USA using a method outlined previously [2]. Titanium and zirconium films were selected because of their ubiquitous application in the nuclear power industry. Lithium ions were employed in this preliminary study as their generation was straightforward at energies where significant charge cycling processes were expected and so could be measured with comparative ease.

The modelling of charge cycling in Monte Carlo track structure simulations will also be presented.

The data gained from this research will allow a better understanding of energy transfer of ions in materials and thereby shed light on the deleterious effects of ionising radiation on material properties.

[1] J.F. Ziegler, M.D. Ziegler, J.P. Biersack, Nuclear Instruments and Methods in Physics Research Section B: Beam Interactions with Materials and Atoms, 268, 1818-1823 (2010).

[2] C. Schmitt, J. LaVerne, D. Robertson, M. Bowers, W.T. Lu, P. Collon, Phys Rev A 80 (2009).

## Proton induced ionization cross sections of the elements Al, Si, Ti, Fe, and Ni in the 0.7-2.0 MeV energy range

Marcos Vasconcellos<sup>1</sup>, Ana Paula Bertol<sup>1</sup>, Ruth Hinrichs<sup>2</sup>

<sup>1</sup>*Instituto de Física - UFRGS, Brasil*

<sup>2</sup>*Instituto de Geociências - UFRGS, Brasil*

Elemental analysis with particle induced X-ray emission requires the knowledge of several fundamental parameters, such as ionization cross sections and fluorescence yields, to obtain accurate quantitative results. For analysis with protons these parameters can be obtained from theoretical models [1], semi-empirical adjustments comparing theoretical and experimental results [2], or from polynomial functions obtained by fitting a large amount of experimental results [3]. The ionization cross sections of light elements present considerable deviations between experiment and theory [4]. The reference data [2] for elements with  $Z=11-30$  are based on theoretical and experimental data for Ni and on fluorescence yields from Krause [5]. In the Al case, the predicted value was 30% higher than the measured values. In this work we report on experimental results for ionization cross sections induced by protons in the 0.7-2.0 MeV energy range on 10 nm films of Al, Si, Ti, Fe and Ni. The ionization cross sections for Ti, Fe and Ni agree well with experimental values and theoretical predictions from the literature, endorsing the experimental method. The Si and Al data agree with recent empirical adjustments [3] and with the high deviation predicted for Al [2]. The production cross sections were compared to the ionization cross sections from ECPSSR theory, using the fluorescence yield values proposed by different authors [6]. The Al discrepancy can be explained when the value of 0.0326 from Kahoul et al. [6] is used, instead of the value 0.039 proposed by Krause [5]. For Si small corrections in the fluorescent yield value are proposed.

[1] G. Lapicki and A. R. Zander, Phys. Rev. A 23, v4, 2072 (1981).

[2] H. Paul and J. Sacher, At. Data Nucl. Data Tables 42, 105 (1989).

[3] A. Kahoul et al., Radiat. Phys. Chem. 80, 1300 (2011).

[4] G. Lapicki, X-Ray Spectrom. 34, 269 (2005).

[5] M. O. Krause, J. Phys. Chem. Ref. Data 8, 307 (1979).

[6] A. Kahoul et al., Radiat. Phys. Chem 81, 713 (2012).

## Analysis of channeling experiments at RBS energies and in the medium energy ion scattering regime

Sveda Rabab Naqvi<sup>1</sup>, Daniel Primetzhofer<sup>1</sup>, M. K Linnarsson<sup>2</sup>, Thawatchart Chulapakorn<sup>1</sup>, Anders Hallén<sup>1,2</sup>, Göran Possnert<sup>1</sup>

<sup>1</sup>*Uppsala University, Division of Applied Nuclear Physics, Department of Physics and Astronomy, P.O. Box 534, SE-751 21 Uppsala, Sweden*

<sup>2</sup>*KTH Royal institute of technology, School of information and Communication Technology, Integrated Circuits and Devices, P. O. Box Electrum 229, SE-16440 Kista-Stockholm, Sweden*

Channeling in crystalline materials has been used as a powerful tool to characterize structural imperfection of single crystals induced by, for instance, ion implantation [1]. In this work we study details of ion channeling experiments with a focus on blocking effects. For example, while small azimuthal rotations of the sample will not affect channeling of incoming particles (under normal incidence) scattered ions can have different exit trajectories and show azimuthal dependent blocking features. We quantify variations in yield from azimuthal dependent blocking under different experimental conditions and compare the observed effects to possible contributions from misalignments in channeling geometries. Results are compared with calculations using the simulation package TRIC (Transmission of Ions in crystals) which yields angular scattering distributions for single crystals [2].

Experiments were carried out at the 5MV tandem accelerator at Uppsala University. Helium ions with an energy of 2 MeV were scattered from a Si[100] surface. Samples were mounted with different azimuth orientations and 2D mappings (polar & tilt) of the scattered intensity were obtained. Spectra were recorded in vicinity of channeling minima and minimum yields were compared. As an example, for a circular detector with acceptance angle of  $2.8^\circ$ , azimuthal rotations result in at most 4% difference in minimum yield. In comparison, changes in intensity of up to 25% were observed  $0.1^\circ$  off the center of channeling minima. Experimental results were found to be in good agreement with simulations and permit predictions for different geometries and detector sizes. Since at keV energies, blocking features span larger solid angles we also investigated lower ion energies. A comparison of experimental blocking patterns with computer simulations will be presented.

[1] J.F. Van Der Veen, Surf. Sci. Rep. 5, 199 (1985).

[2] V.A. Khodyrev et al., Phys. Rev. E 83, 056707 (2011).

## Near-threshold behavior in surface scattering and impact induced multifragmentation of $C_{60}^-$ on gold

Victor Bernstein, Eli Kolodney

*Schulich Faculty of Chemistry, Technion (IIT), Israel*

During recent years we have studied, both experimentally and computationally a new dissociative channel in sub-keV collisions between a large polyatomic projectile and a surface.

The so-called impact induced postcollision multifragmentation process was identified in collision between  $C_{60}^-$  ions and gold or nickel surface at the kinetic energy range of 300 – 900 eV. Molecular dynamics (MD) simulations with extensive trajectory statistics have successfully reproduced the main characteristics of the postcollision multifragmentation event and provided insight into the microscopic details of the dynamics involved.

While our former studies (both experimental and MD simulations) were concerned with the fully developed multifragmentation process, here we focus mainly on the near-threshold behavior (80-160 eV) as revealed by MD, probing the transition from intact scattering to complete multifragmentation. The calculated threshold energy is found to be in fair agreement with the experimental one. At this energy range we observe both intact scattered  $C_{60}$  and  $C_n$  fragments (simultaneously for a given energy) with a gradual increase of multifragmentation events and corresponding decrease of intact scattering with impact energy.

For the intact scattering, a nearly constant relative kinetic energy loss is found. The different contributions to the kinetic energy loss, due to vibrational excitation of the outgoing projectile and energy transfer to the surface, are calculated. Analyzing distinct trajectories we find that for near-threshold impact kinetic energies the multifragmentation event of the highly vibrationally excited fullerene can occur at an exceptionally large distance from the surface after a flight time of more than 20 picoseconds.



## Use of ion-assisted techniques for determining the structure of TiO<sub>2</sub> nanotubes

Renata Pedrolí Renz, Andre Luis Marin Vargas, Roberto Hübler

*Materials and Nanoscience Laboratory - Physics Faculty - Pontifical Catholic University of Rio Grande do Sul, Brazil*

In recent years, several investigators have reported obtaining titanium dioxide nanotubes presenting a variety of advanced and functional properties for high-performance applications, e.g., for solar and fuel cells, gas sensor, self-cleaning and biomedical devices. Electrochemical oxidation of titanium has been widely used as a method for fabrication of self-organized titanium oxide nanotubes (TiO<sub>2</sub> NT), since it is a simple and inexpensive process, which allows a great control over the size and configuration of the formed structure. Normally the morphological and structural characterizations are based on images from scanning or transmission electron microscopy. The use of characterization techniques assisted by energetic ion beams, such as RBS or MEIS, can simultaneously evaluate the composition and structural properties of the nanotubes. In this work TiO<sub>2</sub> nanotubes were grown on plates of commercially pure titanium varying the growth time and the potential applied in order to obtain nanostructures with different diameters and lengths. The characterizations made by RBS were compared by analysis of SEM-FEG demonstrating a good compromise between them.

## Low-loss planar and channel waveguides in $\text{Pr}^{3+}:\text{Y}_2\text{SiO}_5$ fabricated by MeV oxygen ions with low dose

Bing-xi Xiang<sup>1</sup>, Lei Wang<sup>1</sup>, Jing Guan<sup>1</sup>, Yang Jiao<sup>2</sup>

<sup>1</sup>*Shandong University, P.R. China*

<sup>2</sup>*Shandong Normal University, P.R. China*

Low loss planar and channel waveguides in  $\text{Pr}:\text{YSO}$  were fabricated by 6 MeV oxygen ion implantation with a fluence of  $5 \times 10^{14}$  ions/cm<sup>2</sup>. The surface guiding structure has been formatted with an increased refractive index layer as a consequence of ion-induced damage. The dark mode spectroscopy of the planar waveguide was measured using a prism coupling arrangement. The photoluminescence properties of the bulk materials were found to be well preserved within the waveguide core region. The refractive index profile of the planar and channel waveguide was reconstructed using the Reflectivity Calculation Method. The near-field mode profiles of the stripe waveguide were obtained by an end-fire coupling arrangement. For comparison to the experimental results, the finite difference beam propagation method (FD-BPM) was used to simulate the guiding modes of the channel waveguides, the calculated results were in excellent agreement with the measured waveguide modes. After annealing, the propagation loss of the channel waveguides could be reduced down to as low as 0.35dB/cm, respectively.

**Modifications of  $\text{WN}_x\text{O}_y$  films by ion irradiation**

Noriaki Matsunami<sup>1</sup>, T. Teramoto<sup>1</sup>, M. Kato<sup>1</sup>, S. Okayasu<sup>2</sup>, M. Sataka<sup>2</sup>, H. Kakiuchida<sup>3</sup>

<sup>1</sup>*Nagoya University, Japan*

<sup>2</sup>*Japan Atomic Energy Agency, Japan*

<sup>3</sup>*National Institute of Advanced Industrial Science and Technology, Japan*

We have investigated ion-irradiation-induced modifications of electronic- and atomic-structures of  $\text{WN}_x\text{O}_y$  films on C-plane-cut-sapphire ( $\text{C-Al}_2\text{O}_3$ ) substrate. Rutherford backscattering spectroscopy (RBS) of 1.8 MeV  $\text{He}^+$  ions leads to the composition,  $x=1.1$  and  $y=0.4$  within RBS accuracy of 20 %. According to X-ray diffraction (XRD), a strong peak appears at the diffraction angle ( $2\theta$ )  $\approx 37^\circ$  and a weak peak at  $\approx 78^\circ$ . These peaks are assigned as WN, referring to JCPDS card data, though it is known that WN is metastable phase. No peaks were observed other than WN and  $\text{C-Al}_2\text{O}_3$  ( $2\theta=41.7^\circ$ ). It is found that the electrical resistivity of unirradiated film ( $0.03 \text{ } \Omega\text{cm}$ ) is reduced to  $7 \times 10^{-4}$  and  $3 \times 10^{-3} \text{ } \Omega\text{cm}$  by 100 MeV Xe ion irradiation at  $35 \times 10^{12} \text{ cm}^{-2}$  and 100 keV N ion at  $10^{16} \text{ cm}^{-2}$ , respectively, and that the XRD intensity decreases to  $\sim 1/20$  and  $1/10$  by these ion irradiation. These results imply that implantation of N in the film suppress the modification, knowing that considerable fraction of N is remained in the film, since the film thickness of 40 nm is smaller than the projected range of 100 keV N (77 nm). It also appears that the resistivity of unirradiated film increases with decreasing temperature from RT to 30 K like semiconductor and irradiated film shows very weak temperature dependence. Optical absorption monotonically decreases with increasing the wavelength from 200 to 2500 nm, implying that the bandgap does not exist in the region of 0.4- 6 eV and no appreciable change was observed in the optical absorption by the ion irradiation.

**Damage formation in lithium niobate due to electronic energy loss**

Matthias Schmidt<sup>1</sup>, Jura Rensberg<sup>1</sup>, Emanuel Schmidt<sup>1</sup>, Marcel Toulemonde<sup>2</sup>, Werner Wesch<sup>1</sup>, Elke Wendler<sup>1</sup>

<sup>1</sup>*Institut fuer Festkoerperphysik, Friedrich-Schiller-Universitaet Jena, Germany*

<sup>2</sup>*CIMAP, Caen, France*

x- and z-cut lithium niobate (LiNbO<sub>3</sub>) was irradiated with 5 MeV Si, 5 MeV O and 10 MeV O ions at room temperature and 15 K and subsequently analysed by Rutherford backscattering in combination with the channelling technique (RBS/C). For the irradiation conditions used the electronic energy deposition per ion and unit depth,  $Se$ , dominates in the near surface region and reaches a maximum value of  $4.2 \text{ keV nm}^{-1}$ . This is below the common value for amorphous track formation by single ion events. However, in all cases investigated here the relative defect concentration,  $nda$ , calculated from the RBS/C spectra in the depth region of dominating electronic energy loss, steeply increases with the ion fluence  $NI$  until an amorphous layer ( $nda = 1$ ) is formed. For a fixed ion species the damage concentration increases with increasing  $Se$ , e.g. in case of Si irradiation amorphization is reached at  $NI \sim 3 \times 10^{13} \text{ cm}^{-2}$  for  $Se = 4.2 \text{ keV nm}^{-1}$  and  $NI \sim 1 \times 10^{14} \text{ cm}^{-2}$  for  $Se = 2.95 \text{ keV nm}^{-1}$ , respectively. When comparing damage formation caused by Si and O ions with an identical nominal electronic energy deposition of  $Se = 2.95 \text{ keV nm}^{-1}$ , amorphization by O ion irradiation requires an ion fluence being nearly one order of magnitude larger than that for amorphization by Si ion irradiation. This is a consequence of the various ion masses and energies resulting in various ion velocities. This velocity effect, which has been reported for swift heavy ion irradiation in various materials, results in a decreasing deposited energy density with increasing ion energy leading to a smaller defect formation efficiency at higher ion velocities. These effects including the influence of irradiation temperature and crystal cut on defect formation will be discussed in detail. Additionally, on the basis of model calculations the damage formation process for this irradiation regime will be discussed.

## Modification of ultrathin superconducting film under ion beam irradiation

Michael Tarkhov, [Kirill Prikhodko](#), Boris Gurovich, Vladimir Stolyarov, Evgeni Olshansky, Boris Goncharov, Darya Goncharova, Alexander Domantovsky, Evgenia Kuleshova

*National Research Centre Kurchatov Institute, Russia*

The authors present a technique for modification of superconducting properties of ultrathin superconducting films under ion beam irradiation. Our NbN superconducting films with thickness of a few nanometers have the critical temperature  $T_c \sim 13\text{K}$  and very high critical current density  $j_c = 12.5\text{ MA/cm}^2$ . It was been shown that ion beam irradiation influenced on the value of  $T_c$ . Ion beam irradiation technique allows to control the value of critical transition temperature in the range from  $\sim 4\text{K}$  to  $13\text{K}$  by the irradiation dose. This technique can be used in cryoelectronics to develop new functional devices.

## Implantation of Y- and Hf-Ions into a F-doped Ni-base superalloy improving the oxidation resistance at high temperatures

Hans-Eberhard Zschau<sup>1</sup>, Frederik King<sup>2</sup>, Mathias C. Galetz<sup>1</sup>, Michael Schütze<sup>1</sup>

<sup>1</sup>*DECHEMA-Forschungsinstitut, Germany*

<sup>2</sup>*Goethe-Universität Frankfurt, Germany*

At temperatures above 1000°C the widely used Ni-base superalloys with Al-contents of 3-5 wt.% are unable to form a protective aluminium oxide scale. However after doping the metal surface with fluorine by e. g. ion implantation and heating to 1050°C a dense protective alumina scale can be formed by the halogen effect [1-2] which is stable under isothermal conditions. This protective scale may partly spall during cyclic oxidation. Subsequent implantation of F and of Y or Hf resp. was carried out to improve the scale adherence for the Ni-base alloy IN738. To choose the suitable ion energies for realizing the same implantation depth for F/Y and F/Hf resp., range calculations were performed by using SRIM. The elemental concentrations for several fluences of the implanted elements have been calculated by using the Monte Carlo software T-DYN. By changing the implantation sequence the depth profiles of F and Hf show a distinct difference. If the heavy Hf-ion is implanted first, followed by light F-ion bombardment (case 1) the resulting F-concentrations reach values necessary for the fluorine effect. If the light F-ion is implanted first, followed by Hf-bombardment (case 2), the resulting F-concentration is much lower. In case 1 the results obtained by ion beam analysis with PIGE (for F) and RBS (for Hf) are in good agreement with the data of the simulation, whereas in case 2 differences occur. A similar behaviour has been obtained for the implantation of F and of Y in IN738. Based on these results oxidation tests with IN738 reveal an improved adherence of the formed protective alumina scale for implantations according to case 1. In contrast to this the samples implanted according to case 2 show the formation of a non-protective scale.

[1] H.-E. Zschau, D. Renusch, P. Masset and M. Schütze, *Materials at High Temperatures* 26, No. 1, 85-89 (2009).

[2] H.-E. Zschau, M. Schütze, *Materials Science Forum* 696, 366-371 (2011).

## Surface modifications of hydrogen storage alloy by heavy ion beams at energies from keV to MeV

Hiroshi Abe<sup>1</sup>, Shinnosuke Tokuhira<sup>2</sup>, Hirohisa Uchida<sup>2</sup>, Takeshi Ohshima<sup>1</sup>

<sup>1</sup>*Quantum Beam Science Center, Japan Atomic Energy Agency, Japan*

<sup>2</sup>*Department of Applied Science, Graduate School of Engineering, Tokai University, Japan*

This study reports the surface modifications of hydrogen storage alloys ( $\text{LaNi}_{4.6}\text{Al}_{0.4}$ ) by heavy ion beams at energy ranges from keV to MeV. This alloy is widely used as a negative electrode of Ni-MH (Nickel-Metal Hydride) battery. We aimed to improve the initial rate of hydrogen absorption using defects such as vacancies, dislocations, micro-cracks or added atoms, effectively induced into the surface region of the metal alloys [1, 2].

Oxygen (O) ion beams at acceleration energies from 100 keV to 12 MeV with a dose of  $1 \times 10^{16} \text{ cm}^{-2}$  were irradiated onto the surface of the alloys at TIARA (Takasaki Ion Accelerators for Advanced Radiation Application), JAEA (Japan Atomic Energy Agency). The hydriding rate for samples with and without O ion irradiation was measured electrochemically. As a result, the increase in hydriding rate for samples irradiated with O ion irradiation is obtained. This indicates that the modified surface is responsible for the promotion of the dissociation rate of  $\text{H}_2\text{O}$  in electrochemical process, and as a result, the initial hydrogen absorption rate is enhanced.

Since defective layer near the surface can easily be oxidized, the conductive oxide layer is formed on the sample surface by O ion beam irradiation, and the conductive oxide layer might cause the improvement of hydrogen absorption rate [2]. This paper demonstrates an effective surface treatment of hydrogen storage alloys using heavy ion beams.

[1] H. Abe, R. Morimoto, F. Satoh, Y. Azuma and H. Uchida, J. Alloys Comp. 404-406, 288 (2005).

[2] H. Abe, R. Morimoto, F. Satoh, Y. Azuma and H. Uchida, J. Alloys Compd. 408, 348 (2006).

[3] H. H. Uchida, Y. Watanabe, Y. Matsumura and H. Uchida, J. Alloys Compd. 231, 679 (1995).

## Measurement of different implanted depth profiles of fluorine in titanium aluminum using proton induced gamma emission

Daniel Brenner<sup>1</sup>, Hans-Eberhard Zschau<sup>2</sup>

<sup>1</sup>*Institut für Kernphysik, Goethe-Universität, Frankfurt a.M., Germany*

<sup>2</sup>*DEHEMA-Forschungsinstitut, Frankfurt a.M., Germany*

Due to their high specific strength at high temperatures the TiAl based alloys are believed to have a high application potential in high temperature technologies, especially in aerospace and automotive industries. In contrast to the presently used Ni-based super alloys their specific weight is reduced by about 50%. However the oxidation resistance of TiAl inhibits an industrial use at temperatures above 750°C. The oxidation resistance can be improved by using the so-called “halogen-effect”. The most promising results are achieved using fluorine. To adjust the surface treatment of TiAl with F the measurement of fluorine depth profiles plays a key role. To investigate this topic single and double implantations with different fluences of fluorine were performed. For double implantation two different profile shapes were realized. All implantations were simulated using the T-DYN software in advance. The implanted depth profiles were analyzed using the non-destructive PIGE-technique (Particle Induced Gamma Emission). Digital signal processing was used for data acquisition. The resulting fluorine profiles are also used to determine the detection limit of the existing experimental instruments.



## **The use of plasma immersion ion implantation in the high-temperature oxidation protection of low-Al-content Ti-base alloys and TiAl intermetallics**

Rossen Yankov<sup>1</sup>, Johannes Von Borany<sup>1</sup>, Bernadeta Pelic<sup>1</sup>, Alexander Donchev<sup>2</sup>, Michael Schütze<sup>2</sup>

<sup>1</sup>*Institute of Ion Beam Physics and Materials Research, Helmholtz-Zentrum  
Dresden-Rossendorf, Germany*

<sup>2</sup>*DECHEMA Forschungsinstitut, Germany*

Low-Al content Ti-base alloys and TiAl intermetallics are attractive lightweight materials for advanced medium-temperature (500°-750°C) structural applications including components such as jet engine and industrial gas turbine blades, turbocharger rotors and automotive engine valves. However, envisaged service temperatures are in the range of 750° to 1050°C at which these alloys are prone to both destructive oxidation and oxygen embrittlement. Therefore, development of surface-engineering techniques for preventing high-T environmental damage is critical in exploiting the advantages of the TiAl alloys to their fullest extent.

We propose two techniques for protecting candidate Ti-base and TiAl alloys from high-temperature (>750°C) oxidation environments. The first technique involves a single step, namely treating the alloys directly by plasma immersion ion implantation (PIII) of fluorine using a mixture of CH<sub>2</sub>F<sub>2</sub>+6.25% Ar as the precursor gas. This technique is applicable to TiAl alloys of an Al content of ~ 45 to 55 at.%. The F implant dose has been found to depend critically on the gas flow rate ratio (GFRR, i.e. CH<sub>2</sub>F<sub>2</sub>/Ar) while the resulting F depth profiles show dependence on both the GFRR and the alloy material. Optimum implantation conditions have been established under which the F-implanted alloy surface is able to form a highly protective Al<sub>2</sub>O<sub>3</sub> film upon subsequent oxidation in air. Oxidation resistance has been evaluated by thermal gravimetric analysis (TGA) at temperatures as high as 1050°C for extended exposure times.

The alternative technique is applicable to low-Al-content Ti-base alloys (< 40 at.% Al). It involves the fabrication of a barrier coating in a three-step process, namely formation of a Ti+Al layer by magnetron co-sputtering of Ti and Al followed by vacuum annealing to form a gamma-TiAl coating and, finally, PIII of fluorine. The coating so formed has been shown to prevent further oxidation of the base material at elevated temperatures.

## Study of heavy ion irradiation induced softening in various compositional ZrCuAl bulk glassy alloys

Koji Ishii<sup>1</sup>, Taishi Ishiyama<sup>1</sup>, Akihiro Iwase<sup>1</sup>, Fuminobu Hori<sup>1</sup>, Yoshihiko Yokoyama<sup>2</sup>

<sup>1</sup>*Department of Materials Science, Osaka Prefecture University, Japan*

<sup>2</sup>*Institute for Materials Research, Tohoku University, Japan*

The bulk glassy alloys, which have no long range ordered structure, are expected to be useful for various applications due to their superior mechanical properties such as hardness, strength, corrosion resistance and so on. We suggest that the properties of bulk glassy alloys are further improved by irradiation. So far, we have reported the hardness change in eutectic Zr<sub>50</sub>Cu<sub>40</sub>Al<sub>10</sub> bulk glassy alloy by electron and ion irradiations [1, 2]. On the other hand, it is known that the relaxation behavior of local domains in bulk glassy alloys by annealing is not unique but depends on their chemical compositions [3]. Hardness and local structure changes have been investigated by using micro Vickers hardness, X-ray diffraction, positron annihilation lifetime and Doppler broadening techniques for hypoeutectic Zr<sub>x</sub>Cu<sub>90-x</sub>Al<sub>10</sub> (x= 55, 60, 65) bulk glassy alloys compared to Zr<sub>50</sub>Cu<sub>40</sub>Al<sub>10</sub> eutectic alloy after 200 MeV Xe ion irradiation with a fluence of  $5 \times 10^{13}$  ions/cm<sup>2</sup>. Irradiation induced softening was observed in all composition alloys. On the other hand, remarkable change of positron lifetime, which reflects shrinking of open volume, appears only in the case of eutectic alloy. In contrast, change in positron lifetime gradually decreases with increasing of Zr concentration.

[1] Y. Fukumoto, A. Ishii, A. Iwase, Y. Yokoyama, F. Hori, J. Phys.: Conf. Ser. 225, 012010 (2010).

[2] N. Onodera, A. Ishii, Y. Fukumoto, A. Iwase, Y. Yokoyama, F. Hori, Nucl. Instrum. Method B 282, 1-3 (2012).

[3] Y. Yokoyama, T. Yamasaki, P. K. Liaw and A. Inoue, Acta Mater. 56, 6097–6108 (2008).

## **Enhanced hardness and thermal stability of copper thin films prepared by ion beam assisted deposition**

Huan Ma, Yu Zou, Ralph Spolenak

*Laboratory for Nanometallurgy, Department of Materials, ETH Zurich, Switzerland*

Materials with good mechanical properties and high thermal stability are highly desired for applications under extreme conditions, e.g. high temperatures. The strength of metallic materials can be significantly enhanced by grain refinement down to nanometer scale. Unfortunately, these nano-crystalline materials are not suitable for high-temperature applications due to their thermally sensitive microstructure. In this work, we present that ion beam assisted deposition (IBAD) has the potential to simultaneously enhance the hardness and thermal stability of material. Copper thin films with 500 nm thickness were deposited either by normal magnetron sputtering or IBAD. For ion beam energy of 1 KeV, the IBAD Cu film exhibits the maximum hardness of 5.06 GPa, which is 1.8 GPa higher than that of the normally deposited film (3.26 GPa). The significant enhancement of hardness could be due to the incorporation of ion-beam-induced point defects, which hinder dislocation activities and, therefore, harden the film. After annealing at 400°C for one hour, the grain size of the normally deposited film is increased by one order of magnitude and the hardness is decreased by 40%. However, no obvious grain growth was observed in IBAD film, the hardness of which only decreased by 16%. Even after annealing, the hardness of this IBAD film is still 1 GPa higher than the normally deposited film before annealing. The absence of grain growth of IBAD films upon annealing is attributed to the ion-beam-induced damage at grain boundaries, pinning the movement of grain boundaries. The hardness decrease without grain growth in IBAD films is probably due to the defect annihilation or agglomeration in the interior of grains.

## Influence of pulsed plasma treatment on the corrosion resistance of 12% Cr ferritic-martensitic steel

Pavel Dzhumaev<sup>1</sup>, Vladimir Yakushin<sup>1</sup>, Aung Thurein Khein<sup>1</sup>, Boris Kalin<sup>1</sup>, Maria Leontyeva-smirnova<sup>2</sup>, Irina Naumenko<sup>2</sup>, Valeriy Polsky<sup>1</sup>

<sup>1</sup>National Research Nuclear University MEPhI (Moscow Engineering Physics Institute), Russia

<sup>2</sup>JSC A.A. Bochvar All-Russian Scientific Research Institute for Inorganic Materials, Russia

12% Cr ferritic-martensitic steels are considered as a promising fuel element cladding material for new generation fast breeder reactors with liquid metal coolant. One of the promising methods for modifying the microstructure of the surface layers of steels to improve their corrosion resistance is the use of concentrated energy fluxes, in particular their treatment by high-temperature pulsed gas plasma flows (HTPPF).

The experimental results of the investigations on the corrosion resistance improvement by HTPPF treatment (including the liquid phase surface alloying method) of 12% Cr ferritic-martensitic steels (EP823 (16Cr12MoWSiVNbB) and EP900 (16Cr12MoWSiNbVCeNB)) in flowing liquid lead conditions are presented.

The surface alloying technique involved deposition of thin (0,4–0,8  $\mu\text{m}$ ) homogeneous layers of alloying elements (Al or Cr) on the outer surface of the tube and liquid-phase surface mixing of the coating and base material surface layers under HTPPF action.

Processing of chromium steels fuel cladding tubes using nitrogen pulsed plasma flows ( $\sim 20$  ms) with a specific power  $q \sim 1 \text{ MW/cm}^2$  ( $N \geq 2$ ) leads to the surface melting. At the same time hardening creates a two-dimensional nanocrystalline structure in the surface layers. The mean grain size of cellular structure is about 100 nm. Pulsed nitrogen plasma modification of the microstructure of the surface layers of fuel cladding tubes leads to an increase in their microhardness up to 50 % depending on the processing conditions.

Corrosion tests were carried out in a dynamic liquid lead loop with an increased and controlled oxygen content at the temperature of 620-650C and the test duration of 1000 - 5000 h. SEM investigations of the surface and cross-section of samples after corrosion tests have shown that the surface alloying significantly increases the corrosion resistance of the steel.

## Surface modification of low activation ferritic-martensitic steel EK181 (rusfer) by high temperature pulsed plasma flows

Olga Emelyanova<sup>1</sup>, Vladimir Yakushin<sup>1</sup>, Pavel Dzhumaev<sup>1</sup>, Maria Ganchenkova<sup>1</sup>, Boris Kalin<sup>1</sup>, Aung Khein<sup>1</sup>, Maria Leontyeva-smirnova<sup>2</sup>, Ruslan Valiev<sup>3</sup>, Nariman Enikeev<sup>3</sup>

<sup>1</sup>*National Research Nuclear University MEPhI (Moscow Engineering Physics Institute),  
Moscow, Russia*

<sup>2</sup>*JSC A.A. Bochvar All-Russian Scientific Research Institute for Inorganic Materials, Moscow,  
Russia*

<sup>3</sup>*Ufa State Aviation Technical University, Ufa, Russia*

The ferritic-martensitic steels are considered as promising materials for the fuel element claddings of the fast breeder reactors. This work presents the results of an experimental study of the pulsed plasma flows treatment effects on the microstructure and the strengthening of the chromium ferritic-martensitic steel EK 181 (16Cr12W2VTaB) surface layers. The samples used for the investigation were made in three initial states: hot-rolled and annealed, traditional heat treatment (hardening from 1100°C, tempering at 720 °C for 3 h), and nanostructured by severe plastic deformation processing (SPD).

Modification of the samples surface was made by high-temperature nitrogen pulsed plasma flows (HTPPF) with a specific energy (Q) of an incident flow changing in the range of 17–28 J/cm<sup>2</sup> with a pulse duration of 20x10<sup>-6</sup> s. The number of irradiation pulses was up to 8. The microstructure of the initial samples and samples treated by plasma flows was investigated by optical and scanning electron microscopy.

It has been found that the treatment of EK181 steel samples by nitrogen plasma flows with a specific power of ~ 1.0 MW/cm<sup>2</sup> (the number of pulses N = 3) leads to the surface melting. The heating and subsequent high-speed cooling of the surface layers make it possible to fix a non-equilibrium martensitic structure with formation of cellular nanostructure. Characteristic mean size of grain of the cellular structure is 140 - 150 nm, and the depth of the modified layer ranges from 3 to 10 microns depending on the pulsed plasma flows specific energy.

It has been shown that these microstructural changes lead to the surface hardening up to 1.20–2.4 times. The degree of microhardness increase depends on the initial state and the plasma treatment conditions (Q and N).

It is revealed that independent of the samples fabrication technology and their heat treatment, HTPPF processing allows to create the gradient materials with the similar two dimensional nanostructured surface layers.

**Copper and silver nanoparticles synthesised in PMMA by ion implantation: structure and optical properties of the nanocomposites**

V.N. Popok<sup>1</sup>, A.L. Stepanov<sup>2,3</sup>, V.F. Valeev<sup>2</sup>, V.I. Nuzhdin<sup>2</sup>, A. Mackova<sup>4</sup>, R. Miksova<sup>4</sup>

<sup>1</sup>*Aalborg University, Denmark*

<sup>2</sup>*Kazan Physical-Technical Institute Russian Academy of Sciences, Russia*

<sup>3</sup>*Kazan Federal University, Russia*

<sup>4</sup>*Nuclear Physics Institute of the Academy of Sciences of the Czech Republic and J.E. Purkinje University, Czech Republic*

In recent years, thin metal/polymer nanocomposite films attract considerable attention due to a number of practical applications. In particular, optical properties of polymers with gold, silver and copper nanoparticles (NPs) are of interest due to localized surface plasmon resonance (LSPR). These materials are considered to be promising for nanoscale plasmonics, fabrication of non-linear optical devices and optical sensors.

Polymethylmethacrylate (PMMA) samples are implanted by 40 keV Cu and 30 keV Ag ions with various fluences to synthesize metal NPs in shallow polymer layers. The produced metal/polymer nanocomposites are studied using atomic force microscopy, Rutherford back-scattering and optical transmission spectroscopies. It is found that NPs nucleation and growth are strongly fluence dependent as well as they are affected by the structural and compositional changes of PMMA. High-fluence irradiation causes considerable sputtering of the polymer surface and as a result the shallow synthesized NPs are partly towered above the surface. Implantation and particle formation significantly change optical properties of PMMA reducing transmittance in the visible range due to structural and compositional evolution and causing specific absorption band related to LSPR on NPs. The role of ion species and polymer degradation under the implantation on the LSPR is discussed and the experimental results are compared with the modelling of optical extinction of NPs. NP formation at the surface and considerable LSPR response make these composite materials promising for applications as optical sensors.

**Study of degradation of polymers irradiated by  $C_n^+$  and  $O_n^+$  9.6 MEV heavy ions**

Romana Miksova<sup>1</sup>, Petr Slepicka<sup>2</sup>, Petr Malinsky<sup>1</sup>, Anna Mackova<sup>1</sup>

<sup>1</sup>*Nuclear physics institute of the Academy of Science of the Czech Republic V.V.I., 25068 Rez, Czech Republic*

<sup>2</sup>*Department of solid state engineering, Institute of chemical technology, 166 28 Prague, Czech Republic*

Polypropylene (PP), polyethylene terephthalate (PET), polycarbonate (PC) and polyetheretherketone (PEEK) foils were irradiated with 9.6 MeV  $C_n^+$  and  $O_n^+$  ions at fluencies of  $10^{10} - 10^{13}$  ions/cm<sup>2</sup> during the experiments of heavy ion energy loss and energy straggling study in polymers. Structural and compositional changes of the implanted polymers after the irradiation are very important to estimate the influence of these effects to the experimentally determined ion energy losses. Rutherford back-scattering (RBS), elastic recoil detection analysis (ERDA) were used for the elemental compositional study, UV-Visible spectral study (UV-VIS) and Fourier Transformation Infrared spectroscopy (FTIR) were used to follow the structural changes (polymeric functional group appearance, double bonds, carbon cluster creation etc.) of the irradiated polymers. The heavy ion irradiation can cause a release of hydrogen and oxygen from the polymers penetrated by the ion beam, the chemical and structural changes, new radical appearance, polymeric chain crosslinking especially at the ion fluencies above  $10^{12}$ - $10^{13}$  ions/cm<sup>2</sup>. The compositional changes and structural changes related to the ion specie, ion irradiation fluence and the type of polymer were studied and discussed in the connection to the energy loss measurement.

The research was realized at the CANAM (Center of Accelerators and Nuclear Analytical Methods) infrastructure LM 2011019 and has been supported by project No. P108/12/G108.

**Ion-beam induced damage in polymers: removal by argon cluster ion beam**

Laurent Nittler, Jean-Jacques Pireaux

*UNamur - PMR - LISE, Belgium*

It is well known that an atomic beam can induce structural and molecular damages on organic samples [1]. It has been demonstrated that cluster ion guns ( $\text{SF}^{5+}$ ,  $\text{Au}^{3+}$ ,  $\text{C}^{60+}$ ,  $\text{Ar}^{n+}$ , ...) induced much less chemical damage on organic samples, so that the possibilities of depth profiling significantly increases. Also it has been shown on polyimide that  $\text{Ar}^{n+}$  gas cluster ion beam (GCIB) can be used to remove the damage previously induced by monoatomic Ar bombardment [2,3].

In this study we bombarded a PMMA layer with a defined amount of monoatomic  $\text{Ar}^+$  ions to voluntarily induce damage until a certain depth. By successively eroding the damaged surface by a GCIB, we show that the XPS fingerprint of the PMMA can be recovered only under certain cluster ion beam conditions of cluster size and energy. By calibrating the sputtering rates, we could also estimate the thickness of the previously damaged layer.

[1] I.P. Jain, G. Agarwal, Surf. Sci. Rep. 66, 77–172 (2011).

[2] T. Miyayama, N. Sanada, S.R. Bryan, J.S. Hammond, M. Suzuki, Surf. Interface Anal. 42, 1453–1457 (2010).

[3] C.M. Mahoney, Mass Spectrom. Rev. 29, 247–93 (2010).



**Effect of cold atmospheric pressure plasma jet on DNA change and bacterial mutation**

Chaitawat Yaopromsiri, Prutchayawoot Thopan

*Chiang Mai University, Thailand*

Cold atmospheric plasma jets have recently been developed and applied as a type of convenient and useful medical treatment tools especially for skin care. While impressive and massive successes have been achieved in the application, concerns about its safety are also growing. In this study we investigated the plasma jet effect on DNA change. It has been believed that ions with low energy can change or damage DNA in certain degree and thus cause potential mutation or cancers. Since plasma jets emit low-energy ions and also other physical and chemical agents such as radicals and photons, there must be some dangers to DNA in the cells. Our experiment utilized a home-developed cold atmospheric-pressure helium plasma jet to directly treat naked DNA plasmid pGFP with varied frequency and radiofrequency (RF) power. Plasma species were measured by using Optical Emission Spectroscopy (OES). OH, N<sub>2</sub>, N<sup>2+</sup>, and He radicals were found. After the plasma jet treatment, DNA topological form change was analyzed by gel electrophoresis. The original DNA supercoiled form was found to change to the relaxed and linear forms, indicating single strand break or double strand break. The plasma jet treated DNA was transferred into bacterial E. coli cells and a certain amount of mutation was observed. This result demonstrated that the atmospheric pressure helium plasma jet was possible to break DNA strands and thus potential to cause genetic modification of living cells.

**Plasma immersion ion implantation of Poly(lactic acid) to covalent attachment of antimicrobial agent for non-migrating antimicrobial surface**

Chanokporn Chaiwong, Tanwivat Jaikuna

*Department of Physics and Materials Science, Faculty of Science, Chiangmai University,  
Thailand*

Non-migrating antimicrobial surface is one of alternative approaches to control microbial growth or kill microbes in the vicinity that can be applied in many fields, such as packaging materials and implanted medical devices. In this work we investigated the adsorption of nisin, an antimicrobial agent, on the surface of plasma-treated poly(lactic acid) (PLA). PLA samples were functionalized using plasma immersion ion implantation of argon and nitrogen at a negative bias voltage of 15 kV. Oxygen plasma was also used to treat the samples. X-ray photoelectron spectroscopy (XPS) and Fourier transform infrared spectroscopy (FTIR) were utilized to investigate the chemical surface modification. Surface topography was obtained using atomic force microscopy (AFM). Nisin was adsorbed on the pristine and plasma-treated PLA samples. Antimicrobial activity of adsorbed nisin was evaluated against staphylococcus aureus (*s. aureus*). Diffusion of nisin from the surfaces of PLA samples was studied. The observed antimicrobial activities and the migration of nisin will be correlated to the adsorbed amount of nisin, the surface topography and the functional groups on the plasma-treated surfaces.

## Interface defects in a-Si:H/c-Si heterojunction solar cells

Alice Defresne<sup>1</sup>, Olivier Plantevin<sup>1</sup>, Igor P. Sobkowicz<sup>2,3</sup>, Pere Roca I Cabarrocas<sup>2</sup>

<sup>1</sup>*Université Paris-Sud CSNSM-CNRS, France*

<sup>2</sup>*LPICM-CNRS, France*

<sup>3</sup>*TOTAL-New Energies, USA*

Combining crystalline silicon with thin film deposition techniques has made important progress these recent years. Specifically, a-Si:H/c-Si heterojunction solar cells have now reached record efficiencies of 24.7%. They consist of a n-type crystalline silicon wafer on which a thin (~10 nm) p-type hydrogenated amorphous silicon (a-Si:H) layer is deposited by plasma enhanced CVD at low temperature (~200 °C). The electrical contact is usually achieved by sputtering a thin transparent conducting oxide (80 nm thick) on the cell. Both sputtering and plasma deposition processes may introduce defects at the c-Si/a-Si:H interface which in turn will determine the conversion efficiency of the cell. The goal of this study is to understand the fundamental aspects of this interface via defect formation using a controlled introduction of point defects. Ion implantation of argon at low energy allows the modification of the a-Si:H thin layer (about 45 nm thick in our case). We can control the depth and concentration of irradiation defects by varying the ion energy and fluence. Varying the energy from 1 keV to 20 keV, we can tune the energy loss maximum position at a depth between 4 nm and 20 nm, while defect concentration is adjusted by varying fluence. Starting at a fluence of  $1\text{E}10\text{ Ar}^+/\text{cm}^2$  we obtain a defect threshold as low as some 0.0001 at.%, showing the extreme cell sensitivity to interface defects. We follow the changes in the effective lifetime of minority carriers upon defect creation and annealing through photoconductance and low temperature photoluminescence measurements. At low energy, defects are created only in the amorphous layer, away from the crystalline interface. The role of ion induced hydrogen diffusion within the amorphous silicon layer is tentatively proposed as the origin of the heterojunction interface modification and correlated to the solar cell characteristics.

## Near-infrared waveguides in Gallium Nitride single crystal produced by MeV carbon ion implantation

Bing-Xi Xiang<sup>1</sup>, Lei Wang<sup>1</sup>, Yang Jiao<sup>2</sup>

<sup>1</sup>*Shandong University, P.R. China*

<sup>2</sup>*Shandong Normal University, P.R. China*

We report on the fabrication of planar waveguides in Gallium Nitride by 5 MeV carbon ion implantation with different fluence at room temperature. The waveguide were characterized by the methods of prism coupling, Rutherford Backscattering/Channeling and High-resolution X-ray Diffraction analysis. Positive change of extraordinary refractive index was confirmed in the waveguide region. The thermal stability of the ion-implanted GaN waveguide was investigated by annealing at different temperatures.

## Formation of SIMOX-SOI structure by high-temperature oxygen implantation

Yasushi Hoshino, Tomohiro Kamikawa, Gosuke Yachida, Jyoji Nakata

*Kanagawa University, Japan*

It is known that silicon on insulator (SOI) technology makes it possible to reduce stray capacitances and leak-currents between transistors and a substrate due to separation by insulating layer of SiO<sub>2</sub>, compared to ordinary Si-based transistors. The SOI structure is therefore expected to be energy-saving and high-performance electronic devices. However, the process to make the SOI structure is complicated and requires high costs. We performed oxygen ion implantation in silicon at very high substrate temperatures for the purpose of avoiding the damage in the SOI layer during the implantation and simultaneously stabilizing the box SiO<sub>2</sub> and the SOI-Si layers. The effect of the implantations at various temperatures (RT – 1000 °C) has been investigated, and we have compared the SOI structures formed by the present processes to that done by the ordinary ones. Such a high-temperature implantation can make it possible to reduce post-annealing process. In the present implantation, oxygen ions with 180 keV were incident on Si(001) substrates at the various substrate temperatures. The ion fluencies were in order of  $10^{17} - 10^{18}$  ions/cm<sup>2</sup>. Some of the oxygen-implanted samples were postannealed at various temperatures of more than 1000 °C. The samples have been analyzed by micro-Raman spectroscopy (MRS), Rutherford backscattering (RBS) and transmission electron microscope (TEM). In the analysis with Raman spectroscopy, we used two kinds of excitation LASERs with different wave lengths of 532 (green) and 442 (blue) nm. We first investigated the crystallinity of the SOI-Si layer by the MRS as a function of ion-fluencies. We will discuss the details of the results on SIMOX-SOI structure formed by high-temperature oxygen implantation and show the advantage of this method at the conference.

## Two-dimensional dopant profiling of gallium nitride p-n junctions by scanning capacitance microscopy

Mohamed Lamhamdi<sup>1,2</sup>, Daniel Alquier<sup>1</sup>, Frédéric Cayrel<sup>1</sup>, A.E. Bazin<sup>3</sup>, A. Yvon<sup>3</sup>, E. Collard<sup>3</sup>

<sup>1</sup>*GREMAN- Université de Tours, France*

<sup>2</sup>*ENSAK Université Hassan 1<sup>er</sup>, Morocco*

<sup>3</sup>*STMicroelectronics, Tours, France*

Gallium Nitride offers an interesting alternative for a large variety of applications even if technological challenges still have to be faced. For power devices, obtaining local p and n-type doping remains crucial. This step requires reliable characterizations to provide electrical and physical information at nano-scale. Scanning Capacitance Microscopy (SCM) measurements, combined with classical AFM imaging, can provide reliable and quantitative information. In this work, local doping of GaN is investigated as well as the impact of surface and bulk defects using AFM measurements. To do so, a thick n- on n+ GaN layers were grown by MOCVD on sapphire. Different samples were used for better understanding of GaN doping using ion implantation. First, Mg and Si were implanted on different samples using multiple energies in order to create a box-like profile to study n and p-type doping. A p-doped GaN layer was also deposited in-situ on the initial structure (reference). Samples were then annealed and prepared for characterization. Samples were then analyzed under the same conditions to extract dopant profiles and surface damages. GaN roughness, dislocation density and hexagonal pits density were first investigated, evidencing a drastic increase of pits when facing high temperature annealing. Then, the SCM measurements allowed us to distinguish reliably and qualitatively doping concentrations for the different regions (both p and n type). We first demonstrate that Si implantation may lead to n-type activation. If n and p-type regions as well as space charge one are clearly observed for the in situ Mg-doped sample, it is not the case for the Mg-implanted sample, evidencing a very low efficiency of the annealing step. Additionally, it has been possible to quantify the dopant profiles using a calibration structure. This work clearly demonstrates the interest of SCM measurements and the progresses that are still needed for obtaining local p-type doping by Mg implantation.

## Structural analysis of thin silicon layers implanted by carbon ions

N. Beisenkhanov, K. Nussupov, S. Zharikov, I. Beisembetov, B. Kenzhaliev

*Kazakh-British Technical University, Almaty, Kazakhstan*

Microcrystalline  $\mu\text{c-SiC:H}$  alloys or amorphous p-type a-SiC/nc-Si hybrid layer [1] have a very high potential as transparent window layers in thin-film solar cells. SiC antireflection coatings improve the solar cell efficiency up to 1.3 times.

Synthesis of silicon carbide layers of different thicknesses was carried out by implantation of  $^{12}\text{C}$  ions with energies 40, 10 or 2.5 keV and doses  $(3.56, 1.56, 2.7) \times 10^{17} \text{ cm}^{-2}$ , respectively, into (100) or (111) oriented silicon wafers at implantation conditions as in [2]. Through decomposition of infrared absorption spectrum, it is shown, that, in case of 10 and 40 keV, the proportion of the amount of elongated weak Si-C-bonds of the amorphous phase, strong shortened Si-C-bonds on the surface of small nanocrystals, tetrahedral Si-C-bonds of the crystalline phase after the high temperature annealing (1300-1400°C) of the layers are about 29/29/42 and 22/07/71 percent, respectively.

Intensive carbon sublimation and desorption from thin layer (2.5 keV) during long-time annealing (8 hours) at 1200–1400°C are observed. LO-phonon peak of SiC were observed from layers with a thickness less than 30 nm (10 keV). Analysis of growth in the number of the tetrahedral Si-C-bonds shows, that, in case of 40 keV, synthesis of SiC nanocrystals in (100)-oriented silicon substrate is preferably carried out at temperatures of 1000–1200°C and, in Si(111) – at 1200–1300°C. Detection of LO-phonon peak of SiC allowed to calculate the values of low-frequency dielectric constant  $\epsilon_0$  (9.82), the effective charge  $e^*/e$  (0.89) and the dimensionless parameter  $\rho$  (0.25). X-ray reflectometry data on the intensity fluctuations near the main maximum are explained by a density variation in the layer depth from 2.55 g/cm<sup>3</sup> (SiC<sub>0.25</sub> layer), 2.90 g/cm<sup>3</sup> (SiC<sub>0.65</sub>) up to 3.29 g/cm<sup>3</sup> (SiC<sub>1.36</sub>).

[1] J. Ma, J. Ni, J. Zhang et al., Solar Energy Materials and Solar Cells. 114, 9 (2013).

[2] K.Kh. Nussupov, V.O. Sigle, N.B. Beisenkhanov, Nucl. Instr. Meth. B 82, 69 (1993).

## Silicon oxide films prepared by bipolar type plasma immersion ion implantation

Nakao Setsuo<sup>1</sup>, Atsushi Kinomura<sup>1</sup>, Hiroshi Kojima<sup>2</sup>

<sup>1</sup>*AIST, Japan*

<sup>2</sup>*Hiroshima Prefectural Technology Research Institute, Japan*

Silicon based films, such as  $\text{SiO}_x$ ,  $\text{SiN}_x$  and  $\text{SiCN}$ , are expected to be the protecting coatings for the soft materials, such as polycarbonate, because of high transparency, high abrasion resistance and the impermeability of moisture and oxygen. A low temperature deposition process is necessary to perform the coatings on such polymeric substrates. However, low temperature deposition usually degrades the properties and causes the poor adhesion between the films and the substrates.

Plasma immersion ion implantation (PIII), sometimes called plasma based ion implantation (PBII), has a potential to improve the microstructure of the films and the adhesion properties at low temperature by ion bombardment effect. In the review paper [1], the surface modification of engineering polymers is described in detail using PBII system. However, the improvement of the microstructure of the films using PIII system is not always clarified yet. In this study, silicon oxide ( $\text{SiO}_x$ ) films are prepared at different conditions by bipolar type PIII system and the microstructure and composition are examined.

$\text{SiO}_x$  films are deposited on Si substrates using source gases of tetramethylsilane (TMS:  $\text{Si}(\text{CH}_3)_4$ ) and  $\text{O}_2$ . The ratio of O to Si increases up to 2 with increasing  $\text{O}_2$  flow rate. The results of XRD measurements show that no significant peak appears except for the peak originating from Si substrate. These results suggest that the compositional ratio of O to Si can be controlled by the  $\text{O}_2$  flow rate and the prepared films have amorphous nature. The details will be presented.

[1] A. Toth, K. Kereszturi, M. Mohai and I. Bertoti, *Surf. Coat. Technol.* 204, 2898 (2010).



## Implantation damage in a-, c- and m-plane GaN

Katharina Lorenz<sup>1</sup>, N. Catarino<sup>1</sup>, A. Redondo-Cubero<sup>1</sup>, E. Alves<sup>1</sup>, M. P. Chauvat<sup>2</sup>, P. Ruterana<sup>2</sup>, E. Wendler<sup>3</sup>

<sup>1</sup> *Instituto Superior Técnico, IPFN Lisbon, Portugal*

<sup>2</sup> *ENSICAEN, France*

<sup>3</sup> *Friedrich-Schiller-Universität Jena, Germany*

Despite the overwhelming success of blue LEDs and lasers based on InGaN/GaN, III-nitride devices emitting at longer wavelength still suffer from low efficiencies due to strong polarization effects in conventional c-plane wurtzite material. Non-polar GaN grown on the a- or m-plane of the wurtzite lattice are under intense investigation in order to avoid these polarization effects. Implantation damage build-up in c-GaN has been investigated by several groups while the radiation effects on non-polar material remain widely unknown. Recently it was suggested that a-GaN is more resistant to implantation damage than c-GaN [1].

In this work, a-, c- and m-plane epitaxial GaN layers were implanted with 200 keV Ar-ions at 15 K with fluences ranging from  $2 \times 10^{12}$  to  $4 \times 10^{16}$  cm<sup>-2</sup>. In-situ Rutherford Backscattering Spectrometry in the Channelling mode was performed, measuring the damage after each implantation step without changing the sample temperature. Ex-situ transmission electron microscopy was carried out on selected samples. The damage build-up proceeds in three steps separated by large fluence regions where the maximum damage level saturates. While the three steps occur at similar fluences for the three orientations, the second saturation regime reveals a significantly lower damage level in a-plane layers while m- and c-plane samples have a similar behaviour with 3-4 times higher damage levels. The complete loss of the channelling effect is observed in all crystals at fluences around  $1-3 \times 10^{16}$  cm<sup>-2</sup> occurring first in c-GaN, then in m-GaN and finally in a-GaN. This loss of monocrystalline order is due to the formation of two nanocrystalline layers one at the surface and one buried at a deeper depth. The position of the latter is found between the depths of maximum nuclear energy deposition and maximum Ar-concentration.

[1] N. Catarino, K. Lorenz et al., Europhysics Lett. 97, 68004 (2012).

## Comparison of damage formation in low-temperature Ar implanted In-group V semiconductors

Elke Wendler<sup>1</sup>, Rüdiger Goldhahn<sup>2</sup>, Katharina Lorenz<sup>3</sup>, Lutz Wendler<sup>4</sup>

<sup>1</sup>*Institut fuer Festkoerperphysik, Friedrich-Schiller-Universitaet Jena, Germany*

<sup>2</sup>*Abteilung Materialphysik, Otto-von-Guericke-Universität Magdeburg, Germany*

<sup>3</sup>*Instituto Superior Técnico, IPFN Lisbon, Portugal*

<sup>4</sup>*Friedrich-Schiller-Universitaet Jena, Germany*

Ion implantation induced damage formation in semiconductors has been studied since many years. However, there is continuous research in this field because the microscopic processes and the role of atomic binding properties during ion-beam induced defect formation are not yet fully understood. In this presentation various In-group V semiconductors (InN, InP, InAs and InSb) are compared with respect to damage formation during low-temperature Ar ion implantation. Rutherford backscattering spectrometry in channelling configuration (RBS) is used for quantification of damage. Ar ion implantation and subsequent RBS analysis are performed in a special target chamber at 15 K without change of the temperature or the environment of the samples. From the RBS spectra measured in aligned and random direction the depth distribution of damage is calculated. The evolution of maximum damage versus ion fluence is well represented assuming damage formation by two processes: (i) by direct ion impacts and (ii) by stimulated growth of damage already existing from previous ions. The corresponding cross-sections are related to quantities representing the primary energies deposited in the displacement of lattice atoms and in electronic interactions by empirical formulas [1, 2]. In the case of InN, these dependencies are used to estimate a lower limit of the displacement energy of about 12 eV. Further it is shown that the cross sections of direct impact damage formation decreases exponentially with increasing iconicity of the materials which increases with decreasing mass of the group-V element. The decrease as a function of the iconicity is consistent with general concepts for classifying crystalline materials with respect to their amorphisibility by ion irradiation [3].

[1] E. Wendler, L. Wendler, Appl. Phys. Lett. 100, 192108 (2012).

[2] E. Wendler, M. Schilling, L. Wendler, Vacuum 105, 102 (2014).

[3] K. Trachenko, J. Phys.: Condens. Matter 16, R1491 (2004).

## Surface treatment of DLC films by reactive Ar/CF<sub>4</sub> high power pulsed magnetron sputtering plasmas

Takashi Kimura<sup>1</sup>, Ryotaro Nishimura<sup>1</sup>, Kingo Azuma<sup>2</sup>, Setsuo Nakao<sup>3</sup>, Tsutomu Sonoda<sup>3</sup>,  
Takeshi Kusumori<sup>3</sup>, Kimihiro Ozaki<sup>3</sup>

<sup>1</sup>*Nagoya Institute of Technology, Japan*

<sup>2</sup>*University of Hyogo, Japan*

<sup>3</sup>*National Institute of Advanced Industrial Science and Technology (AIST), Japan*

DLC films have attracted for material industries because they have unique properties, such as high hardness, low friction, chemical inertness, high wear resistance and optical transparency. Hydrogen-free and hydrogenated DLCs have been conventionally deposited by physical vapor deposition and plasma enhanced chemical vapor deposition, and are widely used in various industries. The applications of fluorinated DLC thin films deposited by plasmas containing fluorocarbon gases to the microelectronics and medical fields have been also expected due to functionality of low dielectric constants and highly hydrophobic properties. Recently, high power pulsed magnetron sputtering (HPPS) technique has been attracted. In addition to improvement of ionization rate of target materials, the technique can take another advantage of functionality of films deposited by pulse magnetron sputter plasma of reactive gas mixture, because high density of active species can be also achieved in the plasmas.

In this study, DLC films are firstly deposited by HPPS of pure Ar gas and then the surface treatment of films are carried out by HPPS of Ar/CF<sub>4</sub> mixture. Both the mechanical properties of film surface related to hardness and surface energy and the composition of film surface are investigated, changing the treatment time (5-30 min. ) by Ar/CF<sub>4</sub> HPPS and CF<sub>4</sub> fraction (2.5-10%). The results show that the contact angle increases from 65 degree (fluorine free DLC) to 110 degree (fluorinated DLC) owing to increase in CF<sub>x</sub> content on the film surface, whereas the hardness relatively abruptly decreases with increase in CF<sub>4</sub> fraction. These results suggest that the film properties, such as film hardness and contact angle, can be controlled by an appropriate treatment time under the condition of low CF<sub>4</sub> fraction. The details will be presented.

## **In situ variations of the scintillation characteristics in GaN and CdS layers under irradiation by 1.6 MeV protons**

Tomas Ceponis, Eugenijus Gaubas, Jevgenij Pavlov, Audrius Tekorius

*Vilnius University, Lithuania*

Evolution of the non-radiative and radiative recombination in GaN and CdS 2.5-20 mkm thick layers has been examined by the in situ measurements of the 1.6 MeV proton induced luminescence and laser excited photoconductivity characteristics. The ex situ characteristics of the microwave probed photoconductivity and steady-state/time-resolved photoluminescence spectroscopy are compared for 1.6 MeV protons and reactor neutrons irradiated GaN. It has been revealed that proton excited luminescence intensity ascribed to the radiative recombination through defects is obtained to be significantly larger in comparison with laser excited photoluminescence spectral bands. The defect introduction rate has been evaluated by the comparative analysis of the laser and proton beam induced luminescence for the examined GaN and CdS layers. The difference of a carrier pair generation mechanism inherent for light and for a proton beam has been revealed and discussed.

## **Operation characteristics and radiation damage of particle detectors based on GaN**

Eugenijus Gaubas, Tomas Ceponis, Jevgenij Pavlov, Jozas Vysniauskas

*Vilnius University, Lithuania*

The pulsed characteristics of the Schottky diode and capacitor type detectors based on GaN have been simulated using a drift-diffusion and Ramo's current models. The drift-diffusion current simulations have been implemented by employing the software package Synopsys TCAD Sentaurus. Particle detection is emulated through photo-excitation of an excess carrier domain at different locations of the active volume of a detector. The bipolar and monopolar drift regimes have been analyzed by applying the Ramo's current model. It has been shown that the pulse shape of current strongly depends on the excess carrier injection location due to the considerable difference of the electron and hole mobility in GaN and changing of the bipolar to the monopolar drift regimes.

The combined charge collection and scintillation detection regimes have been also considered. The radiation hardness and operation characteristics have been evaluated based on the results obtained during in situ measurements of the proton induced luminescence spectral and fluence dependent characteristics. The reliable detector operation range has been estimated by analysis of the radiation introduced centres of radiative and non-radiative recombination.

## Studies redistribution of implanted boron and nitrogen in a- and c-oriented SiC during anneal

Alexander Suvorov<sup>1</sup>, Kenneth Irvine<sup>1</sup>, Igor Usov<sup>2</sup>

<sup>1</sup>*CREE, INC., USA*

<sup>2</sup>*Los Alamos National Laboratory, USA*

High channel mobility and discovery of excellent ion implantation induced lattice damage recovery in a-oriented 4H-SiC stimulated a number of studies aimed at comparison of electronic devices made out of SiC with different crystallographic orientations. In addition to promising device parameters, ion implanted a-oriented 4H-SiC demonstrated suppressed surface roughening, lack of cubic polytype inclusions, and low sheet resistance upon annealing. A possibility to reduce implantation and annealing temperatures, which is crucial for device processing, was also suggested for a-oriented 4H-SiC. SIMS concentration profile measurements revealed that diffusion depth of implanted atoms in a-oriented 4H-SiC was noticeably deeper compared to c-oriented 4H-SiC. From a device fabrication viewpoint, location of implanted boron atoms must be precisely controlled and their redistribution, induced by post implantation annealing, should be preferably suppressed. In this report, we'll present a study of B- and N-implanted atoms redistribution in a- and c-oriented 4H-SiC induced by annealing. 4H-SiC samples of both orientations implanted with B<sup>+</sup> ions and co-implanted with N<sup>+</sup>/B<sup>+</sup> ions at room temperature and subsequently annealed at 1700°C for 30 minutes. The annealing influence on in- and out-diffusion of B atoms will be presented and a method to suppress deep B diffusion by nitrogen implantation will be demonstrated.

## **The influence of the ion beam on the structure and optical properties of Titanium Nitride nano-scale thin films.**

Ibrahim Odeh, Rajaa Elian

*Yarmouk University, Jordan*

Titanium Nitride nano-scale thin films have been prepared by ion beam assisted reactive DC magnetron sputtering. The films are characterized by XRD, SEM and TEM. The films are found to be amorphous. The effect of the use of ion beam during deposition was evident from smoothness of film surface (SEM and TEM images) and modifications in optical properties. Investigation of the optical constants show stable refractive index dominating most of the visible range. The films are not highly absorptive in the visible range. An energy gap of  $2.9 \pm 0.1\text{eV}$  is estimated for the IBAD amorphous Titanium Nitride nano-thin films. The stability of the films at normal laboratory environment in addition to the golden colour make the nano-thin films suitable for hard and decorative coatings.

## Pulsed laser irradiation-induced microstructures in the Mn ion implanted Si

Muneyuki Naito<sup>1</sup>, Yusuke Koshiba<sup>2</sup>, Akira Sugimura<sup>2</sup>, Tamao Aoki<sup>2</sup>, Ikurou Umezu<sup>2</sup>, Ryo Yamada<sup>1</sup>, Nobuya Machida<sup>1</sup>

<sup>1</sup>*Department of Chemistry, Konan University, Japan*

<sup>2</sup>*Department of Physics, Konan University, Japan*

Intermediate band semiconductors have attracted considerable attention due to their potential applications in photovoltaic devices such as high performance solar cells. Ion implantation combined with pulsed laser melting is a promising way to fabricate supersaturated semiconductors with intermediate band structures. To optimize physical properties of such supersaturated semiconductors detailed structural information is required. In the present study, we synthesized Mn-hyperdoped Si using ion implantation technique and examined microstructural change induced by pulsed laser melting in the ion-implanted region using transmission electron microscopy (TEM).

Single crystalline Si(001) wafers were irradiated with 65 keV Mn ions to a fluence of  $1.0 \times 10^{15} / \text{cm}^2$  at room temperature. Pulsed laser melting was performed using YAG laser beam (355 nm). Cross-sectional TEM samples were prepared by a combination of mechanical polishing and ion thinning. Microstructures of as-implanted and pulsed laser melted samples were investigated using a JEOL JEM-2100 electron microscope. Elemental distributions were analyzed using energy dispersive X-ray spectroscopy (EDS) and X-ray photoelectron spectroscopy (XPS).

Cross-sectional TEM and nanobeam electron diffraction experiments revealed that the amorphous Si layer was formed on the topmost layer of the as-implanted sample. After pulsed laser irradiation with an appropriate laser intensity the surface amorphous layer recrystallized into single crystalline Si without the formation of planar defects such as stacking faults and twins. EDS and XPS analyses indicated that Mn migration to the surface region became pronounced with increasing laser fluence. Furthermore, amorphous regions with relatively high Mn concentration were formed via cellular breakdown. We discuss the formation process of pulsed laser melting induced microstructures in the Mn implanted Si on the basis of the atomistic structural information.



## **Formation of amorphous silicon carbonitride diaphragm for environmental-cell transmission electron microscope by low-energy ion beam induced chemical vapor deposition**

Takaomi Matsutani<sup>1</sup>, Tadahiro Kawasaki<sup>2</sup>, Kayo Yamasaki<sup>1</sup>, Norihiro Imaeda<sup>2</sup>

<sup>1</sup>*Department of Electric & Electronic Engineering, Kinki University, Japan*

<sup>2</sup>*Department of Electrical Engineering, Nagoya University, Japan*

Formation of amorphous silicon carbonitride (a-SiCN) diaphragm for environmental-cell transmission electron microscope (E-TEM) was achieved by a low-energy ion beam induced chemical vapor deposition (LEIBICVD) method with hexamethyldisilazane (HMDSN). E-TEM has been developed to determine the reaction mechanism of catalytic gold nanoparticles and the behaviour of biological specimen. E-TEM includes a specimen holder with a small chamber that employs a diaphragm to isolate the vacuum for TEM observations from the reaction gas about the specimen. The diaphragm is the most important component of the E-TEM system because it both maintains the pressure difference between the vacuum and the reaction gas and allows an electron beam to pass through it. Therefore, the diaphragm should have the conditions of high hardness, no pin-hole, no electron diffraction contrast, and low electron scattering.

The present study investigates the suitability of a-SiCN film for the diaphragm of the E-TEM. Films for the diaphragm were prepared by LEIBICVD. One of advantages of the LEIBICVD technique is that film deposition with smooth surface can be carried out.

Desorption of CH<sub>3</sub> and NH in the films which were enhanced by increasing of ion energy was confirmed by Fourier transform infrared spectroscopy and X-ray photoelectron spectroscopy. The films were amorphous and transparent at 200 kV was observed by TEM. The increasing of the nitrogen concentration and the decreasing of the hydrogen bonds in the film led to increase the hardness of the film was confirmed by the pressure resistant test.

## Interdependence between training and magnetization reversal in granular Co-CoO exchange bias systems

Enric Menéndez Dalmáu<sup>1</sup>, Thiago Dias<sup>2</sup>, André Vantomme<sup>1</sup>, Kristiaan Temst<sup>1</sup>, Julian Geshev<sup>2</sup>, José Francisco Lopez-Barbera<sup>4</sup>, Josep Nogués<sup>4,5</sup>, Roland Steitz<sup>6</sup>, Brian J. Kirby<sup>7</sup>, Julie A. Borchers<sup>7</sup>, Lino Pereira<sup>1</sup>

<sup>1</sup> IKS, KU Leuven, Belgium

<sup>2</sup> Instituto de Física, Universidade Federal do Rio Grande do Sul (UFRGS), Porto Alegre, 91501-970 Rio Grande do Sul, Brazil

<sup>4</sup> ICN2-Institut Català de Nanociència i Nanotecnologia, Campus UAB, 08193 Bellaterra, Barcelona, Spain

<sup>5</sup> ICREA-Institució Catalana de Recerca i Estudis Avançats, Barcelona, Spain

<sup>6</sup> Helmholtz-Zentrum Berlin für Materialien und Energie GmbH, 14109 Berlin, Germany

<sup>7</sup> NIST Center for Neutron Research, National Institute of Standards and Technology, Gaithersburg, Maryland 20899, USA

Controlled O ion implantation in Co thin films has been shown to be an advantageous route to improving the magnetic properties of Co-CoO exchange bias (EB) systems by forming multiple nanoscaled ferromagnetic (Co)/antiferromagnetic (CoO) interfaces homogeneously distributed throughout the Co layer. By designing the implantation conditions and the structure of the films, uniform O profiles across the Co layer can be achieved using a single-energy ion implantation approach. This results in superior properties (e.g., enhanced exchange bias loop shifts or increased blocking temperature) with respect to both Co/CoO bilayers and O-implanted Co films with a Gaussian-like O depth profile. The interdependence between training and magnetization reversal in these granular Co-CoO systems with a uniform distribution of O (i.e., CoO) along the Co layer is demonstrated by polarized neutron reflectometry. While high-fluence O-implanted thin films show reduced relative training values and no asymmetry in magnetization reversal (reversals by domain wall nucleation and motion), low-fluence O ion implantation results in an increased relative training and a magnetization reversal asymmetry between the first descending and the first ascending branches. Whereas the untrained decreasing field reversal occurs mainly by domain wall nucleation and motion, traces of a domain rotation contribution are evidenced in the increasing field reversal. This is explained by the evolution of the CoO structure and the contribution of the out-of-plane magnetization with ion implantation. The amount of incorporated O, which determines the threshold between both behaviors, is around 20 at.%. This reveals that the interdependence between training and magnetization reversal is insensitive to the morphology of the constituents (i.e., granular or layered), indicating that this is an intrinsic EB effect, which can be tailored by the interplay between the intrinsic properties of the materials and ion implantation.

**Ion beam solutions for surface synthesis, modification and patterning**

Alfonz Luca, Alexander Hoerold, Frank Richter, Margit Sarstedt

*Roth & Rau AG, Germany*

The presentation is focusing on the topic of the principle and advantages of our ion beam processing equipment for micro and nanometer surface treatment. As we provide a broad product portfolio in ion beam technology we will here focus on two different systems. The IonScan series as a production ready tool is a scanning technique with a focused ion beam. This allows local correction of surfaces. The ion beam source with full automatic RF matching network is developed for this purpose and is used successfully and stable in the semiconductor industry for high volume production. One of the main applications is ion beam trimming i.e. tuning of resonant frequency of SAW and BAW filters, where inhomogeneities over the wafer and wafer to wafer during the whole production line would lead to high spread of frequencies and sequentially to a high failure rate. The similar principle of ion beam scanning is successfully applied for deterministic correction of the form of optical surfaces also known as ion beam figuring (IBF). The Gaussian removal profiles with different sizes ranging from sub millimeter to some cm (FWHM) are as predestinated for manufacturing optics of variety of sizes and correcting small and high spatial frequencies left by preprocesses.

With the IonSys series, based on our in-house developed ion beam sources, we offer a system for sensitive and well controllable surface processes for high-precision deposition or etching processes. These etching processes are used for e.g. magnetoresistance nanopillars, facets etching and ion beam smoothing. The deposition processes are used for multilayer coatings, X-ray filters, optical elements, anti-reflective coating, highly reflective mirrors, sensors or gradient layers. Especially characteristic with the IonSys is the excellent etch rate and deposition uniformity that meets the highest standards of reproducibility and stability. The components used in the IonSys set the standard for high quality ion beam processes.

## Ion – induced nanostructures on surfaces: comparing the effect of slow highly charged ions to grazing incidence swift heavy ions

Brigitte Ban-d'Etat<sup>1</sup>, Pierre Salou<sup>1</sup>, Friedrich Aumayr<sup>2</sup>, Elisabeth Gruber<sup>2</sup>, Abdenacer Benyagoub<sup>1</sup>, Clara Grygiel<sup>1</sup>, Stéphane Guillous<sup>1</sup>, Delphine Levavasseur<sup>1</sup>, Jimmy Rangamma<sup>1</sup>, Henning Lebius<sup>1</sup>, Marika Schleberger<sup>3</sup>

<sup>1</sup>CIMAP (CEA-CNRS-ENSICAEN-UCBN), Bd Henri Becquerel, 14070 Caen Cedex 5, France

<sup>2</sup>Inst. of Applied Physics, TU Wien – Vienna University of Technology, 1040 Vienna, Austria

<sup>3</sup>Fakultät für Physik and CENide, Universität Duisburg-Essen, Germany

Ion impact on surfaces can induce surface modifications on the nano-scale, like hillocks, pits or craters [1]. To study the mechanisms responsible for nanostructure formation, we compare the effects of two different types of ions: slow highly charged ions (HCI), where mainly the potential energy plays a role in the surface structuring process [1-5], as well as swift heavy ions (SHI), where the kinetic energy is important [1, 6-8]. For both types of ions the surface damage process usually exhibits a threshold, either in the charge state (HCI) or the kinetic energy (SHI) [1]. While both types of ions excite the electronic system of the target, they induce their main damage in different locations: slow HCI produce predominantly surface damage, whereas SHI do their damage in the bulk (ion track). In our comparison, we therefore concentrate on grazing incidence with SHI. This collision geometry brings the track to a region close to the surface [6], comparable with the shallow damage of slow HCI. We present the results of our comparative studies carried out with normal incidence slow HCI from the ARIBE facility and grazing incidence SHI from the IRRSUD line (at GANIL) impacting on three target materials, CaF<sub>2</sub>, SrTiO<sub>3</sub> and TiO<sub>2</sub> and discuss similarities and differences in the mechanisms responsible for nanostructure formation.

The experiments were supported by the French-Austrian collaboration SIISU, co-financed by ANR (France) and FWF (Austria).

[1] F. Aumayr, et al., J. Phys.: Cond. Mat. 23, 393001 (2011).

[2] A.S. El-Said, et al., Phys. Rev. Lett. 100, 237601 (2008).

[3] R. Heller, et al., Phys. Rev. Lett. 101, 096102 (2008).

[4] A.S. El-Said, et al., Phys. Rev. Lett. 109, 117602 (2012).

[5] R. Ritter, et al., Appl. Phys. Lett. 102, 063112 (2013).

[6] S. Akcöltekin et al., Nature Nanotechn. 2, 290 (2007).

[7] S. Akcöltekin et al., Appl. Phys. Lett. 98, 103103 (2011).

[8] O. Ochedowski et al., Appl. Phys. Lett. 102, 153103 (2013).

## Nano-structured surfaces by low energy ion beam sputtering of amorphous metal silicide films

Hans Hofsäss<sup>1</sup>, Kun Zhang<sup>2</sup>, Christoph Brüsewitz<sup>2</sup>, Clemens Beckmann<sup>2</sup>

<sup>1</sup>University Göttingen, 2nd Institute of Physics, Germany

<sup>2</sup>University Göttingen, Germany

It is well known that metallic surfactants induce pronounced dot and ripple patterns on Si substrate surfaces during normal ion incidence sputter erosion. These surfactant atoms are co-deposited on the substrate surface either from intentional co-deposition or inadvertently contaminations from sputtering of the vacuum chamber walls. In this contribution we investigate the pattern formation on amorphous  $\text{Fe}_x\text{Si}_{1-x}$  thin films with different Fe atomic fraction  $x$ , irradiated with Xe ions of 5 keV and 10 keV energies and normal incidence. In this situation the Fe atoms work as surfactants, but are supplied from the bulk of the substrate. The resulting surface morphologies were examined ex-situ by AFM, while the Fe concentration and the Fe depth profiles were determined with RBS and high resolution RBS. Some samples were also prepared with isotopically enriched 57-Fe and characterized with Mössbauer spectroscopy. Nanopattern are formed on the substrates with  $x = 0.02 - 0.08$ . In this case Fe atoms accumulate in the surface near region (13 nm in depth) after ion irradiation, revealing a phase separation towards a  $\text{FeSi}_2$  phase. For the samples with  $x > 0.09$ , the average Fe concentration near the surface exceeds  $x=0.33$  and the surface remains flat. For  $x < 0.02$  no pattern formation occurs. The results give further evidence of phase separation as a major driving force for metal surfactant induced the pattern formation on Si substrates.

## Shape elongation of embedded Zn nanoparticles irradiated with swift heavy ions of different species and energies

Hiro Amekura<sup>1</sup>, Satyabrata Mohapatra<sup>2</sup>, Devesh Avasthi<sup>3</sup>, Nariaki Okubo<sup>4</sup>, Norito Ishikawa<sup>4</sup>

<sup>1</sup>*Nat. Inst. for Mater. Sci., Japan*

<sup>2</sup>*Guru Gobind Singh Indraprastha Univ., India*

<sup>3</sup>*Inter-University Accelerator Centre, India*

<sup>4</sup>*Japan Atomic Energy Agency, Japan*

The elongation of metal nanoparticles (NPs) in silica induced by swift heavy ion (SHI) irradiation has been receiving much attention. In this paper, the fluence dependence of the shape elongation of Zn NPs in silica are discussed under seven different ion species and energies, i.e., 200 MeV Au, 200 MeV Xe, 60 MeV Ti, 140 MeV Si, 50 MeV Si, 8 MeV Si, and 1.7 MeV Si. The degrees of the shape elongation were evaluated by the optical linear dichroism spectroscopy [1], and were plotted with the electronic energy deposition, i.e., the product of the electronic stopping power  $S_e$  and the fluence  $F$ . The scaling using the electronic energy deposition was successful for the SHI beams having higher  $S_e$  than  $\sim 3$  keV/nm, i.e., 200 MeV Au, 200 MeV Xe, 60 MeV Ti, and 8 MeV Si. The data from these beams fell on roughly the same curve when plotted with the electronic energy deposition, although it was not the case for the beams with lower  $S_e$  than  $\sim 3$  keV/nm, i.e., 140 MeV Si and 1.7 MeV Si.

Recently it has been proposed that (assumption A) “the low-density cores of the ion-tracks in silica played an important role for the shape elongation.” Furthermore, it was also believed that (assumption B) “the low-density cores were formed by the vaporization of silica in the tracks.” According to the thermal spike calculations, the 200 MeV Xe irradiation induces the vaporization of silica cores but the 60 MeV Ti irradiation does not. If both the assumptions were correct, a big difference could be observed in the elongation efficiency between the two beams, because of with/without the low-density cores. However, the difference was approximately a factor of  $\sim 3$ , which can be explained by the above-mentioned scaling, i.e., the difference in  $S_e$  between 200 MeV Xe and 60 MeV Ti beams. Consequently, either of the two assumptions, A or B, probably the latter, should be excluded.

[1] H. Amekura, et al. Phys. Rev. B 83, 205401 (2011).

## Vibrational dynamics of Sn nanoparticles synthesized by ion implantation in amorphous SiO<sub>2</sub>

Sébastien Couet<sup>1</sup>, Yana De Pauw<sup>1</sup>, Rudolf Rueffer<sup>2</sup>, Margriet Van Bael<sup>3</sup>, Kristiaan Temst<sup>1</sup>, André Vantomme<sup>1</sup>, Kelly Houben<sup>3</sup>, Sara Bals<sup>4</sup>, Maria Filippou<sup>4</sup>, Sam Roelants<sup>4</sup>, Bart Partoens<sup>4</sup>, Francois Peeters<sup>4</sup>

<sup>1</sup>*IKS, KU Leuven, Belgium*

<sup>2</sup>*European Synchrotron Radiation Facility, France*

<sup>3</sup>*Laboratory of Solid-State Physics and Magnetism, KU Leuven, Belgium*

<sup>4</sup>*University of Antwerpen, Belgium*

In the last decade, metallic particles embedded in an insulating matrix have been intensively investigated for their optical and electro-optical properties. These systems are also ideal candidates to study how superconductivity evolves in confined nanoparticles. Resolving their vibrational properties, embodied in the phonon density of states (PDOS), is a key aspect since it is expected that the electron-phonon coupling is modified in nanoscale structures. However, it remains extremely challenging to isolate and measure the PDOS of embedded nanoparticles.

In this research, we have used the isotope-sensitive technique of nuclear inelastic scattering to study the vibrational dynamics of Sn nanoparticles embedded in an amorphous SiO<sub>2</sub> matrix. Isotopically pure <sup>119</sup>Sn has been implanted in SiO<sub>2</sub>. The implantation process allowed to control the size of the nanoparticles (10 to 30 nm) and hence to study the size dependent evolution of their vibrational properties. HR-TEM confirmed the single crystalline nature of the nanoparticles and the eventual presence of a metallic core/oxide shell structure. The experimental phonon spectra have been compared to *ab-initio* calculations of bulk Sn.

We found that the experimental PDOS could be well represented as a combination of Sn and SnO<sub>2</sub> PDOS, the ratio of each component depending on the particle size and thickness of the oxide shell. A gradual broadening of the spectrum is observed for decreasing particle sizes. This broadening is surprisingly well reproduced by taking into account a decreasing phonon lifetime with particle size. These measurements provide a unique insight in the vibrational properties of embedded nanoparticles and the potential influence of a matrix around them. We are currently developing methods to measure the superconducting properties of these nanoparticles and link them to the observed change in the PDOS.

**Ion beam analysis in a helium ion microscope - concepts, challenges and first experiments -**

René Heller, Nico Klingner, Stefan Facsko, Johannes Von Borany

*Helmholtz-Zentrum Dresden-Rossendorf, Bautzner Landstr. 400, 01328 Dresden, Germany*

Helium ion microscopes (HIM) have become powerful imaging devices within the last decade. Their excellent lateral resolution and the ultimate depth of field make them a unique tool in surface imaging. However, so far there is no possibility to analyze target compositions (elements) in a quantitative manner.

In this contribution we present concepts as well as first experiments on the capability, efficiency and the limits of applying (Rutherford) Backscattering Spectrometry (RBS) within a HIM device to image samples with target mass contrast and to analyze target compositions. In particular, the capability of different kind of particle detectors (Si detector, TOF, electrostatic and magnetic analyzers) with respect to their use for IBA in a HIM will be discussed.

The basic considerations and design studies are accompanied by first He backscattering investigations with by use of an electrostatic analyzer.



## Magneto-optical study of ordered composite nanosystems made by masked bi-metal ion implantation

Nianhua Peng<sup>1</sup>, Wei Guan<sup>2</sup>, Jing Jing Wang<sup>3</sup>, Chris Jeynes<sup>1</sup>, Russell Gwilliam<sup>1</sup>, Roger Webb<sup>1</sup>, Beverley Inkson<sup>4</sup>, Günter Möbus<sup>4</sup>

<sup>1</sup>*Surrey Ion Beam Centre, University of Surrey, Guildford GU2 7XH, England*

<sup>2</sup>*School of Physics and Astronomy, The University of Edinburgh, James Clerk Maxwell Building, Mayfield Road, Edinburgh EH9 3JZ, Scotland*

<sup>3</sup>*Centre for Science, Engineering and Technology, Trinity College Dublin, College Green, Dublin 2, Ireland*

<sup>4</sup>*Department of Materials Science and Engineering, The University of Sheffield, Sir Robert Hadfield Building, Mappin Street, Sheffield S1 3JD, England*

Many unusual optical properties and a wide range of novel applications have been demonstrated by nanostructures of noble metals such as gold (Au) and platinum (Pt), in particular those associated with localized surface plasmon resonances. Magnetic nanoparticles of iron (Fe) and cobalt (Co) have long been a focus of research because of not only their applications in data storage, medicine, imaging, but also being special candidates for fundamental magnetic study. An effective approach to integrate these two distinct functions into one composite nanosystem would offer an even greater opportunity for future research and application.

We have developed a nanopattern transfer technique in synthesising composite bi-metal nanoparticles by ion implantation through anodised aluminium oxide (AAO) masks. Key parameters such as nanoparticle shape and size, inter-particle distance and chemical composition of nanoparticles could be tuned by a combinatorial adjustment of the structure parameters of AAO nanomasks and implantation fluences of ions.

In this presentation, AAO nanomasks with pore sizes 50, 100 and 200 nm and inter-pore distances 100, 200 and 500 nm were prepared and transferred onto SiO<sub>2</sub> and Al<sub>2</sub>O<sub>3</sub> substrates for bi-metal ion implantation. By matching the projected ion ranges in SiO<sub>2</sub> and Al<sub>2</sub>O<sub>3</sub> substrates, 21 keV ferromagnetic metal ions (Fe and Co) and 30 keV noble metal ions (Au and Pt) were implanted with an identical ion fluence of  $5 \times 10^{16}$  ions/cm<sup>2</sup> at room temperature. The physical sizes and chemical compositions of these binary metal nanoparticles were characterized by analytical electron microscopy. The well ordered nano bi-metal composite array is clearly following the AAO nano mask geometry. A few selected nanocomposite arrays were further studied by magneto-optical Faraday and Kerr rotation both at room temperature and at low temperature (10K). Surface plasmon resonance-enhanced magneto-optical behaviour was observed in these bi-metal composite nanosystems.

## Optimization of Si-nanoparticle synthesis using ion implantation

Thawatchart Chulapakorn<sup>1</sup>, Anders Hallén<sup>2</sup>, Ilya Sychugov<sup>2</sup>, Sethu Saveda Suvanam<sup>2</sup>, Syeda Rabab Naqvi<sup>1</sup>, Daniel Primetzhofer<sup>1</sup>, Jan Linnros<sup>2</sup>, Göran Possnert<sup>1</sup>

<sup>1</sup>*Department of Physics and Astronomy, Uppsala University, Sweden*

<sup>2</sup>*KTH Royal Institute of Technology, School of Information and Communication Technology, Sweden*

Si-nanoparticles show a high luminescent intensity upon excitation by photons where the luminescence is blue-shifted for smaller size particles [1]. It was early shown that ion implantation followed by annealing is a useful method to form such nanoparticles. It has also been shown that implantation parameters, such as the sample temperature and post-implant annealing conditions are important for the final nanoparticle size distribution [2] and the luminescence. In this work, 50 keV Si-ions are implanted into a thermally grown SiO<sub>2</sub>-layer on-top of Si-substrate by varying fluence in a range of  $7.5 \times 10^{15} - 7.5 \times 10^{16}$  ions/cm<sup>2</sup> (1 – 10 at.%) and also at different implantation temperatures from room temperature to 400 °C. The samples are then annealed at around 1000-1100 °C for activating the Si-nanoparticles nucleation. Standard silicon processing techniques (e.g. forming gas annealing, FGA) are also employed in order to passivate the nano-particle surfaces. The aim is to optimize the synthesis of Si-nanoparticles with spherical shape and about 2 – 10 nm-diameter and to minimize the influence of surface defects on the quantum efficiency. The particle size is measured via photoluminescence and compared with electron microscopy images. Furthermore, ion beam analysis technique is involved to characterize the nanoparticles.

## Temperature dependent retention characteristics of ion-beam modified SONOS memories

Dimitrios Simatos<sup>1</sup>, Panagiotis Dimitrakis<sup>1</sup>, Vassilios Ioannou-sougleridis<sup>1</sup>, Nikolaos Nikolaou<sup>1</sup>, Pascal Normand<sup>1</sup>, Konstantinos Giannakopoulos<sup>1</sup>, Spyridon Ladas<sup>2</sup>, Beatrice Pecassou<sup>3</sup>, Gerard Benassayag<sup>3</sup>

<sup>1</sup>*Department of Microelectronics, NCSR "Demokritos", Attika, Greece*

<sup>2</sup>*Department of Chemical Engineering, University of Patras, Greece*

<sup>3</sup>*CEMES-CNRS, Toulouse, France*

For more than 10 years, charge-trap (CT) memory in the form of SONOS (PolySi-Oxide-Nitride-Oxide-Si)-type cell has been produced in high volume manufacturing and constitutes one of the most promising technologies for the downscaling continuation of non-volatile memories. A promising option to increase SONOS performance is via low-energy Si-ion implantation into oxide nitride (ON) stacks followed by low thermal budget wet-oxidation [1]. Here, we report on the structural and electrical properties of ONO structures using silicon and nitrogen implanted ON stacks. Oxide-nitride stacks (2.5 nm/ 6 nm) were formed on n-type Si substrates, further implanted with 1 keV Si or N to a dose of  $1\text{E}16$  ions/cm<sup>2</sup>, and finally wet oxidized at 850°C for 15 min. TEM imaging showed that the thickness of the blocking oxide layer, formed during wet oxidation, strongly depends on the implanted species being 10 nm in the case of Si and 5 nm for N. Electrical characterization of the structures was performed using standard aluminum gate MONOS capacitors. Program/erase (P/E) testing revealed that Si implanted stacks can trap either electrons or holes resulting to a memory window as large as 8.5 V for a +15/-14V P/E regime at 1ms. In turn N implanted stacks can trap only electrons with a corresponding memory window of 4 V. Room-temperature charge retention measurements showed that the electron loss rate is faster in samples implanted with Si ( $\sim 0.32\text{V/decade}$ ) compared to N-samples ( $\sim 0.1\text{V/decade}$ ). The 10-year extrapolated memory windows were 1.7 and 2.5V for Si and N-implanted devices, respectively. Retention measurements within the temperature range of 25 -150 °C indicate that the Si implanted stacks exhibit a thermally activated retention which is not the case for the N-implanted stacks. This retention behavior is mainly attributed to the different nature of traps generated by ion implantation and wet oxidation processing.

[1] V. Ioannou-Sougleridis et al, APL 90(26), 263513 (2007).

## A model for GISAXS characterization of ion-beam induced tracks in surface region of thin films

Maja Buljan<sup>1</sup>, Marko Karlusic<sup>1</sup>, Iva Bogdanovic Radovic<sup>1</sup>, Igor Mekterovic<sup>2</sup>, Darko Mekterovic<sup>1</sup>, Schleberger Marika<sup>3</sup>, Nikola Radic<sup>1</sup>, Sigrid Bernstorff<sup>4</sup>

<sup>1</sup>*Rudjer Boskovic Institute, Bijenicka cesta 54, 10000 Zagreb, Croatia*

<sup>2</sup>*Faculty of Electrical Engineering and Computing, Zagreb, Croatia*

<sup>3</sup>*Fakultät für Physik and CeNIDE, Universität Duisburg-Essen, 47048 Duisburg, Germany*

<sup>4</sup>*Elettra-Sincrotrone Trieste, SS 14 km 163.5, 34149 Basovizza, Italy*

Heavy ions with a kinetic energy in the MeV range are a powerful tool for the design of material properties via changes induced within the ion tracks. Characterization of these changes is usually difficult, especially if the tracks are completely or partially below the surface as well as in amorphous systems where the contrast between the track and surrounding material is low. Therefore, a simple and efficient method for the characterization of ion beam induced changes in materials is of great importance.

Here we present a new model/program for the analysis of ion beam induced tracks at the material surface or just below it by GISAXS (grazing incidence small angle x-ray scattering). The structure of the formed tracks is often non-continuous, i.e. the tracks consist of nano-sized structures aligned along the ion beam trajectory. The proposed method allows determination of all important ion track properties including their structure, shape, size, separation as well as all properties of the formed nano-objects for the non-continuous tracks. The efficiency of the method is demonstrated using ion tracks produced in Ge+ITO mixture film irradiated by 15 MeV Si ions. The model will be incorporated into a new freely available program for processing and analysis of materials modified by ion beams using GISAXS.

### Electron beam modification of polymeric materials

Danay Dupeyron<sup>1,2</sup>, Jacques Rieumont<sup>2</sup>, Guillermo Solorzano<sup>3</sup>, Rafael Martinez<sup>4</sup>

<sup>1</sup>*Department of Pharmacy, Instituto Macapaense do Melhor Ensino Superior, IMMES, Brazil*

<sup>2</sup>*Polymer Laboratory, Instituto de Ciencia y Tecnología de Materiales, Universidad de la Habana, Cuba*

<sup>3</sup>*Department of Materials Science and Engineering, Pontifícia Universidade Católica do Rio de Janeiro, Brazil*

<sup>4</sup>*FAEM Laboratory, Physics Department, Universidade Federal do Amapá, Brazil*

Structural modifications not only on the surface but also throughout the bulk of materials can be triggered by radiation, depending on the incident energy [1]. Electrons are used to irradiate samples for several purposes, from sample analysis to structural modification [2]. In Transmission Electron Microscope (TEM) a beam of highly energetic electrons is used to analyze samples. During the irradiation process interactions occur between primary electrons (TEM electrons) and bulk sample. Due to these interactions high-resolved images are obtained allowing detailed micro-structural examination. In this sense, TEM electrons can cause transitory or permanent modifications on the surface or bulk structure of a specimen. The irradiation effects on polymeric materials has attracted increased attention since molecular changes occurring in polymers, as a result of radiation-induced chemical reactions, can modify their physical and chemical properties such us strength, solubility, etc. In this study, interesting results of polymeric nanoparticles irradiated by TEM electrons are presented: new ordered conformations as structure like carbon nanotubes were observed. These structure modifications are showed through morphological analyses, which also indicate that those modifications are function of irradiation time.

Keywords: Structural modification, Electron beam, Irradiation, Materials, Polymers.

[1] C. R. Ponciano, R. Martinez, L. S. Farenzena et al., J. Mass Spectrom. 43, 1521-1530 (2008).

[2] N. Cheremisinoff, Electron Beam Processing of Polymers. Advanced Polymer Processing Operations, Noyes Publications, USA 157-186 (1998).

### Comparative catalytic activity of PET track-etched membranes with embedded silver and gold nanotubes

Daryn Borgekov, Anastassiya Mashentseva, Sergey Kislitsyn, Maxim Zdorovets, Anastassiya Migunova

*Institute of Nuclear Physics Republic of Kazakhstan, Kazakhstan*

Irradiated by heavy ions nanoporous track-etched membranes (TeMs) has significant applications not only in separation processes as a filter but also in nanotechnology as a flexible template for the synthesis of highly ordered nanowires or nanotubes arrays. TeMs, prepared by  $+15\text{Kr}84$  ions bombardment (1.75 MeV/nucl with the ion fluency of  $1 \times 10^9 \text{ cm}^{-2}$ ) of polyethylene terephthalate (PET) film, was applied in this research as a template for development of composites with catalytically enriched properties. A highly ordered silver and gold nanotubes arrays were embedded in 100 nm pores of PET TeMs via electroless deposition technique at  $4^\circ\text{C}$  during 1 h. The wall thickness of nanotubes not exceeds 30-50 nm, the crystal structure and fcc parameters according to XRD data are correlated to metallic gold and silver, crystallite sizes are calculated by Scherrer formula. Chemical composition and structure of nanotubes were confirmed by EDX assay. All “as-prepared” composites (size of tested sample -  $5 \times 5 \text{ cm}$  was a similar in all experiments) were examined for catalytic activity using reduction of p-nitrophenol to p-aminophenol by sodium borohydride as a common reaction to test metallic nanostructures- catalysts. The effect of temperature on the catalytic activity was investigated in range of 288 -323 K and the reusability of catalyst was investigated. The apparent constant rates as well as activation energy for Ag/PET and Au/PET composites were calculated.

## Electrospray ion beam deposition – from surface science of individual nonvolatile molecules towards functional thin films

Stephan Rauschenbach, Klaus Kern

*Max-Planck-Institute for Solid State Research, Germany*

Vapor deposition in vacuum is an extremely important technology with applications ranging from food packaging to high-performance semiconductor devices. Vacuum processing is successful because of the chemical purity of the environment and the ability to control the growth. Just as well, high performance material characterization methods require a perfectly controlled environment that is provided by high- and ultrahigh vacuum (HV/UHV). However, large, highly functional molecules of either natural or synthetic origin tend to be non-volatile or thermally labile, which hinders the conventional vacuum processing by evaporation.

To fabricate and characterize organic surface coatings made from nonvolatile molecules in vacuum, we developed electro-spray ion beam deposition (ES-IBD) as a method for the vacuum deposition of non-volatile molecules. ES-IBD is based on electrospray ionization, a soft ambient ionization method, creating intact molecular gas phase ions of even fragile molecules. The deposition apparatus is differentially pumped and contains ion optics in each stage, which convey the ion beam to the target in UHV. The use of charged particles allows for the full control over all deposition parameters including mass-, charge state- and energy-selection. While this makes the ES-IBD source an extensive apparatus it also greatly extends the possibilities for growth control over that of conventional vapor deposition.

We use high resolution scanning tunneling microscopy (STM) in UHV to characterize the adsorbed molecules after deposition with submolecular/atomic resolution. Examples presented here range from proteins and peptides, single molecule magnets, and dye molecules, to crystalline films grown from reactive polymer building blocks and large organic salt clusters. Based on these examples it is shown how the properties of the ion beam can be utilized for controlling the growth.

**Poster session B**  
**Tuesday, September 16, 2014**  
**16.50 – 19.00**



## **Chemical modification and sputtering of metal surfaces by CO<sub>2</sub>-hydrate cluster ion beams**

Gikan Takaoka, Hiromichi Ryuto, Mitsuaki Takeuchi, Hiroki Kobayashi

*Kyoto University, Japan*

The inclusion of gas molecules into water cluster cages with specific number of cluster sizes could be performed by introducing gas into liquid water for the cluster formation. In this work, a vapor of water bubbling with carbon dioxide (CO<sub>2</sub>) gas was ejected through a nozzle into a vacuum region, and CO<sub>2</sub>-hydrate clusters were produced. TOF measurement showed that mixed beams of water clusters and carbon dioxide-hydrate clusters were produced. With regard to the irradiation of CO<sub>2</sub>-hydrate cluster ions on solid surfaces, Q-mass measurement showed that several peaks such as H<sub>2</sub>O, OH, CO and CO<sub>2</sub> peaks appeared as residual gas peaks.

Cu and Au substrates were irradiated by water cluster ions and CO<sub>2</sub>-hydrate cluster ions. For Au surfaces, the incident energy of the cluster ions had an important role in sputtering the surfaces. The sputtered depth for the water cluster ion and CO<sub>2</sub>-hydrate cluster ion irradiation was similar at the same acceleration voltage. On the other hand, for Cu surfaces, the sputtered depth for CO<sub>2</sub>-hydrate cluster ion irradiation was larger than that for water cluster ion irradiation. In addition, it increased with increase of CO<sub>2</sub> flow rate. This is ascribed to the chemical modification of Cu surfaces, and the formation of CuCOOH on the surfaces caused the enhancement of sputtering Cu surfaces. Furthermore, AFM measurement showed that the surface roughness of Cu surfaces increased with increase of CO<sub>2</sub> flow rate. XPS measurement showed that C1s peaks corresponding to COOH bond appeared onto the Cu surfaces. The chemical reaction occurred between H<sub>2</sub> and CO<sub>2</sub> molecules, which resulted in the formation of COOH radicals. Thus, the chemical modification by CO<sub>2</sub>-hydrate cluster ion irradiation was enhanced, resulting in the formation of soft structures on the Cu surfaces.

## **Physical and chemical modification of amorphous carbon surface with Ar or CF<sub>4</sub> gas cluster ion beams**

Noriaki Toyoda, Asahi Kimura, Masahiro Hayashi, Isao Yamada

*University of Hyogo, Japan*

Recently, various carbon materials are widely used. Among various carbon materials, amorphous carbon (a-C) film has favorable aspects of hardness, low-friction coefficient, stability and so on. However, sp<sup>3</sup> bond decreases when the film is extremely thin. Therefore, increase of sp<sup>3</sup> bond on a-C is necessary. Besides physical modification, chemical modification of a-C films is important to realize functional surface. For example, interaction between lubricant and a-C film is crucial for hard disk media. In order to modify surface layer, ultra-low-energy ion beam is necessary.

Gas cluster ion beam (GCIB) is an ultra-low energy ion beam, which alters only top surface of films. Besides low energy aspect, GCIB induces transient dense energy deposition in local area, which realizes densification of films and enhances chemical reactions. In this study, physical and chemical modifications of a-C films were performed with GCIB.

At first, transformation of sp<sup>2</sup> and sp<sup>3</sup> bond in a-C films was characterized with in-situ XPS and near edge X-ray absorption fine structure (NEXAFS) using synchrotron radiation facility. After irradiation of Ar-GCIB, fraction of sp<sup>3</sup> bond on a-C film increased with the acceleration voltage (V<sub>a</sub>) to 10 kV. With further increase of V<sub>a</sub>, sp<sup>3</sup> bond decreased due to degradation by high-energy GCIB. NEXAFS results also showed the same tendency.

By using reactive GCIB, chemical modification at low substrate temperature is anticipated because of local and transient heating effects. When CF<sub>4</sub>-GCIB irradiation was carried out, formation of fluorinated layer on a-C was confirmed from XPS and NEXAFS. Contact angle measurement also suggested surface fluoridation. When V<sub>a</sub> of CF<sub>4</sub>-GCIB was 7 kV, fluoridation of a-C with appropriate smoothness was realized. Both physical and chemical modifications of a-C surface are realized with GCIB owing to its dense energy deposition.

## **Modification of diamond-like carbon films by nitrogen incorporation via plasma immersion ion implantation**

Stefan Flege<sup>1</sup>, Ruriko Hatada<sup>1</sup>, Koumei Baba<sup>2</sup>, Marion Hoefling<sup>1</sup>, Wolfgang Ensinger<sup>1</sup>

<sup>1</sup>*Darmstadt University of Technology, Germany*

<sup>2</sup>*Industrial Technology Center of Nagasaki, Japan*

The properties of diamond-like carbon (DLC) films can be altered by the incorporation of additional elements. In the case of nitrogen, there are effects on the inner stress of the film, the conductivity, biocompatibility and wettability. Nitrogen-DLC films are also used as electrode materials in electrochemical applications.

The nitrogen content is limited, though, and the maximum concentration depends on the preparation method. Here, plasma immersion ion implantation was used for the deposition of the films, without the use of a separate plasma source, i.e. the plasma was generated by a high voltage pulse. The plasma gas consisted of a mixture of C<sub>2</sub>H<sub>4</sub> and N<sub>2</sub>, the substrates were silicon and glass.

By changing the plasma parameters (high voltage, pulse length and repetition rate and gas ratio) layers with different N content were prepared. Additionally, some samples were prepared using a DC voltage. The nitrogen content and bonding was investigated with SIMS, AES, XPS, FTIR and Raman spectroscopy.

Depending on the preparation conditions different nitrogen contents were realized. Those values were compared with the nitrogen concentration that can be achieved by implantation of nitrogen into a DLC film.

## **Combinatorial ion beam sputter approach by rf-ion thrusters**

Martin Becker, Angelika Polity, Bruno K. Meyer

*I. Physics Institute, JLU Giessen, Germany*

Ion beam sputter deposition (IBSD) has been under focus of research for a number of years due to the flexibility it provides in the deposition of novel thin film materials. One of the unique characteristics of this kind of technique is the ability to deposit multilayered or multicomponent materials using a multi-target scheme with single ion gun bombardement. Furthermore the demand of new combinatorial capabilities for both the synthesis of new solid state optoelectronic materials and optimization of existing materials has driven the interest in multibeam arrangements.

We have developed the deposition tool necessary for a combinatorial approach to thin film metal oxides, with a special focus on transparent conducting oxides (TCOs). We are presently depositing compositionally graded libraries using multi-target sputtering. The initial collection of characterization tools includes UV/VIS/NIR transmission/reflection, Raman scattering and X-ray diffraction. In addition to allowing for a more complete empirical optimization of TCO properties, we expect to develop an improved basic understanding of TCOs.

**An example of low damage surface processing by GCIB : Comparison with monomer ion beams**

Katsumi Hanazono, Izumi Kataoka

*O.S.I Industry Co., Ltd., Japan*

Many reports have shown that GCIB (Gas Cluster Ion beams) processes could realize low damage processes. In cluster ion beam bombardment of solid surfaces, the concurrent energetic interactions between many atoms making up a cluster and many atoms at a target surface result in highly nonlinear sputtering and implantation effects. Cluster ion beams have become useful surface-processing techniques in a number of industrial applications. Experimental verification of surface damages using different substrates has already been shown by using damage sensitive materials such as Si,  $\text{CaF}_2$ ,  $\text{Fe}_7\text{Co}_3$  and organic materials by Ar,  $\text{N}_2$ , and  $\text{SF}_6$  cluster beams. However, it became important when the process is requested in sub-nanometer accuracy the evaluation of the surface damage must be extremely accurate. Then, the measurement of such surface damage after the GCIB process must not be influenced by preparing the following evaluation process which might modify by exposure by air and by other surface processing for evaluation.

In this paper, in-situ XPS evaluation of the surface damage during and after GCIB sputtering of BBO crystal surface is shown. For the comparison, Ar monomer ion irradiation has also been done in the same UHV chamber. BBO is a common nonlinear optical material with the chemical formula  $\text{BaB}_2\text{O}_4$  and the optical characteristics are extremely influenced by surface smoothness and composition. Experimental results show that after GCIB irradiation, the surface compositions remained constant without changes, whereas the sputtering by monomer Ar ions created surface composite alternation due to different sputtering yield in each elements. XPS analysis of the crystal which was exposed in the air after GCIB irradiation showed different surface composition.

**Effects of negative pulse voltage on microstructure of TiCN films prepared by plasma immersion ion implantation combined with sputtering**

Setsuo Nakao<sup>1</sup>, Tsutomu Sonoda<sup>1</sup>, Takeshi Kusumori<sup>1</sup>, Kimihiro Ozaki<sup>1</sup>, Kingo Azuma<sup>2</sup>, Takashi Kimura<sup>3</sup>

<sup>1</sup>*AIST-Chubu, Japan*

<sup>2</sup>*University of Hyogo, Japan*

<sup>3</sup>*Nagoya Institute of Technology, Japan*

Hard coatings, such as TiN, TiCN and DLC, are useful for expanding the life time of the mold. Recently, the application of sintering is widespread to various materials, such as magnetic materials, so that further improvement on the property of hard coatings is also required. Therefore, many investigations on the preparation of hard coatings are carried out by physical and chemical vapor depositions. Especially, sputtering method is widely used in industry. However, the microstructure and property of the coatings are not always controllable.

On the other hand, plasma immersion ion implantation (PIII) is emerged as a conventional ion implantation or ion bombardment technique to modify the microstructure and property of the coatings. In a previous study [1], it is reported that the microstructure and property of DLC coatings are widely varied by ion bombardment effects which are adjusted by negative pulse voltage.

It is expected that a combination of PIII and sputtering is useful to improve the microstructure and property of the coatings by the aid of ion bombardment. In this study, TiCN films are prepared by bipolar type PIII combined with sputtering system and the microstructure and composition are examined as a function of negative pulse voltage. The results of XRD measurements indicate that the peak of TiN(111) decreases in intensity and broadens, and the broad peak of TiCN(200) appears with increasing negative pulse voltage. These results suggest that TiN and TiCN crystals are reduced in size and the coatings are composed of TiCN nanocrystals as negative pulse voltage increases. The details will be presented.

[1] S. Nakao, J. Choi, J. Kim, S. Miyagawa, Y. Miyagawa and M. Ikeyama, *Diamond Relat. Mater.* 15, 884 (2006).

**Interaction of bipolar type plasma immersion ion implantation with high power pulsed magnetron sputtering discharge**

Kingo Azuma<sup>1</sup>, Takeshi Kusumori<sup>2</sup>, Kimihiro Ozaki<sup>2</sup>, Takashi Kimura<sup>3</sup>, Setsuo Nakao<sup>2</sup>, Tsutomu Sonoda<sup>2</sup>

<sup>1</sup>*University of Hyogo, Japan*

<sup>2</sup>*National Institute of Advanced Industrial Science and Technology, Japan*

<sup>3</sup>*Nagoya Institute of Technology, Japan*

The bipolar type PIII (Plasma immersion ion implantation) is a conventional ion implantation method, which applies the positive and negative high voltage pulse alternately to a work-piece. The positive pulses ignite plasma and heat the work-piece. On the other hand, the negative pulses pull out ions from plasma to implant into the work-piece. A functionality of thin film with high adhesion is obtained by this method. For example, the conductive DLC coating is materialized when using the carbon-based gas plasma. Providing the use of the metallic plasma instead of gas plasma, more various surface treatments by metallic ions are expected to be realized.

One of the plasma production methods generated metallic plasma is HPPMS (High Power Pulsed Magnetron Sputtering). HPPMS can ionize most of the sputtered metallic atoms by applying more negative voltage pulses as compared with dc operation.

We inserted the planar magnetron sputtering source with a titanium target of 2 inch diameter into the reaction chamber of PIII equipment. HPPMS power source was connected to the sputtering target, individually. The positive voltage pulses were applied to the work-piece through the substrate holder electrode, when the HPPMS power source was into an inactive state. Then, the sputtering plasma was discharged, subsequently. In the case of the voltage of +4 kV, the sputter target current became the maximum of approximately 35 A at 1.8  $\mu$ s later from the positive pulse ON. The results showed that HPPMS discharge was immediately kept up just after the HPPMS power source was activated. It is confirmed that the bipolar type PIII and HPPMS are congenial. The details will be presented.

## **Sputter yield of heavy monatomic and polyatomic ions: dependence on impact angle and substrate temperature**

Lothar Bischoff<sup>1</sup>, Roman Böttger<sup>1</sup>, Stefan Facsko<sup>1</sup>, Karl-Heinz Heinig<sup>1</sup>, Wolfgang Pilz<sup>2</sup>

<sup>1</sup>*Helmholtz-Zentrum Dresden-Rossendorf, Germany*

<sup>2</sup>*TU Dresden, Germany*

Focussed ion beam irradiation can be used to pattern surfaces at a scale of tens of nm by direct writing as well as by self-organization. Both patterning modes are controlled by ion beam erosion, where the sputter yield depends on the ion species, i.e. their mass, energy and angle of incidence. It depends also on the composition, temperature and surface roughness of the substrate.

Here, peculiarities of sputtering with heavy monatomic and very heavy polyatomic ions will be presented. Ion erosion of Si, SiO<sub>2</sub>, Ge and GaAs with Au<sub>n</sub> and Bi<sub>n</sub> ions from a liquid metal ion source has been investigated for different irradiation conditions.

The sputter yield per incoming atom is, compared with monatomic ions, considerably higher for polyatomic ions, even if the kinetic energy per atom is chosen to be equal. A newly developed sample holder allows irradiation at substrates temperatures up to 500°C and angles of ion incidence in the range from 0° to almost 90°, which will be used to elaborate sputter yield data of polyatomic ions in a range not yet explored so far. Due to the extremely high energy density deposition into the collision cascade volume by a very heavy polyatomic ion impact, an almost classical but tiny, transient melt pool can form, which adds to the collisional sputtering a loss of atoms by evaporation [1]. The latter contribution can be increased by substrate heating. Besides of the increased sputter yield, the repeated melting and resolidification of tiny pools leads to well-ordered surface pattern [2], which in turn influence the sputter yield.

[1] C. Anders, K.-H. Heinig and H. Urbassek, Phys. Rev. B 87, 198 (2012).

[2] L. Bischoff, K.-H. Heinig, B. Schmidt, S. Facsko and W. Pilz, Nucl. Instr. Meth. Phys. Res. B 272, 198 (2012).



**Production and transport of symmetric neutralized ion beams**

Nathaniel Hicks

*University of Alaska, Anchorage, USA*

A computational plasma physics study using particle-in-cell modeling is performed on the generation of beams composed of positive ion and negative ion species such that the net charge is close to zero. Formation and propagation of the beam, especially encountering and crossing a transverse magnetic field region, is studied. Applications for delivery of a neutralized ion beam with relatively little electron content are explored.

**Andromede project: surface analysis and nano-particle surface interactions in the keV to MeV energy range**

Michael Eller<sup>1</sup>, Evelyne Cottureau<sup>1</sup>, Anne Delobbe<sup>2</sup>, Stanislav V. Verkhoturov<sup>3</sup>, Emile A. Schweikert<sup>3</sup>, Serge Della-Negra<sup>1</sup>

<sup>1</sup>*Institut de Physique Nucléaire d'Orsay, UMR8608, CNRS/IN2P3, Université Paris-Sud 11, F-91406 Orsay, France*

<sup>2</sup>*Orsay Physics, ZA Saint Charles, 13710 Fuveau, France*

<sup>3</sup>*Department of Chemistry, Texas A&M University, College Station, Texas 77843-3144, USA*

The Andromede project (ANR-10-EQPX-23)[1] is a new imaging mass spectrometry instrument for surface analysis. With this new instrument surface modification and analysis will be performed using the impact of nano-particles ( $\text{Au}_{400}^{+4}$ ) in the keV to MeV range, the impacts will be localized using an electron proton emission microscope. The instrument will be the center of a multidisciplinary research team, however a series of experiments will be devoted to studying the fundamentals of ion-surface interactions, in particular the nano-particle surface interaction. It has been shown that impacting a surface with nano-particles in the keV or MeV range induces chemical modification of the molecules in the surface including: the promotion of cationization, formation of adduct ions with gold from the nano-particle, molecular fragmentation and implantation of intact nano-particles. In additional, a large volume of material is sputtered from the surface, the ionized portion of can be analyzed by mass spectrometry. In such conditions, the yield of molecular ions is significant, often exceeding one molecular ion per nano-particle impact.

This new instrument will use a new FIB column equipped with a gold LMIS which has been developed in collaboration with Orsay Physics. Initial tests show that the source is capable of producing more than 900pA of  $\text{Au}_{400}^{+4}$  with up to 20kV impact energy, this large beam intensity allows for the rapid implantation of a high dose of nano-particles on a large surface area (approximately 1 hour for  $10^{12}$  nano-particles/cm<sup>2</sup> for a 1cm<sup>2</sup> area). The FIB column is designed for direct injection of a parallel beam of nano-particles into the first stage of the 4MV van de Graaff accelerator.

The characterization of the FIB column, outlook of the Andromede project and fundamental studies for ion-surface interaction and surface modification will be presented.

The Andromede Project is funded by the program for future investment: EQUIPEX, ANR-10-EQPX-23.

**Plasma immersion ion implantation in conducting tubes using ExB fields**

Elver Juan De Dios Pillaca, Mario Ueda, Rogerio Oliveira

*National Institute for Space Research, Brazil*

Plasma immersion ion implantation (PIII) is an efficient technique used for the three-dimensional surface modification of materials. Recently, applications of PIII in ExB fields proved to be suitable for increasing the implanted dose compared with the standard PIII. Taking advantage of this result, PIII using ExB fields was tested in conducting tubes with different diameters. The experiment was carried out in a stainless steel cylindrical vacuum chamber of 0.38 meter length and 0.13 meter radius. In order to produce the required magnetic field, the PIII vacuum chamber was equipped with a magnetic coil system. The tubes were placed on the axis, in position coinciding with the magnetic trap region. The sequential experiments were started with the analysis of the electrical discharge at tubes with smaller (1.5cm), medium (4.0cm) and larger (11cm) diameters, while changing the magnetic field intensity, pressure and high voltage pulse intensity. Finally, the effect of the PIII with ExB fields on the tube inner wall is analyzed by various surface analysis methods. Samples of stainless steel (SS304) were placed inside the tube wall and then treated for 60 min. Our results showed that the discharge process in presence of magnetic field was stable, with a much better performance with respect to the case without B. Furthermore, the PIII current is strongly influenced by operating gas pressure ( $> 2.0 \times 10^{-2}$  mbar) and moderate magnetic field ( $\sim 40 - 90$  G). In these conditions, a high intensity of light produced by the discharge inside the tube was observed, which became more evident for smaller diameter tubes. By analyzing SS304 samples placed inside the tubes, DRX results demonstrated formation of expanded austenite phase in the nitrogen PIII treated samples. This may be explained by the rising of the tube temperature caused by the high ion flux hitting the tube inner wall when the magnetic field is applied.

**Proton beam generation using Au-coated plastic target from Laser Ion Source**

Masafumi Kumaki<sup>1</sup>, Masahiro Okamura<sup>2</sup>, Shunsuke Ikeda<sup>1</sup>, Yasuhiro Fuwa<sup>1</sup>, Takeshi Kanesue<sup>2</sup>, Masakazu Washio<sup>3</sup>

<sup>1</sup>*RIKEN, Japan*

<sup>2</sup>*Brookhaven National Laboratory, USA*

<sup>3</sup>*Waseda University, Japan*

A Laser Ion Source (LIS) produces high current and low emittance pulsed ion beams. It is a useful source for ion implantation since it can produce practically any metal beams only by changing target materials. However it has been very difficult to provide stable proton beam. We have tried to create a hydrogen plasma using frozen hydrogen and metal hydride targets, but these methods were not appropriate as an ion source for accelerators. Then we propose to use a plastic plate as laser targets. Normally most of plastics are transparent to laser lights and sharp energy deposition could not be expected. To help to make initial plasma which reads efficient classical laser energy absorption, we examined metal coating on the plastic which may promote plasma formation process. We prepared a 125 nm Au-coated polycarbonate plate and measured the plasma properties using a Nd:YAG laser (wavelength: 1064 nm; pulse energy: 300 mJ; pulse width: 270 ps). The result shows that the Au coating increased the plasma expansion velocity and the boost effect was most clearly observed on protons.

In this conference, we will explain the results of current density measurements and ion charge-state distributions.

## **Changes in the young modulus of hafnium oxide thin films**

Andre Luis Marin Vargas, Fabiana De Araujo Ribeiro, Roberto Hübler

*Pontificia Universidade Catolica do Rio Grande do Sul, Brazil*

Hafnium oxide ( $\text{HfO}_2$ ) thin films have attracted the interest of researchers due the great potential for use in optical materials and electronic devices.  $\text{HfO}_2$  stands out for its high resistance to diffusion of impurities and mixing on the interface. It is known that reactive DC magnetron sputtering technique can produce films with different Young Modulus. Modulating these properties open a wide range of applications on electronics and opto-electronics. The aim of this work is study the alteration of mechanical properties induced by the increasing of Ar / O ratio content in the deposition chamber. The thin films were deposited by DC reactive magnetron sputtering with different Ar / O concentrations. After deposition, films were characterized through XRD, AFM, RBS and XRF. In this regard, it was observed that the as-deposited  $\text{HfO}_2$  films were mostly amorphous in the lower Ar / O ratio and transformed to polycrystalline with monoclinic structure as the Ar / O ratios grows. RBS technique shows good compromise between the experimental data and the simulated ones. It was possible to tailored the Young Modulus of the films by alter the Ar / O content on the deposition chamber without thermal treatment.

## **Low temperature crystallization of sputter-deposited film**

Noriyuki Sakudo, Noriaki Ikenaga, Naotake Sakumoto, Kei Matsui

*Kanazawa Institute of Technology, Japan*

We have been developing a technique to crystallize sputter-deposited metal-compound film at low temperature by using low-energy PIII (plasma immersion ion implantation). Combining magnetron-sputter deposition with simultaneous ion implantation of Argon enabled forming crystalline film directly on plastics, although most solid materials that were simply sputter-deposited on a cold substrate were amorphous and needed high-temperature post annealing in order to be crystallized. In this study, titanium nickel film formed on polyimide was proved crystalline from its X-ray diffraction file. The optimum ion energy for crystallization was experimentally investigated. After processing the experimental data, it was found that the ion energy in the low-energy PIII was not determined not only by the pulse bias voltage but also by the plasma potential. Namely, the ion energy in PIII for very low energy implant less than several hundred eV would change dependently on the plasma parameters even if the pulse bias voltage for ion acceleration was unchanged. The exact ion energy is discussed in detail. Beam-line implanters that are practically used for semiconductor device production will have the same issue in common as long as they are applied to ultra-low energy implantation, because the ion generation in their ion sources depends on plasma.

## **Raman spectra of graphene irradiated by highly charged ions**

Haibo Peng<sup>1</sup>, Tieshan Wang<sup>1</sup>, Xin Du<sup>1</sup>, Yongtao Zhao<sup>2</sup>, Yuyu Wang<sup>2</sup>, Rui Cheng<sup>2</sup>

<sup>1</sup>*School of Nuclear Science and Technology, Lanzhou University, P.R. China*

<sup>2</sup>*Institute of Modern Physics, Chinese Academy of Sciences, P.R. China*

The graphene is the single layer which is made of honeycombed carbon atoms. It has attracted the comprehensive interesting. Because of peeling off many bonding electrons, the highly charged ion has huge potential energy. In this work, the graphene layers and Highly Oriented Pyrolytic Graphite (HOPG) were bombarded by highly charged Xe ions. The Raman spectra of irradiated graphene and HOPG were measured. After irradiation of highly charged ions, the D peak of  $1350\text{cm}^{-1}$  presented on both HOPG and grapheme spectra, which indicated formation of the defects by the impaction. The spectra were fitted with multi-Lorentzian function. For the fitting curve of HOPG, as the irradiation doses grew, the ratio of D peak intensity to G peak increased. For the graphene, the ratio saturated with high irradiation doses. This result suggested the potential energy deposition on the graphene affected the Raman spectra.

### **Sputtering analysis of astrophysical ices and silicate analogs**

Rafael Martinez<sup>1,2</sup>, Thomas Langlinay<sup>1</sup>, Philippe Boduch<sup>1</sup>, Amine Cassimi<sup>1</sup>, Frédéric Ropars<sup>1</sup>, Hermann Rothard<sup>1</sup>, Cassia R. Ponciano<sup>3</sup>, Enio F. Da Silveira<sup>3</sup>, Maria Elisabetta Palumbo<sup>4</sup>, Giovanni Strazzulla<sup>4</sup>, John R. Brucato<sup>5</sup>, Hussein Hijazi<sup>6</sup>

<sup>1</sup>*Centre de Recherche sur les Ions, les Matériaux et la Photonique (CEA/CNRS/ENSICAEN/Université de Caen-Basse Normandie UCBN) CIMAP-CIRIL-Ganil, Boulevard Henri Becquerel, BP 5133, 14070 Caen Cedex 05, France;*

<sup>2</sup>*Departamento de Física, Universidade Federal do Amapá, Brazil*

<sup>3</sup>*Departamento de Física, Pontifícia Universidade Católica do Rio de Janeiro, Brazil*

<sup>4</sup>*INAF-Osservatorio Astrofisico di Catania, Italy*

<sup>5</sup>*INAF-Osservatorio Astrofisico di Arcetri, Firenze, Italy*

<sup>6</sup>*Physics Division, Oak Ridge National Laboratory - ORNL, TN, USA*

In specific astrophysical environments ices (condensed gases) and silicates are the dominant materials of the surfaces of many objects. They can e.g. be found on asteroids, on moons of many planets and on dust grains in the interstellar medium. They are exposed to solar wind, cosmic rays, and energetic ions present in the magnetospheres of the giant planets. The ion populations consist, besides H and He, of multiply charged heavy ions. Ion bombardment (solar wind, cosmic rays, etc.) is able, among other effects, to influence the reflectance spectra of irradiated silicates by inducing physico-chemical changes known as a whole as “space weathering”. Sputtered particles also contribute to the composition of the exosphere of planets or moons [1]. The sputtering of such astrophysical materials was studied at PUC-Rio and CIMAP-GANIL by time-of-flight mass spectrometry (TOF-SIMS), with projectiles in a wide energy range from  $\approx 200$  keV to  $\approx 600$  GeV [1,2]. A general result, also valid for other materials such as LiF, is the important contribution of cluster emission [2,3] to sputtering. Also, imaging XY-TOF-SIMS allows to measure energy distribution of sputtered secondary ions [1,3,4], which can provide important information about the emission profile of sputtered particles from planetary surfaces.

The CAPES-COFECUB French-Brazilian exchange program, a CNPq postdoctoral grant, and the EU Cost Action “The Chemical Cosmos” supported this work.

[1] M.A. Allodi, R.A. Baragiola, G.A. Baratta, M.A. Barucci, G.A. Blake, Ph. Boduch et al., *Space Science Reviews* 180, 101-175 (2013).

[2] D. P. P. Andrade, A. L. F. de Barros, S. Pilling, A. Domaracka, H. Rothard, P. Boduch, E. F. da Silveira, *Monthly Notices of the Royal Astronomical Society* 430, 787-796 (2013).

[3] H. Hijazi, H. Rothard, P. Boduch, I. Alzaher, Th. Langlinay A. Cassimi et al, *Eur. Phys. J. D* 66:305 (2012).

[4] R. Martinez, C.R. Ponciano, and E.F. da Silveira, *Eur. Phys. J. D* 66:251 (2012).



**Friction characteristics of a-C:H films deposited by plasma immersion ion implantation using pulsed-DC plasma**

Noriaki Ikenaga, Noriyuki Sakudo

*Kanazawa Institute of Technology, Japan*

An amorphous carbon (a-C:H) film formed by plasma chemical vapor deposition (CVD) combined with plasma immersion ion implantation (PIII) is known to have both high hardness and low friction at the same time. In this case, the plasma on PIII is generated by RF or DC power supply separate from pulsed bias voltage for ion implantation or irradiation. We therefore developed a new PIII deposition technique without RF or DC power supply for plasma generation with the purpose to become easier to use as a PIII apparatus. The apparatus consist of a process chamber and a negative pulse power supply to realize this technique. In this apparatus, a negative pulse power supply is substituted for RF or DC as a source of plasma generation, and it has two roles in this apparatus. One of the roles is to generate pulsed-DC plasma only around substrate by applying a pulse bias voltage to substrate. The other role is to irradiate ions for deposition and modification during a-C:H film formation. In this time, we developed this apparatus and made a comparison between the friction coefficient of each a-C:H films deposited by RF plasma and pulsed-DC plasma. Furthermore, those deposited films were investigated about the relationship between the friction and the pulsed-DC parameters. As a result, the formed a-C:H films by using this apparatus demonstrated equivalent friction coefficient to the traditional a-C:H films. The friction coefficient of a-C:H films formed by pulsed-DC plasma showed lower value than case of RF plasma at low-range pulse repetition frequency (less than 1kHz), although that showed the same tendency about pulse duty ratio and pulse bias voltage.

**Formation of large cluster anions of C, Cu and Au with a Cs-sputtering source**

Alfredo Galindo-Uribarri<sup>1</sup>, Ran Chu<sup>2</sup>, Shiyu Fan<sup>2</sup>, Yuan Liu<sup>1</sup>, Gerald Mills<sup>1</sup>, Elisa Romero-Romero<sup>2</sup>

<sup>1</sup>*Oak Ridge National Laboratory, USA*

<sup>2</sup>*University of Tennessee, USA*

Intense beams of Cu cluster negative ions have been observed with a cesium sputter negative ion source of the ORNL 25-MV tandem accelerator. The formation of large cluster anions in the Cs-sputter source is being investigated. Using different bombarding energies up to 8 keV, sputtered Cu cluster anions containing up to about 50 atoms have been obtained. The sputter targets were made of natural copper metal or powder. Also an electroformed ultra pure Cu sample was analyzed. Mass analyses reveal that the Cu clusters comprise <sup>63,65</sup>Cu isotopes and the composition distributions of the two isotopes follow a binomial distribution of their corresponding natural abundances. We observed breaks in the Cu cluster anion intensity distributions at certain "magic numbers" and odd-even alternation with the odd clusters more abundant than the adjacent even clusters. The experimental results in Cu, Au and C clusters will be presented. Possible future applications will be discussed.

**Ion irradiation effects in epitaxial graphene on SiC**

Jin-Hua Zhao<sup>1</sup>, Xuelin Wang<sup>2</sup>

<sup>1</sup>*Shandong Jianzhu University, P.R. China*

<sup>2</sup>*School of Physics, Shandong University, P.R. China*

Graphene is a one-atom-thick planar sheet of carbon atoms that are densely packed in a honeycomb crystal lattice. Graphene is attracting tremendous interest since discovered in 2004, due to its unconventional electronic properties, such as high and nearly equal mobilities at room temperature for both electron and hole conduction. Graphene has a wide range of applications, for example it has the potential for technological applications as a successor of silicon, in quantum computing or as a terahertz oscillator. Epitaxial growth on silicon carbide (SiC) is an effective method to obtain graphene with high quality. In our work, the effect of irradiation on epitaxial graphene on SiC was studied. The samples were irradiated with B and P ions at energy of 25 keV and different fluence with  $5 \times 10^{12}$  ions/cm<sup>2</sup> to  $1 \times 10^{15}$  ions/cm<sup>2</sup>. X-ray photoelectron spectroscopy is used to investigate the graphene lattice and form new chemical bonds with carbon atoms. The results of Raman measurement indicate that ion beam irradiation causes defects and disorder to the graphene crystal structure, and the level of defects increases with increasing of ion fluence. Surface morphology images are obtained by atomic force microscope (AFM) and scanning electric microscope (SEM).

## Radiation damage induced in $\text{Al}_2\text{O}_3$ single crystal by 90 MeV Xe ions investigated by optical and Raman spectroscopy

Hamza Zirour<sup>1</sup>, Mahmoud Izerrouken<sup>2</sup>

<sup>1</sup>*Faculté de Physique, USTHB, Bp. 32 El-Alia, Bab-Ezzouar, Algiers, Algeria*

<sup>2</sup>*Centre de Recherche Nucléaire de Draria, BP.43, Sebbala, Draria, Algiers, Algeria*

Despite numerous studies of radiation damage induced by swift heavy ions in  $\text{Al}_2\text{O}_3$  single crystal, point defect kinetics is not well understood. The aim of the present investigation is to get additional information on the point defect evolution with increasing fluence.

The irradiation was performed at the GANIL accelerator in Caen, France with fluences extending from  $10^{12}$  to  $6 \times 10^{13}$  Xe ions/cm<sup>2</sup>. After irradiation the samples were characterized by optical measurements (absorption and photoluminescence) and Raman spectroscopy techniques.

According to the present study it is found that with increasing fluence the  $\text{F}^+$  centre concentration increases and reaches a maximum value at  $3 \times 10^{13}$  Xe/cm<sup>2</sup>, then decreases little bit at  $6 \times 10^{13}$  Xe/cm<sup>2</sup>. At the same time the absorption band at 450 nm attributed to  $\text{F}22+$  intensity increases with increasing fluence as well revealed by photoluminescence measurements. The 550 nm emission band intensity attributed to  $\text{F}22+$  increases with fluence. This explains that at high fluence the F type centre (F and  $\text{F}^+$ ) aggregates to form F center clusers ( $\text{F}22+$ ). Raman Analysis of the non irradiated sample show four bands centred at 379.5, 418, 431 and 645  $\text{cm}^{-1}$  corresponding to the characteristic peaks of  $\text{Al}_2\text{O}_3$  single crystal. After irradiation, the relative peak area of the most-active Raman mode (418  $\text{cm}^{-1}$ ), decreases with increasing fluence up to  $3 \times 10^{13}$  Xe/cm<sup>2</sup>, indicating the Al-O bond breaking. Then increases at  $6 \times 10^{13}$  Xe/cm<sup>2</sup> in accordance with optical measurements. The position of the same peak (418  $\text{cm}^{-1}$ ) shifts towards lower wave vector and its FWHM increases with about 0.2  $\text{cm}^{-1}$ . This may be attributed to the stress resulted from the Xe ion defect agglomeration. However, according to our experimental data, Raman analysis reveals no amorphysation of  $\text{Al}_2\text{O}_3$  crystal irradiated with 90 MeV Xe ions up to a fluence of  $6 \times 10^{13}$  Xe/cm<sup>2</sup>.

## Color centers, dislocations and nanostructures in LiF irradiated with fast ions

Alma Dauletbekova<sup>1</sup>, Kurt Schwartz<sup>2</sup>, Ilze Manika<sup>3</sup>, Janis Maniks<sup>3</sup>, Robert Zabels<sup>3</sup>, Abdirash Akilbekov<sup>1</sup>, Muratbek Baizhumanov<sup>1</sup>

<sup>1</sup>*L.N. Gumilyov Eurasian national university, Kazakhstan*

<sup>2</sup>*GSI Helmholtzzentrum für Schwerionenforschung, Planckstr. 1, 64291 Darmstadt, Germany*

<sup>3</sup>*Institute of Solid State Physics, University of Latvia, 8 Kengaraga Str., LV 1063 Riga, Latvia*

Color center creation and nanostructure formation are studied in LiF irradiated with <sup>12</sup>C, <sup>14</sup>N, <sup>40</sup>Ar, <sup>84</sup>Kr, and <sup>130</sup>Xe MeV energy ions using optical spectroscopy, scanning electron (SEM) and atomic force microscopy (AFM). Optical spectroscopy (in the range of 190 – 1100 nm) detected the main electron color centers (F and Fn) whereas the complementary hole centers with absorption in the vacuum UV (maximum at 114 nm) was outside of our study. By irradiation with light ions (<sup>12</sup>C, <sup>14</sup>N) the concentration of single F centers (NF, cm<sup>-3</sup>) increases with the fluence (absorbed energy), saturates at NF~10<sup>19</sup> cm<sup>-3</sup> and at higher fluences a decrease both of single F and Fn centers takes place due to the formation of larger aggregates. In LiF irradiated with heavy ions (<sup>40</sup>Ar, <sup>84</sup>Kr, and <sup>130</sup>Xe) no decrease of F and Fn centers was observed up to the absorbed energy of 2x10<sup>25</sup> eV/cm<sup>3</sup> (corresponding to fluencies of about 10<sup>15</sup> ions/cm<sup>2</sup>).

Nanostructures were investigated in ion irradiated LiF on the surface and in the bulk after short etching. In LiF crystals irradiated with 150 MeV <sup>84</sup>Kr ions nanostructures consisting of columnar grains with the size of 30 – 90 nm were observed using SEM and AFM. Such nanostructures are created along the ion tracks where the energy loss exceeds the threshold of 10 keV/nm. At lower energy loss in the deeper part of the track only dislocation loops are observed. In LiF irradiated with light ions (<sup>12</sup>C, <sup>14</sup>N) to high fluencies, which ensure the overlapping of tracks and aggregation of color centers, structural study reveals only numerous dislocations.

Comparing our results with previous data we can conclude that nanostructuring takes place as a stress-driven ordering of ion induced defects and their aggregates.

## **Systematic multiple-energy self-ion implantation of silicon for the formation of continuous, thick amorphous layers**

Jim Williams<sup>1</sup>, L.A. Smillie<sup>1</sup>, T.T. Tran<sup>1</sup>, M.O. Thompson<sup>2</sup>, J.E. Bradby<sup>1</sup>

<sup>1</sup>*Australian National University, Australia*

<sup>2</sup>*Cornell University, Ithaca, NY USA*

Amorphous Si formed by self-ion implantation is desirable for applications that require near ideal density, pure, void free and continuous amorphous layers. However, there are few references in the literature that provide the implantation conditions and procedures necessary for reliably producing high quality amorphous layers of desired thickness. The primary aim of this study is to establish the implantation conditions (temperature, energies, doses, dose rates, etc.) required for reproducibly producing amorphous layers that are either buried or continuous to the surface as desired.

A series of Si implants were undertaken at liquid nitrogen temperature using various energies (0.08-4.5MeV) at low dose rates (dependent on energy) to damage Si (100) wafers. Samples were analysed by Raman microspectroscopy to detect the presence of any crystalline material within the 'amorphous' layers resulting from the implantation. Rutherford backscattering and channelling spectroscopy (RBS) was carried out to examine the depth distribution of disorder and the depth of the 'amorphous' layers for both continuous and buried layers. For selected samples transmission electron microscopy (TEM) was used to validate the RBS data and monitor any nanocrystallinity within the amorphous layers. RUMP was used to fit data and (with the aid of TEM) a channelled stopping power was obtained that allowed channelled spectra to be simulated using RUMP by adding two additional parameters. These parameters are the channelled stopping power for an incident channelled path and a minimum yield beyond the disorder/amorphous layer in the RBS spectra. Finally, implant schedules are tabulated that will reliably result in continuous amorphous layers up to a thickness of about 3.5 $\mu$ m, as well as a range of buried layers.

## Formation of germanium oxide microcrystals on the surface of Te-implanted Ge

Jacques Perrin Toinin<sup>1</sup>, Yauheni Rudzevich<sup>2</sup>, Khalid Hoummada<sup>1</sup>, Michael Texier<sup>1</sup>, Sandrine Bernardini<sup>1</sup>, Alain Portavoce<sup>3</sup>, [Lee Chow](#)<sup>2</sup>

<sup>1</sup>*Aix-Marseille Université, IM2NP, Faculté des Sciences et Techniques de Saint-Jérôme Case 142, 13397 Marseille, France*

<sup>2</sup>*University of Central Florida, USA*

<sup>3</sup>*CNRS, IM2NP, Faculté des Sciences et Techniques de Saint-Jérôme Case 142, 13397 Marseille, France*

The formation of voids on the surface of heavily implanted germanium has been known for more than 30 years. Recently there is renewed interests in germanium due to its potential application in complementary metal oxide semiconductor (CMOS) devices. Here we report the observation of germanium oxide microcrystals formed on the surface of tellurium implanted into a germanium substrate. The target used was a <100> polished single crystalline germanium wafer and the implantation was carried out at room temperature with Te ions at 180 keV and a fluence of  $3.6 \times 10^{15}$  at/cm<sup>2</sup>. Under scanning electron microscope (SEM), the surface of the Ge substrate is evenly covered by microcrystals with a diameter about  $1 \sim 2 \mu\text{m}$  and a coverage density of  $\sim 10^7$  particles/cm<sup>2</sup>. The initially smooth surface of the polished germanium substrate becomes very rough and mostly consists of voids with an average diameter of  $40 \sim 60$  nm, which is consistent with reports of heavily implanted germanium. The composition of the microcrystals was studied using energy dispersive X-ray analysis (EDX) and atom probe tomography (APT) and will be presented. Preliminary results indicate that tellurium is not detected in the microcrystals. The origin of the microcrystals will be discussed.

**Corundum-to-spinel phase transformation in Zr-ion irradiated  $\text{Al}_2\text{O}_3$** 

Shogo Adachi<sup>1</sup>, Manabu Ishimaru<sup>1</sup>, Younes Sina<sup>2</sup>, Carl McHargue<sup>2</sup>, Kurt Sickafus<sup>2</sup>, Eduardo Alves<sup>3</sup>

<sup>1</sup>*Kyushu Institute of Technology, Japan*

<sup>2</sup>*University of Tennessee, USA*

<sup>3</sup>*Universidade de Lisboa, Portugal*

Many polytypes exist in  $\text{Al}_2\text{O}_3$ , and they transform to a stable alpha-phase with a hexagonal corundum structure on thermal annealing. Here, we demonstrate that the alpha- $\text{Al}_2\text{O}_3$  directly transforms to a metastable crystalline phase by ion irradiation, and the volume fraction of the metastable phase increases with thermal annealing. Single crystalline (0001) sapphire wafers were irradiated at room temperature with 175 keV Zr ions to a fluence of  $2 \times 10^{16} \text{ Zr/cm}^2$ . Post-irradiation thermal annealing was performed at 1073K-1273 K for 1 hr in argon. The radiation- and annealed-induced microstructures were analyzed using x-ray diffraction and transmission electron microscopy (TEM). The as-irradiated specimen possesses a layered structure consisting of defective crystal, amorphous, defective crystal, and unirradiated substrate from the surface. It was found that an eta- $\text{Al}_2\text{O}_3$  with a cubic spinel structure is formed in the as-irradiated specimen. High-resolution TEM observations revealed that the alpha- and eta-phases coexist in the topmost layer, suggesting that ion-irradiation induces structural phase transformation from the hexagonal corundum to cubic spinel. The volume of alpha-phase decrease with increasing the annealing temperature, and finally it disappears at 1173K-annealing: the corundum-to-spinel phase transformation occurs by thermal treatments.



**Defect accumulation in Ar-ion bombarded ZnO single crystals**

Anna Stonert<sup>1</sup>, Renata Ratajczak<sup>1</sup>, Przemysław Jozwik<sup>1,2</sup>, Andrzej Turos<sup>1,2</sup>, Jarosław Gaca<sup>2</sup>,  
Marek Wojcik<sup>2</sup>, Edyta Wierzbicka<sup>2</sup>

<sup>1</sup>*National Centre for Nuclear Research, Warsaw, Poland*

<sup>2</sup>*Institute of Electronic Materials Technology, Warsaw, Poland*

Mechanism of damage buildup in ZnO single crystals implanted with Ar ions has been studied by means of Rutherford Backscattering Spectrometry/channeling (RBS/c) and High Resolution X-Ray Diffractometry (HRXRD). Bulk single crystals were implanted with 300 keV Ar – ions to fluences ranging from  $1\text{E}14$  to  $4\text{E}16/\text{cm}^3$ . Depth defect concentration profiles have been obtained by RBS/c and analyzed with the Monte-Carlo McChasy code. Basing on these profiles the defect accumulation curves have been determined. McChasy allows to distinguish between simple defects and the extended ones. This fact results in two accumulation curves: one for randomly displaced atoms (RDA) and the second one for extended defects (dislocations). Each accumulation curve has been evaluated according to the Multistep Defect Accumulation Model (MSDA). According to both curves the damage buildup process is a multistep one. The HRXRD method was used to elucidate the mechanism of the defect transformation between individual steps. At low fluencies HRXRD profiles revealed the tensile strain buildup which grows with implantation fluence. It disappears at some critical fluence. Rapid growth of defect concentrations has also been observed at this fluence leading to the conclusion that plastic deformation of implanted region took place. This behaviour seems to be typical for the wide-gap compound semiconductors [1]

[1] A. Turos et al. Nucl. Instr. Meth. B 332, 50 (2014).

## The channeling effect of Al and N ion implantation in 4H-SiC during JFET integrated device processing

Mihai Lazar<sup>1</sup>, Farah Laariedh<sup>1</sup>, Pierre Cremillieu<sup>2</sup>, Dominique Planson<sup>1</sup>, Jean-Louis Leclercq<sup>2</sup>

<sup>1</sup>*Université de Lyon, Laboratoire AMPERE, INSA Lyon, UMR CNRS 5005, 21 Avenue Jean Capelle, 69621 Villeurbanne, France*

<sup>2</sup>*Université de Lyon, Institut des Nanotechnologies de Lyon, Ecole Centrale de Lyon, UMR CNRS 5270, 36 Avenue Guy de Collongue, 69134 Ecully, France*

Due to the low values of diffusion coefficients of dopants in silicon carbide (SiC), ion implantation is required during fabrication of power SiC devices. Al and N are the typical dopants to form p and n-type layers in 4H-SiC. Power discrete SiC devices are already commercialized as Schottky diodes, BJT, JFET and MOSFET transistors. A monolithic integration of this type of devices in SiC single crystal wafers is suitable to improve performance and reliability in power electronics. The size of the resulting converters is thus reduced, improving the switching operation and significantly decreasing the power loss. For this purpose, structures must be fabricated involving a numerous specific technological steps as plasma reactive-ion-etching and doping by ion implantation.

In 4H-SiC, due to the hexagonal crystalline structure, a strong channeling effect of Al and N implanted ions is observed, especially in the case of Al. This makes difficult to accurately estimate the depth of the formed junctions by multiple ion implantation steps. The sizes of the functional layers, and even an optimal operation of the final fabricated converters could be predicted, but with uncertainties.

We fabricated various JFET transistors (with different geometries) integrated on the same 4H-SiC wafer. A considerable number of ion implantations have been performed in order to realize p and n-type wells under the contact electrodes, buried channels and other specific layers necessary to prevent the electric field increase inside the device. In order to quantify and control the influence of the channeling effect of the implanted ions, we have performed an experimental study based on Secondary Ion Mass Spectrometry measurements and Monte-Carlo simulations with a dedicated code considering the 4H-SiC crystalline structure. Several batches have been fabricated and finally a new technological process was defined that enables to obtain devices working even with the presence of the channeling effect.

## Analysis and modification of blue sapphire from Rwanda by ion beam techniques

Saweat Intarasiri<sup>1</sup>, Duangkhae Bootkul<sup>2</sup>, Chaiyon Chaiwai<sup>3</sup>, Udomrat Tippawan<sup>3</sup>

<sup>1</sup>*Science and Technology Research Institute, Chiang Mai University, Chiang Mai 50200, Thailand*

<sup>2</sup>*Department of General Science (Gems & Jewelry), Faculty of Science, Srinakharinwirot University, Bangkok 10110, Thailand*

<sup>3</sup>*Plasma and Beam Physics Research Facility, Department of Physics and Materials Science, Faculty of Science, Chiang Mai University, Chiang Mai 50200, Thailand*

Blue sapphire is categorised in a corundum ( $\text{Al}_2\text{O}_3$ ) group. The gems of this group are always amazed by their beauties and thus having high value. In this study, blue sapphires from Rwanda, recently came to Thai gemstone industry, are chosen for investigations. On one hand, we have applied Particle Induced X-ray Emission (PIXE), which is a highly sensitive and precise analytical technique that can be used to identify and quantify trace elements, for chemical analysis of the sapphires. Here we have found that the major element of blue sapphires from Rwanda is Al with trace elements such as Fe, Ti, Cr, Cu and Mg as are commonly found in normal blue sapphire. Further analysis of the relationship among trace elements has assisted in segregation of the Rwanda blue sapphire from other blue sapphire origins, such as Cambodia and Sri Lanka. On the other hand, we have applied low and medium ion implantations for color improvement of the sapphire. It seems that a high amount of energy transferring during cascade collisions have altered the gems properties. We have clearly seen that the blue color of the sapphires have been intensified after nitrogen ion bombardment. In addition, the gems were also having more transparent and luster. The UV-VIS-NIR spectrograms measured after implantation recording the increase in absorption peak of the  $\text{Fe}^{3+}/\text{Fe}^{3+}$  pairs peaked at 377 nm,  $\text{Fe}^{2+}/\text{Ti}^{4+}$  pair peaked at 565 nm and  $\text{Fe}^{2+}/\text{Fe}^{3+}$  pairs peaked between 840 and 900 nm. These bands are responsible for the intense blue after implantation. Here the mechanism of these modifications is postulated and reported. In any point of view, the bombardment by using nitrogen ion beam is a promising technique for quality improvement of the blue sapphire from Rwanda.

## Effects of 5.4 MeV alpha-particles irradiation on electrical properties of nickel schottky diodes on 4H-SiC

Ezekiel Omotoso, Walter Meyer, Danie Auret, Alexander Paradzah, Johan Janse Van Rensburg, Sergio Coelho, Phuti Ngoepe, Mmantsae Diale

*University of Pretoria, South Africa*

Current-voltage, capacitance-voltage and conventional DLTS at temperature ranges from 40-300 K have been employed to study the influence of  $^{254}\text{Am}$  irradiation on the Ni/4H-SiC Schottky contacts. Nickel Schottky barrier diodes were resistively evaporated on n-type 4H-SiC samples of doping density of  $7.10 \times 10^{15} \text{cm}^{-3}$ . It was observed that radiation damage caused an increase in ideality factors of the samples from 1.03 to 1.10, a decrease in the Schottky barrier height from 1.44 to 1.38 eV, an increase in saturation current from  $1.54 \times 10^{-20}$  to  $4.10 \times 10^{-20}$  A and an increase in series resistance from 11.1 to 12.6  $\Omega$  from I-V plots at room temperature which indicate the deviation from the thermionic emission current transport mechanism. The free carrier concentration of irradiated sample was slightly different from as-grown because of low dose introduced. Conventional deep level transient spectroscopy showed deep energy level of three peaks with activation energy, as determined by means of an Arrhenius plot, of 0.08, 0.15 and 0.65 eV for the as-grown material. After irradiation, four peaks with activation energy 0.06, 0.15, 0.67 and 0.62 eV for alpha particle irradiated sample. The modified Richardson plot assuming a Gaussian distribution of barrier heights for the as-grown and alpha particles irradiated samples were 132.57 and 150.86  $\text{Acm}^{-2}\text{K}^{-2}$  respectively. These values are similar to literature values.

## Influence of the surface on the luminescence properties of $\text{ZnWO}_4$ crystals

Liudmila Lisitsyna<sup>1</sup>, Irina Tupitsyna<sup>2</sup>, Victor Lisitsyn<sup>3</sup>

<sup>1</sup>*Tomsk State University of Architecture and Building, Tomsk, Russia*

<sup>2</sup>*Institute for Scintillation Materials, Kharkov, Ukraine*

<sup>3</sup>*National Research Tomsk Polytechnic University, Tomsk, Russia*

The effect of oxygen ions implantation and heat treatment in oxygen or hydrogen atmosphere at 900° C for 10 hours on spectral-kinetic characteristics of  $\text{ZnWO}_4$  crystals photoluminescence is discussed. The luminescence spectra were measured with nanosecond time resolution. The energy of the accelerated oxygen ions and the fluence were 28 MeV and  $10^{15} \text{ cm}^{-2}$ , respectively.

It is shown that in as-grown crystals the excitation spectrum of the emission band at 2.6 eV contains the energy threshold at 4.1 eV, close to the value of the band gap  $\sim 4.6$  eV, and then a slight (15%) emission intensity decrease with the photon energy increasing up to 6.2 eV.

By our estimates the penetration depth of photons in a crystal varies from 40 to 5 nm in the energy region of 4 – 6 eV.

Under heat treatment, in the crystal surface layer of  $d$  thickness, a new short-lived emission centers (transition at 3.1 eV) appear as a result of transformation/destruction of the emission centers with the transition at 2.6 eV. The occurrence of the concentration gradient leads to decrease of 90% the emission intensity at 2.6 eV excited by the photon in the energy region  $> 4.6$  eV, where the penetration depth of the photons in the crystal is comparable to the thickness of the crystal layer  $d$  disturbed by heating.

Oxygen ion implantation in heated crystals leads to healing of the crystal surface and restoration of the excitation spectrum of the emission band at 2.6 eV.

The nature of the phenomenon and structure of the emitting centers are discussed.

## Molecular dynamics modeling of defect formation and lattice thermal conductivity in multilayer hexagonal boron nitride

Kelly Stephani<sup>1</sup>, Iain Boyd<sup>2</sup>

<sup>1</sup>*University of Illinois at Urbana-Champaign, USA*

<sup>2</sup>*Department of Aerospace Engineering at the University of Michigan, USA*

Molecular dynamics simulations [1,2] are conducted to examine lattice defect formation in a hexagonal boron nitride (h-BN) lattice by high-energy xenon ion impact. Previous studies [3-5] established a dependence of the lattice thermal conductivity with the lattice depth (layers) and isotopic enrichment, which fundamentally modify the intrinsic phonon transport within the lattice. This study aims to examine the influence of lattice defects on phonon transport and lattice thermal conductivity. Lattice defect formation is first examined in single-layer hexagonal boron nitride.  $\text{Xe}^+$  particles over a range of energies (0.1-10 keV) are used to randomly impact the central lattice in the shaded region of the hexagonal structure. Good agreement is found with a previous molecular dynamics study [6] that examined lattice defect formation over a range of  $\text{Xe}^+$  energies. Similar results are obtained for a multilayer h-BN lattice involving 10 layers. The defect formation in the top layer is examined for comparison. It is found that single and interstitial vacancies are prominent in the lattice sub-layers with increasing ion energy. The influence of the resulting lattice defects on phonon transport and lattice thermal conductivity is analyzed using the Green-Kubo linear response formulation [7] to establish a relationship between defect distribution and size with thermal transport in h-BN materials.

[1] J.A. Anderson, C.D. Lorenz and A. Travesset, J. Comp. Phys. 227(10) 5342-5359 (2008).

[2] HOOMD-blue web page: <http://codeblue.umich.edu/hoomd-blue>.

[3] I. Jo et. al., Nano Lett. 13 550-554 (2013).

[4] L. Lindsay and D.A. Broido, Phys. Rev. B: Condens. Matter 84, 155421 (2011).

[5] L. Lindsay and D.A. Broido, Phys. Rev. B: Condens. Matter 85, 035436 (2012).

[6] O. Lehtinen, et al., Nucl. Instr. Meth. Phys. Res. B 296 1327-1331 (2011).

[7] R. Kubo, M. Toda and N. Hashitsume, Statistical Physics II, Nonequilibrium Statistical Mechanics, Springer-Verlag, Berlin (1991).

## Radiation damage in insulators via both electronic and nuclear energy deposition

Flyura Djurabekova<sup>1</sup>, Marie Backman<sup>2</sup>, Aleksi Leino<sup>1</sup>, Szymon Daraszewicz<sup>3</sup>, Olli Pakarinen<sup>1</sup>,  
Marcel Toulemonde<sup>4</sup>, Yanwen Zhang<sup>5</sup>, William Weber<sup>2</sup>, Kai Nordlund<sup>1</sup>

<sup>1</sup>*University of Helsinki, Finland*

<sup>2</sup>*University of Tennessee, USA*

<sup>3</sup>*University College London, UK*

<sup>4</sup>*University of Caen, France*

<sup>5</sup>*Oak Ridge National Laboratory, USA*

By means of atomistic simulations, we study the radiation damage as a result of both nuclear and electronic energy deposition. The inelastic thermal spike model of the interaction of swift heavy ions with insulators describes the damage observed in experiments at very high energies of irradiation ( $>1$  MeV/amu) surprisingly well. In the low energy regime, when the effect of electronic energy deposition is not significant, the radiation damage has been studied to a great extent. Presently, by employing the inelastic thermal spike model in molecular dynamic simulations, we attempt to estimate the effect of both channels of radiation damage in materials in the intermediate range of energies.

Ion irradiation in the transition energy regime might lead to a synergy between the two channels of energy transfer, interactively producing the damage, which cannot be found if both mechanisms act independently. Here, by synergy we understand the possible collaborative or competitive effects, which may occur if the energy is deposited via both channels in the same place and at the same time. The collaborative effect between these two mechanisms will most likely result in enhanced damage production, but the competition between them might lead to the enhanced recombination or partial annealing during damage formation.

We analyze the interplay of both channels of energy deposition with respect to the damage produced by the Au ions of transient energies in silica and by Kr ions in  $\text{ZrSiO}_4$ . We also consider two models of introducing the electronic energy deposition, i) via a single event of inelastic thermal spike along the ion path or ii) as a two-temperature exchange model, naturally dissipating energy in the lattice and electronic subsystems. We show that the latter model agrees excellently with experimental results in silica, and in particular can explain why RBS and SAXS experiments give different track radii.

## Effects of substrate temperature during ion implantation on residual damage and defects in Si

Naotake Sakumoto<sup>1</sup>, Hiroyuki Ito<sup>1</sup>, Noriaki Ikenaga<sup>2</sup>, Osamu Ueda<sup>2</sup>, Noriyuki Sakudo<sup>2</sup>,  
Kalipatnam Vivek Rao<sup>1</sup>

<sup>1</sup>*Applied Materials Japan, Japan*

<sup>2</sup>*Kanazawa Institute of Technology, Japan*

In order to minimize the residual damage, two different implantation methods have been recently proposed for silicon wafer applications. One is called “Cryo” implantation and the other called “Hot” implantation. The former maintains the substrate at very low temperature such as -160 °C during implantation. This low temperature implantation process enhances amorphization of implanted layer on Si wafer, therefore, it can realize complete recrystallization of Si during anneal without leaving any residual damage in the end of range (EOR) region. The latter uses a heated substrate (400 °C or more), which to eliminates accumulation of damage by enhancing the recombination of Si-interstitials and vacancies at the time of their generation, which minimizes crystal damage after implantation.

In this work, the effects of substrate temperature during high dose Arsenic ion implantations on residual damage and defects in Si have been investigated systematically using TEM and other metrological analyses such as EDS and RBS. The results showed that in the case of cryogenic temperature implantation the “as-implanted” layer becomes “damage free” after annealing due to complete recrystallization. On the other hand, the damage recovery of hot implantation appears to be more complex as a certain thickness of amorphous layer still remains after RTA. Furthermore, the junction depth shifted slightly deeper with hot implantation, which indicated a presence of enhanced diffusion of Arsenic at low temperature. This diffusion mechanism is different from Transient Enhanced Diffusion (TED) as Arsenic is known to diffuse through vacancies rather than interstitials.



**A DLTS study of hydrogen doped Czochralski-grown silicon**

Moriz Jelinek<sup>1</sup>, Johannes Laven<sup>1</sup>, Stefan Kirnstoetter<sup>2</sup>, Werner Schustereder<sup>1</sup>, Hans-Joachim Schulze<sup>1</sup>, Mathias Rommel<sup>3</sup>, Lothar Frey<sup>4</sup>

<sup>1</sup>*Infineon Technologies Austria AG, Austria*

<sup>2</sup>*Institute of Solid State Physics, Graz University of Technology, Austria*

<sup>3</sup>*Fraunhofer IISB, Germany*

<sup>4</sup>*Chair of Electron Devices, FAU Erlangen-Nuremberg, Germany*

Proton implantations find wide-spread application in tailoring the electrical characteristics of modern silicon power devices. At moderate activation temperatures below 200 °C proton-induced lattice damage is used to reduce the local minority carrier lifetime, thus improving the switching capability of bipolar devices, such as power thyristors. Another application is the formation of shallow hydrogen-related donors (HDs) at annealing temperatures between 350 and 550 °C. Although the creation of HDs through proton implantation is known since 1970, the microscopic composition of these complexes is still under debate. In this study we examine proton implanted and subsequently annealed commercially available CZ-wafers with the DLTS method. Depth-resolved spreading resistance measurements are shown, indicating an additional peak in donor concentration, not seen in oxygen-lean FZ. The additional peak lies about 10 – 15 microns deeper than the main peak near the projected range of the ions. DLTS-measurements of this second peak are presented.

## Wavelength-dependent ripple propagation on ion-irradiated pre-patterned surfaces driven by viscous flow corroborates two-field continuum model

Detlef Kramczynski<sup>1</sup>, Bernhard Reuscher<sup>2</sup>, Hubert Gnaser<sup>1,2</sup>

<sup>1</sup>*TU Kaiserslautern, Germany*

<sup>2</sup>*Institut für Oberflächen- und Schichtanalytik (IFOS) GmbH, Germany*

Glass surfaces were patterned by milling periodic trench structures with wavelengths from 150 to 750 nm in a focused ion beam (FIB) system. Upon exposure to 30 keV Ga<sup>+</sup> ion irradiation under an incidence angle of 52° with respect to the surface normal, those patterns were found to transform into “ripple”-like nanostructures. Their evolution was monitored in situ for ion fluence from  $5 \times 10^{16}$  to  $2.4 \times 10^{18}$  Ga<sup>+</sup> ions/cm<sup>2</sup> using the scanning electron microscope incorporated in the FIB. With increasing fluence, the wavelengths of the ripples remain constant (and equal to their original feature size) while they propagate across the surface, in a direction which coincides with the projection of the ion beam's incident direction onto the surface. The propagation velocities  $v$ , being in the range (60-100) nm/(10<sup>17</sup> ions/cm<sup>2</sup>), were determined to be inversely proportional to the wavelengths  $\lambda$ , with  $v = A+B/\lambda^2$  (the constants A and B derive from various ion beam and target material parameters). Such a dependence is in accordance with the predictions of a theoretical two-field continuum model of ripple formation which treats the surface as being composed of a thin layer of mobile species on the substrate. A quantitative agreement of the experimental findings with this model is obtained if the presence of a viscous flow is effective in that thin surface layer. Ex situ atomic force microscopy was employed to derive the final crest-to-valley amplitudes of the ripple structures; their values were ~50-100 nm and thus similar to the depth of the original trenches. On the pristine surface areas (which had not been patterned) ripples were also formed by ion bombardment. Their wavelength increases with ion fluence  $\Phi$  from ~250 nm to ~420 nm, following a dependence  $\lambda \sim \Phi^{0.19}$ .

## Tailoring the broadband optical functionalities of self-organised nanopatterned

Christian Martella<sup>1</sup>, Carlo Mennucci<sup>1</sup>, Marina Giordano<sup>1</sup>, Diego Repetto<sup>1</sup>, Daniele Chiappe<sup>1</sup>, Iure Usatii<sup>2</sup>, Lucia Mercaldo<sup>2</sup>, Paola Delli Veneri<sup>2</sup>, Francesco Buatier De Mongeot<sup>1</sup>

<sup>1</sup>*Physics Department, University of Genoa, Italy*

<sup>2</sup>*ENEA, Portici (Naples), Italy*

Here we report on the optical functionalization of glass, semiconductor (Silicon and GaAs) and Transparent Conductive Oxide (TCO) substrates in view of light trapping and photon harvesting in photovoltaic devices [1,2].

Defocused Ion Beam Sputtering, assisted by a sacrificial self-organised Au stencil mask, is exploited in order to project in the underlying substrate a pattern of high aspect ratio nanoscale features.

We describe the formation of a quasi-periodic array of one-dimensional nanostructures with RMS roughness ranges from 80 nm up to 130 nm as a function of the total ion dose (corresponding to a vertical dynamic range of the nanostructures of roughly 500 nm) [1]. The characteristic lateral size of the nanostructures, estimated from the height-height correlation function, is in the range of 200 nm [1]. The tailored optical properties of the substrates are characterised in terms of total reflectivity and haze by means of integrating sphere measurements as a function of the morphological modification at increasing ion fluence. A broad-band anti-reflection effect (of the order of 10-20% with respect to a flat reference) is found in the VIS-NIR range. At the same time the patterned substrates have shown enhanced broadband light scattering functionalities as quantitatively highlighted by the Haze functions (reflection and transmission) which can be tailored in the 30%-60% range [1,2]. The first encouraging results demonstrate that a:Si solar cells grown on patterned glasses exhibit a 15% relative enhancement in photocurrent due to light trapping in the active layers [1].

The sacrificial Au stencil mask has been successfully replaced by an Al mask, with the aim of reducing the cost of the pattern transfer process.

[1] C. Martella, D. Chiappe, P. Delli Veneri, L.V. Mercaldo, I. Usatii, F. Buatier de Mongeot, *Nanotechnology* 24 (22), 225201 (2013).

[2] C. Martella, D. Chiappe, C. Mennucci and F. Buatier de Mongeot, *J. Appl. Phys.* 115, 194308 (2014).

## The role of composition profile and evolution on ion induced patterning of III-V semiconductor surfaces

Brandon Holybee<sup>1</sup>, Jean Paul Allain<sup>1</sup>, Scott Norris<sup>2</sup>, Stefan Facsko<sup>3</sup>

<sup>1</sup>*University of Illinois, USA*

<sup>2</sup>*Southern Methodist University, USA*

<sup>3</sup>*Helmholtz-Zentrum Dresden-Rossendorf, Germany*

The formation of hexagonally ordered dot patterns on GaSb by ion irradiation has been a known effect since 1999 [1], yet the mechanisms leading to the formation remain unclear. There are several proposed theoretical models, but so far there has not been a direct coupling between modeling and experiment. This work presents depth profile measurements of GaSb crystals at various stages of ion irradiation, and are used as improved inputs into BCA simulations to connect the gap between modeling and experiments.

Results on the compositional changes of GaSb at the surface during ion irradiation have seen conflicting data due to experimental inconsistencies. In order to eliminate these effects, we cleaved in-situ GaSb crystals and performed angular resolved AES and LEISS to obtain the compositional depth profile evolution with fluence up to the appearance of pattern formation. Ion irradiations were performed with Ne<sup>+</sup>, Ar<sup>+</sup>, and Xe<sup>+</sup> at energies from 500eV to 1keV and fluences up to 10<sup>16</sup> cm<sup>-2</sup>.

The resulting depth profiles are then used to create experimentally accurate BCA targets. Using the TRI3DST BCA simulation package [3] and the extension of the crater function framework to binary materials [4], we provide significantly improved estimates of the model parameters that account for the proper depth profile, the preferential dislocations at the surface, and the curvature dependence of the target [5]. These estimates provide better insight into the driving mechanism behind ordered nanostructure formation.

[1] S. Facsko, T. Dekorsy, C. Koerdt, C. Trappe, H. Kurz, a Vogt, and H. Hartnagel, Science 285, 1551 (1999).

[2] S.A. Norris, J. Appl. Phys. 114, 204303 (2013).

[3] W. Möller, Nucl. Instr Meth Phys. Res. Sect. B Beam Interact. with Mater. Atoms 322, 23 (2014).

[4] S.A. Norris, J. Samela, M. Vestberg, K. Nordlund, and M.J. Aziz, Nucl. Instr. Meth Phys. Res. Sect. B Beam Interact. with Mater. Atoms 318, 245 (2014).

[5] R. Bradley and J. Harper, Vac. Sci. Technol. A (1988).

**Nanopattern formation on metallic surfaces with focused ion beam**

Tomas Skeren<sup>1</sup>, Martin Vesely<sup>2</sup>, Jaroslav Kral<sup>1</sup>, Pavel Capek<sup>2</sup>

<sup>1</sup>*Czech Technical University in Prague, Czech Republic*

<sup>2</sup>*Institute of Chemical Technology, Prague, Czech Republic*

Low energy ion irradiation of surfaces can lead to the formation of well-defined periodic morphologies. This phenomenon can provide an efficient tool for nanopatterning of large scale areas but its detailed physical background remains unclear.

Although these nanopatterns are typically prepared by irradiation with a broad, unfocused ion beam, using a focused ion beam (FIB) tool brings numerous possibilities to study in detail the pattern formation process and obtain deeper insight in this phenomenon.

We present a study of the pattern formation on Ni(001) surface irradiated with a 20 keV Ga<sup>+</sup> focused ion beam. The general patterning behavior in this case is similar to the irradiation of Ni surface with a noble gas ion beam – at low angles of incidence (below ~60° from the surface normal) an isotropic mound structure forms on the surface. With increasing angle, this pattern becomes gradually elongated in the direction parallel to the ion beam and at 80° angle of incidence the pattern turns into a highly organized ripple structure with a periodicity of about 25 nm. The degree of organization of the mound pattern at low angles of incidence is slightly inferior to the pattern created by noble gas ion bombardment. However, the quality (quantified by the pattern correlation length) of the grazing incidence ripple pattern is comparable to or better than the ripples created with noble gas ions.

The combination of the FIB with the in-situ scanning electron microscopy (SEM) observation allowed us to investigate the in-plane movement of the surface morphology during the ion irradiation. Our observations are in agreement with the classical theory – for low angles of incidence the pattern is virtually static, for moderate angles (around 60°) the pattern travels slightly towards the ion source and at grazing incidence, the pattern travels rapidly away from the ion source.

**Dual-beam ion irradiation of silicon: experimental results and modeling**

Zachariah Koyn, Zhangcan Yang, Brandon Holybee, Michael Lively, Jean Paul Allain

*University of Illinois at Urbana-Champaign, USA*

Dual-beam ion irradiation has been shown on several materials, notably metals [1] to produce various kinds of nanostructures beyond ripples, which are usually induced by single ion beam irradiation. However, experiments thus far have mainly been exploratory, and have not been systematically performed to explore the underlying mechanisms compared directly with modeling. Moreover, the existing continuum theories are not able to explain the pattern formation by dual-beam ion irradiation [1,2]. We have developed a hybrid MD/kMC multiscale atomistic model to simulate ion beam nanopatterning of silicon [3, 4]. This model uses crater functions to model the prompt mass redistribution. Defect migration is treated by a kMC Arrhenius model. In this work we validate the predictive ability of the model as compared directly to experiments for dual-beam ion irradiation of silicon.

Silicon pattern formation at 500eV – 1keV and fluences up to  $1\text{E}18\text{ cm}^{-2}$  is performed under varying fluxes of perpendicular noble gas beams. Simulations reveal a strong correlation between single-beam and dual-beam pattern formation. The surface remains flat at low angles, similar to single-beam irradiation. For intermediate angles where ripples start to form for single-beam irradiation, ordered dots develop that coarsen with increasing fluence. Equal beam fluxes only generate dot structures whereas unequal fluxes induce compound dot and ripple features, moving toward only ripples at high flux mismatch. Feature dimensions are shown to depend on incident ion species. Experimental results are analyzed and compared to simulations under the same conditions.

[1] M. Joe, et al., J. Phys.: Condens. Matter 21, 224011 (2009)

[2] T. Yasserli and R. Kree, Nucl. Instr. Meth. Phys. Res. B, 268, 2496–2503 (2010)

[3] Z. Yang, M. Lively, J.P. Allain, Nucl. Instr. Meth. Phys. Res. B, 307, 189-195 (2013)

[4] Z. Yang, M. Lively, J.P. Allain, to submit, (2014)

## Chemical and structural metastability response of nano-particles through equilibrium and nonequilibrium kinetic pathway in ODS material

Joel Ribis<sup>1</sup>, Eric Bordas<sup>1</sup>, Patrick Trocellier<sup>1</sup>, Yves Serruys<sup>1</sup>, Yann De Carlan<sup>1</sup>, Alexandre Legris<sup>2</sup>

<sup>1</sup>CEA, France

<sup>2</sup>CNRS, France

The Oxide Dispersion Strengthened (ODS) steels are potential candidates as cladding tubes for Sodium-cooled Fast Reactors. The nano-oxides are finely dispersed within the grains and confer excellent mechanical properties to these alloys. So far, their structure and chemical compositions still lack of clarity, especially whether they are metastable or not. Hence, improving knowledge on this aspect remains crucial to guarantee the nano-oxide stability under irradiation.

Under ion beam irradiation, it is believed that nano-particle metastability can be sustained by kinetic mechanisms involving ballistic diffusion and point defects annihilation at sinks than can generate solute drag. Using Energy Filtered and High Resolution Transmission Electron Microscopy, it is proposed to explore and learn about nano-oxide metastability by comparing the nano-particle response when the Fe-14Cr<sub>0.3</sub>Ti<sub>0.3</sub>(Y<sub>2</sub>O<sub>3</sub>) material is placed under thermodynamic condition (1300°C, 1h), or driven far from equilibrium by means of Fe+ ion beam (150 dpa at 500°C).

In the as-received condition, nano-particles appear to display both chemical and structural metastability since they are unknown YTiCrO compounds with a cubic crystallographic structure. Under ion beam, radiation-induced Ostwald-ripening and Cr mobility ensured by point defect drag mechanism, make nano-oxide self-organize such that chemical metastability has been sustained. This result rationalizes the immiscible YTiCrO system as being stabilized through a nonequilibrium kinetic pathway. Under thermodynamic condition, the initial YTiCrO nano-particles changed into fcc Y<sub>2</sub>Ti<sub>2</sub>O<sub>7</sub> particle surrounded by a Cr shell. The Cr shell varies linearly with the particle size. Its formation may result in that Cr has to be released out so that particles achieve to relax toward equilibrium.

## **Roughness evolution of sol-gel optical coatings under ion beam sputtering**

Patrick Gailly, Olivier Dubreuil, Karl Fleury-Frenette

*Centre Spatial de Liège - Université de Liège, Belgium*

The surface roughness evolution of two silica-based sol-gel materials under 650 eV argon ion beam sputtering has been investigated. The liquid sol-gel solutions had been applied on silicon substrates using the dip coating technique and then thermally cured to obtain solid thin films. Their thickness had then been controlled over the samples surface using spectroscopic ellipsometry. The surface roughness of the sol-gel films has been measured using both interferometric profilometry and atomic force microscopy at different sputtering depths. Roughness increases significantly faster with sputtering depth in sol-gel layers than on bulk fused silica. Interestingly, the sputtering rates of the sol-gel layers are also observed to be approximately twice that of bulk fused silica. The development of micron scale holes with relatively stable interstices rules the surface roughness evolution. AFM measurements revealed a regular submicron scale lateral structure which nanometric amplitude is amplified under sputtering. The origin of the surface features is discussed.



## Columnar nano-void formation on germanium under $\text{Sn}^+$ ion implantation: $\text{Ge}_{1-x}\text{Sn}_x$ walls

Maria Secchi<sup>1,2</sup>, Evgeny Demenev<sup>1</sup>, Damiano Giubertoni<sup>1</sup>, Lia Vanzetti<sup>1</sup>, Massimo Bersani<sup>1</sup>

<sup>1</sup>FBK - Fondazione Bruno Kessler, Italy

<sup>2</sup>Department of Physics - University of Trento, Italy

As it is well known, Ge undergoes a peculiar surface nanostructuration under heavy ion implantation at room temperature [1,2]. In fact, once a threshold dose ( $\sim 5\text{-}10 \times 10^{14}$  at/cm<sup>2</sup>) is reached, the formation of a relatively regular nanostructured network of columnar voids with  $\sim 20$  nm diameter and  $\sim 100$  nm depth occurs. The formation mechanism of these structures seems to be strongly dependent on the different vacancy and interstitial mobility in Ge and clustering of vacancy [2].

In this work, Ge (1.5  $\mu\text{m}$  thick film epitaxial on Si(100) or bulk) was implanted with  $5\text{-}100 \times 10^{14}$   $\text{Sn}^+$ /cm<sup>2</sup>. A protective layer ( $\text{SiN}_x$ ) with different thickness (0, 10 nm, 20 nm) was deposited on Ge to prevent contamination of the nanostructures and to act on voids formation, to modify their size, dimension and symmetries [3]. The implantation energies were tuned in order to obtain the same Sn distribution in samples with the same dose but different protective layer thickness. Our goal is the formation of nanostructures with  $\text{Ge}_{1-x}\text{Sn}_x$  walls through thermal treatment of our samples, in order to combine the peculiar properties of  $\text{Ge}_{1-x}\text{Sn}_x$  alloy (tunable bandgap[4], high electron and hole mobility[5]) with the Ge nanostructures.

Electronic microscopy (TEM cross sections and SEM plan views) and AFM measurements allowed the morphologic characterization of our samples. SAD measurements gave information on the crystallization degree. Moreover SIMS and RBS measurements provided information on Sn distribution and damaged layer thickness. XPS characterization was used to investigate the Ge oxidation degree as a function of the air exposition time and the identification of other contaminants.

[1] I. Wilson, J. Appl. Phys. 53, 1698 (1982).

[2] N.G. Rudawski and K.C. Jones, J. Mater. Res. 28, 1633 (2013).

[3] T. Janssens et al., J. Vac. Sci. Technol. B 24, 510 (2006).

[4] G. He and H.A. Atwater, Phys. Rev. Lett. 79, 1937 (2007).

[5] J.D. Sau and M.L. Cohen, Phys. Rev. B 75, 045208 (2007).

## **Novel microstructures on the surfaces of metal and single crystal silicon irradiated by intense pulsed ion beams**

Jie Shen, Yanyan Zhang, Gaolong Zhang, Haowen Zhong, Xiao Yu, Jie Zhang, Miao Qu, Xiaofu Zhang, Xiaoyun Le

*Beihang University, P.R. China*

IPIB (Intense Pulsed Ion Beams) have been developed over decades for various applications, including surface treatment, films deposition and nanophase powder synthesis. The beams' (with ion currents  $I \sim 5\text{kA}$ , and ion energies  $E \sim 400\text{keV}$ ) short pulse duration ( $\leq 1\mu\text{m}$ ) and high deposited energy density ( $\sim \text{J}/\text{cm}^2$ ) without reflection make them promising for wide commercial use. The key process of the IPIB surface treatment is the induced rapid melt and re-solidification at up to  $10^{10}\text{ K/s}$ , which may at the same time, introduce non-equilibrium microstructures or defects, such as the familiar craters, cracks and ripples, thus affecting the performance of modified materials. Many related researches have been presented.

In our recent work, metal specimens like copper and titanium, single crystal silicon with high purity were chosen to study the IPIB material processing. After surface irradiation by IPIB (given by BIPPAB-450 accelerator in Beihang University) with different pulse numbers, and corresponding analysis, some novel forms of microstructures such as flower-like craters and closed bubbles were found on or inside the surface layer. Some possible mechanisms for their formation were presented respectively.

## Helium depth profiling by NRA, PES and HI-ERD: Application to advanced nuclear materials

Patrick Trocellier<sup>1</sup>, Thomas Loussouarn<sup>1</sup>, Frederic Lepretre<sup>1</sup>, Sylvain Vaubailon<sup>1</sup>, Helene Lefaix-Jeuland<sup>2</sup>, Sofia Gorondy-novak<sup>2</sup>, Yves Serruys<sup>1</sup>, Lucile Beck<sup>1</sup>

<sup>1</sup>CEA, Laboratoire JANNUS, France

<sup>2</sup>CEA, DMN-SRMP, France

The solubility of helium atoms is generally extremely low in metallic and non-metallic compounds. The helium accumulation in nuclear materials may induce detrimental effects on their thermo-mechanical properties and deep modifications of their microstructure.

The quantitative characterization of helium isotopes is not a so easy task mainly due to the extreme stability of  $^3\text{He}$  and  $^4\text{He}$  nuclei. Ion beam analysis offers several opportunities in order to determine the depth profile of both isotopes. Direct observation of deuteron-induced nuclear reactions (d-NRA), proton enhanced scattering (PES) and high energy heavy ion-induced elastic recoil spectrometry (HI-ERD) can be used to follow the helium behavior accumulated in materials submitted to thermal and/or radiation treatments.

This paper is devoted to the comparison of experimental conditions and performances allowed by the use of d-NRA, PES and HI-ERD in quantitative analysis of helium. Several application examples to model advanced nuclear materials implanted with helium ions and then submitted to fully controlled thermal annealing tests are presented and discussed.

## Specific features of helium retention mechanisms in inorganic compounds

Patrick Trocellier, Shradha Agarwal, Sandrine Miro, Sylvain Vaubaillon, Yves Serruys

*CEA, Laboratoire JANNUS, France*

Ageing processes of candidate materials for applications in future fission reactors, fusion devices and radioactive waste management include a lot of physico-chemical phenomena in which temperature and radiation play a major role. The consequences of the accumulation of helium generated by neutron-induced nuclear reactions or  $\alpha$ -decay of actinides constitute one of the most exciting challenges to be solved.

Ion implantation is a useful technique to introduce a precise quantity of helium in inorganic materials such as metals (Fe, W), binary oxides ( $\text{ZrO}_2$ ,  $\text{UO}_2$ ), carbides (SiC, TiC, ZrC) or nitrides (TiN) and more complex mineral matrices (britholite, zirconolite, glass) used to simulate the behaviour of advanced nuclear materials submitted to realistic operation conditions.

This paper presents specific features observed in the study of retention mechanisms of helium in a broad range of materials. After a brief description of our experimental methodology based on the use of the  $^3\text{He(d, p)}^4\text{He}$  nuclear reaction analysis in millibeam or microbeam modes (NRA) coupled with transmission electron microscopy (TEM), we discuss some typical results in order to illustrate:

- the broad variation range of apparent diffusion coefficients and thermal activation energy [1],
- the role of implanted ion fluence,
- the influence of grain size and crystallinity degree of the implanted sample,
- the evolution of helium release with annealing temperature and duration,
- the evolution of the morphology of helium bubbles under thermal annealing.

[1] P. Trocellier, S. Agarwal, S. Miro, J. Nucl. Mater. 445, 128-142 (2013).

## Micro-characterization of ion-irradiated materials for nuclear applications

Junhyun Kwon<sup>1</sup>, Hyung-Ha Jin<sup>1</sup>, Chansun Shin<sup>2</sup>, Peter Hosemann<sup>3</sup>

<sup>1</sup>*Korea Atomic Energy Research Institute, South Korea*

<sup>2</sup>*Myongji University, South Korea*

<sup>3</sup>*UC Berkeley, USA*

One of key issues in the field of nuclear materials is to evaluate the degradation of material properties as a result of neutron irradiation. Tests of neutron-irradiated materials are rather limited due to activation, cost, time and the availability of proper facilities. Ion beam irradiation can be used to simulate neutron irradiation of materials in a controlled way but has the limitation of small penetration depth in the order of micro-meter. We develop the techniques for micro-scale materials test, which will allow us to obtain mechanical properties of ion-irradiated sample with its limited penetration depth. Also, it is expected that this method will be directly applicable to neutron-irradiated samples.

In this work, we performed micro-compression tests on two alloys irradiated by ions, including oxide dispersion-strengthened (ODS) steels and nanostructured stainless steels. The specimens were fabricated in the shape of circular pillars by an FIB (Focused ion Beam) machine. To obtain pillars that contain the ion-irradiated zone in the order of micro-meter from the surface, pillars were manufactured at the edge of a bulk sample, which are perpendicular to the ion irradiating direction. Circular pillars with a diameter ranging from 0.7  $\mu\text{m}$  to tens of  $\mu\text{m}$  were made to minimize the taper angle and were tested with a conical diamond flat indenter. From micro-compression tests, we evaluated the engineering stress-strain curves depending on the pillar size. While no changes in yield strength were found in irradiated and non-irradiated samples for ODS steels, the effect of the pillar size on mechanical properties were observed from stainless steels. Below the critical size of a pillar, the smaller one exhibits the weaker strength. The fact that the bulk mechanical properties can be obtained with pillars as small as a few micro-meters is promising in the nuclear materials field.

## Microstructural evolution of austenitic stainless steel after helium and hydrogen ion irradiation

Hyung-Ha Jin, Eunsol Ko, Junhyun Kwon

*Korea Atomic Energy Research Institute, South Korea*

Ion irradiation method has been conventionally used to understand various radiation induced phenomena in structural materials under neutron irradiation. The objective of this work is to study the effects of helium and hydrogen on radiation induced changes in microstructure in austenitic stainless steel by ion irradiation experiment and transmission electron microscopy.

Helium and hydrogen ion irradiations in the 50 – 490 keV energy range were used to obtain uniform radiation damage of about 5 dpa. Depth profiles of displacement damage and stopped helium and hydrogen ions were calculated by SRIM code. Typical radiation induced microstructural changes such as the formation of fine dislocation loop in the matrix and radiation induced segregation (or depletion) at grain boundary were observed in both the helium and the hydrogen irradiated samples. The structure of the ion-irradiation-induced dislocation loop was identified as frank loops formed on {111} planes. The size of the frank loops after helium ion irradiation is smaller than that after hydrogen ion irradiation. The helium irradiation leads to the formation of bubble at grain boundary as well as in the matrix whereas the depletion of Cr and the segregation of Ni were occurred more considerably at grain boundary after the hydrogen irradiation. In addition, the transformed martensites (or ferrite) were observed along the grain boundary as well as at surface in the hydrogen irradiated sample.

## **Influence of ion irradiation coupled with He implantation on the swelling microstructure of austenitic stainless steels**

Stéphanie Jublot-Leclerc<sup>1</sup>, Xiaoqiang Li<sup>1</sup>, Marie-Laure Lescoat<sup>2</sup>, Franck Fortuna<sup>1</sup>, Cédric Pokor<sup>2</sup>, Aurélie Gentils<sup>1</sup>

<sup>1</sup>*CSNSM, Univ Paris-Sud et CNRS-IN2P3, 91405 Orsay, France*

<sup>2</sup>*EDF R & D, Groupe Métallurgie, Les Renardières, France*

Extending nuclear power plants lifetime requires a very good knowledge and a good control of the mechanisms of ageing of all their components. This study deals with nuclear reactors material components of Pressurized-Water Reactors (PWR), such as Reactor Pressure Vessel Internals, made of austenitic stainless steels, which are subjected to intense irradiation at elevated temperature. These extreme conditions alter significantly their properties, and a phenomenon of swelling due to irradiation may be possible under PWR conditions. The sensitivity of materials to swelling when irradiated has been studied mainly in the context of work on fast breeder reactors (FBR) above 400°C. It is not therefore possible to extrapolate the FBR data to the operating conditions in PWRs without considering additional factors, and in particular, the effect of He gas produced by the “thermal” neutrons in the PWR spectrum. The main objective of our study is to define, at the nanoscale, mechanisms and kinetics of swelling occurring in austenitic stainless steels under long-term neutron irradiation, while taking into account synergistic effects of irradiation and helium gas. In this study, experiments were carried out on 316LSH1 industrial austenitic stainless steels at the JANNuS-Orsay facility using simultaneous ion irradiation and helium ion implantation in the transmission electron microscope. Ion irradiations and implantations were performed at elevated temperatures (200, 450 and 550°C) to doses obtained after several years in reactors. Detailed and quantitative results on the microstructure of the material will be shown and in particular, the influence of temperature, dose and helium on the formation of cavities will be discussed.

We acknowledge financial supports from the French National Research Agency through project ANR-11-BS09-006, and from the French EMIR network.

## Deuterium-hydrogen isotope exchange in self-damaged tungsten studied by in-situ nuclear reaction analysis

Heun Tae Lee<sup>1</sup>, Thomas Schwarz-Selinger<sup>2</sup>

<sup>1</sup>*Osaka University, Japan*

<sup>2</sup>*Max Planck Institute for Plasmaphysics, Germany*

Presently, tungsten (W) is the leading plasma facing material in magnetic fusion devices. Tritium (T) will be used as a fuel species, and its retention in W must be strictly controlled as it impacts both the safety and operation of a fusion device. These considerations have motivated extensive studies on hydrogen retention behavior in W, and a large database now exists. However, a general and quantitative understanding has not been achieved in many of the areas studied due to: (1) the uncertainty of hydrogen binding with a variety of matrix entities (e.g. solute atoms and defects), which recent atomistic simulations have greatly advanced, and (2) the inability to rigorously test theoretical treatments of transport processes that encompass such hydrogen interactions with matrix entities (i.e. trapping kinetics). To meet such deficiency, we have leveraged the unique capabilities of in-situ ion implantation and nuclear reaction depth profiling to study the kinetics of D trapping and release.

W sample was first implanted with 20 MeV W ions to introduce defects, followed by recrystallization at 2000 K. Next, the sample was implanted with 9 keV D<sup>3+</sup> up to a fluence of  $\sim 10^{24}$  D/m<sup>2</sup> over several implantation steps. The experiments were performed at 300 K and 450 K to examine surface and bulk (up to 8  $\mu$ m) trapping and release kinetics, respectively. Following each D implantation step, the depth distribution of trapped D was measured in-situ using the D(<sup>3</sup>He,p)<sup>4</sup>He reaction. Measurements confirm diffusion limited trapping kinetics as D diffuses inwards into the bulk. Following D implantation, H was implanted over several implantation steps, and the loss of D measured. This yielded information on the de-trapping and release kinetics of D by H, which showed that the D loss within the first 30 nm decays linearly with time, whereas, the D loss at depths greater than 3  $\mu$ m decays exponentially with time, indicating recombination and diffusion limited processes, respectively.



## Nanomechanical properties of Ar-irradiated zirconia polymorphs developed on pure zirconium.

Lukasz Kurpaska<sup>1</sup>, Jacek Jagielski<sup>1</sup>, Iwona Jozwik-Biala<sup>2</sup>

<sup>1</sup>*National Center for Nuclear Research, Poland*

<sup>2</sup>*Institute of Electronic Materials Technology, Poland*

Due to its high corrosion resistance, good mechanical properties and low neutron absorption rate, zirconium and its alloys are commonly used in nuclear reactors. Zr-based alloys can serve as a future fuel claddings, spreaders for fuel elements and for core structural materials. During their operation time in reactor these elements are irradiated by neutrons which results in radiation damage. Ion implantation is not only an excellent tool for modifying surface of materials but also for simulating radiation damage. Despite of abundant amount of research, corrosion behavior and mechanical properties of zirconium and zirconium polymorphs subjected to the influence of neutrons or effect of ion implantation damage are still under consideration.

Study of materials exposed to neutron radiation requires placing them into the reactor, which activates the sample and is a very expensive and long-lasting process. Therefore, the most effective way of study mechanical properties occurring during long term exposure to radiation is implementation of accelerated ion beams. Such technique provides certain advantages i.e.: a) high displacement rate resulting in short irradiation time and b) precise control of bombardment conditions.

In this study, effect of Ar—irradiation on nanomechanical properties of pure zirconium and its oxide at room temperature were investigated. In order to simulate the irradiation damage, the argon ions were implanted in the pure zirconium and zirconia oxide with fluences ranging from  $1 \times 10^{15}$  to  $1 \times 10^{17}$  ions / cm<sup>2</sup>. In order to reveal grain structure, surface of zirconium samples were chemically polished in a solution of HF/HNO<sub>3</sub>/H<sub>2</sub>O. Then, nanomechanical properties of big/small grains, grain boundaries and monoclinic zirconia phase were measured using a nanoindentation technique. The results revealed correlation between effect of Ar-implantation dose, hardness and Young modulus of grains, grain boundaries and oxide phases.

## Slow positron annihilation studies on helium irradiated tungsten

M.H. Cui, Z.G. Wang, C.F. Yao, T.L. Shen, L.L. Pang, B.S. Li, J.R. Sun, Y.B. Zhu

*Institute of Modern Physics, CAS, P.R. China*

The divertor in future International Thermonuclear Experimental Reactor (ITER) will have to face a very severe environment, e.g. intense neutron, helium and hydrogen isotopes irradiations. Therefore the materials used as divertor must possess intrinsic advantages such as low sputtering yield for light elements, high melting point and good thermo-mechanical behaviour etc. Tungsten is such a candidate divertor material. The defects evolution and defects-helium interaction studies have been a focus in the frame of materials for fusion reactors. Slow positron annihilation technique is a very promising probe because it has been proved to be very efficient in sensing the micro structural evolution which cannot be detected using conventional transmission electron microscopy.

In our present investigation, high pure tungsten samples were irradiated at room temperature to fluence from  $1 \times 10^{16}$  to  $5 \times 10^{17}$  ions/cm<sup>2</sup> with 200 keV He ions and fluence from  $1 \times 10^{16}$  to  $1 \times 10^{17}$  ions/cm<sup>2</sup> with 500 keV He ions respectively. Irradiation experiment was completed at the 320 kV Multi-discipline Research Platform for Highly Charged Ions in Institute of Modern Physics. After irradiation, the Doppler broadening of the positron annihilation gamma ray lineshape has been adopted to infer the damage evolution process in helium-implanted tungsten as a function of irradiation fluence at room temperature. The doppler broadening spectroscopy shows, that with increasing fluence, the S parameters increase first and then decrease when the fluence is above  $5 \times 10^{16}$  ions/cm<sup>2</sup>. Based on roles of the displacement damage level, as well as helium diffusion and occupation induced by high density helium or ratio between helium and dpa, the formation and evolution of vacancy type defects are discussed.

## Surface swelling and spectroscopic investigations of Au-ion irradiated monazite-(Ce) crystals

Andreas Artac<sup>1</sup>, Bernhard Jachs<sup>2</sup>, Christoph Lenz<sup>1</sup>, Shavkat Akhmadaliev<sup>3</sup>, Gerlinde Habler<sup>1</sup>, Dominik Talla<sup>1</sup>, Lutz Nasdala<sup>1</sup>

<sup>1</sup>*University of Vienna, Austria*

<sup>2</sup>*Johannes Kepler University Linz, Austria*

<sup>3</sup>*Helmholtz-Zentrum Dresden-Rossendorf, Germany*

The accumulation of radiation damage in minerals and other solids is associated with dramatic changes in chemical and physical properties [1], therefore making irradiation-induced amorphisation, and its accompanying effects, an important issue for the Earth sciences (e.g. interpretation of geochronological data) and materials sciences (e.g. potential use of mineral-based ceramics as nuclear waste forms [2]). In this present research, volume swelling of natural monazite-(Ce) (monoclinic  $\text{CePO}_4$ ), and synthetic analogues, as induced by irradiation with MeV Au ions, is investigated. Samples were irradiated with combinations of 1 MeV, 4 MeV and 10 MeV Au ions, with fluences ranging between  $2.25 \times 10^{13}$  and  $7 \times 10^{14}$  ions/cm<sup>2</sup>.

Volume expansion at the surface of irradiated bulk samples was measured using an AFM (atomic force microscopy) system. For this, special apertures were applied to limit irradiation to definite surface areas. In addition, widths of Raman bands related to internal  $\text{PO}_4$  vibrations were determined for irradiated FIB (focused ion beam) foils. Lamellae, 1.5 micrometres in thickness, were prepared for these irradiations, to ensure that sample thicknesses corresponded to the trajectory lengths of the ions irradiated.

Both macroscopic volume swelling and widths of Raman bands increase as a function of the ion fluence. At very high irradiation damage, the tabular volume swelling is virtually “framed” by ridges emerging at the edges of the areas irradiated. Opportunities to use parameter changes for quantifying irradiation effects in unknowns are discussed.

The authors acknowledge funding by the University of Vienna Doctoral School IK052, and the Austrian Science Fund (FWF) through project P24448-N19 to L.N.

[1] W.J. Weber, J Mater Res 5: 2687-2697 (1990).

[2] J.M. Montel, CR Geosci 343: 230-236 (2011).

## Ion-damaged diamond and graphite in deuterium plasma

Alec Deslandes<sup>1</sup>, Mathew C. Guenette<sup>1</sup>, Inna Karatchevtseva<sup>1</sup>, Matthew Thompson<sup>2</sup>, Lars Thomsen<sup>3</sup>, Mihail Ionescu<sup>1</sup>, Cormac S. Corr<sup>2</sup>, Daniel P. Riley<sup>1</sup>, Gregory L. Lumpkin<sup>1</sup>

<sup>1</sup>*Australian Nuclear Science and Technology Organisation, Australia*

<sup>2</sup>*Australian National University, Australia*

<sup>3</sup>*Australian Synchrotron, Australia*

Fusion materials will suffer radiation damage effects due to energetic particles, including hydrogen and helium ions, and high energy neutrons from the fusion fuel and its reaction products. Of the pure carbon materials, diamond has the strongest chemical bonds, greatest resistance to radiation damage, and exhibits lower erosion rates than other forms of carbon in hydrogen plasma. Impinging fluxes of energetic ions and neutrons modify the structure of diamond from the sp<sup>3</sup>-bonded lattice to disordered sp<sup>3</sup> or graphitic states, which may degrade the attributes that make the as-prepared material an attractive choice. Of particular concern for carbon materials is the retention of hydrogen isotopes via implantation or erosion and redeposition processes.

In this work diamond and graphite samples were irradiated with 5 MeV carbon ions to simulate the damage created by the collision cascades of 14 MeV neutrons. Samples were also exposed to deuterium plasma in the MAGnetised Plasma Interaction Experiment (MAGPIE), a linear plasma device at the Australian National University (ANU) capable of creating fusion-relevant plasma conditions. For the case of diamond, Raman spectroscopy results revealed 5 MeV carbon ion irradiation induced broad disordered and graphitic carbon peaks, and isolated defect peaks, which increased in intensity with increased ion fluence. Preferential erosion of disordered and graphitic carbon was observed in the Raman spectra after exposure to deuterium plasma in MAGPIE. Changes to the surface chemistry were characterised using Near-Edge X-ray Absorption Fine Structure spectroscopy. The sp<sup>2</sup> signal was observed to increase with fluence of carbon ions, but then decreased following exposure to deuterium plasma. Retention of deuterium was measured using elastic recoil detection analysis. Retention was observed to increase for the case of 5 MeV carbon ion-irradiated diamond, but the retained deuterium was less than for the case of ion-irradiated graphite.

## Ion implantations of oxide dispersion strengthened steels

Stanislav Sojak<sup>1</sup>, Jana Simeg Veternikova<sup>2</sup>, Vladimir Slugen<sup>1</sup>, Martin Petriska<sup>1</sup>

<sup>1</sup>*Institute of Nuclear and Physical Engineering, Faculty of Electrical Engineering and Information Technology, Slovak University of Technology, Slovakia*

<sup>2</sup>*Slovak University of Technology, Slovakia*

Oxide dispersion strengthened steels (ODS) are one of the candidate structural materials for application in future nuclear facilities as Gen IV. and fusion reactors. These steels fulfill demands on radiation, thermal and mechanical resistance during operation of nuclear reactor.

Our work was focused on study of radiation damage of ODS steels, simulated by hydrogen ion implantations at linear accelerator at Slovak University of Technology. The ODS steels MA 956 and PM 2000 were available for study in as-received state after different thermal treatments and in ion implanted state. Energy of hydrogen ions chosen for implantation was 800 keV and the dose of  $6.24 \times 10^{17}$  ions/cm<sup>2</sup>.

Specimens were measured by non-destructive technique Positron Annihilation Spectroscopy (PAS) in order to study defects behavior after different thermal treatments in as-received state and after the hydrogen ion implantations. Different resistance to defects production was observed in both MA 956 and PM 2000 steels.

**Xe ion irradiation of ZrN-coated U-Mo/Al dispersion fuel**

Bei Ye, Di Yun, Edward O'Hare, Abdellatif Yacout, Mo Kun, Walid Mohamed, Yeon Soo Kim, Gerard Hofman, Jeffrey Fortner, Michael Pellin, Thomas Wiencek

*Argonne National Laboratory, USA*

High-density U-Mo alloy dispersion fuel in an Al matrix has been developed for high-performance research reactors under the Global Threat Reduction Initiative (GTRI) conversion program. Interdiffusion between U-Mo and Al is one of the major obstacles in this fuel development because it decreases fuel-zone thermal conductivity, produces volume expansion while consuming the Al matrix, and in some high power tests, showed the formation of large fission-gas-filled pores that can lead eventually to a fuel plate failure. As a remedy, applying a coating such as ZrN on U-Mo particles as a diffusion barrier has been proposed. In order to examine the stability and effectiveness of the ZrN coating on U-Mo, we tested dispersion fuel samples containing ZrN-coated U-Mo particles or bare U-Mo particles using a high-energy (84 MeV) Xe ion beam at the ATLAS facility in Argonne National Laboratory. Xe was selected considering it is a dominant gaseous fission product. Post-irradiation examinations include scanning electron microscopy (SEM), transmission electron microscopy (TEM) and X-ray analyses.

## Effects of multilayer and multimaterial structure on space proton radiation protection

Guoliang Ma, Xingji Li, Chaoming Liu, Jianqun Yang, Chunfeng Hou

*Harbin Institute of Technology, P.R. China*

An investigation of multilayer (and multimaterial) structure for space proton radiation protection is presented. In this research, both the role of the material itself on the shielding efficiency and the effect of the structure of the shield were considered. By simulations with the Geant4, the possibility of combining optimized properties of given materials (aluminum, copper and tantalum) in a multilayer structure was given for solar proton protection. Based on the simulation results, it is valuable to change a monomaterial absorber as an optimized multilayer or multimaterial shield for shielding the high energy protons. In order to prove the validity of simulation results, 9 MeV protons irradiation were performed. The good agreement between simulation results and experimental data confirms that the Geant4 code can be used to accurately calculate high-energy proton radiation protection.

## Ion beam studies of plasma first wall materials - tungsten

Yongqiang Wang<sup>1</sup>, S. Pathak<sup>1</sup>, N. Mara<sup>1</sup>, J. Tesmer<sup>1</sup>, E. Dechaumphai<sup>2</sup>, J. Barton<sup>2</sup>, R.K. Chen<sup>2</sup>, G. Tynan<sup>2</sup>, R.P. Doerner<sup>2</sup>

<sup>1</sup>*Los Alamos National Laboratory, USA*

<sup>2</sup>*University of California at San Diego, USA*

The plasma facing material faces not only harsh plasma erosion but also fast neutron damage. To facilitate experimental research on plasma-first wall interactions, deuterium plasma has been used as a surrogate for D-T plasma exposure and ion irradiation as a surrogate for neutron in studying radiation damage. In this report, we explore three depth-sensitive techniques to study near surface deuterium retention profile, mechanical strength, and thermal conductivity of ion irradiated tungsten.

First, we study the effects of ion irradiation damage on the deuterium retention rate and deuterium depth profile using  $D(^3\text{He}, p)^4\text{He}$  nuclear reaction analysis technique. ITER grade W specimens were pre-damaged with varying ion beam conditions at Los Alamos National Laboratory before D-plasma exposure in the PISCES linear plasma device at UCSD. Deuterium concentration profiles are discussed along with the irradiation induced defects as various trap sites in W.

Second, we study the local mechanical response of radiation-induced changes in ion irradiated W using spherical nanoindentation stress-strain curves. We will discuss the capabilities of spherical nanoindentation stress-strain curves, extracted from the measured load-displacement dataset, in characterizing the local mechanical behavior within individual grains in polycrystalline W as a function of radiation-induced damage.

Third, we study the thermal conductivity of near-surface regimes damaged by ion irradiation using a technique referred to as the 3-omega 'method. By modulating the frequency of the heating current in a micro-fabricated heater strip, the technique enables the probing of near-surface thermal properties as a function depth. The technique was applied to measure the thermal conductivity of a thin ion-irradiated layer on a tungsten substrate. , which was found to decrease by more than 50% relative to pristine tungsten for a moderate damage dose of less than 1 dpa.



## Magnetization and X-ray absorption spectroscopy of Mn implanted Ge after flashlamp annealing

Shengqiang Zhou

*Helmholtz-Zentrum Dresden-Rossendorf, Institute of Ion Beam Physics and Materials Research, Germany*

Ge-based diluted magnetic semiconductors have drawn extensive attention over the past decades due to their potential to be applied in spintronic devices and to be integrated with the mainstream Si microelectronics as well. In this contribution, we will present the magnetic properties and X-ray absorption spectroscopy of Mn implanted Ge annealed by flashlamp.

Ge(001) wafers were implanted with Mn ions, resulting in a box-like distribution of Mn ions with concentration around 10 at.% (or 2 at.%) over a depth of 100 nm. After implantation the samples were subjected to flashlamp annealing (FLA) with the pulse duration of 3 ms and with the energy density between 44 and 56 J/cm<sup>2</sup>. All samples show ferromagnetism with the Curie temperature between 250 and 300 K which may be interpreted as the co-contribution of the Ge matrix diluted with Mn ions and of Mn-rich nanoclusters [1]. SQUID measurements show evidence for multiple distinct magnetic phases or a bimodal size distribution for the Mn-rich nanoclusters. In X-ray absorption spectroscopy (XAS), clearly x-ray magnetic circular dichroism is observed. However, the XAS is much different from Mn<sub>5</sub>Ge<sub>3</sub>, which shows a featureless and broad spectrum [3]. It is also different from the spectrum of tetrahedrally coordinated Mn<sup>2+</sup> in the high spin S=5/2 configuration [4]. XAS results also indicate multiple electronic configuration of Mn, in agreement with the magnetic properties. Moreover, we measured large positive magnetoresistance for these samples. The enhancement of magnetoresistance is consistent with the magnetization as well as the inhomogeneous nature of the implanted layer [5].

- [1] S. Zhou et al., PRB 81, 165204 (2010).
- [2] S. Zhou, et al., APL, 95, 192505 (2009).
- [3] P. De Padova, et al., PRB 77, 045203 (2008).
- [4] L. Ottaviano, et al., APL 90, 242105 (2007).
- [5] I.-S. Yu, et al., JAP 109, 123906 (2011).

**Possible defect-induced ferromagnetism in Cr doped SiC single crystals**

Yu Liu<sup>1</sup>, Shengqiang Zhou<sup>1</sup>, Gang Wang<sup>2</sup>, Shunchong Wang<sup>2</sup>, Wei Sun<sup>2</sup>, Xiaolong Chen<sup>2</sup>

<sup>1</sup>*Institute of Ion Beam Physics and Materials Research, Helmholtz-Zentrum  
Dresden-Rossendorf (HZDR), Germany*

<sup>2</sup>*Institute of Physics, Chinese Academy of Sciences, P.R. China*

Defect-induced ferromagnetism (FM) was realized in non-magnetic materials, such as highly oriented pyrolytic graphite (HOPG), HfO<sub>2</sub>, and Li doped ZnO. Recently, such FM was also found in SiC by doping, neutron bombardment and ion implantation. As now SiC crystals are available in microelectronic grade, the good crystallinity makes SiC a kind of potential materials for spin electronics. However, one problem in defect-induced FM in bulk SiC crystals is that the magnetization induced by defects is not strong, which might increase the difficulty for the further study. Here, we demonstrate the enhanced defect-induced FM in Cr doped SiC. The 4H-SiC single crystals were grown by physical vapor transport method. The SiC sample is diamagnetic when the nominal doping density of Cr is below 0.5%, whereas the room-temperature FM reaching  $1.5 \times 10^{-3}$  emu/g is observed in SiC with 1% Cr doping. However, the actual Cr concentrations in magnetic SiC measured by secondary ion mass spectroscopy are nearly equal in both the nominal 0.5% and 1% samples, so Cr doping is not the origin of the FM. After annealing, the decreased magnetization suggests that the FM is closely associated with defects. However, we can not distinguish the defect types by positron annihilation lifetime spectroscopy or photoluminescence. The defects with higher dimensions rather than divacancies are proposed to induce the FM in Cr doped SiC. More efforts are needed to clarify this puzzling phenomenon.

**Ion induced modifications of Mn-doped ZnO films**

Noriaki Matsunami<sup>1</sup>, M. Itoh<sup>1</sup>, M. Kato<sup>1</sup>, S. Okayasu<sup>2</sup>, M. Sataka<sup>2</sup>, H. Kakiuchida<sup>3</sup>

<sup>1</sup>*Nagoya University, Japan*

<sup>2</sup>*Japan Atomic Energy Agency, Japan*

<sup>3</sup>*National Institute of Advanced Industrial Science and Industry, Japan*

We have studied modifications of Mn(6%)-doped ZnO films (known as n-type transparent semiconductor) on SiO<sub>2</sub>-substrate by ion irradiation. For 100 MeV Xe ion irradiation at room temperature, we find the reduction of the XRD intensity to 1/50 of that of unirradiated film, lattice compaction of 0.4 % at the ion fluence of  $4 \times 10^{14} \text{ cm}^{-2}$ , little bandgap change (<0.02 eV) and five order of magnitude reduction of the electrical resistivity to  $\sim 30 \text{ } \Omega\text{cm}$ . The electrical resistivity modification can be ascribed to the increase of the carrier (electron) density due to replacement of Zn by Mn induced by ion irradiation as in the case of In-doped ZnO [1]. We also find that temperature (T) dependence of the magnetic susceptibility ( $\chi$ ) of Mn-doped ZnO (SiO<sub>2</sub>-substrate was replaced by Al<sub>2</sub>O<sub>3</sub> to reduce the influence of the substrate) follows the Curie law:  $\chi = \chi_0 + C/T$  (i.e., para-magnetic) and the Curie constant C decreases to a half of that before irradiation ( $C_0 = 0.012 \text{ emu} \cdot \text{cm}^{-3}$ ) at the ion fluence of  $10^{12} \text{ cm}^{-2}$ . Modifications of the magnetic property can be explained by change of the valency of Mn induced by ion irradiation.

[1] N. Matsunami et. al., Nucl. Instrum. Meth. B268, 3071 (2010).

## Magnetic domains with non-collinear magnetizations fabricated by He ion bombardment

Alexander Gaul<sup>1</sup>, Arno Ehresmann<sup>1</sup>, Martin Wilke<sup>1</sup>, Hans Peter Oepen<sup>2</sup>, Sebastian Hankemeier<sup>2</sup>

<sup>1</sup>*University of Kassel, Germany*

<sup>2</sup>*University of Hamburg, Germany*

Arbitrary micro magnetic domain patterns are fabricated by light ion bombardment induced magnetic patterning (IBMP) of exchange biased thin films. In this way the size and shape of the magnetic domains and the direction and value of the anisotropy parameters of adjacent domains can be set independently.

Magnetic domains modified via ion bombardment are investigated by scanning electron microscope with polarization analysis (SEMPA) and magnetic force microscopy (MFM). Thereby magnetic ripples are revealed in the subdomain structure and analyzed via fast fourier transform algorithm. Furthermore the domain wall configuration between the particular domains is resolved and analyzed in dependence on the anisotropy configuration of the surrounding domains. Vibrating sample magnetometry (VSM) is performed to investigate the magnetic properties of the individual domain types, i.e. anisotropy, exchange bias field and coercivity.

## Room temperature ferromagnetism after low energy $H^+$ implantation in Li-doped ZnO microwires

Israel Lorite<sup>1</sup>, Benjamin Straube<sup>2</sup>, Carlos Zandelazini<sup>2</sup>, Pablo Esquinazi<sup>1</sup>, H. Ohldag<sup>3</sup>, Silvia P. Heluani<sup>2</sup>

<sup>1</sup>*Institut für Experimentelle Physik II, University of Leipzig, Linnéstraße 5, D-04103 Leipzig, Germany*

<sup>2</sup>*Laboratorio de Física del Sólido, Dpto. de Física, FCEyT, Universidad Nacional de Tucumán, Argentina*

<sup>3</sup>*Stanford Synchrotron Radiation Lightsource, Stanford University, Menlo Park, CA 94025, USA*

ZnO-based dilute magnetic semiconductors have attracted attention in the last years and many groups reported room temperature ferromagnetism (RTFM) in magnetic ions-doped ZnO. On the other hand, it has been pointed out that magnetic dopants are not necessary to obtain RTFM. Magnetic order has been observed in ZnO samples after introducing certain density of point defects like zinc vacancies (VZn). The control of such point defects to induce magnetic order at room temperature is, however, a difficult task and a rather weak reproducibility has been achieved up to now [1].

In the challenge to introduce point defects in a controlled way, high energy implantation of non magnetic ions is under intensive study [2]. However, high energy implantation has also a drawback, since it could reduce the crystallinity of ZnO affecting negatively the electrical and magnetic properties required for spintronic devices.

In this work, we present a 300 eV  $H^+$  implantation in Li-doped ZnO microwires as alternative to the high energy implantation for the creation of magnetic point defects. Our results indicate that Li can stabilize VZn formed during the low energy irradiation, triggering magnetic order at room temperature. As expected from this defect-induced magnetism phenomenon, the amount of stabilized VZn necessary to have magnetic order at room temperature is in the several percent range. The magnetic characterization of the microwires was done using a commercial Superconducting Quantum Interference Device (SQUID), X-ray magnetic circular dichroism (XMCD) and magnetoresistance measurements of single microwires.

[1] P. Esquinazi, W. Hergert, D. Spemann, A. Setzer, and A. Ernst, IEEE Transactions on magnetics 49, 4668 (2013).

[2] R.P. Borges, R.C. da Silva, S. Magalhães, M. M. Cruz, M. Godinho, J. Phys.: Condens. Matter 19, 476207 (2007).

## Rare-earth doped zinc oxide: Unravelling magnetic ordering, electrical and magnetotransport properties

John Kennedy<sup>1</sup>, Peter Murmu<sup>1</sup>, G.V.M. Williams<sup>2</sup>, Ben Ruck<sup>2</sup>, Jérôme Leveneur<sup>1</sup>, Andreas Markwitz<sup>1</sup>

<sup>1</sup>*GNS Science, New Zealand*

<sup>2</sup>*MacDiarmid Institute for Advanced Materials and Nanotechnology, New Zealand*

Spintronics is an emerging field with a potential for realizing smaller, faster and cheaper devices owing to their exploitation of intrinsic spin of a charge carrier in electronic devices [1]. There are number of semiconducting materials capable of displaying inherent spintronic properties, although, their low magnetic transition temperatures demands alternative materials such as dilute magnetic semiconductors to mitigate these issues. Rare-earth (RE) elements were reported to result in large magnetic moment due to spin polarization of host semiconductors [2].

In this paper, we report the results from 30-40 keV RE implanted with various fluences into ZnO single crystals and thin films. RBS and channelling results showed that in as-implanted ZnO:RE, majority of RE atoms occupy substitutional lattice sites [3]. Upon annealing a fraction of Gd atoms were found in random interstitials. The electronic transport properties are consistent with a degenerate semiconductor [4]. Non-linear Hall voltage along with an anomaly in temperature dependent resistivity at low temperatures are associated with inhomogenous transport mechanism in ZnO:Gd. Ferromagnetic ordering was observed in ZnO and ZnO:Gd annealed samples persistent up to room temperature [4]. Detailed results will be presented in conference highlighting the origin of magnetic ordering, electrical and magnetotransport properties in ZnO:RE.

[1] F. Pulizzi, Nat. Mater. 11, 367 (2012).

[2] S. Dhar, O. Brandt, M. Ramsteiner, V.F. Sapega, and K.H. Ploog, Phys. Rev. Lett. 94, 037205 (2005).

[3] P.P. Murmu, R.J. Mendelsberg, J. Kennedy, D.A. Carder, B.J. Ruck, A. Markwitz, R.J. Reeves, P. Malar, and T. Osipowicz, J. Appl. Phys. 110, 033534 (2011).

[4] J. Kennedy, G.V.M. Williams, P.P. Murmu, and B.J. Ruck, Phys. Rev B. 88, 214423 (2013).

## Magnetic properties of plasma-nitrided austenitic stainless steel single crystals

Enric Menéndez Dalmau<sup>1</sup>, Claude Templier<sup>2,3</sup>, José Francisco Lopez-Barbera<sup>4</sup>, Kristiaan Temst<sup>1</sup>, André Vantomme<sup>1</sup>, Jordi Sort<sup>5,6</sup>, Josep Nogués<sup>4,6</sup>

<sup>1</sup>*Instituut voor Kern- en Stralingsfysica (IKS), KU Leuven, Belgium*

<sup>2</sup>*Institut P', Université de Poitiers*

<sup>3</sup>*ENSMA, 86962 Futuroscope-Chasseneuil, France*

<sup>4</sup>*ICN2-Institut Catala de Nanociencia i Nanotecnologia, Campus UAB, 08193 Bellaterra (Barcelona), Spain*

<sup>5</sup>*Departament de Física, Facultat de Ciències, Universitat Autònoma de Barcelona, E-08193 Bellaterra, Spain*

<sup>6</sup>*ICREA-Institució Catalana de Recerca i Estudis Avançats, Barcelona, Spain*

Ferromagnetic single crystalline [100], [110] and [111]-oriented expanded austenite is obtained by plasma nitriding of paramagnetic 316L austenitic stainless steel single crystals for 1 hour at either 300°C or 400°C. Nitriding was carried out in the URANOS reactor where plasma is created in a quartz tube using a 13.56 MHz electromagnetic excitation with an incident input power of 700 W. After nitriding at 400°C, the [100] direction appears to constitute the magnetic easy axis due to the interplay between a large lattice expansion and the expected decomposition of the expanded austenite, which results in Fe and Ni-enriched areas. However, a complex combination of uniaxial (i.e., twofold) and biaxial (i.e., fourfold) in-plane magnetic anisotropies is encountered. It is suggested that the former is related to residual stress-induced effects while the latter is associated to the in-plane projections of the cubic lattice symmetry. Increasing the processing temperature strengthens the biaxial in-plane anisotropy in detriment of the uniaxial contribution, in agreement with a more homogeneous structure of expanded austenite with lower residual stresses. In contrast to polycrystalline expanded austenite, single crystalline expanded austenite exhibits its magnetic easy axes along basic directions. Moreover, the magnetic properties of a gradually nitrided austenitic stainless steel are also studied. Plasma nitriding at 400°C of a [100]-oriented 316L single crystal is carried out using a loose shadow mask to produce an in-plane lateral gradient of nitrogen concentration that extends up to 100 micrometers. Fingerprints of the expected transition from a nitrogen supersaturated solid solution to a multiphase nature of expanded austenite are evidenced along the gradually nitrided area.

## Ferromagnetism in BiFeO<sub>3</sub> enhanced by Co-implantation

Hiwa Modarres<sup>1</sup>, Enric Menéndez Dalmau<sup>1</sup>, Vera Lazenka<sup>1</sup>, Michael Lorenz<sup>2</sup>, Manisha Bisht<sup>1</sup>, Marius Grundmann<sup>2</sup>, Margriet J. Van Bael<sup>3</sup>, André Vantomme<sup>1</sup>, Kristiaan Temst<sup>1</sup>

<sup>1</sup> *Instituut voor Kern- en Stralingsfysica (IKS), KU Leuven, Belgium*

<sup>2</sup> *Institut für Experimentelle Physik II, Universität Leipzig, Linnéstraße 5, D-04103 Leipzig, Germany*

<sup>3</sup> *Laboratorium voor Vaste-stoffysica en Magnetisme, KU Leuven, Belgium*

Artificial multiferroic materials are attractive alternatives to intrinsic multiferroic materials as their ferroelectric (FE) and/or ferromagnetic (FM) properties can be externally tuned. An approach, which differs from the conventionally used FM/FE bilayers, is to implant ion species which might enhance and/or induce ferromagnetism in a ferroelectric host crystal. In this study, magnetic property of the BiFeO<sub>3</sub> (BFO) is enhanced through Co ion-implantation. BFO intrinsically shows both ferroelectricity and antiferromagnetism and, moreover in thin film with thickness below a few hundred nanometers, BFO exhibits weak ferromagnetism due to the suppression of the spin spiral structure. The BFO films are epitaxially grown on SrTiO<sub>3</sub> using pulsed laser deposition. It is well known that ferroelectric property depends crucially on the crystalline order. Therefore, in order to bring ferromagnetism into the ferroelectric matrix while at the same time minimizing the damage caused to the host crystal, Co ions have been implanted in the BFO crystals along (001) channeling direction, while the sample was kept at elevated temperature (400 °C). This way, ferromagnetism is introduced into the ferroelectric crystal via embedding Co atoms that have generated ferromagnetic counterparts. A Co-implantation of 1E16 ion/cm<sup>2</sup> with an energy of 60 keV in BFO has led to large enhancement of the coercivity. Although the coercivity improvement is clearly seen at room temperature SQUID measurements, it is the low temperature measurements that result in more fascinating coercivity enhancement. The ferromagnetic response enhancement is attributed to the formation of nanoscale cobalt ferrite particles within BFO which show a gradation of blocking temperatures. In this study, we have chosen an acceleration energy of 60 keV for Co-ions and this way have tuned the cobalt ferrite formation to occur around 30 nm deep under surface which in turn allows for further close-to-surface complementary studies.



## Depth profiling of TiO<sub>2</sub> nanostructures synthesized by ion implantation

Varsha Bhattacharyya<sup>1</sup>, Deepti Rukade<sup>1</sup>, Lokesh Tribedi<sup>2</sup>

<sup>1</sup>*University of Mumbai, India*

<sup>2</sup>*Tata Institute of Fundamental Research, India*

TiO<sub>2</sub> is a wide band gap n-type semiconductor exhibiting in three well known polymorphic phases; rutile, brookite and anatase. The closely balanced surface energies of these polymorphs results in phase transformation over a small difference in surface energy and thus it becomes essential to gain control over the stability of a particular phase. TiO<sub>2</sub> in its nanocrystalline form is studied extensively for a variety of applications such as dye synthesized photovoltaic devices, power circuits, optical coatings. Ion implantation is an efficient technique for synthesis of nanomaterials at the surface and embedded in the matrix up to a desired depth. In this process a thin layer of surface material deposited on a substrate is bombarded with an energetic reactive ion beam of some tens or hundreds of keV that gives rise to collision cascade by nuclear energy loss (Sn). The bombardment of reactive ions on a metallic surface results in formation of a metastable amorphous compound phase. Post implantation annealing in reducing atmosphere stimulates crystalline recovery along with coalescence of the phase formed into nanometer sized structures.

100nm titanium films deposited on SiO<sub>2</sub> are implanted by 60keV oxygen ions from ECR ion source. The energy is chosen using SRIM simulations such that the range results in formation of the oxide phase at the interface of the thin film and substrate. Implantation is carried out at two fluences,  $1 \times 10^{16}$  ions/cm<sup>2</sup> and  $1 \times 10^{17}$  ions/cm<sup>2</sup>. Post implantation annealing is carried out to obtain crystalline phase of TiO<sub>2</sub>. GAXRD and Raman spectroscopy study reveals formation of rutile phases of TiO<sub>2</sub>. The particle size calculated from XRD peaks reveals nanostructure formation and is found to decrease with increasing fluence. Nanostructure formation is also confirmed by the blue shift of the UV-Vis spectra. The RBS analysis confirms the stoichiometry of the oxide phase formed and the distribution of TiO<sub>2</sub> throughout the film.

## Ion beam back-scattering analysis of rough surface samples and elemental depth profiling of non-continuous surface layers

Petr Malinsky<sup>1</sup>, Anna Mackova<sup>1</sup>, Vladimir Hnatowicz<sup>1</sup>, Jakub Siegel<sup>2</sup>, Vaclav Svorcik<sup>2</sup>

<sup>1</sup>*Nuclear physics institute of the academy of science of the Czech Republic v. v. i., 250 68 Rez, Czech Republic*

<sup>2</sup>*Department of solid state engineering, institute of chemical technology, 166 28 Prague, Czech Republic*

Rutherford Backscattering Spectroscopy is often employed for the depth profiling of elements with nanometer depth resolution. In many instances the depth resolution is adversely influenced by surface roughness which may deform RBS energy spectra and lead to wrong evaluation of the depth profiles. On the other hand, the Atomic Force Microscopy is efficient method for independent characterization of surface morphology in the nanometer scale. In this study the RBS spectra from the samples with well defined surface morphology are compared with those simulated using a code taking into account real surface morphology determined by AFM method. The aim is to obtain more definite information on how the surface quality affects the RBS spectra. Samples with regular roughness were prepared by irradiation with KrF laser (248 nm wave length, linear polarization) of polyethyleneterephthalate under the different angles. In this way ripple patterns with periodicity of the order of the wavelength of the laser light and with a corrugation height of several tens nm were created on the PET surface. The irradiated samples were then covered by 35 nm thick Au layer by the means of vacuum evaporation. The surface morphology was characterized by AFM method and basic surface parameters were determined. RBS spectra were measured with 2.0 MeV  $^4\text{He}^+$  at different incident ion beam angles. RBS spectra were simulated using special code based on common simulation procedures [1] and taking into account the results from AFM measurements. Finally, these simulated and experimentally measured spectra were compared and good agreement between spectra was achieved.

The research was realized at the CANAM (Center of Accelerators and Nuclear Analytical Methods) infrastructure LM 2011019 and has been supported by project No. P108/12/G108.

[1] C. Jeynes, N. P. Barradas, P. K. Marriott, G. Boudreault, M. Jenkin, E. Wendler, R. P. Webb, J. Phys. D: Appl. Phys. 36, R97–R126 (2003).

**Nanoparticle formation in Zn ion implanted Si (001) substrate.**

Kseniia Eidelman<sup>1</sup>, Kirill Shcherbachev<sup>2</sup>, Nataliia Tabachkova<sup>3</sup>, Vladimir Privezentsev<sup>4</sup>

<sup>1</sup>*Borisovna, Russia*

<sup>2</sup>*Natl Univ Sci & Technol MISIS, Moscow 119049, Russia*

<sup>3</sup>*Yurievna*

<sup>4</sup>*Inst Phys & Technol RAS, Moscow, Russia*

The last decade of research nanoparticles of metals occupies a huge place in the materials science. Due to nanoscale quantum effects, metal nanoparticles (NPs) have an increased interest in the optoelectronics area to create a high-speed photodetectors in the range of UV, based on the phenomenon of surface plasmon resonance. In this paper was study formation process NP of metallic Zn at implantation and subsequent heat treatment.

A wafer of Cz-Si (001) ( $n = 5 \times 10^{15} \text{ cm}^{-3}$ ) was implanted with  $\text{Zn}^+$  ions with an energy of 50 keV and a fluence of  $5 \times 10^{16} \text{ cm}^{-2}$ . To avoid an amorphization, the target was heated at 350 °C during implantation. A piece of as-implanted wafer was annealed in dry oxygen air at 800 °C for 1 hour. Structural transformations in the implanted layer were investigated by a high-resolution transmission electron microscopy (HRTEM), an X-ray diffraction (XRD) and a photoluminescence (PL) spectroscopy.

Zinc NPs with a size of  $\sim 20 \text{ nm}$  located at the depth of 50 nm were revealed in as-implanted sample. Open pores with a size of 10-20nm on the surface were observed. HRTEM images showed a significant amount of radiation induced defects in the damaged layer. However, an identification of the defects has been hampered due to the blurred image contrast. PL revealed a signal at the wavelength  $\lambda = 340 \text{ nm}$  corresponding to radiation induced defects.

Part of large Zn NPs transforms to  $\text{Zn}_2\text{SiO}_4$  phase. XRD confirmed the simultaneous presence of Zn and  $\text{Zn}_2\text{SiO}_4$  phases. According to HRTEM small size (1-3 nm) crystalline  $\text{Zn}_2\text{SiO}_4$  NPs are located at the depth of 40 nm. All NPs are coherent with the Si matrix. The wavelength of 430 nm PL peak, corresponding to  $\text{Zn}_2\text{SiO}_4$  phase, is appeared.

Thus, used implantation conditions lead to the formation of Zn NPs with a size of  $\sim 20 \text{ nm}$  in Si matrix.  $\text{Zn}_2\text{SiO}_4$  NPs are formed at the "Zn NP - Si matrix" boundary after the subsequent annealing in oxygen. ZnO NPs are not formed under the used processes.

## **Towards covalent chemical modification of surfaces via reactive landing of hyperthermal molecular ion beams**

Stephan Rauschenbach<sup>1</sup>, Girjesh Dubey<sup>1</sup>, Sabine Abb<sup>1</sup>, Gordon Rinke<sup>1</sup>, Michael Dürr<sup>2</sup>, Klaus Kern<sup>1</sup>

<sup>1</sup>*Max-Planck-Institute for Solid State Research, Germany*

<sup>2</sup>*University Giessen, Germany*

Modification of surfaces with functional molecules is important for a wide variety of applications. Often, however, functional molecules are large and thus thermally fragile or even non-volatile. This makes the chemical coupling of functional molecules to solid surfaces a tough challenge, especially in vacuum processing.

Hyperthermal ion beams (1-200 eV) present a unique approach to chemical modification, and are readily formed by increasingly common methods such as electrospray ionization. An electrospray ion beam deposition (ES-IBD) system is employed to carry out the modification of solid surfaces in high vacuum using mass-selected molecular ion beams. The surfaces are investigated by scanning probe microscopy for morphological information at the atomic level, as well as with Raman-Spectroscopy, XPS and Desorption Ionization induced by neutral clusters (DINeC) mass spectrometry.

We investigate model systems like the attachment of 4,4'-azobis(pyridine) to graphene or N<sub>3</sub>-dyes to TiO<sub>2</sub> anatase. On the surface we find homogeneous coverage of adsorbed molecules on an otherwise atomically clean surface. Raman, XPS and DINeC-MS data indicated that the adsorbates are indeed covalently bound to the surface. The coupling reaction can be steered through the beam parameters, like charge state of the molecular ion or kinetic energy.

This route highlights a facile approach for the controlled modification of surfaces and extends the scope of candidate species that would not otherwise react via existing conventional methods. The present study demonstrates a one-step non-destructive route to covalently functionalize surfaces using the controlled deposition of hyperthermal molecular ion beams.

## **A facial synthesis of Phosphorene via thermal-induced phosphorus Condensation on nitrogen plasma-implanted InP substrates**

Chih-Chung Lai, Hsu-Sheng Tsai, Yu-Lun Chueh

*Department of Material Science and Engineering, National Tsing Hua University, Hsinchu 30013, Taiwan, R.O.C.*

In recent years, the two-dimensional materials attract great research attention due to its' superior physical properties, thus being potential candidates for future application in nano-electronics and opto-electronics. Beyond the most known materials such as graphene and MoS<sub>2</sub>, phosphorene, single layer of black phosphorus, the most stable form among the various allotropies, shows a semiconductor with unique optical and electronic properties. In fact, there are still a few researches regarding the fabrication of phosphorene.[1] In this study, we introduced a simple manufacturing regarding the plasma treatment followed by annealing process in order to achieve large-scale phosphorene films from bulk InP via nitridation-induced phosphorus condensation. After exposure of N<sub>2</sub> plasma, the additional annealing process is performed that promoting nitrogen ions to react with In atoms thus simultaneously condense P around the surface of the InP. The Raman analysis shows typical spectra of black phosphorus [2] and the XPS results reveal that the formation of indium nitride layer. Moreover, the Transmission Electron Microscopy (TEM) analysis indicated that the formation of continuous films of several layer-thick phosphorene, also confirmed by corresponding Electron Energy Loss Spectrum (EELS) mapping. This work demonstrates a route synthesizing large-area phosphorene without complicated manufacturing.

[1] Lu, Wanglin, et al. Nano Research 2014, 7(6), 853-859 (2014).

[2] Sugai, S., and I. Shiotani. "Raman and infrared reflection spectroscopy in black phosphorus." Solid state communications 53, 753-755 (1985).

## Evolution of nanostructures induced by low energy ion sputtering on Si surfaces

Hans Hofsäss, Kun Zhang, Omar Bobes

*Institute of Physics, University Göttingen, Germany*

In order to study the allotropic effect on the ripple formation on silicon surfaces induced by ion-beam sputter erosion, three types of silicon materials, single crystalline silicon, amorphous silicon grown by vapour phase evaporation and amorphous silicon produced by ion irradiation with few hundred keV heavy ions. The three different materials exhibit different atomic densities which may vary up to 13% depending on the preparation method. The atomic densities were measured using RBS and profilometry. The samples were irradiated with 1 keV Ar ions at incidence angles from 30 to 87 degrees with respect to the surface normal. The ion fluence was  $2 \times 10^{17}/\text{cm}^2$  for all irradiations. No ripples were formed for incidence angles smaller than 60° for all three materials. Ripples with wave vector parallel to the beam direction appear at angles between 60° and 75° but with amplitudes strongly dependent on the substrate density. Perpendicular ripples occurred only in amorphous silicon at incidence angles between 82° and 85° but not in crystalline Si. The results show, that ripple formation is influenced by the atom density of the Si substrates. We have also studied the pattern formation as function of ion energy and find flat surfaces for Ar ion energies above 1.3 keV up to at least 10 keV. Reasons for this behavior will be discussed.

## Enhanced sputtering and incorporation of Mn in ion implanted ZnO nanowires

Andreas Johannes<sup>1</sup>, Gema Martinez-Criado<sup>2</sup>, Carsten Ronning<sup>1</sup>, Stefan Noack<sup>1</sup>, Emanuel Schmidt<sup>1</sup>, Mahn-Hung Chu<sup>2</sup>

<sup>1</sup> *Friedrich-Schiller-University Jena, Germany*

<sup>2</sup> *European Synchrotron Radiation Facility, France*

We simulated and experimentally investigated the sputter yield of ZnO nanowires, which were implanted with energetic Mn ions at room temperature. The resulting thinning of the nanowires and the dopant concentration with increasing Mn ion fluency were measured by accurate scanning electron microscopy (SEM) and nano-X-Ray Fluorescence (nanoXRF) quantification, respectively. We observed a clearly enhanced sputter yield for the irradiated nanowires compared to bulk, which is also corroborated by the Monte-Carlo simulations performed with *iradina*. These show a maximum in the sputter yield if the ion range matches the nanowire diameter. As a consequence of the erosion thinning of the nanowire, the incorporation of the Mn dopants is also enhanced and increases non-linearly with increasing ion fluency.

## Enhanced sputtering effects on ion irradiated Au nanoparticles

Henry Holland-Moritz<sup>1</sup>, Andreas Johannes<sup>1</sup>, Stefan Noack<sup>1</sup>, Christian Borschel<sup>1</sup>, Sebastian Scheeler<sup>2</sup>, Claudia Pacholski<sup>2</sup>, Carsten Ronning<sup>1</sup>

<sup>1</sup>*FSU Jena, Germany*

<sup>2</sup>*MPI Stuttgart, Germany*

Nanoparticles can easily be fabricated by different physical and chemical processes, but their customization is restricted by the constraints of thermal equilibrium. Ion beam irradiation, a non-equilibrium method, is one possible subsequent approach in order to tune the properties of nanoparticles. Due to the high surface-to-volume ratio and the 3D-structure, sputtering plays a major role when the size of the nanoparticles is comparable to the ion range. Au nanoparticles of various sizes on Si substrates were irradiated with Ga ions in order to investigate the sputtering yield as a function of the particle diameter. In situ SEM investigations were used to analyze and quantify the sputtering yield. The experimental results will be compared with TRIDYN [1] and iradina [2] simulation results, whereat iradina is a new Monte-Carlo-Code, which takes the specifics of the nanogeometry into account.

[1] W. Möller, W. Eckstein, Nuclear Instruments and Methods in Physics Research B 261 814–818 (1984).

[2] C. Borschel, C. Ronning, Nuclear Instruments and Methods in Physics Research B 269, 2133–2138 (2011).



## Investigation for initial diameter of the gold nanoparticles formed by the solution plasma sputtering

Tsuyoshi Mizutani<sup>1</sup>, Satoshi Ogawa<sup>1</sup>, Takaaki Murai<sup>2</sup>, Hirofumi Nameki<sup>2</sup>, Tomoko Yoshida<sup>3</sup>,  
Shinya Yagi<sup>3</sup>

<sup>1</sup>*Graduate School of Engineering, Nagoya University, Japan*

<sup>2</sup>*Aichi Center for Industry and Science Technology, Japan*

<sup>3</sup>*EcoTopia Science Institute, Nagoya University, Japan*

The nanoparticles (NPs) have been studied for many applications such as optical devices, catalysts and biotechnology. Many preparation methods for NPs have been proposed such as gas evaporation method and chemical reduction method. Recently, the solution plasma method is reported as a new fabrication method. Though, in this solution plasma method, the NPs are prepared by sputtering from the electrodes surface by plasma under glow-like discharge environment, the detail formation mechanism is still unknown. Because the formed NPs react with the solution and/or aggregate with each other based on their high activity, the clarification of the formation mechanism is difficult. In-situ measurement during and after formation by solution plasma sputtering is needed to understand the formation mechanism. The colloidal gold NPs absorb the visible light by the localized surface plasmon resonance (LSPR), and the particle diameters and concentrations are able to calculate by means of this LSPR absorption peak. The in-situ UV-Vis measurement for preparation of gold NPs is appropriate approach to use this calculation method for study the formation mechanism of solution plasma sputtering. This in-situ UV-Vis measurement clarifies that the diameter and behavior of prepared NPs are different according to the kind of electrolyte under same discharge conditions. The prepared gold NPs are dissolved in HCl solution and are stable in NaCl or NaOH solution. We will perform the estimation of the initial diameter under various discharge conditions, and will find out the contributing factors to alter the initial diameter and concentration. The estimation of the initial diameter will be performed by the extrapolation. This is because if the diameter is too small or the concentration of gold NPs is too dilute, the calculated diameter or concentration is not accurate. Based on the contributing factors, we will discuss about the formation mechanism of NPs by the solution plasma sputtering method.

## Formation of GaN nanocrystals in thermally oxidized silicon

Elke Wendler<sup>1</sup>, Kyriakos Filintoglou<sup>2</sup>, Paul Kutza<sup>1</sup>, Philipp Lorenz<sup>1</sup>, Katharina Lorenz<sup>3</sup>, Fadei F. Komarov<sup>4</sup>, S. Ves<sup>2</sup>, Eleni Paloura<sup>2</sup>, Maria Katsikini<sup>2</sup>

<sup>1</sup>*Institut fuer Festkoerperphysik, Friedrich-Schiller-Universitaet Jena, Germany*

<sup>2</sup>*School of Physics, Aristotle University of Thessaloniki, Greece*

<sup>3</sup>*Belarusian State Univ, Minsk 220030, Belarus*

<sup>4</sup>*Department of Physics, Belarusian State University, Belarus*

The formation of GaN nanocrystals in thermally oxidized silicon by ion implantation and halogen-lamp annealing is investigated. The samples were sequentially implanted with 180 keV Ga and 50 keV N ions to ion fluences of several  $10^{16} \text{ cm}^{-2}$ . Halogen-lamp annealing was performed in 1:1  $\text{N}_2:\text{NH}_3$  atmosphere at temperatures between 800 and 1300°C for 30 seconds up to 10 minutes. The Ga and N depth distributions were detected with backscattering spectrometry (RBS/EBS) using 1.4 or 3.7 MeV He ions. The RBS/EBS spectra reveal that the temperature window suitable for annealing is restricted to temperatures below 1000°C since annealing at 1100°C, even for 30 sec, results in significant loss of Ga atoms that is further enhanced for annealing at 1200 and 1300°C. During annealing at 1000°C, a significant Ga loss starts for annealing times of approximately 2 min. A similar dependence on annealing temperature and duration is also observed for the N loss. Complete out-diffusion of N takes place after annealing at 1200°C for 30 sec, whereas annealing at 1000°C has similar effects when the sample is annealed for more than 2 min. In order to detect/identify the formation of GaN nanocrystals, X-ray absorption fine structure (XAFS) and Raman spectroscopies were employed. A weak Raman contribution attributed to the A1(LO) peak of GaN is superimposed to the strong  $\text{SiO}_2/\text{Si}$  signal for annealing at 1000°C for 30 sec. This finding is supported by the Ga-K-edge XAFS spectra that reveal the formation of nano/micro crystalline GaN in this particular sample as well as in the sample annealed at 900°C for 10 min, suggesting that the lower annealing temperature can be compensated by a longer annealing time. In the samples annealed at 800°C and 900°C for 30 sec, Ga seems to substitute Si in the  $\text{SiO}_2$  matrix and no evidence for formation of GaN-phase with mid- or long range order is provided by XAFS. TEM investigations are in progress to verify the formation and determine the size of the GaN nanocrystals.

## The effect of silicon nanocrystal size on the optical gain measured via the variable stripe length method

Rachel Southern-Holland<sup>1</sup>, Iain Crowe<sup>1</sup>, Matthew Halsall<sup>1</sup>, Russell Gwilliam<sup>2</sup>, Andy Knights<sup>3</sup>

<sup>1</sup>*University of Manchester, UK*

<sup>2</sup>*University of Surrey, UK*

<sup>3</sup>*McMaster University, Canada*

The variable stripe length (VSL) technique is useful for determining the presence of optical gain from samples without the need for a resonant cavity [1]. We describe the measurement for two thin (500nm) silica films containing silicon nanocrystals (Si-nc) grown by wet thermal oxidation from sputtered silicon on sapphire. The films were implanted at 80keV with Si<sup>+</sup> to an areal density of  $8 \times 10^{16} \text{cm}^{-2}$ , followed by annealing at 1100°C for 50s (sample 1) and 600s (sample 2). This procedure results in the formation of Si-nc populations with average diameters of 22Å (sample 1) and 27Å (sample 2), as previously verified via X-TEM measurements for similar samples [2]. We obtained a net gain of  $65 \pm 5 \text{cm}^{-1}$  for sample 1 and  $36 \pm 4 \text{cm}^{-1}$  for sample 2, which are similar values to those previously reported [3, 4]. From Shifting Excitation Spot (SES) [5] measurements, performed along the stripe, we obtain a similar difference in the absorption coefficient ( $23 \text{cm}^{-1}$  for sample 1 and  $62 \text{cm}^{-1}$  for sample 2), which likely explains the difference in net gain. This may be due to a combination of increased FCA cross section (for longer wavelength emission) [6] and an increase in the density of surface states for the larger Si-nc population [7].

[1] K.L. Shaklee and R F Leheny, Applied Physics Letters Volume 18 475-477 (1971)

[2] I . F.Crowe, M. P. Halsall, O. Hulko, A. P. Knights, R. M. Gwilliam, M. Wojdak, and A. J. Kenyon, Journal of Applied Physics Volume 109 083534 (2011)

[3] M. Cazzanelli, D. Navarro-Urriós, F. Riboli, N. Daldosso, L. Pavesi, J. Heitmann, L. X. Yi, R. Scholz, M. Zacharias, and U. Gösele, Journal of Applied Physics Volume 96 3164 (2004)

[4] L. Pavesi L. Dal Negro, C. Mazzoleni, G. Franzoa & F. Priolo, Nature Volume 408 440-444 (2000)

[5] J. Valenta, I. Pelant, and J. Linnros, Applied Physics Letters Volume 81 1396 (2002)

[6] R. D. Kekatpure and M. L. Brongersma, Nano Letters Volume 8 3787-3793 (2008)

[7] M. Jivanescu, D. Hiller, M. Zacharias and A. Stesmans, EPL Volume 96 27003(2011)

**Tailoring buried Si-C-N nanocomposite structures by ion implantation**

Alexander Suvorov<sup>1</sup>, Sergey Rubanov<sup>2</sup>, Alexandra Suvorova<sup>3</sup>

<sup>1</sup>*Cree, Inc., USA*

<sup>2</sup>*Bio21 Institute, The University of Melbourne, Australia*

<sup>3</sup>*CMCA, The University of Western Australia, Australia*

Ion implantation is a useful technique to modify technologically important materials and fabricate new materials with stoichiometry, thickness and microstructure control through variation of implantation parameters. Introduction of dopants has been the primary use of ion implantation in SiC device processing, but other possible applications, such as synthesis of integrated layers or regions by high dose ion implantation are of significant interest.

High temperature implantation with nitrogen ion beam have been used to create nanocomposite structures in silicon carbide (4H-SiC). Compositional and structural details of implanted regions have been analyzed at the nanoscale by a range of transmission electron microscopy (TEM) techniques. High resolution TEM imaging and electron diffraction demonstrated that alpha-silicon nitride phase existed in the implanted layer, while energy-filtered TEM (EFTEM) revealed the nanocomposite nature of the implanted layers. A combination of  $7 \times 10^{17} \text{cm}^{-2}$  dose of nitrogen at  $1100^\circ\text{C}$  temperature of SiC has been found to produce a well-defined silicon nitride layer, while implantation at reduced parameters leads to uniformly distributed graphite and silicon nitride phases. We demonstrated experimentally how the implantation parameters affect the layered nanocomposite structures. These new insights into the complex structure of SiC implanted layers are an important step to provide a route to formation of novel integrated materials with potential applications in electronics.

## Nitrogen induced modifications of MANOS memory properties

Nikolaos Nikolaou<sup>1,2</sup>, Vassilios Ioannou-souglерidis<sup>1</sup>, Beatrice Pecassou<sup>3</sup>, Gerard Benassayag<sup>3</sup>, Kaupo Kukli<sup>4,5</sup>, Jaako Niinistö<sup>4</sup>, Mikko Ritala<sup>4</sup>, Markku Leskelä<sup>4</sup>, Panagiotis Dimitrakis<sup>1</sup>, Pascal Normand<sup>1</sup>, Dimitrios Skarlatos<sup>2</sup>, Konstantinos Giannakopoulos<sup>1</sup>, Spyridon Ladas<sup>6</sup>

<sup>1</sup>Department of Microelectronics, NCSR “Demokritos”, 153 10 Athens, Greece,

<sup>2</sup>Department of Physics, University of Patras, 265 04 Patras, Greece

<sup>3</sup>CEMES-CNRS, Toulouse, France

<sup>4</sup>Department of Chemistry, University of Helsinki, FI-00014 Helsinki, Finland,

<sup>5</sup>Institute of Physics, University of Tartu, Riia 142, EE-51014 Tartu, Estonia

<sup>6</sup>Department of Chemical Engineering, University of Patras, 26504 Patras, Greece

We report on the electrical properties of MANOS stacks modified by low-energy nitrogen implantation.  $\text{Al}_2\text{O}_3/\text{Si}_3\text{N}_4/\text{SiO}_2$  stacks having thicknesses of 15/6.5/3.5 nm were fabricated on n- and p-Si substrates. The  $\text{Al}_2\text{O}_3$  layer was implanted with 1 keV nitrogen at a dose of  $1 \times 10^{16}$  ions/cm<sup>2</sup>. Post-Implantation Annealing (PIA) was performed in  $\text{N}_2$  ambient at 850 (low-T) or 1050 °C (high-T) for 15 min. Non-implanted stacks were also fabricated for comparison purposes. Electrical characterization of the stacks was performed using platinum gate capacitors. TEM imaging indicates the following: a) After PIA a low-contrast amorphous layer is formed at 3-4 nm from the surface of the implanted samples. Such a layer is not observed for the non-implanted samples. In the case of low-T PIA this layer has a thickness of 3 nm, while for high-T PIA it is non-uniform with a thickness within the 0-2 nm range. b) The crystallization process of  $\text{Al}_2\text{O}_3$  during PIA is retarded due to nitrogen enrichment. c) High-T PIA densifies the modified  $\text{Al}_2\text{O}_3$  to 13 nm as compared to 16 nm after the low-T PIA. Memory testing reveals that the implanted and non-implanted samples exhibit similar programming / erasing characteristics except the case of the low-T PIA implanted sample where enhanced hole charging and thereby, increase erase efficiency is observed. Finally, the retention of the programmed state of the high-T PIA samples appears improved by 25% as compared to the non-implanted samples. These results suggest that the transport properties which control the erase and the retention characteristics of the blocking  $\text{Al}_2\text{O}_3$  layer can be tailored by nitrogen implantation and the PIA conditions and thereby, be used for memory performance optimization.

## Synthesis and structure of Fe/Ni nanotubes fabricated in polyethylene-terephthalate ion-track films

Artem Kozlovskiy<sup>1</sup>, Arman Zhanbotin<sup>1</sup>, Kairat Kadyrzhanov<sup>1</sup>, Viacheslav Rusakov<sup>2</sup>

<sup>1</sup>*L.N. Gumilyov Eurasian National University, Astana, Kazakhstan*

<sup>2</sup>*Lomonosov Moscow State University, Moscow, Russia*

This work describes structure and properties of an array of free-standing Fe/Ni nanotubes grown inside of ion-beamed PET polymer films. Highly oriented, free standing Fe/Ni nanotubes were electrochemically grown in the pores of 12  $\mu\text{m}$  thickness track etched PET films with pore density of  $1.0\text{E}+07\text{ cm}^{-2}$ . SEM, TEM, X-ray and Mossbauer analysis was used due to determine crystal structure and elemental composition of Fe/Ni solid solution.

One of the most popular techniques of synthesis of metallic nanostructures is an electrochemical deposition. The main advantages of this method are ability to control metal deposition rate inside of channels of nanoporous template and possibility to synthesis of poly-component materials. PET films as a template material, gives possibility to make pore density from  $1.0\text{E}+06\text{ cm}^{-2}$  to  $1.0\text{E}+09\text{ cm}^{-2}$ , pore diameters from 50 nm to 1000 nm, film thickness 6, 12, 19 and 23  $\mu\text{m}$  [1].

The work considers the synthesis and structure of ordered arrays of Fe/Ni nanotubes. Choice of these materials is caused to their unique magnetic properties [2] and the prospective application in technique [3].

EDAX analysis has showed  $\text{Fe}_{15}\text{Ni}_{85}$  atomic percentage of Fe/Ni nanotubes. This ratio has been confirmed by Mossbauer spectroscopy. TEM spectroscopy definitely shows tube-like structure of received Fe/Ni samples.

According to X-ray analysis, nickel lattice parameter is slightly larger than the standard parameter values ( $a = 3,523\text{ \AA}$ ). FCC lattice parameter changes possibly due to the fact that this phase is a solid solution of Fe in Ni. Parameter of nickel lattice for the sample #1 is equal to  $a = 3,5337 \pm 0,0008\text{ \AA}$ .

X-ray analysis and Mossbauer spectroscopy doesn't demonstrate crystal and magnetic texture of Fe/Ni nanotubes.

[1] A.A. Mashentseva, M.V. Zdorovets, KazNU Bulletin. Chemical series. №1 (69) (2013).

[2] J.C. Hulteen, C.R. Martin, J. Mater, Chem 7, 1075 (1997).

[3] S.K. Chakarvarti, J. Vetter, Radiation Measurements 29, 149-159 (1998).

## The loading effect of silver nanoparticles prepared by impregnation and solution plasma methods on the photocatalysis of Ga<sub>2</sub>O<sub>3</sub>

Muneaki Yamamoto<sup>1</sup>, Tomoko Yoshida<sup>2</sup>, Naoto Yamamoto<sup>1</sup>, Toyokazu Nomoto<sup>3</sup>, Shinya Yagi<sup>2</sup>

<sup>1</sup>*Graduate School of Engineering, Nagoya University, Japan*

<sup>2</sup>*EcoTopia Science Institute, Nagoya University, Japan*

<sup>3</sup>*Aichi Synchrotron Radiation Center, Japan*

Silver nanoparticle-loaded gallium oxide (Ag/Ga<sub>2</sub>O<sub>3</sub>) has exhibited photocatalytic activity for CO<sub>2</sub> reduction with water to produce CO, H<sub>2</sub> and O<sub>2</sub>. We prepared Ag/Ga<sub>2</sub>O<sub>3</sub> samples by impregnation method (Ag/Ga<sub>2</sub>O<sub>3</sub> (imp)) and solution plasma method (Ag/Ga<sub>2</sub>O<sub>3</sub> (SPM)), and compared their photocatalytic activities. We also investigated the effects of the chemical states and the size of the Ag nanoparticles on the photocatalytic CO<sub>2</sub> reduction mechanism by TEM, XAFS and FT-IR measurements.

The photocatalytic reduction of CO<sub>2</sub> with water proceeds over all Ag/Ga<sub>2</sub>O<sub>3</sub> samples and the CO production rates are higher than that of a bare Ga<sub>2</sub>O<sub>3</sub>. The optimum amount of Ag loading for CO production is 0.06 and 0.20 wt% for Ag/Ga<sub>2</sub>O<sub>3</sub> (SPM) and Ag/Ga<sub>2</sub>O<sub>3</sub> (imp), respectively, and the photocatalytic activity of the latter is higher than that of the former. However, the CO production rates decrease with the reaction time, and the decrease in the CO production rates is remarkable for Ag/Ga<sub>2</sub>O<sub>3</sub> (SPM) samples.

As for Ag/Ga<sub>2</sub>O<sub>3</sub> (imp) samples, their TEM images and XAFS spectra show the predominant formation of Ag metal and oxide nanoparticles with the size of less than 10 nm. These Ag species are likely dispersed atomically, especially in the lower Ag loading samples. In addition, in-situ FT-IR measurements reveal the following reaction mechanism of Ag/Ga<sub>2</sub>O<sub>3</sub> (imp) samples: carbonate and bicarbonate species are formed when CO<sub>2</sub> molecules chemisorb on the catalyst surface. These species change to bidentate formate species under photoirradiation and it subsequently converts to CO by interacting with water molecules, not chemisorbed OH on the catalyst surface.

At the conference, we will discuss the results of TEM, FT-IR and XAFS measurements for Ag/Ga<sub>2</sub>O<sub>3</sub> (SPM) samples to compare the loading effect of silver nanoparticles on Ag/Ga<sub>2</sub>O<sub>3</sub> (imp) and Ag/Ga<sub>2</sub>O<sub>3</sub> (SPM) samples.

## Fabrication of dendritic nanostructured photoactive tungsten materials by helium plasma irradiation

Katsuyuki Komori<sup>1</sup>, Tomoko Yoshida<sup>2</sup>, Toyokazu Nomoto<sup>3</sup>, Muneaki Yamamoto<sup>1</sup>, Chie Tsukada<sup>1</sup>, Yagi Shinya<sup>2</sup>, Miyuki Yajima<sup>1</sup>, Shin Kajita<sup>2</sup>, Noriyasu Ohno<sup>1</sup>

<sup>1</sup>*Graduate School of Engineering, Nagoya University, Japan*

<sup>2</sup>*EcoTopia Science Institute, Nagoya University, Japan*

<sup>3</sup>*Aichi Synchrotron Radiation Center, Japan*

In the plasma engineering field, it has been reported that the helium plasma irradiation fabricates dendritic nanostructures on the surface of tungsten plates. The dendritic tungsten shows a broad photo-absorption in the wide energy range from 1 to 5 eV in the diffuse reflection measurements. Such a nanosized WO<sub>3</sub> with a high specific surface area might promote a photoinduced reaction.

In the present work, we examined the photoactivity of the nanostructured tungsten material, which is expected to consist of both nanosized W and WO<sub>3</sub>, fabricated by the He plasma technique followed by gentle oxidation.

The photoinduced reaction experiments were conducted for the dendritic tungsten samples with 20~100 % surface oxidation ratios, and the reaction activities were evaluated with the decolorization rate of methylene blue (MB) in an aqueous solution under near-infrared light (<1.55 eV), whose energy is lower than the band gap of WO<sub>3</sub>. The photoinduced reaction rate varied with the oxidation ratio of the samples, and reached the maximum around 50 %, suggesting that WO<sub>3</sub> /W interface is an active site for the photoinduced reaction. On the other hand, the reaction rate over fully oxidized sample was slower, suggesting that WO<sub>3</sub> species is the lower active site. Unfortunately, the high active WO<sub>3</sub>/W interface species was found to be deactivated in cycle tests while less deactivation was observed for the low active WO<sub>3</sub> species.

The photoinduced MB decomposition process was confirmed by XAFS, XPS and SEM analyses, i.e., in the dark, MB molecules are adsorbed on the sample surface and stacked each other by the  $\pi$ -orbital interaction while under the light, S-C bonds of MB molecule are broken to produce SO<sub>4</sub><sup>2-</sup>. The active W/WO<sub>3</sub> interface species could be deactivated by adsorption of the reaction products on the metal tungsten sites of the sample surface.



## Structural transformation of implanted diamond layers during high temperature annealing

Sergey Rubanov<sup>1</sup>, Barbara Fairchild<sup>2</sup>, Alexandra Suvorova<sup>3</sup>, Paolo Olivero<sup>4</sup>, Steven Prawer<sup>1</sup>

<sup>1</sup>*University of Melbourne, Australia*

<sup>2</sup>*RMIT, Melbourne, Australia*<sup>3</sup>*The University of Western Australia, Australia*

<sup>4</sup>*University of Torino, Italy*

In the recent years ion implantation became the basic tool for device fabrication in diamond. The lift-off method with high fluence MeV ion implantation is used to create a buried damage layer and eventually a graphite-like layer upon annealing [1]. The etchable graphitic layer can be removed to form a free-standing membrane into which the desired structures can be sculpted using FIB milling. We have also demonstrated the possibility of ultrathin membranes fabrication in diamond using double implantation technique [2]. The combination of double-implantation technique and FIB milling allows device fabrication in diamond at the nano-scale. The optical properties of these devices are assumed on the model of sharp diamond-air interface. The real quality of this interface could depend on the degree of graphitization of the amorphous damage layers after annealing. Also, graphitization of ion-beam induced amorphous layers in diamond has attracted significant interest due to ability to fabricate device structures containing two structural forms of carbon. In the present work the graphitization process was studied using conventional and analytical TEM. It was found that annealing at 550 °C results in a partial graphitization of the implanted volume. Annealing at 1400 °C resulted in complete graphitization of the amorphous layers. The average size of graphite nano-crystals did not exceed 5 nm with predominant orientation of c-planes normal to the sample surface.

[1] P. Olivero et al., Adv. Mater. 17, 2427 (2005).

[2] B.A. Fairchild et al., Adv. Mater. 20, 4793 (2008).

## Effects of electron irradiation on LDPE/MWCNTs composites

Jianqun Yang, Xingji Li, Chaoming Liu, Erming Rui, Liqin Wang

*Harbin Institute of Technology, P.R. China*

Low density polyethylene (LDPE) is a polymer that is widely used in industrial and space applications. In this study, multiwalled carbon nanotubes (MWCNTs) were incorporated into LDPE in different concentrations (2, 4 and 8%) using a melt blending process. LDPE/MWCNTs composites were irradiated by 110 keV electrons to improve the interaction between MWCNTs and the LDPE matrix. Structural, thermal and mechanical characterizations of LDPE/MWCNTs composites were investigated by means of scanning electron microscopy (SEM), small angle X-ray scattering (SAXS), electron paramagnetic resonance (EPR) spectroscopy, differential scanning calorimetry (DSC), thermogravimetric analysis (TGA) and uniaxial tensile techniques. Based on the results of SEM analysis, MWCNTs were found to be well-dispersed in the LDPE matrix even at 8 wt.%, and no radiation-induced morphological changes were observed. The analysis results of the thermal stability and tensile property revealed that the LDPE/MWCNT composites exhibited a higher radiation resistance in comparison to the pure LDPE, which was dependent on the MWCNTs content. This improved radiation resistance can be ascribed to a number of factors including the homogeneous distribution of MWCNTs in LDPE matrix, the aberrance zone between MWCNTs and LDPE matrix, and the incorporation of the radical scavenging MWCNTs into the LDPE matrix.

## Effect of the initial thickness on the thinning rate of polymer nanolayers under ion irradiation

Raquel Thomaz<sup>1</sup>, Bárbara Friedrich<sup>1</sup>, Leandro Izê Gutierrez<sup>1</sup>, Ricardo Meurer Papaléo<sup>1</sup>,  
Pedro Grande<sup>2</sup>

<sup>1</sup>*Pontifical Catholic University of Rio Grande do Sul, Brazil*

<sup>2</sup>*Federal University of Rio Grande do Sul, Brazil*

We report on the thickness decrease of poly(methyl methacrylate) thin and ultrathin layers after ion bombardment with 300 keV H<sup>+</sup>, 2 MeV H<sup>+</sup> and 18 MeV Au<sup>7+</sup> ions. Thin films with initial thickness  $h_0$  from 2 up to 100 nm were spun onto Si wafers with a native oxide layer. The thickness of the layers after ion beam irradiation with a fluence  $\phi$ ,  $h(\phi)$ , was measured offline with a Dimension Icon scanning force microscope (SFM) and by ellipsometry. As expected, the qualitative effect of the irradiation with all different beams was a decrease in thickness with increasing fluence. However, we observe a clear thickness dependent thinning rate of the irradiated polymer films, which becomes progressively slower the smaller the thickness. For 300 keV H<sup>+</sup> and thick samples ( $\sim 50$  nm) the rate (or cross-section) was  $\sim 2 \times 10^{-14}$  cm<sup>2</sup>, whilst for the 26 nm thick film it slowed down to  $\sim 6 \times 10^{-15}$  cm<sup>2</sup>. Moreover for the H<sup>+</sup> beam the thinning tends to saturate, what is not observed for the 18 MeV Au beam, at least in the fluence range investigated. Such differences are attributed to the different contributions of compaction and sputtering to the overall thinning rate for the different types of beams.

## Ta ions implantation induced by high density laser for plasma diagnostics

Mariapomea Cutroneo<sup>1</sup>, Petr Malinsky<sup>1,2</sup>, Anna Mackova<sup>1,2</sup>, Jindrich Matousek<sup>2</sup>, Lorenzo Torrisi<sup>3</sup>, Ullschmied Jiri<sup>4</sup>

<sup>1</sup>*Nuclear Physics Institute, ASCR, 25068 Rez, Czech Republic*

<sup>2</sup>*Department of Physics, Faculty of Science, J.E. Purkinje University, Ceske mladeze 8, 400 96 Usti nad Labem, Czech Republic*

<sup>3</sup>*Physics Department & of Earth Sciences, Messina University, V.le F.S. d'Alcontres 31, 98166 S. Agata, Messina, Italy*

<sup>4</sup>*Institute of Physics, ASCR, v.v.i., 182 21 Prague 8, Czech Republic*

The production of ion beams from laser-generated plasma is prospective in different applications from fundamental point of view for nuclear physics and new Laser Ion Sources, Bio-medicine, to micro-electronics.

The present work is focused on implantation of Ta ions in Silicon substrates covered by 50 Å - 3000 Å silicon dioxide layer, by using a sub-nanosecond pulsed laser ablation at 438 nm wave-length, 300 ps pulse, 200 J energy and  $10^{15}$  W/cm<sup>2</sup> intensity at the Laser Plasma Department, Institute of Plasma Physics, AS CR with an objective of non-equilibrium plasma ions acceleration. Accelerated Ta ions are implanted on exposed substrates of silicon at energies of the order of 20 keV per charge state and with charge states higher than 20+, characterized by Boltzmann-like distribution. By varying few variables in the laser pulse (time of the pulse, incident laser energy, laser intensity, focal position) it is possible to control the kinetic energy, the yield, and the angular distribution of the emitted ions. Rutherford Back-Scattering analysis was performed using 2 MeV He<sup>2+</sup> as the probe ions to determine the elemental depth profiles and the chemical composition of laser implanted substrates. The depth distribution of implanted Ta ions was compared to the SRIM - 2011 simulation. Evaluated results of energy distribution, were compared with on-line techniques such as Ion Collectors (IC) and Ion Energy Analyzer (IEA) for a detailed identification of produced ion species and their energy-to-charge ratios (m/z) energy respectively. Further XPS analysis was carried out, for the study of chemical bonds created in the modified implanted layers.

### Acknowledgement

The research has been realised at the CANAM (Center of Accelerators and Nuclear Analytical Methods) infrastructure and has been supported by project No. P108/12/G108.

## **Ion mass effect on DNA change induced by ultra-low-energy ion bombardment**

Prutchayawoot Thopan, Liangdeng Yu

*Chiang Mai University, Thailand*

This study was aimed at further investigating ultra-low-energy ion bombardment effect on DNA change by focusing on the ion mass effect. Ultra-low-energy ion interaction with naked DNA has been an interesting research topic as it can reveal fundamentals involved in charged particle irradiation effect on life as well as biological evolution. It has been known from previous studies that ion energy as low as 10 eV/u is able to induce DNA change and potential mutation. As the diversity of the charged particles, their mass should have effect on changing DNA when they interact with DNA. In our model study, inert elements of various masses such as He, Ar and Xe were used as the ion beam species and they were decelerated by a home-developed deceleration lens to energy lower than 1 keV to bombard naked DNA plasmid pGFP. After ion bombardment, gel electrophoresis was operated to analyze changes in the DNA topological form. The result showed that the DNA form change certainly depended on the ion mass. At the same ion energy and beam fluence, the higher mass ion beam could induce more changes in the DNA form from supercoiled to relaxed and to linear form than lower mass ion beam. Quantitative analysis showed near-linear relationship between the ion mass and the number of the DNA form change. Physics involved in the process was discussed. The investigation concluded that the heavier ions, the more the danger to DNA damage.

**Self-cleaning ion source for ultra-low energy implantation**

Timur Kulevoy<sup>1</sup>, Dmitry Seleznev<sup>1</sup>, Efim Oks<sup>2</sup>, Alexander Kozlov<sup>1</sup>, Rostislav Kuibeda<sup>1</sup>,  
Gennady Kropachev<sup>1</sup>, Ady Herscovitch<sup>3</sup>, Vasily Gushenets<sup>2</sup>, Oleg Alexeyenko<sup>4</sup>, Sergey  
Dugin<sup>4</sup>

<sup>1</sup>*ITEP, Russia*

<sup>2</sup>*HCEI, Russia*

<sup>3</sup>*BNL, USA*

<sup>4</sup>*State Scientific Center of the Russian Federation State Research Institute for Chemistry and  
Technology of Organoelement Compounds, Russia*

The main goal of ongoing international collaborative research program is the development of intense ion-beam sources for low-energy ion implanters. The results of self-cleaning operation mode of ion source by using the carborane acid are presented. As well the results of ion source operation with oxygen as an in-city cleaning gas are presented.

## Temperature dependent formation, elastic response and recrystallization of swift heavy ion tracks in quartz

Daniel Schauries<sup>1</sup>, Boshra Afra<sup>1</sup>, Patrick Kluth<sup>1</sup>, Matias Rodriguez<sup>1</sup>, William Weber<sup>2</sup>, Christina Trautmann<sup>3</sup>, Nigel Kirby<sup>4</sup>, Kai Nordlund<sup>5</sup>, Olli Pakarinen<sup>5</sup>, Aleksi Leino<sup>5</sup>, Flyura Djurabekova<sup>5</sup>, Maik Lang<sup>2</sup>

<sup>1</sup>*Australian National University, Australia*

<sup>2</sup>*University of Tennessee, USA*

<sup>3</sup>*GSI Helmholtz Centre for Heavy Ion Research, Germany*

<sup>4</sup>*Australian Synchrotron, Australia*

<sup>5</sup>*University of Helsinki, Finland*

Ion tracks in solids are narrow trails of permanent damage generated along the paths of highly energetic heavy ions facilitated by their inelastic interactions with the target electrons. They have applications in a variety of disciplines including materials science and engineering, nuclear physics, geochronology, archaeology, and interplanetary science.

Here, we present results on the formation of ion tracks in quartz at elevated temperatures as well as their elastic response/recrystallization upon annealing using synchrotron based small angle x-ray scattering (SAXS) in combination with in situ annealing. The ion tracks were generated using GeV Au and U ions at the UNILAC accelerator at GSI in Germany. Ion tracks are comprised of cylindrical amorphous regions with a density difference of about 2% compared to the quartz matrix [1]. When generated at elevated temperatures, the track radii increase by approximately  $1 \text{ \AA}/100^\circ\text{C}$  as a consequence of increased local temperature leading to a larger melting radius in the thermal spike [2]. A complex post-formation annealing behaviour is apparent for ion tracks generated at room temperature. Below  $600^\circ\text{C}$  an irreversible increase in the track radius is observed followed by a reversible decrease near the transition temperature from  $\alpha$ - to  $\beta$ -quartz. The latter is well described by an analytical model of the ion tracks as cylindrical elastic inclusions, using experimental values of the temperature dependent elastic properties of fused silica and quartz for the track and matrix material, respectively, and a consequence of a dramatic change in the Poisson-ratio of quartz. At temperatures above  $800^\circ\text{C}$ , re-crystallisation of the ion tracks is apparent and is critically dependent on the crystallographic direction the ion tracks are aligned with.

[1] B. Afra et al., J. Phys.: Condens. Matter 25, 045006 (2013).

[2] ) o K" #

### Energy threshold for swift heavy ion tracks in GaN

Marko Karlusic<sup>1</sup>, Roland Kozubek<sup>2</sup>, Branko Santic<sup>1</sup>, Henning Lebius<sup>5</sup>, Richard A. Wilhelm<sup>4</sup>, Maja Buljan<sup>1</sup>, Ferdinand Scholz<sup>5</sup>, Tobias Meisch<sup>5</sup>, Milko Jaksic<sup>1</sup>, Sigrid Bernstorff<sup>6</sup>, Marika Schleberger<sup>2</sup>

<sup>1</sup> *Ruder Boskovic Institute, Bijenicka cesta 54, 10000 Zagreb, Croatia*

<sup>2</sup> *Fakultät für Physik and CENIDE, Universität Duisburg-Essen, 47048 Duisburg, Germany*

<sup>3</sup> *CIRIL/GANIL, 14070 Caen cedex 5, France*

<sup>4</sup> *Helmholtz-Zentrum Dresden-Rossendorf, Bautzner Landstraße 400, 01328 Dresden, Germany*

<sup>5</sup> *Universität Ulm, Institut für Optoelektronik, Albert Einstein Allee 45, 89081 Ulm, Germany*

<sup>6</sup> *Elettra-Sincrotrone Trieste, SS 14 km 163.5, 34149 Basovizza, Italy*

The passage of a swift heavy ion through a solid material can result in permanent damage called ion track. The most common description of the ion track formation, the thermal spike model, suggests that the kinetic energy of the projectile that is deposited as dense electronic excitation along the ion trajectory, can lead to melting of the material. In this case, ion tracks originate from the quenching of the molten phase on the nanosecond time scale, resulting in an amorphous inclusion. Thus, the threshold for ion track formation and the track size depend on ion beam parameters and material properties.

One of the most important material properties related to the swift heavy ion track formation is the energy bandgap [1,2]. In this work we present experimental results of ion track formation in thin GaN epi-layer grown by MOVPE on sapphire. As a follow up of our previous work on the wide bandgap semiconductors SrTiO<sub>3</sub> ( $E_g = 3$  eV) [3] and TiO<sub>2</sub> ( $E_g = 3$  eV), the material investigated here presents an opportunity for further studies since its bandgap energy is  $E_g = 3.4$  eV.

The GaN samples were irradiated by swift heavy ions under both normal and grazing angle of incidence. Irradiation parameters were chosen to investigate the material's response close to the ion track formation threshold, and to complement previous works using higher energy ion beams [4,5]. We investigated ion irradiation effects both on the material surface by means of AFM and GISAXS and in the bulk by means of RBS/c. Our results are discussed in the framework of the thermal spike model.

[1] M. Toulemonde et al., Nucl. Instrum. Meth. B 166-167, 903 (2000).

[2] G. Szenes, Nucl. Instrum. Meth. B 269, 2075 (2011).

[3] M. Karlušić et al., New J. Phys. 12, 043009 (2010).

[4] S. Mansouri et al., Nucl. Instrum. Meth. B 266, 2814 (2008).

[5] S.O. Kucheyev et al, J. Appl. Phys. 95, 5360 (2004).



**Poster session C**  
**Thursday, September 18, 2014**  
**16.40 – 18.40**

## Structural modifications induced by ion irradiation and temperature in boron carbide B<sub>4</sub>C

Guillaume Victor<sup>1</sup>, Yves Pilon<sup>1,2,3</sup>, Olivier Rapaud<sup>4,5</sup>, Nikolay Djourellov<sup>6</sup>, Nicolas Bérerd<sup>1,2,3</sup>, Nathalie Moncoffre<sup>1,3</sup>, Nelly Toulhoat<sup>1,7</sup>, Dominique Gosset<sup>7</sup>, Sandrine Miro<sup>7</sup>, Alexandre Maître<sup>4,5</sup>, Nicolas Pradeilles<sup>4,5</sup>

<sup>1</sup>*Institut de Physique Nucléaire de Lyon, France*

<sup>2</sup>*UCBL, France*

<sup>3</sup>*CNRS, France*

<sup>4</sup>*SPCTS, France*

<sup>5</sup>*Unilim, France*

<sup>6</sup>*INRNE, Bulgaria*

<sup>7</sup>*CEA, France*

Already used as neutron absorber in nuclear reactors, boron carbide B<sub>4</sub>C is also considered in the future Sodium Fast Reactors of the next generation (Gen IV). Due to severe irradiation conditions occurring in these reactors, it is of primary importance that this material presents a high structural resistance under irradiation, both in the ballistic and electronic damage regimes. Previous works have shown an important structural resistance of boron carbide even at high neutron fluences. Nevertheless, the structural modification mechanisms due to irradiation are not well understood.

In this paper, we aim at studying the structural modifications induced in B<sub>4</sub>C samples in different damage regimes. The boron carbide pellets were shaped and sintered by using the non-conventional spark plasma sintering method. They were then irradiated in several conditions, either by favoring the creation of ballistic damage, with 600 keV <sup>+</sup> ions or 800 keV Ar<sup>+</sup> ions at the fluence of 1x10<sup>16</sup>at.cm<sup>-2</sup> (about 1 and 3 dpa max respectively) at room temperature, or by favoring the electronic excitations using 100 MeV swift Iodine ions at 5x10<sup>15</sup>at.cm<sup>-2</sup> (Se ≈ 15000 keV/μm). In these last conditions, the effect of temperature was also investigated (room temperature and 800°C). Ex-situ Raman microspectrometry and Doppler broadening of annihilation radiation technique with variable energy slow positrons were used to follow the evolution of the B<sub>4</sub>C structure under irradiation. Raman results clearly show that, in both regimes, irradiation induces a local disorder of B<sub>4</sub>C structure and that temperature prevents this disorder. Complementary results are reported in the communication of D. Gosset et al.

## Pattern formation during ion beam assisted growth of carbon-nickel nanocomposite films: the effect of nickel concentration

Matthias Krause<sup>1</sup>, Wolfhard Möller<sup>1</sup>, Stefan Facsko<sup>1</sup>, Matthias Zschornak<sup>1</sup>, Sebastian Wintz<sup>1</sup>, Jose L. Endrino<sup>2</sup>, Sibylle Gemming<sup>1,3</sup>, Maja Buljahn<sup>4</sup>

<sup>1</sup>*Helmholtz-Zentrum Dresden-Rossendorf, PF-510119, 01314 Dresden, Germany*

<sup>2</sup>*Cranfield University, Cranfield, Bedfordshire MK43 0AL, UK*

<sup>3</sup>*Institute of Physics, TU Chemnitz, Germany*

<sup>4</sup>*Ruder Bošković Institute, 10000 Zagreb, Croatia*

Ion assistance provides unique opportunities to influence the microstructure of growing films due to energy and momentum transfer. Recently the formation of a three-dimensionally ordered pattern of Ni rich nanoparticles in an amorphous carbon matrix was reported. The pattern was attributed to the transfer of compositionally modulated surface ripples into the bulk of a bi-component carbon:nickel thin film. The essential experimental features were reproduced by three-dimensional binary collision computer simulations. Ion-induced preferential displacements were proposed as the driving force for the pattern formation [1]. Here the influence of the Nickel content on the morphology of C:Ni (~ 5 at.% Ni to ~ 36 at.% Ni) nanocomposite (NC) films deposited by dual ion beam sputtering using 130 eV assisting Ar<sup>+</sup> ion irradiation is reported. Surface and bulk structure were analyzed by SEM, Raman spectroscopy, XTEM, and GISAXS. For all C:Ni NC films surface ripple formation with the wave vector parallel to the surface-projected ion-beam projection is found. The structural order and the period of the ripples are strongly dependent from the Ni concentration. The film microstructure is discussed as interplay of different displacement mechanisms such as relocation and sputtering and the effects of phase separation and ion-enhanced diffusivity.

[1] M. Krause, M. Buljan, A. Mücklich, W. Möller, M. Fritzsche, S. Facsko, R. Heller, M. Zschornak, S. Wintz, J.L. Endrino, C. Baehtz, A. Shalimov, S. Gemming, G. Abrasonis, Phys. Rev. B, 89, 085418 (2014).

Acknowledgement: The work is funded by the European Union, LEI Folgeprojekt D1, "C-basierte Funktionsschichten für tribologische Anwendungen (CarboFunctCoat)", No. 7310000211. G. Abrasonis (EPO Munich) is gratefully acknowledged for initiation and long-term supervision of this work. The authors thank A. Mücklich, M. Fritzsche, C. Baehtz, A. Shalimow for technical assistance and helpful discussions.

## Development of nano-topography during SIMS characterization of $\text{Ge}_{1-x}\text{Sn}_x$ alloy

Maria Secchi, Evgeny Demenev, Damiano Giubertoni, Erica Iacob, Massimo Bersani

*FBK - Fondazione Bruno Kessler, University of Trento, Italy*

$\text{Ge}_{1-x}\text{Sn}_x$  is a semiconductor alloy, compatible with silicon technology, with a bandgap tunable with Sn concentration ( $3\% < x < 7\%$  can change the Ge bandgap from indirect to direct) [1], high electron and hole mobility [2,3]. For all those applications, it is mandatory to define analytical approaches able to provide accurate measurements of Sn content. SIMS can be a valuable choice but quantification and matrix issues due to the high Sn content need to be addressed. Therefore, we developed a SIMS protocol using Sn ion implants on Ge as reference samples. Ion implantation was carried out at liquid nitrogen temperature, in order to avoid the well-known phenomenon of Ge nanostructuration under heavy ion implantation at room temperature [4,5]. Implant fluences varied between  $1 \times 10^{14}$  at/cm<sup>2</sup> and  $5 \times 10^{15}$  at/cm<sup>2</sup> and implant energy was set at 45keV. SIMS characterization was performed in different configurations, i.e. using  $\text{O}^{2+}$  as primary beam and collecting positive secondary ions,  $\text{Cs}^+$  and negative secondary ions,  $\text{Cs}^+$  collecting  $\text{MCs}^+$  ions; the final results were compared with quantitative measurements obtained by RBS, revealing a good accuracy for the  $\text{MCs}^+$  protocol. However, it was observed that the applied sputtering conditions ( $\text{Cs}^+$  1 keV, 55° incidence vs. normal) induced an early formation of surface topography resulting in a variation of sputtering yield. AFM images will be reported showing the peculiar topography developed on Ge and corrections to improve depth calibration accuracy will be discussed. The obtained protocol was then used to quantify also SIMS profiles of room temperature Sn implants, i.e. nanostructured Ge samples, with good accuracy.

[1] S. Gupta et al. IEDM (2011).

[2] G. He and H.A. Atwater, Phys. Rev. Lett. 79, 1937 (2007).

[3] J.D. Sau and M.L. Cohen, Phys. Rev. B, 75, 045208 (2007).

[4] I.H. Wilson, J. Appl. Phys. 53(3), 1698 (1982).

[5] N.G. Rudawski and K.C. Jones, J. Mater. Res. 28(13), 1633, (2013).

**Ion irradiation induced morphological instability of thiol-functionalized Au surfaces**

Annika Venäläinen, Minna Räisänen, Benoit Marchand, Kenichiro Mizohata, Jyrki Räisänen

*University of Helsinki, Finland*

Self-assembled monolayers (SAMs) are ordered molecular assemblies formed by adsorption of an active surfactant on a solid surface. SAMs are materials with promising applications, as controlled modification of the surface enables new opportunities in different technological fields. In the present study Ar ion irradiation induced changes in the surface morphology of both bare and 1-dodecane-thiol (DDT) covered Au(111) – surfaces have been investigated. The surface morphological changes, induced by varying the ion charge ( $Ar^{1+}$ ,  $Ar^{4+}$ ), energy (10-40 keV) and fluency ( $10^{12}$  -  $10^{13}$   $1/cm^2$ ), was followed by performing scanning tunnelling microscopy (STM) and x-ray photoelectron spectroscopy (XPS) measurements of the surfaces.

## **Roughness evolution in polymer thin films submitted to ion irradiation and thermal treatments near the glass transition**

Danieli Born Guerra, Bárbara Friedrich, Christian Roberto Becker Esteves, Raquel Thomaz, Pedro Grande, Leandro Izê Gutierrez, Ricardo Meurer Papaléo

*Pontifical Catholic University of Rio Grande do Sul, Brasil*

Polymer thin films are commonly used in a large number of technological applications, such as sensors, lithography, smart packaging, membranes and medical implants. During deposition by spin-coating, there is rapid decrease in the chains mobility due to the fast evaporation of the solvent, leading to a molecular conformation far from equilibrium. Because of that, these materials may present structure evolution or even full dewetting upon mild thermal treatments. Ion bombardment may also induce perturbations in the samples that could trigger structural evolution of the films. In this study, we investigated the thermal stability of poly(methyl methacrylate) thin films after exposure to 300 keV and 2 MeV  $H^+$ , and 18 MeV  $Au^{7+}$  ions combined to thermal treatments at 100°C. Depending on the irradiation conditions, the films showed either roughening or smoothing upon annealing. When the samples were bombarded by  $H^+$  ions and annealed at 100°C, the effect of the radiation was to decrease the roughness of the surface, stabilizing its value at levels below those of the films not exposed to the beam. On the other hand, the irradiation with  $Au^{7+}$  destabilized the films and caused strong changes on the surface morphology upon annealing. Increasing the irradiation fluence (at moderate levels) did not influence much the roughness evolution with treatment time. We will also discuss the effect of the type of interface ( $SiO_x$  or Ti substrates) on the stability of the films.

## Nano-size metallic oxide cluster formation in high-purity Fe-10%Cr alloy by ion implantation

Ce Zheng<sup>1</sup>, Aurélie Gentils<sup>1</sup>, Joël Ribis<sup>2</sup>, Odile Kaïtasov<sup>1</sup>, Vladimir Borodin<sup>3</sup>

<sup>1</sup>*CSNSM, Univ Paris-Sud, CNRS/IN2P3, France*

<sup>2</sup>*CEA/DEN/SRMA/LA2M, France*

<sup>3</sup>*NRC Kurchatov Institute, Russia*

Controlling the synthesis of nano-particles (size, distribution and composition) in a material is a fundamental problem for broad applications from electronics and photonics to nuclear industry. Ion implantation is a powerful technique to achieve the synthesis under well-controlled conditions. In this presentation we demonstrate that ion implantation can be successfully applied to create nano-size oxide precipitates in Fe-Cr steel.

We report the results of the metal-oxide particle formation in a high purity Fe-10wt.%Cr steel by ion implantation (using JANNuS-Orsay facility, where two accelerators are linked to a Transmission Electron Microscope), together with a structural characterization of these nano-oxide clusters [1]. The behaviour of these particles under *in situ* thermal annealing will be also addressed.

A dispersion of nano-size precipitates of metallic oxides is known to strongly improve mechanical properties of ferritic-martensitic steels especially at high temperature. The Oxide Dispersion Strengthened (ODS) steels are promising candidates for structural components of future nuclear reactors. The broad application of these steels is however hindered by the relatively complicated and expensive production technology (powder co-grinding and high-pressure thermomechanical treatment). Our experimental results indicate the feasibility of unconventional ways for nano-size oxide ensemble creation with high potential for control over the steel property amelioration by tailoring the parameters of oxide ensembles.

[1] C. Zheng et al., Phil. Mag., in press (2014).

### Damage accumulation in irradiated powellite studied by ionoluminescence method

Jacek Jagielski<sup>1</sup>, Grzegorz Gawlik<sup>1</sup>, Iwona Jozwik-biala<sup>1</sup>, Gerard Panczer<sup>2</sup>, Nathalie Moncoffre<sup>3</sup>, Renata Ratajczak<sup>4</sup>, Swirkowicz Marek<sup>1</sup>, Lionel Thomé<sup>5</sup>

<sup>1</sup>*Institute of Electronic Materials Technology, Poland*

<sup>2</sup>*Universite Claude Bernard Lyon I, France*

<sup>3</sup>*Institut de Physique Nucleaire Lyon, France*

<sup>4</sup>*National Centre for Nuclear Research, Poland*

<sup>5</sup>*Centre de Sciences Nucleaires et de Sciences de la Matiere, France*

It is well known, that many materials glow when hit by ion beams. It is thus clear, that the ion beams may serve a twofold purpose: induce material modification and in the same time provide the information about the changes caused by irradiation. In this work we studied Ar-irradiated CaMoO<sub>4</sub> (single crystalline powellite, an oxide precipitating from nuclear waste glass) by using three complementary techniques: Rutherford Backscattering/Channeling (RBS/C), cathodoluminescence (CL) and ionoluminescence (IL). The main aim of the study is to get a better insight into potential of the IL technique, especially for the damage accumulation analysis in polycrystalline solids, when the use of the RBS/C method is impossible.

The CaMoO<sub>4</sub> crystals were irradiated with increasing fluences of 320 keV Ar ions in order to create various levels of radiation damage. RBS/C measurements provided quantitative data about damage concentration in the samples, these values were compared to the luminescence measurements. All measurements point to a two-step damage accumulation mechanism involving the defect transformation at about  $10^{15} \text{ cm}^{-2}$ . The main difference between luminescence and RBS/C results is the fact that the main decrease of the luminescence signal is observed in the first stage of the damage accumulation (characterized by the formation of small defect clusters), whereas huge changes in the RBS/C spectra are observed in the second stage (when dislocations are preferentially formed). Both methods appear thus as complementary techniques. The huge advantage of the luminescence measurements relies in the fact that such an analysis may be performed also for polycrystalline samples and allows one to extract the threshold irradiation fluence for defect transformation and cross-sections for defect formation at each step of the damage accumulation process.



## **Ion beam induced luminescence in fused silica: role of the stopping power**

Diana Bachiller-Perea<sup>1</sup>, Ángel Muñoz-Martín<sup>1</sup>, Fernando Agulló-López<sup>1</sup>, David Jiménez-Rey<sup>2</sup>

<sup>1</sup>*Centro de Micro-Análisis de Materiales (Universidad Autónoma de Madrid), Spain*

<sup>2</sup>*National Fusion Laboratory – CIEMAT, Spain*

Amorphous silica is a fundamental material in fusion technology: optical viewports, plasma diagnostics, and safety and control systems are based on fused silica. Degradation of optical and structural properties of silica due to irradiation is an important issue with a considerable number of features not yet sufficiently understood.

Ion Beam-Induced Luminescence (IBIL) is a very sensitive technique for the analysis of impurities and defect centers, such as those introduced by irradiation. In-situ ionoluminescence during ion beam irradiations can be used to investigate the microscopic processes accompanying the generation of damage and its kinetic evolution with the irradiation fluence.

In this work we have compared the ionoluminescence in three different types of  $\alpha$ -SiO<sub>2</sub>: KU1 and two commercial types of silica fabricated by CRYSTRAN. These three materials contain a different amount of OH impurities, giving rise to some differences in their luminescent behavior. For all samples, the IBIL spectrum shows two main peaks at 460 and 650 nm which have been associated with different defects in the material. We have observed that, at the beginning of the irradiation, the red emission is much higher in the samples with high OH-content than in the samples with low OH-content, while the blue emission is higher in low OH-content samples than in high OH-content ones.

We have paid special attention to comparing the IBIL produced by the different ions and energies (i.e., different stopping powers). The kinetic evolution of the ionoluminescence is different depending on these parameters. For light ions, the yields of both peaks increase monotonically with the dose. However, when we irradiate with heavy ions, the yields of the two main emissions increase with the fluence and reach a maximum at a certain dose, where they start to decrease. We have studied the dependence of the dose at which this maximum is produced with the stopping power of the incident particle.

**Behavior of mesoporous silica under ionic irradiation**

Yu Lou<sup>1</sup>, Xavier Deschanel<sup>2</sup>, Cyrielle Rey<sup>3</sup>, Guillaume Toquer<sup>4</sup>, Sandrine Dourdain<sup>5</sup>, Clara Grygiel<sup>6</sup>

<sup>1</sup>*CEA Marcoule (French atomic energy commission), France*

<sup>2</sup>*ICSM - UMR5257, France*

<sup>3</sup>*Université de Montpellier 2, France*

<sup>4</sup>*ENSCM, France*

<sup>5</sup>*CEA, France*

<sup>6</sup>*GANIL, France*

In the prospective of radioactive waste conditioning, the mesoporous silica material represents several advantages:

1. Its large specific surface, able to be functionalized, is expected to efficiently adsorb radionuclides.
2. Once having retained radionuclides, the mesoporosity could be closed by chemical or thermal ways, which give the possibility for long term waste confinement.
3. Low relatively temperature (~100°C), compared to the conventional borosilicate nuclear glass (~1200°C), could be advantageous in confining volatile radionuclides.

During these processes, with the presence of radionuclides, the mesoporous structure will be exposed to self-irradiation. External heavy ion irradiation is used to simulate this irradiation, as the intense beam allows achieving a high dose in a short period, making the material little radioactive at the same time.

In our recent work, two mesoporous silica materials, SBA-15 and MCM-41 were irradiated, along with some preliminary post-irradiation characterizations. SBA-15 and MCM-41 are model materials synthesized under mild conditions. Notably SBA-15 possesses considerably large pore size (~6-7 nm). The beam used was 278 MeV 20Ne on SME, GANIL, France, at a maximum fluence of  $2.5 \times 10^{14}$  ions/cm<sup>2</sup>.

Post characterizations of nitrogen adsorption (BET) and SAXS all confirm that SBA-15 resists under the highest fluence while mesoporous structure of MCM-41 collapses before the lowest one. Data treatment also gives the evolution of specific surface, porous volume, pore size distribution, microporosity volume and constant C representing porosity surface state. Other characterizations like infrared and solid state NMR are being undertaken.

## Ion tracks formation threshold and structural changes in Simple and Complex Borosilicate's

Anamul Haq Jeri Mir<sup>1</sup>, Peugeot Sylvain<sup>1</sup>, Toulemonde Marcel<sup>2</sup>, Bouffard Serge<sup>2</sup>, Monnet Isabelle<sup>2</sup>, Mechin Laurence<sup>3</sup>, Michael Gennison<sup>1</sup>, Kluth Patrick<sup>4</sup>, Olivares Jose<sup>5</sup>, Jegou Christophe<sup>1</sup>

<sup>1</sup>CEA, DEN/LMPA, 30207 Bagnols-sur-Cèze, France

<sup>2</sup>Laboratoire CIMAP-GANIL, Caen, France

<sup>3</sup>GREYC, CNRS, ENSICAEN Université de Caen, France

<sup>4</sup>Electronics Materials Engineering Department, ANU, Canberra, Australia

<sup>5</sup>Centro de Microanálisis de Materiales, CMAM Madrid, Spain

Simple borosilicate's (BS3; 3 oxide and ISG; 6 oxide borosilicate) and complex glass (30 oxide R7T7); the latest glass serving as confining matrix for nuclear waste, have been irradiated with various light and heavy ions with electronic stopping powers ranging from below 1keV/nm to about 16 keV/nm. Ion tracks formation threshold has been determined by extrapolation of damage cross sections which in turn have been determined using different characterization techniques like profilometry for swelling measurement, hardness, AFM, SAXS, Raman spectroscopy and Optical absorption and reflectance measurements. Multiple characterizations allow us to check for the convergence and uniqueness of the threshold. Such damage cross sections are also compared to inelastic thermal spike model calculations to check for compatibility.

It is seen that swelling measurements have minimum damage cross section. Damage cross sections obtained from Raman spectroscopy are consistent with ones obtained from AFM measurements, and both are higher than the ones obtained from hardness or swelling measurements.

Tracks formation threshold for BS3 is determined to be about 2.4keV/nm. This is far above the electronic stopping power of any recoil nuclei generated in the nuclear waste matrix but it is of the same level as their nuclear stopping power.

Structural changes in BS3 and ISG glass have also been studied by NMR spectroscopy using a multinuclear approach (<sup>11</sup>B, <sup>23</sup>Na, <sup>27</sup>Al and <sup>29</sup>Si). Specimens exhibited de-polymerization of the borosilicate network, lower boron coordination number, and a change in the role of fraction of sodium atoms after irradiation, suggesting that the final borosilicate glass structures are a result of fast quenching from a non-equilibrium liquid that is partially relaxed in ion tracks.

## Evolution of vacancy type defects in T91 with self-ion irradiation under different temperature

Huiping Zhu, Zhiguang Wang, Minghuan Cui, Yuanfei Li, Jianrong Sun, Cunfeng Yao, Bingsheng Li, Kongfang Wei, Tielong Shen, Yabin Zhu, Lilong Pang

*Institute of Modern Physics, Chinese Academy of Sciences, P.R. China*

Due to the advantages such as avoidance of activated material owing to neutron irradiation, reduction of irradiation, improved capabilities to vary irradiation conditions and introduction of only displacement damage without foreign atoms, etc., self-ion irradiation is known as an effective method to simulate displacement damage caused by neutron irradiation. Positron annihilation spectroscopy (PAS) is one of the more powerful and well-established techniques to characterize vacancy-type defects of a material [1] and have been widely used on investigating defect structures formed in materials after irradiation. In this paper, the candidate structure material T91 steel was irradiated with 1.625MeV Fe-ions to a fluence of  $2.5 \times 10^{15}$  ions/cm<sup>2</sup> under room temperature, 300, 450 and 550°C. After irradiation, the evolution of vacancy-type defects in the samples was analyzed with doppler broadening spectroscopy (DBS) of positron annihilation measurements. Compare with the unirradiated sample, samples after irradiation at different show different degrees of increase on the value of S parameter, which indicate that vacancy-type defects are generated in all irradiated samples. In our study, the sample irradiated RT has the largest S value when the positron energy is above 1.5 keV. For the samples irradiated at higher temperature, the S value of them are in a trend of  $S_{550^\circ\text{C}} < S_{300^\circ\text{C}} < S_{450^\circ\text{C}}$  and the variation trend of each S plot are not quite the same. For the sample irradiated at different temperature, a second type of vacancy type defect has been found at different implant depth form the S-W plots. These phenomena are closely related to the different evolution mechanism of defects under different temperature, which will be discussed in our paper in detail.

[1] J. Qiu, Y. Xin, X. Ju, et al. Nucl. Instr. and Meth. B. 267, 3162-3165 (2009).

## Study of radiation damage and mechanical properties of 6H-SiC by He and H ion irradiation

S.D. Yao, Q. Bai, L. Li, F.F. Cheng, R. Bin, T. Fa, E. Fu

*State Key Laboratory of Nuclear Physics and Technology, School of Physics, Peking University, Beijing, 100871, P.R. China*

6H-SiC single crystal wafers were radiated by 200 KeV He ions, 100 KeV H ions, and 200 KeV He ions followed by 100 KeV H ions, with the radiation fluences in the range of  $10^{16}$  ions  $\text{cm}^{-2}$ , respectively. After ion irradiation, the samples were annealed at 1000 °C in N<sub>2</sub> atmosphere. XRD, RBS/C, and nano-indentation measurements were carried out to evaluate the damage of the irradiated samples. XRD results show that new diffraction peaks from radiation damage appear at lower angles next to the main diffraction peaks, which indicates that radiation process caused the increase of lattice parameter in the damage region. RBS/C results show that complete amorphization dose not occur even under  $6 \times 10^{16}$   $\text{cm}^{-2}$  He ions follow by  $8 \times 10^{16}$   $\text{cm}^{-2}$  H ions irradiation indicated by  $\chi_{\text{min}}=17.63\%$ . Damage produced by He ions irradiation at a fluence of  $6 \times 10^{16}$  ions  $\text{cm}^{-2}$  is greater than that produced by  $3 \times 10^{16}$   $\text{cm}^{-2}$  He ions and followed by  $4 \times 10^{16}$   $\text{cm}^{-2}$  H ions irradiation, which implied that He ions irradiation effect plays a dominant role in the process of damage producing. The nano-indentation measurements show that hardness variation depends on the irradiation fluences: high dose radiation leads to the decrease of the hardness while low dose irradiation leads to the increase of the hardness. After annealing, the hardness of all the irradiated samples increases. Possible mechanisms are discussed for explaining these phenomena.

## Retention and damage of SiC irradiated with He and H ions

Alec Deslandes<sup>1</sup>, Mathew C. Guenette<sup>1</sup>, Inna Karatchevtseva<sup>1</sup>, Lars Thomsen<sup>2</sup>, Mihail Ionescu<sup>1</sup>, Gregory L. Lumpkin<sup>1</sup>

<sup>1</sup>*Australian Nuclear Science and Technology Organisation, Australia*

<sup>2</sup>*Australian Synchrotron, Australia*

Fusion materials will suffer radiation damage effects due to energetic particles, including hydrogen and helium ions, and high energy neutrons from the fusion fuel and its reaction products. Silicon carbide is a material that offers excellent thermal properties, and less erosion than other carbon-based materials. The retention of hydrogen isotope fuel and helium ash from the fusion environment, as well as the interaction between radiation damage and these retained species, requires further investigation. Results of these investigations will help to understand and predict failure mechanisms of components, and lifetimes for retention of acceptable limits of tritium. Radiation damage is of particular concern for SiC as it is known to degrade its thermal properties. H and He can be produced by neutron transmutation reactions, hence retention of these species and their effects upon the material are also a concern.

SiC samples were irradiated with He ions of energy up to 30 keV to produce damage in the near-surface region. A duplicate set of He ion irradiated SiC samples, as well as undamaged SiC, were also irradiated with H<sub>2</sub><sup>+</sup> ions of energy up to 20 keV to study the interaction of H species with SiC and radiation-damaged SiC. Modification to the surface is observed via Raman spectroscopy, which exhibits development of damage states such as disordered carbon and Si-Si peaks. The retention of H and He were measured using elastic recoil detection analysis with results including fluences required for saturation, and the damage created by He having little affect upon subsequent H retention. Changes to the surface chemistry were characterised using X-ray Photoelectron Spectroscopy and NearEdge X-ray Absorption Fine Structure spectroscopy.

**Positron study of austenitic steel NF 709 after helium ion implantation**

Jana Simeg Veternikova, Veronika Sabelova, Jarmila Degmova, Vladimir Slugen, Martin Petriska

*Institute of Nuclear and Physical Engineering, Faculty of Electrical Engineering and Information Technology, Slovak University of Technology, Ilkovicova 3, 812 19 Bratislava, Slovakia*

NF 709 (Fe-20Cr-25Ni) is an austenitic stainless steel belonging to alloys appropriate for construction of the new generation of nuclear reactors (Generation IV). This steel can be applied for construction of pipelines, heat exchangers or reactor internalities due to its improved thermal and creep resistance as well as its good ductility. Although, austenitic steels have already been used in previous generations of reactors; their radiation swelling is significant which limits lifetime of austenitic components. Therefore, our study is focused on investigation of radiation resistance of the new alloy NF 709. Radiation damage of investigated samples was performed by helium ion implantation with kinetic energy up to 500 keV. The implanted zone with thickness of 1.2  $\mu\text{m}$  was observed by positron annihilation techniques sensitive for a small change of microstructure, especially accumulation of vacancy type-defects. The defect size and defect concentration was compared for NF 709 before and after the implantation and the increase of total defect volume was calculated. The results demonstrated significant defect accumulation, while increase of defect volume was up to 10%.

## Raman spectroscopy studies of damage recovery of the near surface region of ion implanted 6H-SiC

Remeredzai Joseph Kuhudzai, Johan Malherbe, Thulani Hlatshwayo

*Physics Department University of Pretoria, South Africa*

Recrystallisation behaviour of the near surface amorphous layers retained after ion implantation into 6H-SiC at room temperature has been investigated by Raman spectroscopy. Several ions of energy 360 keV including iodine, silver, strontium and xenon were implanted into wafers of 6H-SiC resulting in amorphous layers extending from the surface to depths of about 200 nm. Raman spectroscopy was performed using two laser wavelength excitation regimes. The 514 nm laser, in the visible region and the 244 nm in the deep ultraviolet region (DUV) were employed to characterise the damage recovery of the bulk amorphous layers retained after implantation and the very near surface respectively. The samples were vacuum annealed from 1100-1800 degrees Celsius. Analysis of the characteristic Transverse optical (TO) and Longitudinal optical (LO) 6H-SiC Raman peaks with laser excitation in the visible range showed that while the virgin sample Raman peaks were very thin and symmetrical, the peaks from the as-implanted samples were very broad and approximately Gaussian. Annealing of the samples at 1200 degrees for 5 hours resulted in the peaks becoming thin and symmetrical similar to the virgin samples, albeit with lower intensity due to some retained defects upon recrystallisation of the SiC surface layers. Similarities in the virgin and the annealed sample spectra were due to the deep penetration of the laser in the visible range resulting in the signal from the bulk undamaged SiC contributing to the overall spectra. However, DUV laser excitation which only probes the near surface region shows that after annealing the peaks are broader and asymmetrical compared to the virgin samples. This shows that the SiC has crystallised into a different form which was not be observed with the laser excitation in the visible region and is due to the contribution of the nanocrystals that grow on the surface during annealing as observed by scanning electron microscopy (SEM).



## Irradiation-induced order-to-disorder phase transformation on delta-phase $\text{Sc}_4\text{Hf}_3\text{O}_{12}$

Yongqiang Wang<sup>1</sup>, J. Wen<sup>2</sup>, Y.H. Li<sup>2</sup>, T. Ming<sup>1</sup>, J.A. Valdez<sup>1</sup>, M. Patel<sup>3</sup>, K.E. Sickafus<sup>3</sup>

<sup>1</sup>*Los Alamos National Laboratory, United States*

<sup>2</sup>*Lanzhou University, P.R. China*

<sup>3</sup>*University of Tennessee – Knoxville, United States*

Polycrystalline delta-phase  $\text{Sc}_4\text{Hf}_3\text{O}_{12}$  was irradiated with light and heavy ions under cryogenic conditions ( $\sim 77$  K), in order to examine the possible susceptibility of this compound to radiation damage. The light ion irradiation was performed with 400 keV  $\text{Ne}^{2+}$  ions to fluences ranging from  $1\text{E}14$  to  $1\text{E}15$  ions/ $\text{cm}^2$ , while the heavy ion irradiation was performed with 600 keV  $\text{Kr}^{3+}$  ions to fluences ranging from  $5\text{E}14$  to  $5\text{E}15$  ions/ $\text{cm}^2$ . Irradiated samples were characterized by various techniques including: grazing incidence X-ray diffraction (GIXRD), transmission electron microscopy (TEM), and electron paramagnetic resonance (EPR) spectroscopy. A complete phase transformation from ordered rhombohedral to disordered fluoride was observed by a fluence of  $1\text{E}15$  ions/ $\text{cm}^2$  with 400 keV  $\text{Ne}^{2+}$  ions, equivalent to a peak ballistic damage dose of  $\sim 0.33$  displacements per atom (dpa). Meanwhile, the same transformation was also observed by 600 keV  $\text{Kr}^{3+}$  ions at the same fluence of  $1\text{E}15$  ions/ $\text{cm}^2$ , which however corresponds to a peak ballistic damage of  $\sim 2.2$  dpa. Analysis of the results shows that light ions are more efficient than heavy ions in producing the retained defects that are presumably responsible for the observed O-D transformation in structure. To better quantify the mechanism of the transformation, we also calculated the effect of cation antisite-pair defect and anion oxygen Frenkel defect. Our calculated results appear to support the argument that the O-D phase transformation in delta- $\text{Sc}_4\text{Hf}_3\text{O}_{12}$  is likely caused by anion oxygen Frenkel defects. EPR spectroscopy is also being used to explore the possible charge compensation in irradiation-induced metastable phase of  $\text{Sc}_4\text{Hf}_3\text{O}_{12}$ .

## Effect of recrystallization on the ion-irradiation hardening and microstructural changes in 15Cr-ODS ferritic steel

Yoosung Ha<sup>1</sup>, Akihiko Kimura<sup>2</sup>

<sup>1</sup>*Graduate School of Energy Science, Kyoto University, Japan*

<sup>2</sup>*Institute of Advanced Energy, Kyoto University, Japan*

Oxide dispersion strengthened (ODS) steel is one of the candidate structural materials for nuclear power systems and also fusion reactor with good corrosion resistance, high performance at elevated temperature. Since oxide particles play a role of strengthening in matrix through that the grain size as well as the dispersion morphology of oxide particles greatly influenced their mechanical properties in ODS steels. However, the grains are elongated during the hot-extruded processing, it causes anisotropy which effect on mechanical properties. Thus, recrystallization process for improving the mechanical anisotropy has been studied. Recrystallization processing with grain growth must influence not only their mechanical properties but also on irradiation performance such as hardening or swelling. Therefore, the effect of recrystallization on ion-irradiation hardening of 15Cr ODS ferritic steel is investigated in this research.

The 15Cr-ODS steel used in this study is composed of Fe(bal.)-15Cr-2W-4Al-0.5Zr-0.33Y<sub>2</sub>O<sub>3</sub>. The annealing conditions in order to recrystallize are 1350°C for ODS steel for 1hour, and another specimen of 20% cold rolled specimen after annealing is also prepared. Single-ion beam of 5.1 MeV Fe<sup>3+</sup> for displacement damage and also a dual-ion beam of 5.1 MeV Fe<sup>3+</sup> ions simultaneously with energy-degraded 1.0 MeV He<sup>+</sup> ions were irradiated at 300°C and 470°C up to 10dpa and 30dpa, respectively. Ion-irradiation experiment is performed with DuET facility at Institute of Advanced Energy, Kyoto University in Japan. Irradiation hardening was measured by nano-indentation method and the damage structures were observed by TEM to correlate the hardening with microstructural evolution. At single ion beam condition at 300°C with 10dpa, as-received ODS steel has the largest hardening change, meanwhile, at 470°C with 30dpa, the hardening of recrystallized ODS steel is larger than that of as-received ODS steel and it is similar with the result in dual ion beam with He<sup>+</sup> ion.

## Optical transmission properties of a planar waveguide structure on Nd:Li<sub>6</sub>Y(BO<sub>3</sub>)<sub>3</sub> fabricated by C ion irradiation

Xiao-Fei Yu<sup>1</sup>, Tao Liu<sup>1</sup>, Lian Zhang<sup>1</sup>, Yu-Fan Zhou<sup>1</sup>, Hong-Lian Song<sup>1</sup>, Tie-Jun Wang<sup>1</sup>, Mei Qiao<sup>1</sup>, Jin-Hua Zhao<sup>2</sup>, Xue-Lin Wang<sup>1</sup>

<sup>1</sup>*School of Physics, State Key Laboratory of Crystal Materials and Key Laboratory of Particle Physics and Particle Irradiation (MOE), Shandong University, P.R. China*

<sup>2</sup>*School of Science, Shandong Jianzhu University, P.R. China*

Single crystal of the double alkali-rare-earth borate Li<sub>6</sub>Y(BO<sub>3</sub>)<sub>3</sub> (LYB) has become more and more attractive because of its low density, atomic weight and sensitivity to gamma radiation. The investigation on growth and spectral properties of Nd<sup>3+</sup>:LYB crystal shows that the existence of the covalent bonding in the BO<sub>3</sub> group makes it have a weak concentration quenching effect and a low laser threshold, which makes it a good candidate for laser applications.

There is only once, as reported in ref [2], the Nd<sup>3+</sup>:LYB waveguide structures have been fabricated by oxygen or silicon ion implantation. There is still a huge gap of waveguide structures fabrication on Nd<sup>3+</sup>:LYB. This paper reported a planar waveguide structure on a Nd<sup>3+</sup>:Li<sub>6</sub>Y(BO<sub>3</sub>)<sub>3</sub> sample fabricated by 6MeV C ion irradiation at a fluence of 2.5×10<sup>15</sup> ions/cm<sup>2</sup>. The nuclear and electronic stopping power profiles were simulated with the software Stopping and Range of Ions in Matter (SRIM) 2013. The simulated result shows the procedure and mechanism of the formation of waveguide structure. The effective refractive index profiles of the C-irradiated Nd:Li<sub>6</sub>Y(BO<sub>3</sub>)<sub>3</sub> waveguide were measured using prism coupling method with TM-polarized 632.8-nm and 1539-nm lasers through a Metricon Model 2010 Prism Coupler. The refractive index profiles were reconstructed based on the effective index functions with Reflectivity Calculation Method (RCM). In the calculation, errors between experimental and calculated results for the effective refractive indexes are about 10<sup>-4</sup>. The near-field light intensity files in the visible and near-infrared bands were measured by end-face coupling method with different light sources. The near-field light intensity profiles of the waveguide were simulated with finite difference beam propagation method (FD-BPM) for comparison with the measured results, which can reveal that the experimental and simulated results have a reasonable agreement.

## Ion beam modification of red Spinel for jewelry applications

Duangkhae Bootkul<sup>1</sup>, Saweat Intarasiri<sup>2</sup>, Udomrat Tippawan<sup>3</sup>, Dheerawan Boonyawan<sup>3</sup>

<sup>1</sup>*Department of General Science (Gems & Jewelry), Faculty of Science, Srinakharinwirot University, Sukhumvit 23, Bangkok 10110, Thailand*

<sup>2</sup>*Science and Technology Research Institute, Chiang Mai University, Chiang Mai 50200, Thailand*

<sup>3</sup>*Plasma and Beam Physics Research Facility, Department of Physics and Materials Science, Faculty of Science, Chiang Mai University, Chiang Mai 50200, Thailand*

Natural spinels ( $\text{MgAl}_2\text{O}_4$ ) can be found in several colors similar to corundums, i.e. ruby and sapphire. In particular, spinels of clarity saturated red appearance, called spinel-ruby or balas ruby, are the most valuable. However, the beautiful rich reds spinels are rarely, they can be found in a range of pastel shades blended with either brown, orange or purple. Additionally, the general appearance with inclusions is another obstacle to adopt for the jewelry industry. For spinels, the submicroscopic inclusions are structurally-incorporated of a few ppm of water and gaseous in defect structure at both octahedral and tetrahedral O–O edges. These inclusions cause light scatter, resulting in a slightly sleepy to quite cloudy appearance of a faceted gemstone. Incorporation of water and gaseous can be the cause of damaging of the gems during heat treatment and/or cutting. Therefore, the objectives of the present study are to investigate the origins of the color blending and to remove water and gaseous incorporation in spinels by ion beam technology. Two non-destructive ion beam analysis techniques, i.e., particle induced X-ray emission (PIXE) and iono-luminescence (IL), have been employed for geochemical analysis of the stones. Low and medium energy ion implantations have been applied to the gems for improving their optical appearances. As a new modification technique, ion beam treatment at various ion species, energies and fluences were applied for enhancement of the color qualities of the deep brownish red Burmese spinels. The results shown that the micro-inclusions due to water and gaseous absorption have almost been disappeared, resulting in clarity enhancement. The very interesting is that their colors can be modified to resemble to the spinel-ruby.

## Modification of corundum by Ion Implantation

Thawatchart Chulapakorn<sup>1</sup>, Duangkhae Bootkul<sup>2</sup>, Saweat Intarasiri<sup>3</sup>, Udomrat Tippawan<sup>1</sup>,  
Dheerawan Boonyawan<sup>1</sup>

<sup>1</sup>*Plasma and Beam Physics Research Facility, Thailand*

<sup>2</sup>*Department of General Science (Gems and Jewelry), Faculty of Science, Srinakharinwirot  
University, Bangkok 10110, Thailand*

<sup>3</sup>*Chiang Mai University, Thailand*

Natural corundum, a crystalline form of alumina oxide ( $\text{Al}_2\text{O}_3$ ) with impure elements, is an allochromatic mineral referring to minerals whose color varies based on the presence of impurities in their composition and on defects in their structure. For instance, the red color of ruby is caused by the substitution of  $\text{Cr}^{3+}$  to  $\text{Al}^{3+}$  in the six surrounded oxygen ions. On the other hand, the interchange electron between  $\text{Fe}^{2+}$  and  $\text{Ti}^{4+}$ , as called intervalence charge transfer, generate the deep blue color of sapphires. Either excess or lack of the oxygen during gems growth has the principal effects on the saturation, and tone of color. As a result, the charge state of transition metal element can be either increased or decreased. Ion implantation technology can be utilized for enhancing the optical properties of corundum by selecting the implanted ion type leading to control the surrounding oxygen quantity. As for the appearance of corundum depending on many factors including: brilliance, color, fire (light dispersion), and luster, this research attempts to find out an alternative method for improving the optical appearance and color enhancement of corundum. Ion beam treatment with a variety of ion type, energy and fluence has been applied to ruby and sapphire from Thailand, Myanmar, Cambodia, Sri Lanka, Africa, and USA. Additionally, the ion beam analysis techniques, i.e., particle-induced X-ray emission (PIXE), together with conventional gemological observations such as optical microscope and UV-Vis-NIR spectroscopy have been made out this phenomena description. The advantageous of ion implantation appear to be a new and a sustainable for improving corundum properties.

**Keywords:** Ion implantation, corundum, ruby, sapphire, optical properties.

**Full set of radiation techniques to produce thin film properties transformation under ion beams irradiation for nanotechnology applications**

Kirill Prikhodko, Boris Gurovich, Michael Tarkhov

*National Research Centre Kurchatov Institute, Russia*

Last years we developed a set of techniques to perform radiation-induced atomic composition transformation of thin film insulators, metals, semiconductors, super-conductors under masks-shielded low energy ion beams irradiation to change their properties and form nano-size functional elements for different applications. All techniques are based on one technological approach and may be applied consistently. Different sets of irradiation condition were designed to produce insulator-metal, superconductor-metal/insulator, semiconductor-insulator to and fro transformations.

Selective removal of atoms (SRA) technique was designed to remote some types of atoms, for instance, oxygen from oxides. We use selective association of atoms (SAA) technique to form new chemical compositions by introducing atoms from the composite ion beams-produce transformation of semiconductor or metal to their oxides. Selective displacement of atoms (SDA) technique was used to change one type of atoms to another, for instance, to transform nitrides to oxides. According to our experimental experience, main mechanisms of these transformations were differed from the well-known effects of selective sputtering and ion beam mixing. We can produce transformations to the depth up to the projected range of ions and transform multilayer systems through one mask.

We have made ultra high density patterned magnetic media consisted from separated single domain magnetic cobalt bits in nonmagnetic matrix and also planar metal and semiconductor nanowires separated by high quality insulator for various chemical and biological sensors applications. We also demonstrated high quality planar Josephson junctions and single photon detectors formed on a base of irradiation-induced atomic composition modification of low temperature superconductive NbN thin film.

**Investigation of long-range effects in glasses after ion implantation**

Alla Deshkovskaya

*Belarussian State University of Informatics and Radioelectronics, Dept of Physics, Belarus*

The effect of long-range action, propagation of structural disturbances to distances which greatly exceed the penetration depth of implanted atoms, was found in silicate glasses subjected to ion bombardment.

Conditions of ion beam treatment: ion energy 100-200 keV, fluence  $10^{14}$ - $10^{18}$  cm<sup>-2</sup>, current density 1-5 μA/cm<sup>2</sup>. As bombarding ions were used: B<sup>+</sup>, Ag<sup>+</sup>, Li<sup>+</sup>, F<sup>+</sup>, In<sup>+</sup>, Sb<sup>+</sup>.

The presence of this effect is confirmed experimentally by a sharp increase of microhardness, changes of wear resistance and spectral properties of reverse (relative to the implanted) side of the specimen.

The intensity of the effect decreases with time. The annealing eliminate it only partly. The reason of the long-range action effect is strong dynamic compression of the structural net of the surface layers on the reverse side by shock waves that accompany ion-beam treatment.

**Krypton ion irradiation induced modification in TiO<sub>2</sub> thin films**

Varsha Bhattacharyya<sup>1</sup>, Deepti Rukade<sup>1</sup>, Dinakar Kanjilal<sup>2</sup>

<sup>1</sup>*University of Mumbai, India*

<sup>2</sup>*Inter- University Accelerator Center, India*

Nanocrystalline TiO<sub>2</sub> has a potential for a wide range of technological applications. Properties of polymorphs of TiO<sub>2</sub> are exploited for different applications. The rutile form of TiO<sub>2</sub> is widely used as pigments and catalyst whereas anatase form is used as photocatalytic devices, solar energy conversion and gas sensors. The properties of nanocrystalline TiO<sub>2</sub> are function of its particle size and thus strongly dependent on the method of synthesis. Ion beam processing is a top down approach not only used to decrease the size of a given system but also modify the structure of surface of solids including its mechanical, chemical, optical and morphological properties. In the present investigation, we attempt study of modifications induced in the properties of TiO<sub>2</sub> thin films by Krypton ion irradiation at varying fluences.

TiO<sub>2</sub> thin films of 100 nm corresponding to rutile phase are deposited on fused silica substrate by plasma oxidation technique. The films are irradiated by 500 KeV krypton ions at two different fluences of  $1.5 \times 10^{15}$  ions/cm<sup>2</sup> and  $7.5 \times 10^{16}$  ions/cm<sup>2</sup>. The irradiated films are annealed in oxygen atmosphere for crystalline phase formation. Optical properties of post implantation annealed films are characterized by UV-Vis spectroscopy and photoluminescence spectroscopy (PL). Rutherford Backscattering spectroscopy (RBS) is used to study the elemental composition with depth. The band gap calculated from absorption spectrum corresponds to anatase phase of TiO<sub>2</sub> for both the films. The band gap of the film irradiated with higher fluence shows a larger amount of blueshift which could be attributed to the quantum confinement effect manifested by the nanostructure formation due to irradiation process. PL spectra reveal peaks corresponding to anatase phase and the presence of oxygen defects. RBS spectra show the stoichiometric composition of titanium oxide anatase phase and also the diffusion of krypton in TiO<sub>2</sub>.



## Enhancement of photocatalytic property of titania deposited film by ag-nanoparticles embedded in its substrate of silica glass

Hiroshi Tsuji<sup>1</sup>, Go Miyagawa<sup>2</sup>, Yasuhito Gotoh<sup>2</sup>

<sup>1</sup>*Department of Electronic Science and Engineering, Kyoto University, Japan*

<sup>2</sup>*Kyoto University, Japan*

Nanoparticles (NP) in silica glass showed optical absorption at a certain wavelength by surface plasmon resonance (SPR). This resonance electric field emerged out around NPs. If the electric field is sufficient strong and when a photocatalyst is placed closely from nanoparticles even in substrate, its photocatalytic property might be enhanced by such emerged electric field. We have investigated this effect on TiO<sub>2</sub> film deposited on silica glass including Ag NPs at a shallow depth.

Ag negative ions were implanted in the glass at energy of 10 keV, where the ion range is about 10 nm. From optical absorption measurement after annealing, the steep absorption peak due to SPR of Ag NPs in the glass appeared at around 400 nm in wavelength i.e. 3.1 eV. The electric field of this SPR is considered to be able to activate tetragonal TiO<sub>2</sub> crystals (rutile:3.0 eV, anatase:3.2 eV). TiO<sub>2</sub> film was formed on the Ag-implanted glass by a RF-sputter deposition at substrate temperature of 200-500°C. The thickness of formed TiO<sub>2</sub> film is about 50 nm. From the cross-sectional TEM image of the TiO<sub>2</sub> film on Ag-implanted silica glass, Ag NPs were formed at a size smaller than 10 nm embedded in the shallow surface layer of the glass. Small crystals were found in TiO<sub>2</sub> film in 20 - 40 nm size. XRD revealed the crystals to be anatase and rutile depending on substrate temperature.

Photocatalytic performance of samples was measured by using methylene-blue solution (10 ppm) under irradiation of fluorescent-lamp light, and compared with that of titania film deposited at the same condition on simple silica glass without Ag-implantation. From this test, titania film deposited on silica glass embedded with Ag NPs showed good photocatalytic performance by 3.26 times at maximum higher than that of titania film on a simple silica glass. The best conditions are 10 keV and  $5 \times 10^{15}$  ions/cm<sup>2</sup> at Ag implantation with post annealing at 700°C, and 200°C at TiO<sub>2</sub> deposition.

## Size and oxygen vacancy dependent enhanced photo-absorption from $\text{TiO}_2$ nanostructures

Vanaraj Solanki<sup>1</sup>, Subrata Majumder<sup>2</sup>, Indrani Mishra<sup>1</sup>, Shalish Ram Joshi<sup>1</sup>, Dinakar Kanjilal<sup>3</sup>, Shikha Varma<sup>1</sup>

<sup>1</sup>*Institute of Physics, Bhubaneswar, India*

<sup>2</sup>*School of Advanced Materials Science and Engineering, Sungkyunkwan University (SKKU)  
Suwon, 440746, Republic of Korea*

<sup>3</sup>*Inter University Accelerator Centre New Delhi, India*

Ion beam sputtering is a useful technique to produce self-assembled regular arrays of close-packed nanostructures on thin films or substrates, in a large scale, in a single technological step [1,2].

Room temperature sputtering experiments were performed on rutile  $\text{TiO}_2$  single crystal by utilizing  $\text{Ar}^+$  ion beam with energy of 60 keV and flux of  $1.8 \times 10^{14}$  ions/cm<sup>2</sup>.s from Electron Cyclotron Resonance (ECR) source. The morphological evolution of the  $\text{TiO}_2$  nanostructures has been observed as a function of irradiation fluence. The results show that the photo-absorption response depends, in a complex fashion, on the size of nanostructures. Contrary to the expectation, not the smallest sized nanostructures, but the smallest nanostructures conjugated with the largest oxygen vacancy states, display highest photo-absorbance. With the detailed quantitative investigation of oxygen vacancy states, it is observed that competition between the size of nanostructures and the number of vacancy states controls the photo-absorption properties [3]. The complex relationship between these factors is responsible for the anomalous absorption response, observed here, which can have extensive implications in the area of  $\text{TiO}_2$  based photocatalytic devices.

[1] F. Frost, A. Schindler and F. Bigl, Phys. Rev. Lett. 85, 4116 (2000).

[2] S. Majumder, D. Paramanik, V. Solanki, B. P. Bag, and Shikha Varma, Appl. Phys. Lett. 98, 053105 (2011).

[3] Vanaraj Solanki, Subrata Majumder, I. Mishra, P. Dash, C. Singh, D. Kanjilal and Shikha Varma, Journal of Applied Physics 115, 124306 (2014).

## The structural changes and optical properties of Al<sub>2</sub>O<sub>3</sub> after Er implantation into various crystallographic orientations

Anna Mackova<sup>1</sup>, Petr Malinsky<sup>1</sup>, Romana Miksova<sup>1</sup>, Pavla Nekvindova<sup>2</sup>, Jakub Cajzl<sup>2</sup>, Svecova Blanka<sup>2</sup>, Jiri Oswald<sup>3</sup>

<sup>1</sup>*Nuclear Physics Institute of the Academy of Sciences of the Czech Republic v. v. i., 250 68 Rez, Czech Republic*

<sup>2</sup>*Department of Inorganic Chemistry, Institute of Chemical Technology, Technicka 5, 166 28 Prague 6, Czech Republic*

<sup>3</sup>*Institute of Physics, Academy of Sciences of the Czech Republic, v.v.i., Cukrovarnicka 10, 162 53 Prague, Czech Republic*

The crystalline materials are suitable for preparation of the laser active ions doped optical layers using ion implantation. We have focused on the study of luminescence properties in the erbium implanted different crystallographic cuts of sapphire (Al<sub>2</sub>O<sub>3</sub>). Sapphire was implanted with Er ions at 190 keV with fluencies of  $1.0 \times 10^{16} \text{ cm}^{-2}$  in order to study compositional as well as structural changes occurring after the implantation. Post-implantation annealing at 1000 °C in oxygen atmosphere was also done. Chemical compositions and erbium depth concentration profiles of implanted layers were studied by Rutherford Back-Scattering spectrometry (RBS). Structural properties of the prepared layers were characterized by RBS/channelling; luminescence of the doped samples properties was measured in the region 1400 -1600 nm. Maximal erbium concentration (up to 2 at. %) was observed in 40 nm depth for various crystal cuts. Relative numbers of disordered atoms 70 – 80 % found in the prepared implanted layers were discussed from the point of view of structure of various used cuts. Erbium was found to sit randomly in interstitial positions, though no preferential sites could be denominated. Position of erbium in the host matrix was substantially influenced by the annealing procedure, when Er moved into the subsitutional positions of the crystal matrix. The highest intensity of the luminescence appeared around 1530 nm. As to suitability of particular crystallographic cuts of sapphire for the though purpose, it is clear that the most intensive luminescence was found in the <0001> crystallographic cut.

### Acknowledgements:

The research has been supported by project P108/12/G108 and realized at CANAM (Center of Accelerators and Nuclear Analytical Methods) LM 2011019. This work has been supported by the European Community as an Integrating Activity SPIRIT under EC contract no. 227012.

## **Corrosion protective coating with bi-layered si-dlc/aluminum oxide films by plasma based ion implantation and magnetron sputtering**

Tsutomu Sonoda, Setsuo Nakao, Masami Ikeyama

*National Institute of Advanced Industrial Science and Technology (AIST), Japan*

Some metallic materials such as Fe-Co alloys or Mg alloys respectively feature good magnetic properties or high specific strength, so have been expected to be applied as promising functional materials or light weight structural materials. However, their corrosion resistance is not so adequate or is so poor that the actual use of these alloys requires some surface modification for improving the corrosion resistance. On the other hand, diamond-like carbon (DLC) coatings feature excellent mechanical and chemical properties. Thus the coatings are attractive for industrial applications, especially for surface modifications of the alloys. However, stress concentrations caused at the interface between DLC coatings and metallic substrates. Therefore the coating of magnesium alloy as metallic materials with Si-DLC/aluminum oxide bi-layered films by plasma based ion implantation (PBII) following magnetron sputtering was examined, in order to improve not only the abrasion resistance and the corrosion resistance but also the adhesion of the deposited film to the metallic substrate. For the deposition of aluminium oxide interlayer onto magnesium alloy substrates (Mg-3wt.%Al-1wt.%Zn), the reactive sputtering with a planar target of aluminium oxide was carried out in a gas mixture of argon and oxygen. On the other hand, the deposition of Si-DLC layers onto the aluminium oxide interlayer was performed with our bi-polar type PBII system. Thereby Si-DLC coatings were proceeded with tetramethylsilane (TMS) gas flow and with +pulse of +2kV and -pulse of -4kV. The repetition frequency of the bi-polar pulse was set at 4kHz. Obtained bi-layered films appeared to be uniform and adhesive. The thickness of the oxide interlayer and the Si-DLC layer were respectively around 400nm and 140nm. Furthermore, according to potentiodynamic polarization experiments, it was found that the corrosion current of the coated alloy was smaller than that of the uncoated alloy by three orders of magnitude.

## Characterization of nitrogen ion implanted TiO<sub>2</sub> photocatalysts by XAFS and XPS

Tomoko Yoshida<sup>1</sup>, Satoshi Niimi<sup>2</sup>, Muneaki Yamamoto<sup>2</sup>, Satoshi Ogawa<sup>2</sup>, Toyokazu Nomoto<sup>3</sup>, Shinya Yagi<sup>1</sup>

<sup>1</sup>*EcoTopia Science Institute, Nagoya University, Japan*

<sup>2</sup>*Graduate School of Engineering, Nagoya University, Japan*

<sup>3</sup>*Aichi Synchrotron Radiation Center, Japan*

Photocatalytic reactions at the surface of titanium dioxide (TiO<sub>2</sub>) under UV light irradiation have been attracting much attention in view of their practical applications to environmental cleaning such as self cleaning of tiles, glasses, and windows. Asahi et al. reported that the substitutional doping of N into TiO<sub>2</sub> contributes to band gap narrowing to provide visible-light response [1]. Actually the doped nitrogen has been regarded as the catalytic active site generating the visible-light response in TiO<sub>2</sub>, since the optical absorbance in the visible-light region evolved with increasing nitrogen concentration. In the present study, 5 keV N<sup>+</sup> was implanted into TiO<sub>2</sub> single crystals to distribute nitrogen atoms peaking around 10 nm in depth from the surface.

N<sup>+</sup>-implanted TiO<sub>2</sub> samples promoted the photocatalytic activity for degradation of methylene blue under visible-light irradiation. N 1s XPS and N K-edge XANES spectra of the photocatalytically active sample indicated that N replaces the O sites near the surface, whereas in the inactive samples N-O species are formed. In addition, XPS spectrum of the valence band region was recorded for the photocatalytically active sample. Spectral increase due to the N<sub>2</sub>p states derived from the Ti-N bond appears in the upper part of the O<sub>2</sub>p valence band in the lower region of the gap, strongly indicating the band gap narrowing of TiO<sub>2</sub>.

We also found that the nitrogen concentration of the sample implanted with small amount of N<sup>+</sup> ( $1 \times 10^{21} \text{ m}^{-2}$ ) is a little higher than that with large amount of N<sup>+</sup> ( $3 \times 10^{21} \text{ m}^{-2}$ ). In the low energy (5 keV) N<sup>+</sup> implantation, the sputtering of the sample atoms would be one of the important processes for controlling both the concentration and chemical state of the doped nitrogen.

[1] R Asahi, T. Morikawa, T. Ohwaki, K. Aoki and Y. Taga, Science, 293, 269 (2001).

## **Stoichiometric titanium dioxide ion implantation in AISI 304 stainless steel for corrosion protection**

Alexander Hartwig, Martin Decker, Helmut Karl

*University of Augsburg, Germany*

AISI 304 stainless steel is known to show pitting corrosion when it is connected to more noble materials in chloride containing environment [1]. For a reliable corrosion resistant bond between carbon-fibre reinforced plastics (CFRP) and AISI 304 it is necessary to coat the metal surface with a galvanic barrier for corrosion protection.

In this work highly chemical inert ion beam synthesized titanium dioxide  $\text{TiO}_2$  was investigated for its applicability for corrosion protection of stainless steel. Typically,  $\text{TiO}_2$  is deposited via sol-gel or sputtering [2,3]. Associated with these deposition techniques is the appearance of porosity, cracking and delamination of the coating, which can significantly reduce the corrosion protection properties and bond strength to stainless steel and CFRP. Alternative techniques such as ion implantation could provide a way to avoid those issues inherent to deposition methods. In this work the corrosion behaviour of  $\text{TiO}_2$  synthesized by stoichiometric sequential ion implantation of elements Ti and O into AISI 304 stainless steel was investigated for different implantation and annealing parameters. The energy range of the implanted ions was 50-150 keV ( $\text{Ti}^+$ ) and 20-55 keV ( $\text{O}^+$ ), while the implanted  $\text{Ti}^+$  fluence was varied from  $5 \times 10^{15}$  to  $5 \times 10^{17}$  ions/cm<sup>2</sup>.

Electrochemical characterization methods such as potentiodynamic scans and electrochemical impedance spectroscopy (EIS) in 0.5 M NaCl electrolyte were performed. Microstructure analysis was done via atomic force microscopy (AFM), secondary ion mass spectroscopy (SIMS) and scanning electron microscopy (SEM).

[1] J-H. Wang, C. C. Su, and Z. Szklarska-Smialowska, Corrosion, 44, 10 (1988)..

[2] N. Padhy, S. Kamal et al. Surface and Coatings Techn. 204, 16-17 (2010).

[3] D.S.R. Krishna, Y. Sun and Z. Chen, Thin Solid Films 519, 15 (2011).

## The effect of aluminium on the post-anneal concentration of ion implanted bismuth in silica thin films

Rachel Southern-Holland<sup>1</sup>, Matthew Halsall<sup>1</sup>, Iain Crowe<sup>1</sup>, Russel Gwilliam<sup>2</sup>

<sup>1</sup>*University of Manchester, UK*

<sup>2</sup>*University of Surrey, UK*

Two types of silica thin films were co-implanted with aluminium and bismuth, oxide grown on an n-type silicon substrate and low-florescence silica. The films were then annealed at different times and temperatures. The photoluminescence of the samples were studied and it was found that the samples didn't exhibit the broadband NIR emission reported for bismuth centres [1, 2, 3] but some showed a narrow emission at 1160nm similar to that seen in silicon dislocation loops [4]. It was concluded that the emission had come from the silicon substrate and not the implanted layer. The samples then had Rutherford Backscattering Spectroscopy (RBS) conducted on them to ascertain the concentration of bismuth in the samples after the annealing process. The RBS data showed that the concentration of bismuth was reduced in the samples post anneal and the concentration reduced more the longer the duration and hotter the temperature of the anneal. The concentration of bismuth reduced to around zero when a high initial dose of bismuth ( $7 \times 10^{15} \text{cm}^{-2}$ ) was implanted but around 20% the original implant concentration was retained for a low initial implant dose ( $7 \times 10^{13} \text{cm}^{-2}$ ). The concentration of implanted aluminium in the samples also affected the concentration of bismuth. For a low aluminium dose ( $1.5 \times 10^{15} \text{cm}^{-2}$ ) the bismuth concentration started to reduce at lower anneal times and temperatures than those with a high dose ( $1.5 \times 10^{16} \text{cm}^{-2}$ ).

[1] Y. Miwa, H. Sun, K. Imakita, M. Fujii, Y. Teng, J. Qiu, Y. Sakka and S. Hayashi, Optics Letters 36, 4221-4223 (2011).

[2] L. Zhanga, G. Donga, J. Wub, M. Penga, and J. Qiu, Journal of Alloys and Compounds 531, 10-13 (2012).

[3] I.A. Bufetov, M.A. Melkumov, S.V. Firstov, A.V. Shubin, S.L. Semenov, V.V. Vel'miskin, A.E. Levchenko, E.G. Firstova, and E.M. Dianov, Optics Letters 36, 166-168 (2011).

[4] W.L. Ng, M.A. Lourenco, R.M. Gwilliam, S. Ledain, G. Shao and K.P. Homewood, Nature 410, 192-194 (2005).

## Radiation effects and surface modification of cryogenic solids

Elena Savchenko<sup>1</sup>, Ivan Khyzhniy<sup>1</sup>, Serge Uyutnov<sup>1</sup>, Andrew Barabashov<sup>2</sup>, Alexey Ponomaryov<sup>3</sup>, Galina Gumenchuk<sup>4</sup>, Vladimir Bondybey<sup>4</sup>

<sup>1</sup>*Institute for Low Temperature Physics & Engineering NASU, Kharkiv, Ukraine*

<sup>2</sup>*V.N. Karazin Kharkiv National University, Kharkiv, Ukraine*

<sup>3</sup>*Helmholtz Zentrum Dresden-Rossendorf, Dresden, Germany*

<sup>4</sup>*Lehrstuhl für Physikalische Chemie II TUM, Garching, Germany*

Radiation-induced processes in solids depend on specific properties of projectiles and target materials. Processing of materials based on the subthreshold excitation of solids followed by the energy localization and its conversion into kinetic energy of atoms contributes to any radiation-induced scenario.

In this work we discuss radiation effects and modification of model insulators – cryogenic materials (solidified gases) with the example of solid nitrogen. Radiation-induced ionic centers, and their role in the surface modification are the focus of research. We employed luminescence spectroscopy methods – cathodoluminescence CL, nonstationary luminescence NsL, thermally stimulated luminescence TSL in combination with current activation spectroscopy (thermally stimulated exoelectron emission TSEE) and detection of sputtering yield (Ch. 7 in [1]).

Monitoring of the CL spectra temporal evolution and concurrent measurements of optical and current relaxation emissions revealed stabilization and accumulation of radiation-induced defects – ionic centers, trapped electrons and radicals. Novel phenomenon in molecular solids was detected for the first time – sputtering of highly excited nitrogen molecules under subthreshold irradiation by slow electrons. Analysis of products of electron-ion recombination reactions using spectrally resolved TSL and NsL and the reactions routes suggests formation of  $N_4^+$  and  $N_3^+$  centers. Charge recombination reaction  $N_4^+ + e \rightarrow N_2 + N_2^+ + \Delta E \rightarrow N_2 + N_2 + h\nu + \Delta E$  is supposed to be the stimulating factor for the sputtering. Anomalous strong low temperature “post-irradiation” desorption of own lattice particles first detected in [2] is considered in the context of electron-ion recombination reactions.

[1] M. A. Allodi, R. A. Baragiola, G. A. Baratta et al, Space Sci. Rev. 180, 101 (2013).

[2] E.V. Savchenko, I.V. Khyzhniy, S.A. Uyutnov, A.N. Ponomaryov, G.B. Gumenchuk and V.E. Bondybey, Low Temp. Phys. 39, 446 (2013).



## Effect of plasma-treatment on the metallization of porous low-k dielectrics

Johan Meersschaet, Yiting Sun, Sylvia Armini, Patrick Verdonck, Wilfried Vandervorst

*Imec, Leuven, Belgium*

For future microelectronic applications, low-k materials with an effective dielectric constant of  $k \sim 2$  are required as inter-level insulator. The low-k films consist of a porous material with relatively large open pores. A key issue for the integration of porous films is their susceptibility to material penetration during metallization processes, e.g. by atomic layer deposition. Plasma-treatment is recognized as a potential route to reduce the material penetration during metallization.

We investigate the precursor pore penetration during ALD TiN on porous low-k films ( $k \approx 2.0$ ). Prior to the deposition, the low-k films are modified using a plasma treatment. Here, we use a  $H_2/Ar$  plasma through which the surface is modified with limited impact on the bulk of the low-k layer. More specifically, after plasma treatment the surface is more hydrophilic due to the presence of  $-OH$  groups as evidenced by contact angle measurements and FTIR measurements. Further, the treatment enhances the affinity to bind self-assembled monolayers (SAMs) from (3-aminopropyl)-trimethoxysilane precursor to the surface. Finally, the presence of SAMs at the surface is shown to dramatically affect the tendency of precursor pore penetration during metallization.

The effect of the surface treatment will be illustrated by comparing the penetration after metallization of the pristine low-k, the SAMs-treated low-k without plasma treatment, and the SAMs-treated low-k with plasma treatment. The quantification of the elemental profile for low-k/metal stacks is done through Rutherford backscattering spectrometry (RBS). It is shown that the combined preparation of the low-k using plasma-treatment as well as the application of a self-assembled monolayer are instrumental to effectively seal the pores and to achieve a surface-confined deposition of the metal.

## **Magneto-optical effects of ultrathin materials under low-energy ion irradiation**

Chiung-Wu Su

*National Chiayi University, Taiwan, R.O.C.*

Transformation of magnetic properties of nano cobalt films on a ZnO crystal plate was studied by direct-current ion sputtering of N<sup>+</sup> under ultrahigh vacuum. The magnetic properties of the formed nanoscale nitride material can be precisely controlled using low-energy ions and tuning the vacuum pressure. We designed an ultrahigh vacuum magneto-optic Faraday effect system to monitor the magnetic hysteresis loops in the transformation process. Magneto-optical information in the Faraday effect carries more about surface and interface properties of the material. The ferromagnetic to paramagnetic phase during ion beam irradiation is the characteristic of cobalt nitride. Ions bombardment energy between 0.3-2 keV exhibits different levels on the implantation of the ultrathin materials and on the sputtering of cobalt from the surface. This technique can be used for an application of determining surface magnetic anisotropy due to the ions always interacting first with the top layers. These reacting ions may also solve the existence of perpendicular anisotropy debate on the initial in-plane anisotropy of the grown cobalt films on ZnO(0001).

## Modification of mechanical and magnetic properties of intermetallic compounds by energetic ion bombardment

Akihiro Iwase<sup>1</sup>, Hiroaki Yoshizaki<sup>1</sup>, Akihiro Hashimoto<sup>1</sup>, Yasuyuki Kaneno<sup>1</sup>, Satoshi Semboshi<sup>2</sup>, Hiroshi Kojima<sup>1</sup>, Fuminobu Hori<sup>1</sup>, Yuichi Saitoh<sup>3</sup>, Yoshihiro Okamoto<sup>3</sup>, Tetsuya Koide<sup>1</sup>, Toshiyuki Matsui<sup>4</sup>

<sup>1</sup>*Department of Materials Science, Osaka Prefecture University, Japan*

<sup>2</sup>*Kansai Center, Tohoku University, Japan*

<sup>3</sup>*Japan Atomic Energy Agency, Japan*

<sup>4</sup>*Research organization of the 21st Century, Osaka Prefecture University, Japan*

In this presentation, we will show the effect of energetic ion bombardment on the transformation of lattice structures and mechanical and magnetic properties for FeRh, Ni<sub>3</sub>V and Ni<sub>3</sub>Al binary intermetallic compounds and dual-phase Ni<sub>3</sub>Al-Ni<sub>3</sub>V intermetallic compound.

Bulk specimens of these intermetallic compounds were irradiated with 5-16 MeV heavy ions at room temperature. After the irradiation, the lattice structures of the specimens were investigated by using an x-ray diffraction measurement, an extended x-ray absorption fine structure (EXAFS) at a synchrotron radiation facility, and a transmission electron microscope. The change in surface hardness by the irradiation was measured by means of Vickers microhardness tester. The change in magnetic property was investigated by using a SQUID magnetometer, and MCP and XMCD measurements at a synchrotron radiation facility.

The experiments show that the disordered fcc (A1) phase appears even at room temperature in Ni<sub>3</sub>Al, Ni<sub>3</sub>V and dual-phase Ni<sub>3</sub>Al-Ni<sub>3</sub>V specimens by the ion irradiation. The A1 phase is the high temperature phase in the equilibrium phase diagram of Ni<sub>3</sub>V, but the A1 phase does not exist in the phase diagram of Ni<sub>3</sub>Al. For FeRh, the ion irradiation induces not only the A1 phase but also the L10 phase which does not exist in the phase diagram of FeRh.

The irradiation-induced phase transformations accompany the changes in hardness and magnetic property. For Ni<sub>3</sub>V, Ni<sub>3</sub>Al and dual-phase Ni<sub>3</sub>Al-Ni<sub>3</sub>V, the hardness decreases monotonically with increasing the ion-fluence. The magnetization for FeRh increases by the irradiation and then decreases for higher ion fluences. The result of the present study indicates that the energetic ion bombardment can be used as a useful tool for the modification of mechanical and magnetic properties of intermetallic compounds. In the conference, recoveries of the irradiation-induced lattice structures and physical properties by the thermal treatments will also be discussed.

## The effects of interfacial interactions between Fe-O and Fe-Si induced by ion-beam bombardment on the magnetic properties of Si-oxide/Fe bilayers

Ko-Wei Lin<sup>1</sup>, Johan Van Lierop<sup>2</sup>, Nikolay Galkin<sup>3</sup>, Hsin-Te Liang<sup>1</sup>, Yaro Wrocznskyj<sup>2</sup>

<sup>1</sup>*National Chung Hsing University, Taiwan, R.O.C.*

<sup>2</sup>*University of Manitoba, Canada*

<sup>3</sup>*FEB RAS, Russia*

In this study, we investigated the magnetic properties of a Fe layer coupled to different capping layers (Si and Si-oxide) in order to understand the effects on the magnetism from the formation of Fe-oxides and Fe-silicides due to intermixing at interfaces through energetic oxygen ion-beam bombardment. Si-oxide (10 nm)/Fe (20 nm) bilayers were prepared using a dual ion-beam sputtering deposition technique [1]. Transmission electron microscopy has shown that in a Si/Fe bilayer, the bottom Fe layer was bcc iron (grain sizes ranging from 5-10 nm) and the top Si layer was amorphous Si. The formation of a FeSi layer (~ 4 nm thick) due to intermixing at the interface between Fe and Si was observed in cross-sectional TEM images. By contrast, a Si-oxide/Fe bilayer made with 41% O<sub>2</sub>/Ar, the interfacial layer consisted of both Fe-oxide and Fe-silicide which formed on the Fe surface by chemical reaction of the oxygen ion-beam (from the End-Hall source) and Si atoms (from the Si target), respectively. The formation of this interfacial layer is ascribed to the negative enthalpy of formation of FeSi and Fe<sub>3</sub>O<sub>4</sub>. The temperature dependence of hysteresis loops indicated that no significant changes (constant coercivity, H<sub>c</sub> ~ 15 Oe) from the intermixing were present, except at 10 K where the largest H<sub>c</sub> (~ 60 Oe) was observed for the Si-oxide (8%O<sub>2</sub>/Ar)/Fe bilayer. As the enhanced coercivities occurred only at 10 K in these Si-oxide (8, 21, and 41%O<sub>2</sub>/Ar)/Fe bilayers, this indicated the presence of Fe-oxide (due to oxygen ion-beam bombardment) and was in agreement with structural and compositional characterization. From the above characterization, we ascribe the interfacial layer of a harder ferrimagnetic Fe<sub>3</sub>O<sub>4</sub> phase as the origin of the enhanced coercivities in the Si-oxide/Fe bilayers.

Research was supported by NSC of Taiwan, FEB RAS of Russia, and NSERC of Canada.

[1] K.-W. Lin, T.-C. Lan, C. Shueh, E. Skoropata, and J. van Lierop, J. Appl. Phys. 115, 17D717 (2014).

## Ion beam synthesis of the complete family of III-V:Mn ferromagnetic semiconductors

Shengqiang Zhou

*Helmholtz-Zentrum Dresden-Rossendorf, Institute of Ion Beam Physics and Materials Research, Germany*

Ferromagnetic semiconductors have been under intensive investigation during the last decade. The prototype ferromagnetic semiconductor GaMnAs has revealed a variety of unique features induced by the combination of its magnetic and semiconducting properties. To prepare ferromagnetic semiconductors, one needs to dope the host with up to 5-10% Mn, which is far beyond the solid solubility of Mn in III-V compounds. As a non-equilibrium process, ion implantation can introduce enough dopants as required. However, the activation of dopants remains challenging due to the clustering of implanted ions during post-annealing. Short-time annealing in the millisecond or nanosecond regime allows the epitaxial growth from a liquid phase. The mature development and commercialization of ion implantation promise the versatility. The approach combining ion implantation and pulsed laser melting allows us to prepare ferromagnetic semiconductors covering the full spectrum of III-V compound semiconductors. We have successfully synthesized ferromagnetic Mn doped III-V from InAs and GaAs to InP and GaP with different bandgaps. The results of magnetization, magnetic anisotropy, resistivity, anomalous Hall effect, magnetoresistance and x-ray magnetic circular dichroism obtained from the synthesized samples confirm the intrinsic origin and the carrier-mediated nature of the ferromagnetism. Moreover, in different III-V hosts we observe distinct differences regarding the magnetic anisotropy and conduction mechanism which are related with the intrinsic parameters such as the lattice mismatch, energy gap and the acceptor level of Mn. These results could allow for a panorama understanding of III-V:Mn ferromagnetic semiconductors.

- [1] D. Bürger, S. Zhou, et al. PRB 81, 115202 (2010).
- [2] S. Zhou, et al. APL 96, 202105 (2010).
- [3] S. Zhou, et al. APEX 5, 093007 (2012).
- [4] M. Khalid et al. PRB 89, 121301(R) (2014).
- [5] Y. Yuan, et al. IEEE Trans. Magn., in press (2014).

## **Ferromagnetic InMnAs with perpendicular magnetic anisotropy synthesized by ion implantation**

Ye Yuan<sup>1</sup>, Yutian Wang<sup>1</sup>, Muhammad Khalid<sup>1</sup>, Eugen Weschke<sup>2</sup>, Wolfgang Skorupa<sup>1</sup>,  
Manfred Helm<sup>1</sup>, Shengqiang Zhou<sup>1</sup>

<sup>1</sup>*Institute of Ion Beam Physics and Materials Research, Helmholtz-Zentrum  
Dresden-Rossendorf, P. O. Box 510119, Dresden 01314, Germany*

<sup>2</sup>*Helmholtz-Zentrum Berlin für Materialien und Energie, Wilhelm-Conrad-Röntgen-Campus  
BESSY II, D-12489 Berlin, Germany*

Due to the great potential application in spintronic device, III-Mn-V dilute magnetic semiconductors (DMS) have drawn significant attention during the past two decades. Although of the model member GaMnAs (mostly be prepared by low-temperature molecule beam epitaxy: LTMBE) have been comprehensively investigated, the challenge for preparing other DMS such as InMnAs still exists. Therefore, the understanding about the full family III-Mn-V DMS is far from satisfaction. Ferromagnetic DMS GaMnAs and GaMnP were firstly obtained alternatively by Mn ion implantation and pulsed laser annealing [1, 2], a method rather than LTMBE. The Mn concentration and depth distribution can be controlled through implanting fluence and implanting energy, respectively. When annealing under pulsed laser, due to high temperature gratitude, the large regrowth velocity could trap Mn atoms into the substitutional sites, which is quite effective to obtain high quality layer with less defects which can act as double donors and be harmful to ferromagnetism.

We prepared ferromagnetic InMnAs with different Mn concentrations by ion implantation and pulsed laser annealing. The formation of an epitaxial InMnAs on InAs substrates was proved by Rutherford Backscatting/channeling and X-ray diffraction. The Curie temperature could be as high as around 75 K when the Mn concentration is around 8%. The out-of-plane direction is the easy axis, originating from the compressive strain along the perpendicular direction, as expected from the case of GaMnAs [3, 4]. The perpendicular anisotropy is particularly useful for exploiting spintronics functionalities, such as current induced magnetization switching.

[1] M. A. Scarpulla et al. Phys. Rev. Lett. , 95, 207204 (2005).

[2] M. A. Scarpulla et al. Appl. Phys. Lett., 82, 1251 (2003).

[3] Shengqiang Zhou et al. APEX, 5, 093007 (2012).

[4] K. W. Edmonds et al. Phys. Rev. Lett., 96, 117207 (2006).

## Probing the antiferromagnetic bulk in exchange bias systems using 9 keV He ions

Henning Huckfeldt<sup>1</sup>, Arno Ehresmann<sup>2</sup>, Ali C. Basaran<sup>3</sup>, Thomas Saerbeck<sup>4</sup>, Jose De La Venta<sup>5</sup>, Ivan K. Schuller<sup>4</sup>

<sup>1</sup>*Institute of Physics, University of Kassel, Germany*

<sup>2</sup>*Institute of Physics and Center for Interdisciplinary Nanostructure Science and Technology (CINSA-T), University of Kassel, Germany*

<sup>3</sup>*Materials Science and Engineering, Department of Physics and Center for Advanced Nanoscience, University of California San Diego, USA*

<sup>4</sup>*Department of Physics and Center for Advanced Nanoscience, University of California San Diego, USA*

<sup>5</sup>*Department of Physics, Colorado State University, USA*

The Exchange Bias effect in thin magnetic films consisting of adjacent layers of a ferromagnetic and an antiferromagnetic material manifests as a shift of the hysteresis loop with respect to the external field. Almost all theoretical descriptions of the exchange bias effect are based on the interaction between the ferro- and antiferromagnetic material at the interface while the bulk of the antiferromagnet is neglected.

We present a series of experiments highlighting the influence of the antiferromagnetic bulk on exchange bias in a Ni/FeF<sub>2</sub> bilayer system deposited by electron beam evaporation. By light ion bombardment with 9 keV He<sup>+</sup> ions [1] and changing penetration depths into the material system due to different thicknesses of a gold stopping layer structural defects were created influencing the exchange bias effect [2]. The results were confirmed by numerical simulations of the ion range and damage. Quantitative magnetic and structural characterizations were performed probing the effects of ion bombardment. It is shown that the antiferromagnetic bulk can not be neglected for a quantitative description of the exchange bias effect.

[1] D. Lengemann, D. Engel, A. Ehresmann, Rev. Sci. Instrum. 83, 053303 (2012).

[2] A. Ehresmann, D. Engel, T. Weis, A. Schindler, D. Junk, J. Schmalhorst, V. Höink, M. D. Sacher, G. Reiss, Phys. Stat. Sol. B 243, 29 (2006).

### Paramagnetism in neutron irradiated graphite

Shengqiang Zhou<sup>1</sup>, Yutian Wang<sup>1</sup>, Catherine A Jenkins<sup>2</sup>, Elke Arenholz<sup>2</sup>, Gregor Bukalis<sup>3</sup>,  
Wolfgang Skorupa<sup>1</sup>, Manfred Helm<sup>1</sup>

<sup>1</sup>*Helmholtz-Zentrum Dresden-Rossendorf Institute of Ion Beam Physics and Materials  
Research, (HZDR), P.O.Box 510119, 01314 Dresden, Germany*

<sup>2</sup>*Advanced Light Source, Lawrence Berkeley National Laboratory, Berkeley, California 94720,  
USA*

<sup>3</sup>*Helmholtz-Zentrum Berlin für Materialien und Energie, Wilhelm-Conrad-Röntgen-Campus  
BESSY II, Albert-Einstein-Straße 15, D-12489 Berlin, Germany*

Defect induced magnetism in carbon based materials has many attractive perspectives in understanding of magnetism as well as in future spintronic applications. Although the mechanism of ferromagnetism in carbon-based materials is still an open question, more and more experiments show some common features: First, paramagnetism can be largely enhanced by introducing defects. Second, ferromagnetism only appears under certain defect concentration. Third, defects induced or disturbed electron states play an important role in generating local moments and in establishing the ferromagnetic coupling. In the past, most of researchers have been using ions implantation to introduce defects in graphite or graphene. This technology usually generates defect in the near-surface region and it is hard to effectively increase the total number of defect in the whole matrix. Consequently, the weakness of the magnetic signal confuses the interpretation of the source of the observed ferromagnetism. To obtain more reliable information, it is necessary to enhance the total number of defect states and to keep defect concentration constant when the ferromagnetism appears. In this contribution neutron irradiation is used to introduce defect in the bulk sample in graphite, which will allow for obtaining large magnetic signal.

The magnetic properties were investigated by SQUID-VSM. The paramagnetism increases with neutron fluence. However, the enhanced ferromagnetism is not observed in all irradiated samples. Compared with other report the pronounced difference in X-ray absorption spectroscopy is the absence of new peaks in the Carbon pre-edge region. This indicates the absence of unoccupied states near the Fermi level. We can conclude that neutron irradiation induces more defects so that the paramagnetism is enhanced. However, those defects could not form enough unoccupied states near the Fermi level so that the Stoner instability is not satisfied to generate ferromagnetic coupling.



## Irradiation induced modifications in magnetic behaviour of CoFe/Si interfacial structures

P.C. Srivastava, Arvind Kumar

<sup>1</sup>*Banaras Hindu University, Varanasi (U.P.) India-221005*

Ion irradiation has been successfully used as a tool for interfacial modifications for magnetic behaviour of FM/SC interfaces. In this report, we have studied the swift heavy ion irradiation effect on magnetic behaviour of CoFe/Si interfacial structures, both on p- and n-type Si Substrates.

Interfacial structures of CoFe/Si (on both p- and n-type Si substrates) have been successfully realized by electron beam evaporation technique. The realized structures have been irradiated by 100 MeV  $\text{Ni}^{+7}$  ions for fluences of  $1 \times 10^{11}$  to  $5 \times 10^{13}$ . The structures have been characterized from XRD, AFM/MFM, M-H characteristics and magneto-electronic transport across the structures. AFM results reveal that grain size and rms surface roughness increases with ion fluence for p- and n-Si structures. Magnetization characteristics show that the magnetization has increased significantly by two orders of magnitude with increase of ion fluence for p-Si structures whereas n-Si structures show the increase only for lower fluence of irradiation. The increase of magnetization on the irradiation has been understood due to the formation of various magnetic silicide phases. The XRD data has confirmed the formation of various magnetic silicide phases. It is known that ion irradiation accelerates the interfacial intermixing which may result the formation of various silicide phases. n-Si substrates are known [1] to be more reactive than p-Si substrates which shall damage the substrate at higher fluence for the formation of crystalline phases of silicides.

I-V-H data has shown a magnetic field sensitivity for p-Si structures and not for n-Si structures. From this data, a ~20% MR has been observed for CoFe/p-Si interfacial structure. In conclusion, it has been found that the irradiation induced modifications is significant and favourable for p-Si structures (and not for n-Si structures) for its applications in magneto-electronics.

[1] B. J. Garrison and W. A. Goddard, Phys Rev B 36, 9805 (1987).

## Swift heavy ion (SHI) induced structural and magnetic properties modification in Fe-based amorphous alloys

Sun Jianrong<sup>1</sup>, Wang Zhiguang<sup>1</sup>, Zhu Yabin<sup>1</sup>, Wang Yuyu<sup>1</sup>, Pang Lilong<sup>1</sup>, Li Fashen<sup>2</sup>

<sup>1</sup>*Institute of Modern Physics, Chinese Academy of Sciences, , Lanzhou 730000 P.R. China*

<sup>2</sup>*Key Laboratory for Magnetism and Magnetic Materials of the Ministry of Education, Lanzhou University, Lanzhou 730000, P.R. China*

Amorphous alloy (also known as metallic glass) is a kind of new alloy material synthesized by using modern rapid solidification metallurgical technology, owning excellent mechanical, physical and chemical properties that general metal and glass have. The unique glassy structure makes metallic glass have some high performances such as high strength, corrosion resistance, great ductility, and having a wide supercooled liquid region, etc. which usually belong to the high-quality magnetic functional materials, and hence showing enormous potential for development and application in the fusion reactor [1-3]. In this work, SHI irradiation as a kind of special non-equilibrium and exogenous energy deposition process will be applied to the study on modification of the structural and magnetic properties of the amorphous alloys.

Amorphous FeSiNbZrB alloy ribbons were prepared by melt spinning, and then the amorphous ribbons were irradiated at RT with 2.01 GeV Kr<sup>26+</sup> ions for fluence range from  $1 \times 10^{11}$  to  $1 \times 10^{14}$  ions/cm<sup>2</sup> on the materials research terminal of the HIRFL-SSC (IMP, Lanzhou). X-ray diffraction (XRD), transmission electron microscopy (TEM), vibrating sample magnetometer (VSM), superconducting quantum interference device (SQUID) and mössbauer spectra (MS) were used to measure the structural and magnetic properties of the pristine and irradiated samples.

It's obviously that before and after SHI irradiation, such amorphous FeSiNbZrB alloy systems do not have a long-range order in atomic arrangement and exhibit only a short-range order. Under SHI irradiation at RT, local crystallization phenomenon of amorphous FeSiNbZrB alloy ribbons has been confirmed and formation of finer  $\alpha$ -Fe(Si) phases precipitations with diameter of 1-2 nm has been observed. In addition, after irradiation, magnetic anisotropy considerably changes from its original in-plane direction. Possible mechanism of structural and magnetic properties modification after SHI irradiation is discussed briefly.

## Structural and magnetic characterization of expanded austenite layers on austenitic stainless steel

Orhan Ozturk, Ozgun Karatas, Refika Dal, Mehmet Fidan

*Izmir Institute of Technology, Turkey*

Although they have excellent corrosion resistance, austenitic stainless steels are rather soft materials. Surface hardening of these steels without loss of the corrosion resistance is well realized through surface modification by nitrogen ion beams at moderate substrate temperatures near 400 °C. Nitrogen containing phase formed at 400 °C in the ion beam treated layers is usually called expanded austenite phase,  $\gamma\text{N}$ , due to its structural similarity to the underlying fcc  $\gamma$  phase of austenitic stainless steel. Large and anisotropic lattice expansions, high residual stresses, grain-dependent N contents and diffusion rates are a few unusual characteristics of the  $\gamma\text{N}$  phase. An additional property of this phase is related to its magnetic structure: a paramagnetic to ferromagnetic transition with large amount of nitrogen insertion and associated lattice expansion.

The focus of this research is to investigate the magnetic properties of the expanded phase formed on austenitic stainless steel (316 SS) by nitrogen ion implantation. The N-ion beam processing conditions included the following: beam energy of 0.7 keV, beam current density of 2.0 mA/cm<sup>2</sup>, substrate temperature of 400 °C, and implantation time ranging from 30 minutes to 4 hrs. Implanted layer phases and composition of the near surface region were measured by X-ray diffraction (XRD) and glow discharge optical emission spectroscopy (GDOES). The magnetic structure of the implanted surfaces was studied by magnetic force microscopy (MFM) and a vibrating sample magnetometer (VSM). Based on the XRD data, the expanded phase,  $\gamma\text{N}$ , was the only N-containing phase observed for all processing times. According to the VSM and MFM data, ferromagnetism in the  $\gamma\text{N}$  layers is revealed by the observation of the hysteresis loops and stripe domain patterns. The MFM images show domain size variations and varying magnetic properties from one grain to another.

**Ion-induced coercivity enhancement in BiFeO<sub>3</sub>**

Hiwa Modarresi<sup>1</sup>, Enric Menéndez Dalmáu<sup>1</sup>, Marlies K. Van Bael<sup>2</sup>, Margriet J. Van Bael<sup>3</sup>, Kristiaan Temst<sup>1</sup>, André Vantomme<sup>1</sup>, Vera Lazenka<sup>1</sup>, Nikolina Pavlovic<sup>2</sup>, Manisha Bisht<sup>1</sup>, Michael Lorenz<sup>4</sup>, Marius Grundmann<sup>4</sup>, An Hardy<sup>2</sup>

<sup>1</sup>*Instituut voor Kern- en Stralingsfysica (IKS), KU Leuven, Belgium*

<sup>2</sup>*Institute for Materials Research, Inorganic and Physical Chemistry, Hasselt University, Agoralaan - Building D, B-3590 Diepenbeek, Belgium*

<sup>3</sup>*Laboratorium voor Vaste-stoffysica en Magnetisme, KU Leuven, Belgium*

<sup>4</sup>*Institut für Experimentelle Physik II, Universität Leipzig, Linnéstraße 5, D-04103 Leipzig, Germany*

In thin films with thickness below a few hundred nanometers, BiFeO<sub>3</sub> exhibits weak ferromagnetism due to the suppression of its spin spiral structure. BiFeO<sub>3</sub> is also well-known to be an intrinsic room temperature (RT) multiferroic material showing coupled antiferromagnetic and ferroelectric properties. We have demonstrated that the ferromagnetic response of polycrystalline single-phase BiFeO<sub>3</sub> films of approximately 300 nm can be significantly enhanced by Co ion implantation and subsequent annealing procedure. This has been achieved by ion modification of the BiFeO<sub>3</sub> film in which Co-ions in a fluence of  $1 \times 10^{16}$  ions/cm<sup>2</sup> have been implanted inside the host matrix. By choosing an acceleration energy of 60 keV, Co-implanted ions are placed around 30 nm deep under the film surface that allows for further close-to-surface complementary studies. Co-ion modification of BiFeO<sub>3</sub> has led the RT hysteresis loops to exhibit a coercivity of around 100 Oe, while, the low-temperature loops show coercivities in excess of 17 kOe. The fascinating coercivity enhancement, is explained by the formation of cobalt ferrite phase which grows coherently within the BiFeO<sub>3</sub> crystal structure. Cobalt ferrite is known to have strong temperature dependent magnetic properties. Whereas at RT the cobalt ferrite formations are largely superparamagnetic and to a much lesser extent ferromagnetic, they become almost fully single-domain ferromagnetic at low temperature. In this study, we have introduced strong ferromagnetism inside the otherwise weak ferromagnetic BiFeO<sub>3</sub> film which allows for further magnetoelectric coupling studies of the system.

## Efficient corrosion protection of TiAl (turbine blades) and CuZn (organ pipes) alloys by plasma based ion implantation

Bernadeta Pelic, Rossen Yankov, Wolfgang Skorupa

*Helmholtz-Zentrum Dresden-Rossendorf (HZDR), Germany*

Experiments have been undertaken to explore the improvement of the high temperature oxidation and aqueous corrosion of Ti-Al and Cu-Zn, respectively, by applying Plasma based ion implantation (PBII).

The atmospheric corrosion of the tongues within the reed pipes which consist of a Cu-20Zn alloy (namely brass) is strongly enhanced by traces of acid vapors (from wooden parts and glue) and also the alloy's instability caused by dezincification. A significant improvement in corrosion resistance has been achieved by applying a 30 nm aluminum oxide film using pulsed laser deposition (PLD) and implanting nitrogen ions into the near surface and the interface regions. In the case of  $\gamma$ -TiAl alloys which exhibit poor oxidation resistance, despite their good mechanical properties at elevated temperatures, this limits their replacement of the nowadays used heavy components made of Ni-alloys. A significant improvement in high temperature oxidation resistance of TiAl alloys (up to 900 °C) has been achieved by implanting fluorine ions ( $10^{17} \text{ cm}^{-2}$ ) at 30 keV into the alloy's subsurface using PBII process. A TiAl alloy modified in this way has been shown to acquire a stable, adherent and highly protective alumina scale ( $\text{Al}_2\text{O}_3$ ) under high temperature oxidation in air. The influence of the implanted  $\text{N}^+$  into CuZn and  $\text{F}^+$  into TiAl samples on the corrosion process has been investigated. For the sample evaluation, different characterization methods including scanning electron microscope with energy dispersive X-ray spectroscopy (SEM / EDX), Auger electron spectroscopy (AES), Rutherford backscattering spectroscopy (RBS), elastic recoil detection analysis (ERDA), and Dektak stylus profiling have been applied to determine the chemical composition, the elemental depth profiles, roughness and defect formation of the samples before and after exposure.

**Modification of surface hardness of Al-Mg-Si alloy by using the combination of energetic ion bombardment and thermal aging**

Daichi Ueyama<sup>1</sup>, Takahito Ohmura<sup>2</sup>, Yuichi Saitoh<sup>3</sup>, Kenji Nishida<sup>4</sup>, Satoshi Semboshi<sup>5</sup>,  
Norito Ishikawa<sup>3</sup>, Fuminobu Hori<sup>1</sup>, Akihiro Iwase<sup>1</sup>

<sup>1</sup>*Osaka Prefecture University, Japan*

<sup>2</sup>*National Institute for Materials Science, Japan*

<sup>3</sup>*Japan Atomic Energy Agency, Japan*

<sup>4</sup>*Central Research Institute of Electric Power Industry, Japan*

<sup>5</sup>*Tohoku University, Japan*

It is well known that the diffusion of supersaturated solute atoms in metals is enhanced under the irradiation. This phenomenon is called the irradiation enhanced diffusion, which causes the precipitation of solute atoms at relatively low temperatures. So far we have irradiated Al-Mg-Si alloy with several kinds of MeV ions at room temperature. After the irradiations, we have observed Si and Mg nano-scaled clusters by means of 3D atom probe tomography. We have found that the ion irradiation induced nano-clusters can harden Al-Mg-Si alloy. In the present study, we have developed the hardening process of the alloy by using the combination of MeV ion irradiation and thermal aging. We have also performed the irradiation with 200 MeV heavy ions, and examined the ion energy dependence of the hardening process. As the effect of ion irradiation on the hardness is localized near the surface, we used the nano-indenter as well as the micro Vickers hardness tester to investigate more precisely the irradiation-induced surface hardening. We performed the thermal aging at 180°C on Al-Mg-Si alloys, which were previously irradiated by energetic ion beam. We found that the hardness of Al-Mg-Si alloy irradiated with ion beam and subsequently thermal-aged was much larger than that of the specimens which were either only irradiated with ion beam or only thermal-aged. The present result indicates that the combination of energetic heavy ion irradiation and the thermal aging is an effective method for the control of the surface hardness of Al-Mg-Si alloy. We also irradiated Al-Mg-Si alloy with 200 MeV Xe ions. The range of 200 MeV Xe ion is about 20  $\mu\text{m}$ . This value is about 7 times larger than that of MeV heavy ions. The energy deposition by 200 MeV Xe ions near the surface is dominated not by the elastic collisions, which is the case of MeV ion irradiation, but by the electronic excitations. In the conference, we will also discuss the ion energy dependence of the hardening of Al-Mg-Si alloy.

## Swift heavy ion irradiation induced interactions in the UMo/X/Al trilayer system (X= Ti, Zr, Nb and Mo)

Hsin-Yin Chiang<sup>1</sup>, Sohyun Park<sup>2</sup>, Mayer Matej<sup>3</sup>, Klaus Schmid<sup>3</sup>, Matrin Balden<sup>3</sup>, Winfried Petry<sup>1</sup>

<sup>1</sup>*Forschungs-Neutronenquelle Heinz Maier-Leibnitz, Technische Universität München, Germany*

<sup>2</sup>*Sektion Kristallographie, Ludwig-Maximilians-Universität München, Theresienstr.41, 80333, München, Germany*

<sup>3</sup>*Max-Planck-Institut für Plasmaphysik, Boltzmannstr.2, 85748 Garching, Germany*

The high density fuel uranium-molybdenum (UMo) alloy embedded in an Al matrix (UMo/Al) is considered as a promising candidate in fuel conversion of research reactors. In this study a modified system with a diffusion barrier, UMo/X/Al trilayer (X = Ti, Zr, Nb, and Mo), was investigated in order to suppress interdiffusion between UMo and the Al matrix. The trilayer was tested by swift heavy ion irradiation, followed by Rutherford backscattering spectroscopy (RBS) and micron X-ray microdiffraction ( $\mu$ -XRD). Atomic mixing at interfaces was resolved by RBS, indicating that Ti interacts strongly with UMo while Zr does with Al.  $\mu$ -XRD revealed the formation of intermetallic AlX compounds which might detain further intermixing. However, Ti and Zr as diffusion barrier can be controversial because their presence might reduce the stability of  $\gamma$ -UMo. The impact of the irradiation-induced phases on the properties of the UMo/X/Al trilayer along with the effectiveness of diffusion barriers will be evaluated.

**Study on mass ablation of metals by intense pulsed ion beam irradiation**

Jie Zhang, Xiao Yu, Haowen Zhong, Binbin Wei, Miao Qu, Jie Shen, Yanyan Zhang, Xiaofu Zhang, Gaolong Zhang, [Xiaoyun Le](#)

*Beihang University, P.R. China*

Ablation effect plays an important role in the process of material modification by intense pulsed ion beam (IPIB). As a direct observable during the process of IPIB irradiation of target, the ablation mass is a crucial physical quantity for understanding the interaction between IPIB and target material and the mechanism of ablation. In the present work, we used IPIB provided by BIPPAB-450 accelerator to bombard Zn, Al, Cu, Pb and W targets. The ablation threshold of different metals material were obtained through analyzing of ablation mass under different energy density. Moreover, correlations between experimental data and incident beam parameters were investigated. The results are helpful to understand the influence of beam parameter on the ablation mass and ablation process.



## Superconducting proximity effect of ion-beam synthesized epitaxial Al/Pb nanocomposites

H. Wang<sup>1</sup>, T. Picot<sup>2</sup>, L. Fernandez Ballester<sup>3</sup>, W. Bras<sup>3</sup>, M.J. Van Bael<sup>2</sup>, A. Vantomme<sup>1</sup>, K. Temst<sup>1</sup>, K. Houben<sup>2</sup>, T. Moorkens<sup>2</sup>, J. Cuppens<sup>2</sup>, J. Grigg<sup>4</sup>, C. Van Haesendonck<sup>2</sup>, E. Biermans<sup>5</sup>, S. Bals<sup>5</sup>, K. Kvashnina<sup>3</sup>

<sup>1</sup>*Instituut voor Kern- en Stralingsfysica, KU Leuven, 3001 Leuven, Belgium*

<sup>2</sup>*Laboratorium voor Vaste-Stoffysica en Magnetisme, KU Leuven, 3001 Leuven, Belgium*

<sup>3</sup>*DUBBLE@ESRF, Grenoble, France*

<sup>4</sup>*The MacDiarmid Institute for Advanced Materials and Nanotechnology, Dept. of Physics and Astronomy, University of Canterbury, 8140, Christchurch, New Zealand*

<sup>5</sup>*EMAT, Dept. Fysica, Universiteit Antwerpen, 2020 Antwerp, Belgium*

High fluence ion implantation and subsequent annealing was used to synthesize epitaxial Pb nanoparticles (NPs) in Si(100) wafers and in single crystalline Al films. The Pb NPs size (5-20 nm) and size distribution were tuned by varying the implantation and annealing parameters [1]. The size, crystal structure, epitaxial orientation and strain of the NPs were investigated by Rutherford backscattering and channeling spectrometry, x-ray diffraction and small angle scattering, and transmission electron microscopy. The scaling behaviors of the average particle radius with the implantation parameters allowed to distinguish different growth regimes upon increasing fluence or increasing annealing duration.

We studied the superconducting properties of Pb NPs in an Al matrix as this forms an interesting heterogeneous mixture of two superconductors with different critical parameters. The heterogeneous Al/Pb nanocomposites display a single superconducting transition, with the critical temperature  $T_c$  increasing with the Pb/Al volume ratio [2]. The experimental  $T_c$  dependence on the Pb/Al volume ratio is compared with theoretical models of the superconducting proximity effect based on the bulk properties of Al and Pb. A very good correspondence with the strong-coupling proximity effect model was found, with an electron-phonon coupling constant in the Pb nanoparticles slightly reduced compared to bulk Pb. Our result differs from other studies on Pb nanoparticle based proximity systems where weak-coupling models were found to better describe the  $T_c$  dependence. We infer that the high interface quality resulting from the ion implantation synthesis method is a determining factor for the superconducting properties. Critical field and critical current measurements support the high quality of the nanocomposite superconducting films.

[1] H. Wang et al. J. Phys. D – Appl. Phys. 45, 035301 (2012).

[2] H. Wang et al. Supercond. Sci. Technol. 27, 015008 (2014).

## Comparison of irradiated and hydrogen implanted German RPV steels using PAS technique

Stanislav Pecko, Vladimír Slugeň, Stanislav Sojak, Tomáš Brodziansky

*Institute of Nuclear and Physical Engineering, Slovak University of Technology, Ilkovičova 3,  
81219 Bratislava, Slovakia*

Radiation degradation of nuclear materials can be experimentally simulated via ion implantation. In our case, German reactor pressure vessel (RPV) steels were studied by positron annihilation lifetime spectroscopy (PALS). This unique non-destructive method can be effectively applied for the evaluation of microstructural changes and for the analysis of degradation of reactor steels due to neutron irradiation and proton implantation. Studied specimens of German reactor pressure vessel steels are originally from CARINA/CARISMA program. Eight specimens were measured in as-received state and two specimens were irradiated by neutrons in German experimental reactor VAK (Versuchsatomkraftwerk Kahl) in the 1980s. One of the specimens which was also in as-received and neutron irradiated condition was also used for simulation of neutron damage by hydrogen nuclei implantation. Defects with the size of about 1-2 vacancies with relatively small contribution (with intensity on the level of 20-40 %) were observed in “as-received” steels. A significant increase in the size of the induced defects due to neutron damage was observed at a level of 2-3 vacancies in the irradiated specimens. The size and intensity of defects reached a similar level as in the specimens irradiated in nuclear reactor due to hydrogen ions implantation with energy of 100 keV (up to the depth <500 nm).

**UV-induced graft polymerization of acrylic acid in the nanochannels of oxidized PET track-etched membrane**

Ilya Korolkov<sup>1</sup>, Anastassiya Mashentseva<sup>2</sup>, Olgun Güven<sup>3</sup>, Abzal Taltenov<sup>1</sup>

<sup>1</sup>*The L.N.Gumilyov Eurasian National University, Astana, Kazakhstan*

<sup>2</sup>*Institute of Nuclear Physics, Astana, Kazakhstan*

<sup>3</sup>*Department of Chemistry, Hacettepe University, Ankara, Turkey*

Poly(ethylene terephthalate) due to its chemical stability, mechanical strength and thermal stability has found a number of applications in the form of functionalized of track-etched membranes (TeMs). Functionalization of nanochannels of PET TeMs was achieved [1] by grafting of various monomers with different functionalities using chemical, photochemical, radiation or plasma-induced initiation techniques.

In this work acrylic acid monomer was photografted inside the nanochannels of PET TeMs after oxidation process. Among advanced oxidation processes we had chosen ( $H_2O_2$ /UV) system to introduce the maximum concentration of carboxylic acid groups [2]. Benzophenone photo-initiator was first immobilized on the surfaces of nanochannels which are late filled with aq. acrylic acid solution. UV-irradiation from both sides of PET TeMs has led to the formation of grafted PAA chains inside the nanopores. The surface oxidized and AA grafted PET TeMs were characterized by UV-vis, ATR-FTIR, XPS spectroscopies as well as by measuring contact angles and surface physical properties by AFM and SEM.

[1] M. Barsbay, O. Güven, Rad Phys Chem, dx.doi.org/10.1016/j.radphyschem.2014.05.018.

[2] I. Korolkov, A. Mashentseva, O. Güven et al. Polym Degrad Stab, 10.1016/j.polymdegradstab.2014.05.008.

**Preparation of a new anion exchanger by pre-irradiation grafting technique and its adsorptive removal of rhenium**

Jianhua Zu, Ruiqin Liu

*Shanghai Jiao Tong University, P.R. China*

A new anion exchanger with pyridine groups was prepared by grafting of 2-vinyl pyridine (2-VP) onto polypropylene (PP) nonwoven fabrics by pre-irradiation grafting technique using an electron accelerator, and thereafter quaternization of pyridine rings in grafted chains by reaction with bromoethane. The experimental results have shown that the grafting yield increases with the increase of monomer concentrations and longer quaternization time gaining higher conversion ratio. The grafted and quaternized nonwoven fabrics were characterized by FT-IR and DSC. The possibility of adsorption of perrhenate ( $\text{ReO}_4^-$ ), a nonradioactive analogous to pertechnetate ( $^{99}\text{TcO}_4^-$ ), from aqueous solution by anion exchanger was investigated. The results of batch experiments performed at pH 0.1-6, have shown that pH=2.2 was the optimal acidity for  $\text{ReO}_4^-$  adsorption, and the adsorption equilibrium was achieved within 30min. The reaction enthalpy was -12.55kJ/mol, which pointed out that the adsorption process is an exothermic reaction. XPS tests indicated that the nature of  $\text{ReO}_4^-$  uptake was a typical ion exchange between  $\text{Cl}^-$  on anion exchanger and  $\text{ReO}_4^-$ .

**Amino acids multilayer depth profiling with ToF-SIMS and XPS**

Laurent Nittler, Céline Noël, Laurent Houssiau, Jean-Jacques Pireaux

*UNamur - PMR – LISE, Belgium*

Amino acids, being the building blocks of proteins, are the main components of cells. Only a few works exist on their characterization by ToF-SIMS [1-3] and even less by XPS [1,4]. Their response to novel organic depth profiling methods using ultralow energy or cluster ion beams could lead to a complete 3D chemical mapping of biological cells.

In a previous work, it has been shown that under certain beam conditions amino acids model samples can be successfully depth profiled by ToF-SIMS using low energy  $\text{Cs}^+$  ions. The samples consisted in multilayer amino-acid films, which were deposited by successive thermal evaporations of phenylalanine and tyrosine molecules in ultra-high vacuum. Although both amino acids differ only by a hydroxyl group, their characteristic fragments could be differentiated throughout the whole depth profile, with a 5 nm depth resolution.

The current work aims at further studying multilayer amino acids films under ion bombardment in ToF SIMS and XPS. We show that using  $\text{Cs}^+$  ions and  $\text{Ar}_n^+$  cluster beam the multilayer can be depth profiled in ToF-SIMS and XPS, respectively. Results obtained in different analysis conditions are compared to get complementary information on the sputtering yields and chemical structure modification during profiling of amino acids.

[1] R.J. Colton, J.S. Murday et al., Surf. Sci. 84, 235–248 (1979).

[2] N. Wehbe, T. Tabarrant et al., Surf. Interface Anal. 45, 178–180 (2013).

[3] J. Brison, N. Mine et al., Int. J. Mass Spectrom. 321-322, 1–7 (2012).

[4] Y. Zubavichus, M. Zharnikov et al., J. Phys. Chem. A. 108, 4557–4565 (2004).

## **Dosimetry in radiobiological studies with heavy ion beam of the Warsaw cyclotron**

Urszula Kaźmierczak<sup>1</sup>, Dariusz Banaś<sup>2</sup>, Anna Lankoff<sup>3</sup>, Halina Lisowska<sup>3</sup>, Aneta Malinowska<sup>4</sup>, Tomasz Stępkowski<sup>5</sup>, Zygmunt Szepliński<sup>1</sup>, Maria Wojewódzka<sup>5</sup>, Janusz Braziewicz<sup>2</sup>, Joanna Czub<sup>2</sup>, Marian Jaskóła<sup>4</sup>, Andrzej Korman<sup>4</sup>, Marcin Kruszewski<sup>5</sup>

<sup>1</sup>*Heavy Ion Laboratory, University of Warsaw, Warsaw, Poland*

<sup>2</sup>*Institute of Physics, Jan Kochanowski University, Kielce, Poland*

<sup>3</sup>*Institute of Biology, Jan Kochanowski University, Kielce, Poland*

<sup>4</sup>*National Centre for Nuclear Research, Otwock, Poland*

<sup>5</sup>*Institute of Nuclear Chemistry and Technology, Warszawa, Poland*

An experimental set-up with a horizontal heavy ion beam designed for radiobiological research at the Heavy Ion Laboratory (HIL) was used. The aim of this study was to verify the dosimetry in the investigations with <sup>12</sup>C ion beam irradiation of the biological materials at the HIL.

Independent Si-detector systems were used for beam diagnosis and monitoring. One of the detectors was used to measure the particle flux at the position of the cell container and the second on-line detector was applied to monitor particle flux by the intensity of the scattered particles [1].

In order to accurately determine the homogeneity of the irradiation the PM-355 Solid-State Nuclear Track Detectors (SSNTDs) were mounted outside of the beam exit window and irradiated with doses from range 0.05 - 1 Gy. After the irradiation samples were etched and the number of ion tracks was counted using an optical microscope.

In addition, the homogeneity and the number of ions hitting the cell container were verified experimentally by biological γ-H2AX assay. Recent studies have suggested that visualization of γ-H2AX foci can be used to estimate exposure to very low doses of ionizing radiation. Moreover, the yield of foci induced by ionizing radiation increases linearly with the radiation dose. CHO-K1 cells were irradiated with different doses of <sup>12</sup>C ions, incubated and processed for γ-H2AX foci counting. The number of ion traces in individual cells was counted under confocal microscope.

The number of <sup>12</sup>C ions hitting the cell nucleus, calculated on the base of Si-detectors was compared with the number of ions counted on SSNTD-detector and with the number of ion traces detected in CHO-K1 cells by the γ-H2AX assay. The results of these experiments will be discussed.

[1] J. Czub et al., Radiat. Prot. Dosim. 122, 207 (2006).

**SiO<sub>x</sub> / a-C:H / TiO<sub>2</sub> film synthesis on heat-cured PMMA via plasma process for application in prosthodontics**

Dheerawan Boonyawan<sup>1</sup>, Pongrawee Phanbunplook<sup>1</sup>, Theeravat Bunfong<sup>1</sup>, Passakorn Saikrueng<sup>1</sup>, Sakon Sansongsiri<sup>1</sup>, Piriya Yavirach<sup>2</sup>, Saweat Intarasiri<sup>3</sup>

<sup>1</sup>*Plasma and Beam Physics Research Facility, Faculty of Science, Chiang Mai University, Chiang Mai 50200, Thailand*

<sup>2</sup>*Department of Prosthodontics, Faculty of Dentistry, Chiang Mai University, Chiang Mai 50200, Thailand*

<sup>3</sup>*Science and Technology Research Institute, Chiang Mai University, Chiang Mai 50200, Thailand*

Polymethyl methacrylate, PMMA has its own favorable properties such as elastic modulus, biocompatible, good dimensional and chemical stability for metal-free prosthodontics. Particular plasma process was chosen to apply in prosthodontics purposes.

First research proposes silicon film deposition to heat-cured PMMA by using a non-thermal atmospheric plasma jet. Hexamethyldisiloxane (HMDSO) was used as a precursor with argon (Ar) as carrier gas. The result revealed that hydrophobic surface of PMMA can be obtained at 2%HMDSO/Ar mixed gas with 50 W RF power. Surface roughness increases from 133.23 to 422.58 nm within 1-min treatment time. Most of the SiO<sub>x</sub> film are formed by methyl group Si-(CH<sub>3</sub>)<sub>3</sub> and Si-(CH<sub>3</sub>)<sub>x</sub> in HMDSO plasma. Nevertheless, silicon and oxygen percentage are increased during the processing period.

Second, hydrogenated amorphous carbon (a-C:H) film deposition was performed by above system. Acetylene (C<sub>2</sub>H<sub>2</sub>) and argon were utilized as carbon radical source with flow rate 10 sccm and 2.5 slm, respectively, at 50 W RF power. Results from FTIR and XPS affirms the film formation structure compose of sp<sup>2</sup> component over sp<sup>3</sup>. Most of the a-C:H film found strongly adhered to the heat-cured PMMA.

And third, titanium dioxide (TiO<sub>2</sub>) film synthesis by using a filtered cathodic vacuum arc deposition (FCVAD) was carried out. Source of titanium operated at DC-pulse 240 V with arc current 297 A. DC bias between -10 to -50 V was applied to PMMA substrate in oxygen (O<sub>2</sub>) atmosphere for 90 min. As-deposited TiO<sub>2</sub> film was found mostly in amorphous phase. UV irradiation revealed that oxygen vacancies are formed. TiO<sub>2</sub> amorphous film is likely attached to heat-cured PMMA in cohesive and adhesive mixed mode.

**The influence of ion fluence on the development of micropatterns produced in PET foils by proton beam writing**

Cláudia Telles Souza<sup>1</sup>, Elis Moura Stori<sup>1</sup>, Livio Amaral<sup>1</sup>, Ricardo Meurer Papaléo<sup>2</sup>, Johnny Ferraz Dias<sup>1</sup>

<sup>1</sup>*UFRGS, Brasil*

<sup>2</sup>*PUCRS, Brasil*

Proton beam writing is a new direct-write micromachining technique capable of producing 3-D, high aspect ratio microstructures with straight and smooth sidewalls in different materials. In this work we investigated in detail the influence of ion fluence on the development of micropatterns produced by 2.2 MeV H<sup>+</sup> impinging on 12 μm thick PET foils. The microprobe station consists of an Oxford Microbeams® system operating in triplet mode. During the experiments, lines of 1 x 100 μm were patterned on the PET foils with H<sup>+</sup> fluences varying from 1 x 10<sup>11</sup> to 6 x 10<sup>15</sup> ions/cm<sup>2</sup>. After the irradiation, the foils were etched using 6M solution of sodium hydroxide at 60°C during periods of time varying from 0.5 to 60 minutes. Imaging of the etched patterns was performed using scanning electron microscopy (SEM). The curve of the opening times of the microstructured lines as a function of fluence presented an “u-shape”. For fluences between 6x10<sup>14</sup> and 5x10<sup>15</sup> H<sup>+</sup>/cm<sup>2</sup>, the full opening of the lines is produced within 2 minutes of etching, independent of the exact value of fluence. For fluences , below 1x10<sup>14</sup> H<sup>+</sup>/cm<sup>2</sup>, the etching times necessary to completely open the structures increase steeply, reaching values close to 60min. In this fluence range, the lines are also rough and irregular. For very large fluences, the opening times also increase, most probably due to crosslinking of the irradiated polymer. We also observe that at large fluences (~6x10<sup>15</sup> H<sup>+</sup>/cm<sup>2</sup>) the reproducibility was poor, and opening times could vary substantially from line to line. While at low fluences, the removal of the bombarded regions proceeds continuously upon etching, while at large fluences the exposed polymer areas may remain roughly intact after several minutes of etching until they were detached from the foils as a whole block. The variability in the linking points between the exposed block and the rest of the polymer matrix may explain the variations observed in the opening times at high fluences.



**Doping gold ion into living cells with a low energy focused ion-beam increases proliferation activity**

Tatsuhiro Nomaguchi<sup>1</sup>, Naoya Sawamura<sup>1</sup>, Takahiro Shinada<sup>2</sup>, Takashi Tani<sup>1</sup>, Toru Asahi<sup>1</sup>

<sup>1</sup>*Faculty of Science and Engineering, Waseda University, Tokyo, Japan*

<sup>2</sup>*National Institute of Advanced Industrial Science and Technology (AIST), Japan*

Nowadays, the importance of investigating the effect of introduction of heavy-metal to living cells has been increasing since people are frequently being exposed to conditions in which heavy-metals may be introduced into their body. However, the conventional biological techniques for introducing heavy-metal into living cells are not suitable to investigate the effect, because they require the use of mediating substances such as solvents and it is not possible to introduce heavy-metals in a pure state.

Here, we suggest a novel heavy-metal implantation method for living cells using focused ion-beam (FIB). Heavy-ion microbeam has been commonly used in biological fields to induce genetic mutations. Thus far, no studies have reported the implantation of heavy-ion species into living cells with FIB. We decided to apply low acceleration voltage to enable beam ions to remain inside cells, instead of penetrating and causing DNA damage [1].

We performed gold ion ( $\text{Au}^{2+}$ ) doping into living cells by using the FIB implantation method; then intracellular level of adenosine triphosphate (ATP) molecule, which is the energy storing molecule for organisms, was evaluated. The ATP level of the implanted cells was found to be 50% higher than that of the non-implanted control cells. In addition, the implanted cells had a higher proliferation rate than the control cells, which implies that gold ion implantation promotes the energy generating processes.

Our results suggest that the viability of live cells can be modulated by accurately controlling the dopant atom numbers. Our ion implantation technique may be considered as a more accurate tool to quantitatively elucidate the dose-dependent effects of dopants than the conventional methods.

[1] T. Shinada et al., *Biotechnol. Bioeng.* 108, 222 (2011).

**Ion track symmetric and asymmetric nanopores as a universal platform for biomimetic systems and biosensors**

Pavel Apel<sup>1</sup>, Irina Blonskaya<sup>1</sup>, Oleg Orellovitch<sup>1</sup>, Sergei Dmitriev<sup>1</sup>, Bozena Sartowska<sup>2</sup>

<sup>1</sup>*Joint Institute for Nuclear Research, Russia*

<sup>2</sup>*Institute of Nuclear Chemistry and Technology, Poland*

Nanopores in polymer foils and inorganic materials have attracted tremendous interest due to their application as biomimetic systems and as biosensors. A well-known method for the production of uniform pores in dielectrics is particle track etching. Considerable research activity has been focused on the nanometer-sized ion track pores in polymers in recent years. The technique of production of single ion tracks in thin films has become a milestone in advanced studies of intriguing properties of artificial small pores. Conical ion track nanopores have been developed to approach the geometric characteristics of the ion channels. It has been demonstrated that the conical nanopores in polymers such as polyethyleneterephthalate and polyimide are cation selective and possess diode-like voltage-current characteristics. In this report we present several fabrication methods which allow production of ion track nanopore membranes with different pore configurations. Apart from conventional cylinder geometry, symmetrical cigar-shaped pores can be produced as well as various asymmetrical structures with conical pores and pores having funnel-like or bullet-like profile of tip. The factors that were exploited to create a certain pore geometry are (a) atomic number of bombarding ion; (b) etchant composition; (c) one-sided or two-sided etching; (d) application of electric field; (e) exposure to ultraviolet radiation prior to etching. Conductometric measurements during chemical etching combined with FESEM observation allows one to accurately characterize the nanopore geometry. Single- and many-pore membranes were fabricated and investigated. Ion transport properties of the nanopores in electrolyte solutions strongly depend on their geometry. Various examples of ion track nanopores will be presented in light of their potential applications.

### **PDMS compaction by heavy ions**

Istvan Rajta<sup>1</sup>, Szabolcs Szilasi<sup>1,2</sup>, Gyula Nagy<sup>1</sup>, Attila T.T. Szabo<sup>1</sup>, Vladimir Havranek<sup>3</sup>, Vaclav Vosecek<sup>3</sup>, Vasily Lavtentiev<sup>3</sup>

<sup>1</sup>*MTA Atomki, Hungary*

<sup>2</sup>*University of North Texas, TX, USA;*

<sup>3</sup>*Nuclear Physics Institute AV CR, Řež near Prague, 250 68, Czech Republic*

As a continuation of our previous study [1], we have performed irradiations of poly(dimethylsiloxane) (PDMS) samples by focused beam of MeV heavy ions. The irradiations took place at INP ASCR at Řež on the ion microbeam line at the 3MV Tandetron accelerator. The accelerator provided carbon and nitrogen beams, in order to be able to focus them by the Oxford-type nuclear microprobe we chose the C<sup>4+</sup> and N<sup>4+</sup> charge states. This way the beam focus was about 1 μm and the scan size was 1 mm. To achieve different degrees of compaction, each structure was irradiated with a few different fluences.

After the irradiations we investigated the changes of the surface topography, the degree of compaction/shrinkage and its relation to the irradiation fluence and the structure spacing in PDMS. At the irradiated areas the surface topography, the adhesion, the wettability and the rigidity of the surface also changed due to the chemical/structural change of the basic polymer. The surface topography was characterized by atomic force microscopy (AFM).

[1] S.Z. Szilasi, et al. Applied Surface Science 257, 4612 (2011).

## **Irradiation effects of MeV Kr-ions on structural and optical properties of nc-Si:H films**

Yabin Zhu, Zhiguang Wang, Cunfeng Yao, Jianrong Sun

*Institute of Modern Physics, Chinese Academy of Sciences, P.R. China*

As a two-phase mixed material, hydrogenated nano-crystalline silicon film (nc-Si:H) consists of nanoscale silicon crystallites embedded in an amorphous matrix. Researches about irradiation effects on structural and optical properties of nc-Si:H film not only possess the fundamental interest but also the potential application prospects, since the photoelectric properties of nc-Si:H film have great effects on the performance of electronic devices which fabricated by nc-Si:H film, such as solar cells or transistors. In this work, nc-Si:H films were irradiated by 2.0, 3.0 and 4.0 MeV Kr-ions, and were investigated by means of X-ray diffraction (XRD), Raman scattering and UV-Vis-NIR spectroscopies. XRD and Raman results show that the crystalline fraction and crystallite size of the samples decrease with increasing the ion fluence. This gives that the Kr-ion irradiation results in the amorphization of crystallites in nc-Si:H films. Moreover, the crystallographic orientations of nanoscale crystallites have no obvious effects on the amorphization rate. The structural damages become more obvious as the nuclear energy loss of incident ions increases. Thus, a conclusion can be drawn that the observed irradiation effects on microstructure of nc-Si:H films should be mainly attributed to the nuclear collisions. The UV-Vis transmittance spectra results show that the absorption coefficient increases significantly with increasing the fluence at a wavelength range of 400–700 nm. Since the absorption coefficient of amorphous phase is much higher than that of crystalline phase, the irradiation induced amorphization enhances the light absorption of the samples and leads to the decrease of optical band-gap.

## Hydrogen interstitial in H-ion implanted ZnO bulk single crystals: Evaluation by elastic recoil detection analysis and electron paramagnetic resonance

Takuya Kaida<sup>1</sup>, Kazuma Kamioka<sup>1</sup>, Tomoaki Nishimura<sup>1</sup>, Kazuo Kuriyama<sup>1</sup>, Kazumasa  
Kushida<sup>2</sup>, Atsushi Kinomura<sup>3</sup>

<sup>1</sup>*Hosei University, Japan*

<sup>2</sup>*Osaka Kyouiku University, Japan*

<sup>3</sup>*National Institute of Advanced Science and Technology, Japan*

Our recent study [1] reported that the resistivity in H-implanted ZnO bulk single crystals (peak concentration :  $1.45 \times 10^{20} \text{ cm}^{-3}$ ) is about three orders of magnitude lower than that of un-implanted ones, suggesting the presence of the H interstitial as a shallow donor. In this study, the O interstitial was also observed by Nuclear reaction analyses. In the present study, we evaluated H-implanted ZnO bulk single crystals (500 keV using a dose of  $5 \times 10^{15} / \text{cm}^2$ ) by the elastic recoil detection analysis (ERDA) using a 2.0 MeV  $4\text{He}^+$  beam. H can be detected up to 200 nm in depth. In as-implanted samples, H was observed in a range from the surface to 200 nm, indicating that the forward diffusion was caused under the implantation process. The forward diffusion of H was enhanced by 400 °C annealing for 1hr. In the as-implanted samples, a signal with  $g = 1.996$  was observed by electron paramagnetic resonance (EPR) measurements at 77 K. This signal was assigned to the oxygen vacancy (VO) of + charge state [2], which disappeared after illumination with a red LED and appeared after successive illumination with a blue LED as well as VO in the electron-irradiated ZnO [3]. However, the EPR signal for VO was not observed in 400 °C-annealed samples, indicating that the displacement of O atoms was recovered after 400 °C annealing. A peak at  $3337 \text{ cm}^{-1}$  was observed by Fourier transform infrared spectroscopy measurements at room temperature in as-implanted samples, which was assigned to the stretch mode of O-H complexes in ZnO [3]. Therefore, the O-H complexes are the origin of low resistivity in H-implanted ZnO rather than the Vo-H ones.

[1] T. Kaida, K. Kamioka, T. Ida, K. Kuriyama, K. Kushida and A. Kinomura, Nucl. Instr. Meth. Phys Res. B (accepted for publication).

[2] K. Kuriyama, K. Matumoto, Y. Suzuki, K. Kushida and Q. Xu, Solid State Commun. 149, 1347 (2009).

[3] M. D. McCluskey, S. J. Jokela, K. K. Zhuravlev, P. J. Simpson and K. G. Lynn, Appl. Phys. Lett. 81, 3807 (2002).

## Modifying the reaction of thin Ni films with Si by light ion irradiation

Koen Van Stiphout<sup>1</sup>, André Vantomme<sup>1</sup>, Kristiaan Temst<sup>1</sup>, Jelle Demeulemeester<sup>2</sup>,  
Christophe Detavernier<sup>3</sup>

<sup>1</sup> *Instituut voor Kern- en Stralingsfysica, KU Leuven, Belgium*

<sup>2</sup> *IMEC, Belgium*

<sup>3</sup> *Cocoon, UGent, Belgium*

The solid phase reaction of thin (100-10 nm) nickel films deposited on Si has been studied extensively over the last few decades [1]. This reaction starts with the formation of metal-rich phases around 250C, after which the film is converted to NiSi around 350C. Around 800C, the final phase, NiSi<sub>2</sub>, nucleates. Several ways of modifying this reaction have previously been investigated[2-4].

This work focuses on how this reaction is altered when light elements (C,N,O) are implanted into the as-deposited Ni layer, by means of in situ X-ray diffraction (XRD) and Rutherford backscattering and channeling spectrometry (RBS/C). Depending on the implantation energy (25-60 keV), the solid phase reaction is modified in several ways. After implantation at low energy, the metal-rich phases appear at lower temperature, and grow sequentially. After implantation at 40 keV, no metal-rich phases are observed during annealing: either the grains of these are too small, textured, or NiSi is the first phase to form. Additionally, the texture of the NiSi film is different than for unimplanted samples. At the highest energy of implantation, an early onset of NiSi<sub>2</sub> is observed (almost 300C below the thermodynamically expected temperature) during annealing.

The irradiation significantly alters the reaction, likely to due to the crystalline damage and the intermixing of elements caused by implantation. Damage in the Ni layer and Si substrate might increase the diffusion of Ni (and thereby, the kinetics of the reaction), whereas intermixing of Ni and Si at the interface would alter the thermodynamic drive of the reaction[5].

[1] C. Lavoie et al., Microelectronic Engineering 70, 144–157 (2003).

[2] J. Demeulemeester et al., Appl. Phys. Lett. 93, 261912 (2008).

[3] P. Turcotte-Tremblay et al., J. Vac. Sci. Technol. B 31, 051213 (2013).

[4] C. Van Bockstael et al., J. Appl. Phys. 106, 064515 (2009).

[5] R. Pretorius et al., Crit. Rev. Solid State Mater. Sci. 24, 1 (1999).

## **Formation of definite GaN p-n junction by Mg-ion implantation to n--GaN epitaxial layers grown on a high-quality free-standing GaN substrate**

Takuya Oikawa, Yusuke Saijo, Shigeki Kato, Tomoyoshi Mishima, Tohru Nakamura

*Department of Electronics and Electrical Engineering, Hosei University, Tokyo, Japan.*

A selective area doping technology, which is frequently used in processing Si and SiC devices, is required for making high performance GaN devices. Usually, ion implantation is used as a method of the selective area doping but formation of the p-type conductive layer by ion implantation has been difficult for GaN. In previous works, Mg ion implantation into GaN layers grown on Sapphire and SiC substrates were examined [1]. Those GaN layers included large misfit-dislocation density. Such layers have been largely deteriorated optically and electrically by the high temperature annealing for activating the implanted Mg.

The purpose of this paper is p-type conversion of Mg-ion implanted n--GaN layers and formation of device-quality p-n junction as a result, which have been realized by using epitaxial layers grown on a high quality free-standing GaN substrate.

Mg ions were implanted into the GaN layers at two different energies of 30 keV and 60 keV at a dose of  $3.5 \times 10^{13} \text{ cm}^{-2}$  and  $6.5 \times 10^{13} \text{ cm}^{-2}$ . After implanting Mg, samples were capped with SiN layer and annealed at 1230°C for 1min in N<sub>2</sub> gas ambient.

These samples showed low-temperature PL spectra quite similar to those observed from Mg-doped MOVPE-grown p-type GaN, consisting of strong Mg related donor–acceptor pair (DAP) and acceptor bound exciton (ABE) emission. Diodes fabricated by the Mg-ion implantation showed clear rectifying I-V characteristics with turn-on voltage close to bandgap energy (E<sub>g</sub>) of GaN and UV and blue-green electroluminescence was observed at forward biased conditions for the first time. These are definite evidences for the formation of the GaN p-n junction.

These results indicate the p-type conversion was possible using high quality GaN layers grown on free-standing GaN substrates, which can lead new device structures and processing for the GaN devices.

[1] E.V.Kalinina, et al. published in HITEN 99, "Third European Conference on High Temperature Electronics".

**Characterization of crystal structure features of a SIMOX substrate.**

Kseniia Eidelman<sup>1</sup>, Kirill Shcherbachev<sup>2</sup>, Natalia Tabachkova<sup>3</sup>, Dmitriy Podgornii<sup>4</sup>, Dmitriy Pazhin<sup>5</sup>, Vladimir Mordkovich<sup>6</sup>

SIMOX (separation by implanted oxygen) technology is one of the methods to produce SiO<sub>2</sub>-based "silicon-on-insulator" (SOI) wafers, which aims at improving the reliability of the chips and improving their frequency characteristics.

The SIMOX commercial sample (Ibis corp.) was investigated by a high-resolution X-ray diffraction (HRXRD), a high-resolution transmission electron microscopy (HRTEM) and an Auger electron spectroscopy (AES) to determine its actual parameters (the thicknesses of the top Si and a continuous buried oxide layer (BOX) layers, the crystalline quality of the top Si layer). According to the specification, the implantation of oxygen ions with a dose of  $2 \times 10^{18} \text{ cm}^{-2}$  and an energy of 160 keV was performed into the Si(001) at the temperature of 600 °C. The high temperature of the target is necessary to preserve the perfection of the crystal structure of the top Si layer. Then, high-temperature annealing is carried out for 6h at a temperature close to the melting point of Si, followed by slow cooling to form the BOX layer, and annealing of radiation-induced defects in the top Si layer. Under used implantation conditions, the thickness of the top Si and BOX layers were 200 nm and 400 nm correspondingly. XRD intensity distribution near Si(004) reciprocal lattice point was investigated. According to the oscillation period of the diffraction reflection curve defined thickness of the otop silicon layer ( $216 \pm 2$ ) nm. HRTEM determined the thickness of the oxide layer (360 nm) and revealed the presence of Si islands with a thickness of 30-40 nm and a length from 30 to 100 nm in the BOX layer nearby "BOX-Si substrate" interface. The Si islands are faceted by (111) and (001) faces. No defects were revealed in these islands. The signal from Si, which corresponds to the particles in an amorphous BOX matrix, was revealed by AES in the depth profiles. Amount of Si single crystal phase at the depth where the particles are deposited, is about 10-20 %.



## Room temperature photoluminescence from GaAsN dilute nitride using nitrogen-implantation and flash lamp annealing

Kun Gao, Slawomir Prucnal, Wolfgang Skorupa, Manfred Helm, [Shengqiang Zhou](#)

*Helmholtz-Zentrum Dresden-Rossendorf (HZDR), Institute of Ion Beam Physics and Materials Research, Germany*

Nitrogen atoms are isoelectronic substituents for arsenic in GaAs. A small amount of nitrogen doping can lead to a pronounced bandgap reduction. Therefore nitrogen-doping can be applied as a powerful technique to modify GaAs based materials for long wavelength optoelectronic devices.

In this contribution we present the fabrication of dilute nitride material GaAsN by nitrogen-implantation and flash lamp annealing (FLA). N was implanted into the GaAs wafers with atomic concentration of about  $x_{\text{imp1}}=0.38\%$  and  $x_{\text{imp2}}=0.76\%$ . According to the redshift of the near band-edge emission from GaAsN, up to 80% and 44% of the implanted N atoms can be successfully incorporated into the lattice by FLA for  $x_{\text{imp1}}=0.38\%$  and  $x_{\text{imp2}}=0.76\%$ , respectively. According to our investigation, ion-implantation followed by ultrashort flash lamp treatment, which is chip technology compatible and allows for large scale production, exhibits a promising prospect on bandgap engineering of GaAs based semiconductors.

## Physics and technology of an energy filter for tailoring depth profiles in semiconductor doping applications

Michael Rueb<sup>1</sup>, Constantin Csato<sup>1</sup>, Florian Krippendorff<sup>1</sup>, Johannes Von Borany<sup>2</sup>

<sup>1</sup>*University of Applied Sciences Jena, Germany*

<sup>2</sup>*Helmholtz-Zentrum Dresden-Rossendorf e.V., Germany*

Doping of SiC during epitaxial deposition of the active device layer still is a technological challenge. Statistical variations of the doping concentration may be as high as +/- 25% [1]. Ion implantation has the potential of shifting doping accuracy below the +/-5% range. However, particularly in the case of doping areas with  $\mu\text{m}$  vertical dimensions the very small diffusivities of dopants in SiC would require a large number of successive implants with small kinetic energy increments and low ion doses. This results quickly in technically and economically unpleasant situations. We have investigated the physics and technology of a so called energy filter [1,2] which is capable of producing a pre-defined, tailored vertical implantation (concentration) profile from a single monoenergetic ion beam. The filter in its simplest form consists of a thin silicon membrane with etched triangular microstructures on top of it. The triangular structures define the path length of traversing ions and such the kinetic energy of the transmitted ions. Due to scattering the lateral inhomogeneity in energy distribution of the transmitted beam is a strong function of substrate to filter distance.

We will present our findings on physical effects of ions traversing a thin slab of matter such as scattering, its impact on lateral doping homogeneity, sputtering effects and thermal effects. Factors that determine the final concentration profile such as design and different stopping power to energy relations by choosing different filter materials will be discussed. Experimental data on filtered depth profiles of e.g. 7MeV B in silicon and 12MeV N into SiC and a method for analyzing lateral ion distributions will be presented. Some aspects of the filter's micro-manufacturing will also be included.

[1] F. Krippendorff et al. Proceedings MikroSystemTechnik Kongress. Aachen: VDE Verlag, 662-665 (2013).

[2] Bartko, Schlegel, EP000000014516B1, Priority: 04.01.1980.

## Dependence of implantation sequence on surface blistering characteristics due to H and He ions co-implanted in silicon

J.H. Liang<sup>1,2</sup>, H.Y. Hsieh<sup>2</sup>, C.W. Wu<sup>2</sup>, C.M. Lin<sup>3</sup>

<sup>1</sup>*Institute of Nuclear Engineering and Science, National Tsing Hua University, Hsinchu 300, Taiwan, ROC*

<sup>2</sup>*Department of Engineering and System Science, National Tsing Hua University, Hsinchu 300, Taiwan, ROC*

<sup>3</sup>*Department of Applied Science, National Hsinchu University of Education, Hsinchu 300, Taiwan, ROC*

Recently, silicon-on-insulator (SOI) technology has gained growing interest due to its superior advantages such as low leakage current, high isolation, and low parasitic capacitance for modern electronic devices. Among many proposed techniques, the innovative smart-cut (or ion-cut) technique together with the use of H or He ions is believed to be one of the most desirable to fabricate SOI. Hence, an in-depth understanding of the roles of H and He ions in forming surface blisters is highly demanded prior to its industrial applications and thus constitutes the central objective of the present study. In this study, H and He ions were co-implanted into silicon wafers at room temperature and at energy levels of 40 and 50 keV, respectively, in order to have similar depth profiles. The total implantation fluence was  $5 \times 10^{16} \text{ cm}^{-2}$  with various apportionment ratios for He and H ions. The implantation sequences were He+H and H+He. The surface blistering characteristics were probed using dynamic optical microscopy (DOM), Raman scattering spectroscopy (RSS), cross-sectional transmission electron microscopy (XTEM), secondary ion mass spectrometry (SIMS), and atomic force microscopy (AFM). The results revealed that the threshold temperatures of forming blisters and craters in He+H specimens are lower than those in H+He ones. The former has a higher percentage of exfoliation area than the latter. In addition, the existence of He ions lowers the critical H fluence needed for forming blisters with diameter greater than 2 microns when compared to implantation of H ions alone. Furthermore, under the same total implantation fluence, a higher fluence of H ions is beneficial for SOI fabrication.

## **Supersaturated Sn implantation into Ge by ion implantation: towards a group IV direct bandgap semiconductor**

Tuan Tran, Jim Williams, Jennifer Wong-Leung

*Department of Electronic Materials Engineering, Research School of Physics and Engineering, Australian National University, Australia*

Supersaturation of Sn in Ge is predicted to lead to an indirect-to-direct bandgap transition at Sn concentration of 6 to 10%. However, the equilibrium solubility of Sn in Ge is around 1% at ambient temperature. As a result of this limitation, attempts at achieving Sn supersaturation of Ge by non-equilibrium techniques, such as molecular beam epitaxy [1,2] and ion implantation with pulse laser melting [3], have only been partially successful and no direct bandgap material has been demonstrated to date. The best quality sample without Sn precipitation has around 6.5% Sn concentration [1].

In this study various Sn implants (variable energy and doses) have been carried out into n-type Ge, followed by rapid thermal annealing to epitaxially recrystallise the as-implanted amorphous layer. Sn concentrations of up to 5% can be achieved; optimised RTA can lead to substantial Sn supersaturation and good crystal quality of Ge. Rutherford backscattering spectrometry/channelling (RBS-C) has been used to measure the degree of substitutionality and the Sn depth distribution, and transmission electron microscopy (TEM) to monitor crystal quality. RBS-C shows that, for non-optimised RTA, Sn segregation can occur at the surface for the highest Sn concentration ( $\approx 6\%$ ). For short time/high temperature RTA, such Sn segregation can be suppressed with good quality epitaxial growth of Ge. These results are promising for strained Ge-Sn layers and possible direct bandgap behaviour at higher Sn concentrations.

[1] Y. Shimura et al. Thin Solid Films 518(6, Supplement 1): S2-S5 (2010).

[2] R. R. Lieten et al. Appl. Phys. Lett. 102, 052106 (2013).

[3] A. Bhatia et al. Journal of Electronic Materials, 41, 5 (2012).

## Study of the effect of implantation temperature on AlGa<sub>N</sub> compounds implanted with rare earth ions

Maria Fialho<sup>1</sup>, Djibril Nd. Faye<sup>1</sup>, Sérgio Magalhães<sup>1,2</sup>, Joana Rodrigues<sup>3</sup>, Armando J. Neves<sup>3</sup>, Teresa Monteiro<sup>3</sup>, Katharina Lorenz<sup>1</sup>, Eduardo Alves<sup>1</sup>

<sup>1</sup>*Campus Tecnológico e Nuclear, IPFN, Instituto Superior Técnico, Universidade de Lisboa, Portugal*

<sup>2</sup>*IFIMUP/IN, Instituto de Física dos Materiais da Faculdade de Ciências da Universidade do Porto, Instituto de Nanociências e Nanotecnologias, Rua do Campo Alegre, 687, 4169-007 Porto, Portugal*

<sup>3</sup>*Departamento de Física e i3N, Universidade de Aveiro, 3810-193 Aveiro, Portugal*

Light emission from Rare-Earth (RE) doped III-nitride semiconductors has driven much attention for applications on electroluminescence devices. The incorporation of RE ions allows the optical tuning from ultraviolet to infrared wavelengths using the intra 4f<sub>n</sub> sharp emission lines of these ions. Also, the wide band gap of the semiconductors enables the possibility to explore the higher lying RE levels and the temperature quenching of luminescence is expected to decrease with the increase of the semiconductor band gap. The need for high dopant concentration, necessary to reach intense emissions, is limited by the interaction of dopants during the growth process. Alternatively, the ion implantation technique allows the control of dopant profile and concentrations; however, the irradiation damage at higher fluences should be overcome by annealing processes during and/or after implantation.

In this work, Al<sub>x</sub>Ga<sub>1-x</sub>N films grown on (0001) sapphire substrates by Metal Organic Chemical Vapor Phase Deposition (MOCVD) with three different AlN molar fractions (0.15, 0.4, 0.6) were implanted with lanthanides. The ion implantation was carried out for fluences between  $1 \times 10^{14}$  at/cm<sup>2</sup> and  $5 \times 10^{15}$  ion/cm<sup>2</sup>, with the beam aligned with the c-axis to minimize damage. The implantations were studied for two energies, 150 and 300 keV and for different temperatures. In order to access the structural information we used High Resolution X-ray Diffraction (HRXRD) and Rutherford Backscattering / Channeling Spectrometry (RBS/C). Rapid thermal annealing treatments were performed to remove the irradiation damage due to implantation of RE. The optical properties were investigated by Photoluminescence (PL) measurements to account for optical activation of RE ions after annealing treatments. The influence of the AlN molar fraction on the emission intensity is discussed.

## **Ion beam modification of PbTe and Ag doped PbTe for thermoelectric application**

Manju Bala, D.K. Avasth, Srashti Gupta

*IUAC, India*

PbTe is one of the most favorable thermoelectric materials over a wide temperature range (500-900K) for converting waste heat or solar heat into electricity. Present work is focused on the study of ion beam induced modification on surface, structure and thermoelectric properties of thermally evaporated PbTe and Ag doped PbTe thin films. The effects of (i) thermal annealing (at 520 K for 1 hour), (ii) electronic energy loss using 100 MeV Ag ions and (iii) nuclear energy loss using 100 keV Ar ions are studied on pristine and Ag doped PbTe. Samples are characterized by X-Ray Diffraction (XRD), Rutherford Backscattering spectrometry (RBS) and Scanning Electron Microscopy (SEM) for structural, compositional and surface morphological studies, respectively. XRD data exhibits increase in crystallinity and grain sizes of PbTe thin film with Ag doping which further increases with annealing and irradiation. Thermoelectric measurement of PbTe thin film shows an increase in thermo power from  $\sim 290\mu\text{V/K}$  to  $\sim 380\mu\text{V/K}$  after  $\sim 10\%$  Ag doping. The thermoelectric measurements of pristine and Ag doped PbTe after ion irradiation is in progress.

## Implantation of Argon in a-Si:H/c-Si heterojunction solar cells

Alice Defresne<sup>1</sup>, Olivier Plantevin<sup>1</sup>, Igor P. Sobkowicz<sup>2</sup>, Jérôme Bourçois<sup>1</sup>, Pere Roca I Cabarrocas<sup>2</sup>

<sup>1</sup>CSNSM, Univ Paris-Sud, CNRS-IN2P3 et LPICM, CNRS-Ecole Polytechnique, France

<sup>2</sup>LPICM, CNRS-Ecole Polytechnique Palaiseau & TOTAL New Energies La Défense France

a-Si:H/c-Si heterojunction solar cells have reached record efficiencies of 24.7%. They consist of a n-type crystalline silicon wafer on which a thin (~10 nm) p-type hydrogenated amorphous silicon (a-Si:H) layer is deposited by plasma enhanced CVD at low temperature (~200 °C). The electrical contact on the cell is usually a thin transparent conducting oxide (80 nm thick) achieved by sputtering. Both sputtering and plasma deposition processes may introduce defects at the c-Si/a-Si:H interface which in turn will determine the conversion efficiency of the cell[1],[2].

The goal of this study is to understand the fundamental aspects of this interface modification via defect formation using a controlled introduction of point defects. Ion implantation of Argon at low energy (1 to 10 keV at IRMA/CSNSM) allows the modification of the a-Si:H thin layer. We can control the depth and concentration of irradiation defects by varying the ion energy and fluence. The defect concentration maximum is adjusted at a depth between 4 nm and 20 nm and the fluence between  $10^{10} \text{ Ar}^+ \cdot \text{cm}^{-2}$  and  $10^{14} \text{ Ar}^+ \cdot \text{cm}^{-2}$ . The samples are then annealed, under  $\text{H}_2\text{N}_2$  atmosphere, at a temperature close to the deposition temperature, to study the healing of these defects. The modification in the effective lifetime of minority carriers upon defect creation or annealing is characterized via photoconductance and photoluminescence measurements. The migration of hydrogen and vacancies towards the interface during ion irradiation is tentatively proposed to explain the decrease in minority carrier lifetime after ITO deposition. Understanding the degradation mechanisms of the cell under irradiation will allow to improve the efficiency of the future solar cells.

[1] S. De Wolf et al., Green 2, 7–24 (2012).

[2] A. Illiberi et al., Appl. Phys. Lett. 98, 242115 (2011).

### **Diamond and 4H-SiC doping by hot ion implantation and high temperature annealing.**

Laurent Ottaviani<sup>1</sup>, Julien Barjon<sup>2</sup>, Stephane Morata<sup>3</sup>, Gilles Mathieu<sup>3</sup>, Frank Torregrosa<sup>3</sup>,  
Gilles Boccheciampe<sup>3</sup>, Laurent Roux<sup>3</sup>

<sup>1</sup>*IM2NP (UMR6242), France*

<sup>2</sup>*Groupe d'étude de la matière condensée (GEMaC), France*

<sup>3</sup>*Ion Beam Services, France*

We present a current review of the doping process of diamond and 4H-SiC by ion implantation and thermal annealing in the path of ohmic contact formation for high power application.

Doping strategy is the same for both materials: hot ion implantation on IMC200R&D implanter and high temperature annealing up to 1700°C in a vertical furnace.

First, surface modification and graphitization of Phosphorus as-implanted CVD diamonds were respectively studied by AFM and Raman. Donor activity of diamond single crystals implanted with Arsenic or Phosphorus was investigated by Cathodoluminescence [1].

Second, influence of annealing conditions (temperature, heating/cooling rates) on Aluminum-implanted 4H-SiC epitaxial layers is studied by AFM and electrical measurement [2].

High temperature implantation is found to preserve surface roughness and to effectively limit implantation-induced damage in diamond and in 4H-SiC.

Electrical activation of Aluminum-implanted 4H-SiC increases with annealing temperature and is finally improved by a fast heating rate.

At last, new emission lines related to Arsenic excitonic recombinations are observed in Arsenic-implanted diamond after high thermal annealing and an ionization energy of 0.41eV, shallower than Phosphorus, was deduced in good agreement with theoretical predictions.

[1] J. Barjon et al. Phys Rev, B89, 045201 (2014).

[2] L. Ottaviani et al. Mat Sci For Vols, 645-648 (2010).



## Incorporation of oxygen in SiC implanted with hydrogen

Adam Barcz<sup>1</sup>, Rafal Jakiela<sup>1</sup>, George Celler<sup>2</sup>, Maciej Kozubal<sup>1</sup>, Jacek Ratajczak<sup>1</sup>

<sup>1</sup>*Institute of Physics PAS / Institute of Electron Technology, 02-668 Warsaw, Poland*

<sup>2</sup>*Institute for Advanced Materials, Devices, and Nanotechnology (IAMDN) / Department of Materials Science and Engineering; Rutgers University, New Brunswick, NJ 0890, USA*

Oxygen accumulations at buried implantation-damage layers were studied after post-implantation annealing of hydrogen- or deuterium-implanted 4H SiC. In this study  $^2\text{H}^+$  implantation was carried out at energies 600 keV and 1 MeV, to doses ranging from  $2 \times 10^{16}/\text{cm}^2$  to  $1 \times 10^{17}/\text{cm}^2$ . For comparison, the implantation was also done into float-zone (FZ) and Czochralski (CZ) silicon wafers. Annealing at temperatures 400 C to 1100 C was performed either in pure argon or in oxygen enriched with  $^{17}\text{O}$  isotope. Characterization methods included SIMS, RBS and TEM. At sufficiently high doses, hydrogen implantation into semiconductors leads to the irreversible formation of a planar zone of microcavities, bubbles and other extended defects located at the maximum of deposited energy. Such kind of highly perturbed layer, containing large amounts of agglomerated hydrogen, has been reported to efficiently getter a number of impurities. Oxygen was detected in both CZ and FZ silicon subjected to Smart-Cut processing. We have recently identified, by SIMS profiling, a considerable oxygen peak situated at the interface between the SiC substrate and a layer implanted with  $10^{17} \text{ H ions}/\text{cm}^2$  and heated to 1100 C in a nominally pure Ar [1]. In view of a lack of convincing evidence that a hexagonal SiC might contain substantial amounts of oxygen, the objective of the present study was to identify the source and possible transport mechanism of oxygen species to the cavity band. Analysis of several implants annealed at various conditions led us to conclusion that, besides diffusion from the bulk or from surface oxides, an alternative path for oxygen agglomeration is migration of gaseous  $\text{O}_2$  or  $\text{H}_2\text{O}$  from the edge of the sample through the porous layer.

[1]. A. Barcz, M. Kozubal, R. Jakiela, J. Ratajczak, J. Dyczewski, K. Golaszewska, T. Wojciechowski, G. K. Celler,; Journal of Applied Physics (in press).

## Fabrication of dendritic nanostructured photoactive tungsten materials by helium plasma irradiation

Katsuyuki Komori<sup>1</sup>, Noriyasu Ohno<sup>1</sup>, Tomoko Yoshida<sup>2</sup>, Toyokazu Nomoto<sup>3</sup>, Muneaki Yamamoto<sup>1</sup>, Chie Tsukada<sup>1</sup>, Shinya Yagi<sup>2</sup>, Miyuki Yajima<sup>1</sup>, Shin Kajita<sup>2</sup>

<sup>1</sup>*Graduate School of Engineering, Nagoya University, Japan*

<sup>2</sup>*EcoTopia Science Institute, Nagoya University, Japan*

<sup>3</sup>*Aichi Synchrotron Radiation Center, Japan*

In the plasma engineering field, it has been reported that the helium plasma irradiation fabricates dendritic nanostructures on the surface of tungsten plates. The dendritic tungsten shows a broad photo-absorption in the wide energy range from 1 to 5 eV in the diffuse reflection measurements. Such a nanosized WO<sub>3</sub> with a high specific surface area might promote a photoinduced reaction.

In the present work, we examined the photoactivity of the nanostructured tungsten material, which is expected to consist of both nanosized W and WO<sub>3</sub>, fabricated by the He plasma technique followed by gentle oxidation.

The photoinduced reaction experiments were conducted for the dendritic tungsten samples with 20~100 % surface oxidation ratios, and the reaction activities were evaluated with the decolorization rate of methylene blue (MB) in an aqueous solution under near-infrared light (<1.55 eV), whose energy is lower than the band gap of WO<sub>3</sub>. The photoinduced reaction rate varied with the oxidation ratio of the samples, and reached the maximum around 50 %, suggesting that WO<sub>3</sub> /W interface is an active site for the photoinduced reaction. On the other hand, the reaction rate over fully oxidized sample was slower, suggesting that WO<sub>3</sub> species is the lower active site. Unfortunately, the high active WO<sub>3</sub>/W interface species was found to be deactivated in cycle tests while less deactivation was observed for the low active WO<sub>3</sub> species.

The photoinduced MB decomposition process was confirmed by XAFS, XPS and SEM analyses, i.e., in the dark, MB molecules are adsorbed on the sample surface and stacked each other by the  $\pi$ -orbital interaction while under the light, S-C bonds of MB molecule are broken to produce SO<sub>4</sub><sup>2-</sup>. The active W/WO<sub>3</sub> interface species could be deactivated by adsorption of the reaction products on the metal tungsten sites of the sample surface.

## Characterization of the defect formation of 4H-SiC during ion implantation at 625 K

Philipp Schöppe<sup>1</sup>, Leonie Kaczmarek<sup>1</sup>, Andreas Undisz<sup>2</sup>, Markus Rettenmayr<sup>2</sup>, Elke Wendler<sup>1</sup>

<sup>1</sup>*Institut für Festkörperphysik, Friedrich-Schiller-Universität Jena, Germany*

<sup>2</sup>*Otto-Schott-Institut für Materialforschung, Friedrich-Schiller-Universität Jena, Germany*

The damage formation in 4H-SiC during ion implantation at 625 K is investigated. It is found that the evolution of damage density as a function of the ion fluence proceeds in two steps and exhibits similar behaviour for all ion species investigated. The first step occurs at similar values of the number of displacements per lattice atom (dpa) and can be attributed to the formation of point defects and point defect complexes. The saturation of the defect density is due to the balance between defect formation and recombination [1]. At higher ion fluences, a second step with further increasing damage concentration occurs up to a saturation level well below amorphisation.

In this contribution the second step of damage concentration versus ion fluence is studied in detail for different ion species. Rutherford backscattering spectrometry in channelling configuration (RBS) and high-resolution transmission electron microscopy (TEM) are applied. No correlation between the second step and the number of dpa is observed. A possible chemical effect caused by the implanted ions is not substantiated as origin of the second step. Despite the high ion fluences of several  $10^{16} \text{ cm}^{-2}$ , formation of precipitates of implanted ions or bubbles were not observed by TEM. Nevertheless the impurities remain within the implanted layers as detected by RBS. Our results suggest that the implanted impurities occupy interstitial and lattice places. Once the volume introduced by the implanted ions exceeds some critical value, the implanted ions seem to act as effective sinks for the formation of extended defects like dislocations and stacking faults.

[1] E. Wendler, Ph. Schöppe, Th. Bierschenk, St. Milz, W. Wesch, N.G. van der Berg, E. Friedland, J.B. Malherbe, Nucl. Instrum. Methods in Phys. Res. B 286, 93 (2012).

## **Progress in ion implantation technology for devices based on silicon carbide**

Alexander Suvorov

*Cree, Inc., USA*

Silicon carbide is of considerable interest as a material for semiconductor electronic devices used in high temperature, high power, and high radiation conditions under which conventional semiconductors cannot perform. Recent advances in epitaxial growth and significant improvements in the quality of silicon carbide materials have allowed the development of a device technology for a variety of applications and systems, such as Power Modules with Schottky diodes and MOSFETs based on silicon carbide that enable better performance than similar devices based on silicon.

Ion implantation is an irreplaceable technology for selective-area doping and isolation of SiC-based devices. After many years of intensive work and research, significant progress has been made in ion implantation technology for SiC, such as reducing crystal damage and increasing activation of the introduced doping by using high temperature during implantation and protection at the surface of implanted layers destruction during annealing at high temperatures. The high structural quality of the produced silicon carbide implanted layers has allows the growth of epitaxial layers and the buildup of 3D devices with complex architecture. Different approaches for the creation of active areas in SiC devices by ion implantation will be discussed from a process and equipment point of view.

## Lattice location and thermal stability of implanted 3d transition metals in germanium

Valerie Augustyns<sup>1</sup>, Lino Pereira<sup>1</sup>, Ligia Amorim<sup>1</sup>, Ulrich Wahl<sup>2</sup>, Joao Guilherme Correia<sup>2</sup>, Kristiaan Temst<sup>1</sup>, André Vantomme<sup>1</sup>

<sup>1</sup>*KU Leuven, Instituut voor Kern- en Stralingsfysica, Belgium*

<sup>2</sup>*Instituto Tecnológico e Nuclear, Sacavém, Portugal*

The properties of dopants and impurities in semiconductors are determined by the exact position of the dopant/impurity atoms in the host lattice. We investigated the lattice location and thermal stability of 3d transition metals (Mn, Fe, Ni and Cu) implanted in intrinsic Ge, using the emission channeling technique [1]. The experiments were performed at the radioactive ion beam facility ISOLDE at CERN, which provides isotope-pure beams of radioactive <sup>56</sup>Mn, <sup>59</sup>Fe, <sup>65</sup>Ni and <sup>67</sup>Cu. The emission channeling measurements were carried out in the as-implanted state and after thermal annealing at different temperatures up to 600 °C, in vacuum. Apart from the occupation of the expected substitutional position [2,3], interstitial sites were detected as well. For all investigated transition metals, a significant fraction, up to 28%, was found to occupy a near-bond-centered site (0.37 Å displaced from the ideal position), associated with the split-vacancy configuration [2]. For Ni, an additional fraction (up to 28%) was identified in a near-tetrahedral site, which we interpret as being associated with more complex defect structures (e.g. containing more than two vacancies). Upon thermal annealing, substitutional and interstitial sites exhibited comparable thermal stability. For example, the fractions of Ni atoms in all three identified sites decrease to below detection (<3%) between 400 and 500 °C. Such high thermal stability of interstitial transition metals (compared to the typically low thermal stability of free interstitials) can be interpreted as resulting from the energy required to dissociate the defect complexes.

[1] H. Hofsäss and G. Lindner, Phys. Rep. 201, 121 (1991).

[2] S. Decoster, S. Cottenier, B. De Vries, H. Emmerich, U. Wahl, J.G. Correia and A. Vantomme, Phys. Rev. Lett. 102, 065502 (2009).

[3] S. Decoster, S. Cottenier, U. Wahl, J. G. Correia, L.M.C. Pereira, C. Lacasta, M.R. Da Silva and A. Vantomme, Appl. Phys. Lett. 97, 151914 (2010).

## **Distribution and evolution of the thermal field formed by intense pulsed ion beam on a thin target**

Xiao Yu, Miao Qu, Gaolong Zhang, Jie Zhang, Jie Shen, Haowen Zhong, Yanyan Zhang, Xiaofu Zhang, Xiaoyun Le

*Beihang University, P.R. China*

Intense pulsed ion beam (IPIB) is characterized by high pulsed power density. With the strong energy effect in the surface, IPIB is an ideal technic for fast surface thermal processing of materials. Thus, the formation and evolution of thermal field by IPIBs is of great significance to the application. However, due to the short pulsed length and high flux, the study of this field was mainly yield to numerical simulation. In this paper, we studied the distribution and evolution of thermal field formed by IPIB which is produced by a magnetically insulated diode on a thin metal target with a combination of infrared image diagnostic method. Also, the numerical analysis of the evolution of the thermal field was carried out with finite element method (FEM) and the evolution behavior of the thermal field was discussed to clarify its effects on the thin and thick metal films.

**Surface modification and characterization of SiC nanowires**

Xiaodong Zhang<sup>1</sup>, Joachim Bollmann<sup>2</sup>

<sup>1</sup>*Harbin Institute of Technology, China P. R.*

<sup>2</sup>*Institute of Electronic and Sensor Materials, TU Bergakademie Freiberg, Germany*

Silicon carbide (SiC) nanowires have been widely investigated during the past decades. SiC nanowires exhibit the outstanding mechanical properties so that they are regarded as the promising reinforcement materials for metal-, ceramic- and polymer- composites. The surface of SiC nanowires can greatly affect the reinforcement efficiency in composites. Therefore, it is important to modify the surface of SiC nanowires. However, little work has been focused on the surface modification of SiC nanowires.

In this study, we report a novel method to synthesize SiC nanowires. Then, the surface of SiC nanowires is modified to form the SiC@SiO<sub>2</sub> nanostructure by heat-treatment in air atmosphere. The morphologies and structures of nanomaterials are well characterized by scanning electron microscopy (SEM), transmission electron microscopy (TEM) and X-ray diffraction (XRD). And the mechanism of surface modification of nanowires is proposed.

## **Investigation of different phases of Fe-Si structures formed in Si by low energy ion implantation**

Wickramaarachchige Lakshantha, Mangal Dhoubhadel, Tilo Reinert, Floyd Mcdaniel,  
Bibhudutta Rout

Ion Beam Analysis and Modification Laboratory, Department of Physics, University of  
North Texas, Denton, TX 76203, USA

Fe-Si alloy have attracted widespread interest for technological and fundamental reasons. The Fe-Si system provides several iron silicides that have exceptional material properties with wide range applications in the electronic industry. Polycrystalline Fe-Si phases were fabricated by high fluence implantation of 50 keV Fe in Si(100) and subsequent vacuum annealing. The depth profile of the implanted Fe atoms in Si(100) were simulated by the widely used transportation of ion in matter (TRIM) computer code as well as by the dynamic transportation of ion in matter code (T-DYN, TRIDYN and SDTrimSP). The stoichiometry and depth distribution of Fe were determined by Rutherford Backscattering Spectrometry(RBS) and X-ray photoelectron spectroscopy (XPS). The Fe-Si structures were characterized by X-ray diffraction (XRD). Core-level XPS spectra were analyzed for investigation of different Fe-Si phases. Particularly, Chemical shifts and spectral shapes of Fe 2p<sub>3/2</sub> peak for iron silicide phases were studied with heat treatment as well as depth distribution. Scanning Electron Microscope (SEM) with Electron Backscatter Diffraction (EBSD) imaging was used to identify different Fe-Si phases on surface and cross-sectional area.



## Silicon surfaces functionalized by ion implantation

Bruno Nunes, Rogério Colaço, Eduardo Alves, Ana Rego

*Instituto Superior Técnico, Lisbon*

Engineering silicon surfaces is a necessary processing step to improve the nanotribological and wettability response of Si-based materials for MEMS and NEMS applications. In this paper we performed dual ion (??) implantations of Fe+C and Ti+C in silicon wafers with fluences from  $5 \times 10^{16} \text{ cm}^{-2}$  up to  $2 \times 10^{17} \text{ cm}^{-2}$ . Implantation was followed by annealing treatments at 800 °C, 900 °C and 1000 °C. The implanted surfaces were analyzed by Rutherford Backscattering Spectrometry/Channeling (RBS/C), scanning electron microscopy (SEM), X-ray diffraction (XRD) and by X-ray photoelectron spectroscopy (XPS).

After the implantation both X-ray diffractograms and RBS/C results show that the implanted region is fully amorphized. After annealing at 800 °C, SEM observation shows the formation of nanoprecipitates at the surface of the samples and RBS/C indicates the recrystallization of a narrow region close to initial amorphous/crystalline interface. X-ray diffraction and XPS results enabled to identify the precipitates formed as the iron silicide  $\beta\text{-FeSi}_2$  and also two different titanium silicides, the C49 (metastable) and C54 structures, as well as SiC in the case of the higher fluences of the titanium implantations. Moreover, as the annealing temperature increases from 800 °C to 1000 °C, X-ray analysis shows that orthorhombic  $\beta\text{-FeSi}_2$  is progressively replaced by tetragonal  $\alpha\text{-FeSi}_2$  and small peaks of SiC appear, which is confirmed by XPS analysis. The metastable C49-TiSi<sub>2</sub> silicide is fully replaced by the C54-silicide and the formation of SiC is enhanced. The SEM observations of the high temperature annealed samples show the presence of large precipitates emerging from the surface, reaching considerable heights relative to surface.

The nanotribological properties are under assessment and the results suggest the possibility to use ion implantation to improve the nanomechanical performance of silicon with advantages for the micro-nano electromechanical systems.

## Measurement of ultra-low ion energy of decelerated ion beam using a deflecting electric field

Prutchayawoot Thopan, Liangdeng Yu

*Chiang Mai University, Thailand*

In investigation on ultra-low-energy ion bombardment effect on DNA, an ion beam deceleration lens was constructed and installed for high-quality ultra-low-energy ion beam. Measurement of the ion energy after deceleration was necessary to confirm the ion beam really decelerated as theoretically expected. In contrast to conventional methods, this work used a deflecting electrostatic field after the deceleration lens to bend the ion beam. The beam bending distance was related to the ion energy. The paper gives details of the theory and calculation formulae. The ion beam bending was also simulated using the SIMION program. A system for the measurement of the ion beam energy was designed, constructed and installed. The system consisted of a pair of parallel electrode plates to generate the deflecting electrical field, a copper rod measurement piece to detect ion beam current, a vernier caliper to mark the beam position, a stepping motor to translate the measurement rod, and a webcam-camera to read the beam bending distance. The entire system was installed under the ion-beam deceleration lens and the complete system of the deceleration lens with the measurement system was placed inside the large chamber of the 30-kV bioengineering vertical ion beam line at Chiang Mai University. Moving the measurement rod across the decelerated ion beam enabled to obtain beam profiles, from which the beam bending distance could be known and finally the ion beam energy could be calculated. The measurement results were in good agreement with theoretical and simulated results. The performance of the system demonstrated that it was a simple, reliable and accurate method to measure ultra-low energy of decelerated ion beam.

**Optimization of ion tracks in ta-C with the defined charge state**

Srashti Gupta<sup>1</sup>, H.-G. Gehrke<sup>1</sup>, C. Trautmann<sup>2</sup>, D. Severin<sup>2</sup>, M. Bender<sup>2</sup>, J. Krauser<sup>3</sup>, H. Rothard<sup>4</sup>, H. Hofsäss<sup>1</sup>

<sup>1</sup>*2nd Institute of Physics, University of Göttingen, Göttingen, Germany*

<sup>2</sup>*Helmholtz Centre for Heavy Ion Research, GSI, Darmstadt, Germany*

<sup>3</sup>*Department of Automation and Computer Science, University of Applied Science Harz, Wernigerode, Germany*

<sup>4</sup>*CIMAP-GANIL CIRIL-, F-14050 Caen, France*

Ion tracks in a matrix with uniform distribution and reproducibility of track properties are highly desirable for most of the applications. Thus in the present work, it is an interest to look for optimization of conducting ion tracks in ta-C films from swift heavy ions with defined charge state. Tetrahedral amorphous carbon films (ta-C) have been synthesised by mass selected ion beam deposition (MSIBD). Conducting ion tracks have been formed in ta-C films after irradiation using 4.57 MeV/u Pb ions with high charge states of 53<sup>+</sup>, 56<sup>+</sup> and 60<sup>+</sup> at fluence of 1×10<sup>10</sup> ions/cm<sup>2</sup> at GANIL, France. Each ion track can be identified using atomic force microscopy (AFM) by a characteristic hillock at the surface. Topography and conductivity of ion tracks have been characterized by AFM measurement. This study shows that for higher charge state (60+), hillock height and conductivity both are increased. Another approach has also been done for the generation and testing of charge selected swift heavy ion beams at GSI, Darmstadt using stripper foil in the material science beam lines. During irradiation, charge states have been defined with controlling the deflection magnet field in material science beam lines. Ion tracks have been formed using 4.773 MeV/u, Bi ions for high charge states from 50<sup>+</sup> to 61<sup>+</sup> at fluence of 1×10<sup>10</sup> ions/cm<sup>2</sup>. Topography of ion tracks have been characterized by AFM. Optimization of distribution of ion tracks over the ta-C matrix for different charge states has been studied. This study also includes the conductivity of ion tracks as a function of the charge state of swift heavy ions.

**Damage creation in lithium fluoride by swift heavy ions in the electronic energy near the maximum of the Bragg's peak**

Hamdani Benhacine, Soraya Kadid, Ali Meftah

*LRPCSI, Université 20 août 55 Skikda, route El-Hadaeik, Skikda, Algeria*

The Lithium Fluoride crystal are irradiated normal to the lattice plane with lead ions with energy 544 MeV and 840 MeV at fluence between  $10^9$  and  $4.10^{12}$  ions/cm<sup>2</sup>. These samples are characterized by optical absorption in the wavelength range 200 - 900 nm and by photoluminescence (PL) under 458 nm excitation at room temperature. The damage in the tracks is dominated by the creation of simple defects (F centers) and aggregated defects (Fn centers). For LiF crystals two very intense PL bands have been observed at around 545 and 665 nm, which correspond to the emission of F<sup>+3</sup> and F<sup>2</sup> centers respectively.

**Raman study of gallium nitride under swift heavy ions**

Florent Moisy<sup>1</sup>, Mamour Sall<sup>1</sup>, Emmanuel Balanzat<sup>1</sup>, Clara Grygiel<sup>1</sup>, Patrick Simon<sup>2</sup>, Aurélien Canizares<sup>2</sup>, Isabelle Monnet<sup>1</sup>

<sup>1</sup>*CIMAP, Caen, France*

<sup>2</sup>*CEMHTI, Orléans, France*

Wurtzite GaN epilayers, grown on c-plane sapphire substrates, have been irradiated with swift heavy ions (Xe, Ar, U,...) at different energies and fluences, and thereafter studied by Raman scattering spectroscopy. Raman spectra show that strong structural modifications are induced in the GaN layer. Indeed, three new modes appear after irradiation at approximately: 200 cm<sup>-1</sup>, 300 cm<sup>-1</sup> and 670 cm<sup>-1</sup>. The origin of these modes is still debated in the literature [1-3], either attributed to disorder activated Raman scattering [1,3] or to nitrogen vacancy related defects (670 cm<sup>-1</sup>) [2]. The origin of the disorder induced in the GaN layer will be discussed in the communication, particularly the case of the mode at 300 cm<sup>-1</sup>. Using the configuration coordinate approach, we have found that this mode is linked to the optical defects absorbing at 2.8eV in GaN. The combination of optical absorption measurements and Raman spectroscopy allowed us to establish that the irradiation induced optical defects (so the mode at 300 cm<sup>-1</sup>) are Ga vacancy related defects.

The second part of the presentation will be concentrated on the study of the radiation induced stress, since the low wavenumber-shift of E<sub>2</sub> strong mode as a function of the fluence allows to quantify the biaxial stresses in the c-plane.

The influence of nuclear and electronic stopping powers, or an eventual coupled effect of these two phenomenons, will be studied, as we have already done with color center formation in AlN [4].

[1] W. Limmer, W. Ritter, R. Sauer, B. Mensching, C. Liu, B. Rauschenbach, Appl. Phys. Lett. 72, 20 (1998).

[2] M. Katsikini, K. Papagelis, E.C. Palouras, S. Ves, J. Appl. Phys. 94, 7 (2003).

[3] H.W. Choi, S.J. Chua, J. Tripathy, Appl. Phys. 92, 8 (2002).

[4] M. Sall, I. Monnet, C. Grygiel, B. Ban d'Etat, H. Lebius, S. Leclerc and E. Balanzat, Europhys. Lett. 102, 26002 (2013).

## Comparison of AFM and GISAXS capabilities for surface swift heavy ion track analysis

Marko Karlusic<sup>1</sup>, Iva Bogdanovic Radovic<sup>1</sup>, Milko Jaksic<sup>1</sup>, Nikola Radic<sup>1</sup>, Branko Santic<sup>1</sup>,  
Marika Schleberger<sup>2</sup>, Sigrid Bernstorff<sup>3</sup>, Maja Buljan<sup>1</sup>

<sup>1</sup>*Ruder Boskovic Institute, Bijenicka cesta 54, 10000 Zagreb, Croatia*

<sup>2</sup>*Fakultät für Physik and CENIDE, Universität Duisburg-Essen, 47048 Duisburg, Germany*

<sup>3</sup>*Elettra-Sincrotrone Trieste, SS 14 km 163.5, 34149 Basovizza, Italy*

Irradiation of flat solid surfaces by swift heavy ions under the grazing incidence angle can result in the formation of surface ion tracks. These ion tracks can be observed directly using atomic force microscopy (AFM) [1-3]. However, to extract statistical information (average ion track length, length distribution etc.), structural investigations of this type are very time consuming. In the present work we apply grazing incidence small angle X-ray scattering (GISAXS) for the structural analysis of surface swift heavy ion tracks and demonstrate its capabilities on a wide range of investigated materials (SrTiO<sub>3</sub>, TiO<sub>2</sub>, quartz and a-SiO<sub>2</sub>, amorphous Ge+SiO<sub>2</sub> and Ge+ITO thin films). Compared to AFM, GISAXS allows short measuring times with an excellent statistics. Possible applications of surface patterning of Ge+ITO thin films using swift heavy ions, with respect to the modifications of transparent Ge+ITO electrodes for photovoltaics, will be discussed as well.

[1] A. Akcöltekin et al., Nature Nanotechnology 2, 290 (2007).

[2] M. Karlušić et al., New J. Phys. 12, 043009 (2010).

[3] S. Akcöltekin et al., Nucl. Instrum. Meth. B 267, 1386 (2009).

### Structural damage on single-crystal diamond by swift heavy ion irradiation

Jose Olivares<sup>1</sup>, Gastón García<sup>2</sup>, Ovidio Peña-Rodríguez<sup>3</sup>, Manuel Díaz-Hijar<sup>4</sup>, Iullian Preda<sup>2</sup>, Victoria Tormo-Márquez<sup>4</sup>

<sup>1</sup>*Instituto de Óptica, Consejo Superior de Investigaciones Científicas (CSIC), C/Serrano 121, E-28006 Madrid, Spain*

<sup>2</sup>*ALBA Synchrotron Light Source (CELLS-ALBA), 08290, Cerdanyola del Vallès, Barcelona, Spain*

<sup>3</sup>*Instituto de Fusión Nuclear (UPM), José Gutiérrez Abascal 2, E-28006-Madrid, Spain*

<sup>4</sup>*Centro de Microanálisis de Materiales (CMAM), Universidad Autónoma de Madrid (UAM), Cantoblanco, E-28049 Madrid, Spain*

Experimental evidence of diamond synthetic single crystal amorphization under the effect of irradiation with swift heavy ions is shown. Ion beams used have been the following: Si (2.6-20 MeV), Br (11-40 MeV), Au (18.6-33 MeV). The type of sharp thresholding behaviour which characterizes electronic damage is not observed within a range of electronic stopping force covering up to 12 keV/nm. Amorphization is assessed by Rutherford Back Scattering Channeling (RBS-c) measurements done with light ions (H at 3 MeV), after swift heavy ion irradiation. Results are analysed and discussed in order to confirm the hypothesis of a nuclear damage induced process, whereby it is concluded that electronic effects are not relevant in the stopping force range studied. The evolution of the amorphized fraction as a function of the irradiated dose and nuclear stopping force is measured and analysed

**Production of H and Au MeV ion microbeams using glass microcapillaries**

Daniela Sotelo<sup>1</sup>, Danieli Guerra<sup>1</sup>, Cláudia Telles<sup>2</sup>, Ricardo Papaleo<sup>1,2</sup>

<sup>1</sup>*Faculty of Physics, Catholic University of Rio Grande do Sul, Porto Alegre – RS, Brazil*

<sup>2</sup>*Ion Implantation Laboratory, Institute of Physics, Federal University of Rio Grande do Sul, Porto Alegre – RS, Brazil*

In this work, we have used tapered glass microcapillaries with openings between  $\sim 2\text{ }\mu\text{m}$  and  $\sim 118\text{ }\mu\text{m}$  to produce and characterize microbeams of light and heavy ions ( $1\text{ MeV H}^+$  and  $18\text{ MeV Au}^{7+}$ ). The transmission and beam energy straggling from different microcapillaries were measured as a function of tilt angle using the  $1\text{ MeV H}^+$  beam. For some capillaries there was a well defined position corresponding to a maximum transmission of the beam. In other cases, the alignment was lost gradually or the peak position was shifted to lower energies. The energy spectra at maximum transmission presented a FWHM between 18 and 158 keV, and the angular dispersion ranged between  $0.2^\circ$  and  $1.6^\circ$ , depending on the shape of the capillary. The narrowest beams were not obtained with the capillaries with the smallest apertures, but with capillary tips with intermediate diameters between  $\sim 3$  to  $\sim 17\text{ }\mu\text{m}$ . In order to evaluate the beam shape, polycarbonate (PC) foils were exposed to the  $1\text{ MeV H}^+$  and  $18\text{ MeV Au}^{7+}$  microbeams at different fluences (between  $\sim 10^{14}$  and  $\sim 10^{16}\text{ ions/cm}^2$ ). Profiles of the markings produced at  $\sim 1\text{ cm}$  from the capillary exit were evaluated. In some cases the markings were not circular and appeared to be partially blocked. The FWHM of the circular profiles were between 38 to  $90\text{ }\mu\text{m}$ , depending on the ion fluence. The beam angular spread was estimated to be between  $0.15^\circ$  and  $0.20^\circ$  for both beams. We also investigated the performance of a simple PC CCD camera as a detector for the microbeams.



# **Author index**

Abb, Sabine: PB 89  
 Abe, Hiroshi: PA 54  
 Adachi, Shogo: PB 27  
 Afra, Boshra: O 42, PB 114  
 Agarwal, Shradha: O 33, PB 56  
 Agulló-lópez, Fernando: PC 14  
 Ahn, Chihak: O 20  
 Akey, A J: O 19  
 Akhmadaliev, Shavkat: PB 64  
 Akilbekov, Abdirash: PB 24  
 Albarghash, Alyanzan: INV 2  
 Alexander, Duncan T.L.: O 38  
 Alexeyenko, Oleg: PB 113  
 Alix, Kévin: O 38  
 Alkemade, Paul F.A.: PA 21, PA 22  
 Allain, Jean Paul: PB 44, PB 46  
 Allenstein, Uta: O 36  
 Alquier, Daniel: PA 75  
 Alves, E: PA 79  
 Alves, Eduardo: PB 27, PC 108, PC 93  
 Amaral, Livio: PC 78  
 Amarendra, G: O 34  
 Amekura, Hiro: PA 104  
 Amemiya, Kenta: O 35  
 Amorim, Ligia: PC 104  
 Amorim, Lígia: O 18  
 Anahory, Yonathan: INV 10  
 Anders, Christian: O 6  
 Anders, Hallen: O 1  
 Aoki, Takaaki: O 28  
 Aoki, Tamao: PA 89  
 Apel, Pavel: PC 80  
 Appleton, Bill: INV 7  
 Arabi-hashemi, Ariyan: O 36  
 Arenholz, Elke: PC 58  
 Armini, Sylvia: PC 49  
 Arnold, Thomas: O 7  
 Artac, Andreas: PB 64  
 Asahi, Toru: PC 79  
 Augustyns, Valerie: PC 304  
 Aumayr, Friedrich: PA 98  
 Aumayr, Fritz: O 27  
 Auret, Danie: PB 31  
 Avasth, D.K.: PC 94  
 Avasthi, Devesh: PA 104  
 Azarov, Alexander: PA 6  
 Aziz, M J: O 19  
 Azuma, Kingo: PA 81, PB 6, PB 7  
 Baba, Koumei: PB 3  
 Bachelet, Cyril: O 32  
 Bachiller-perea, Diana: PC 14  
 Backman, Marie: PB 35  
 Bai, Q.: PC 20  
 Baizhumanov, Muratbek: PB 24  
 Bala, Manju: PC 94  
 Balanzat, Emmanuel: PC 113  
 Balden, Matrin: PC 67  
 Bali, Rantej: PA 30  
 Ballesteros, Carmen: O 14  
 Bals, S.: PC 70  
 Bals, Sara: PA 105  
 Ban-d'etat, Brigitte: PA 98  
 Banaś, Dariusz: PC 76  
 Baptista, Daniel L.: O 22  
 Barabashov, Andrew: PC 48  
 Baradacs, Eszter: PA 31  
 Barcz, Adam: PC 98  
 Barjon, Julien: PC 97  
 Barozzi, Mario: PA 7  
 Barton, J.: PB 71  
 Basaran, Ali C.: PC 57  
 Bauch, Jürgen: PA 30  
 Bauerdick, Sven: PA 24  
 Bazin, A.E: PA 75  
 Bechade, Jean Luc: O 43  
 Beck, Lucile: PB 55  
 Becker, Martin: PB 4  
 Beckmann, Clemens: PA 103  
 Beisembetov, I.: PA 76  
 Beisenkhanov, Nurzhan: PA 76  
 Belay, Kidane: O 13  
 Benassayag, Gerard: PA 110, PB 102  
 Bender, M.: PC 111  
 Benhacine, Hamdani: PC 112  
 Bennett, Nick: O 20  
 Benyagoub, Abdenacer: O 41, PA 98  
 Berke, Kara: INV 7  
 Bernardini, Sandrine: PB 26  
 Bernstein, Victor: PA 44  
 Bernstorff, Sigrid: O 10, PA 111, PB 116, PC 114  
 Bersani, Massimo: PA 7, PB 50, PC 7

Bertol, Ana Paula: PA 40  
 Beuer, Susanne: PA 25  
 Bhattacharyya, Varsha: PB 84, PC 38  
 Bielejec, Edward: INV 8  
 Biermans, E.: PC 70  
 Bin, R.: PC 20  
 Bischoff, Lothar: O 3, O 6, PB 8  
 Bisht, Manisha: PB 82, PC 63  
 Blanka, Svecova: PC 41  
 Blonskaya, Irina: PC 80  
 Bobes, Omar: PB 93  
 Boccheciampe, Gilles: PC 97  
 Bodnar, Judit: PA 31  
 Boduch, Philippe: PB 18  
 Bogdanovic Radovic, Iva: O 10, PA 111, PC 114  
 Bollmann, Joachim: PA 17, PA 18, PC 106  
 Bondybey, Vladimir: PC 48  
 Boninelli, Simona: O 21  
 Boonyawan, Dheerawan: PC 31, PC 32, PC 77  
 Bootkul, Duangkhae: PB 30, PC 31, PC 32  
 Borany, Johannes Von: PA 107  
 Borchers, Julie A.: PA 93  
 Bordas, Eric: PB 48  
 Borgekov, Daryn: PA 113  
 Borodin, Vladimir: PC 11  
 Borschel, Christian: PB 95  
 Botton, Gianluigi A.: O 38  
 Boucher, Richard: PA 30  
 Bougeard, Dominique: O 3  
 Bourçois, Jérôme: O 32, PC 95  
 Boyd, Iain: PB 33  
 Bracht, Hartmut: O 3  
 Bradby, J E: PB 25  
 Bradley, R. Mark: INV 5  
 Bras, W.: PC 70  
 Braziewicz, Janusz: PC 76  
 Brenner, Daniel: PA 55  
 Brimbal, Daniel: O 33  
 Bringa, Eduardo: O 37  
 Brodziansky, Tomáš: PC 71  
 Brucato, John R.: PB 18  
 Bruchhaus, Lars: PA 24  
 Bruno, Elena: O 20  
 Brüsewitz, Christoph: PA 103  
 Buatier De Mongeot, Francesco: O 8, PB 43  
 Buddhi Tilakaratne, Buddhi: O 17  
 Bukalis, Gregor: PC 58  
 Buljahn, Maja: PC 6  
 Buljan, Maja: O 10, PA 111, PB 116, PC 114  
 Bunfong, Theeravat: PC 77  
 Buonassisi, T: O 19  
 Béland, Laurent K.: INV 10  
 Bérer, Nicolas: PC 2  
 Böttger, Roman: O 6, PB 8  
 Cajzl, Jakub: PC 41  
 Cammelli, Sébastiano: O 43  
 Canizares, Aurélien: PC 113  
 Capek, Pavel: PB 45  
 Carnera, Alberto: O 21  
 Cassimi, Amine: PB 18  
 Castro, Mario: O 14  
 Catarino, N: PA 79  
 Caturla, María Jose: O 37  
 Cayrel, Frédéric: PA 75  
 Celler, George: PC 98  
 Ceponis, Tomas: PA 82, PA 83  
 Chaiwai, Chaiyon: PB 30  
 Chaiwong, Chanokporn: PA 68  
 Chakravarty, Sujoy: O 34  
 Chaudhary, Ramjanay: O 34  
 Chauvat, Mp: PA 79  
 Chen, Feng: O 12  
 Chen, R.K.: PB 71  
 Chen, Xiaolong: PB 73  
 Cheng, F.F.: PC 20  
 Cheng, Rui: PB 17  
 Chiang, Hsin-yin: PC 67  
 Chiappe, Daniele: PB 43  
 Chow, Lee: PB 26  
 Christophe, Jegou: PC 16  
 Chu, Mahn-hung: PB 94  
 Chu, Ran: PB 20  
 Chu, Wei-kan Chu: O 17  
 Chueh, Yu-lun: O 30, PB 92  
 Chulapakorn, Thawatchart: PA 109, PA 41, PC 32  
 Coelho, Sergio: PB 31  
 Colaço, Rogério: PC 108  
 Collard, E: PA 75  
 Corr, Cormac S.: PB 65  
 Correia, Joao Guilherme: PC 104

Correia, João Guilherme: O 18  
 Cottureau, Evelyne: PB 11  
 Couet, Sébastien: PA 105  
 Couillard, Martin: O 38  
 Cowern, Nick: O 20  
 Cremillieu, Pierre: PB 29  
 Crespillo, Miguel Luis: O 37  
 Crowe, Iain: PB 100, PC 47  
 Csato, Constantin: PC 90  
 Cuerno, Rodolfo: O 14  
 Cui, M.H.: PB 63  
 Cui, Minghuan: PC 18  
 Cuppens, J.: PC 70  
 Cuscunà, Massimo: O 21  
 Cutroneo, Mariapomea: PB 111  
 Czub, Joanna: PC 76  
 Da Cunha, Carlo R.: O 22  
 Da Silveira, Enio F.: PB 18  
 Dal, Refika: PC 62  
 Daraszewicz, Szymon: PB 35  
 Das, Kallol: O 2  
 Dauletbekova, Alma: PB 24  
 David, Marie-laure: O 38  
 De Andrade, Antônio Marcos H.: O 22  
 De Araujo Ribeiro, Fabiana: PB 15  
 De Biase, Marco: PA 7  
 De Carlan, Yann: PB 48  
 De La Venta, Jose: PC 57  
 De Pauw, Yana: PA 105  
 De Salvador, Davide: O 20, O 21  
 Debelle, Aurélien: O 32, O 4  
 Dechaumphai, E.: PB 71  
 Decker, Martin: PC 46  
 Decoster, Stefan: O 18  
 Defresne, Alice: PA 70, PC 95  
 Degmova, Jarmila: PC 22  
 Della-negra, Serge: PB 11  
 Delli Veneri, Paola: PB 43  
 Delobbe, Anne: PB 11  
 Demenev, Evgeny: PB 50, PC 7  
 Demeulemeester, Jelle: PC 85  
 Deschanel, Xavier: PC 15  
 Deshkovskaya, Alla: PC 37  
 Deslandes, Alec: PB 65, PC 21  
 Detavernier, Christophe: PC 85  
 Dhoubhadel, Mangal: PC 107  
 Diale, Mmantsae: PB 31  
 Dias, Johnny Ferraz: PC 78  
 Dias, Thiago: PA 93  
 Dimitrakis, Panagiotis: PA 110, PB 102  
 Djourellov, Nikolay: PC 2  
 Djurabekova, Flyura: PB 114, PB 35  
 Dmitriev, Sergei: PC 80  
 Doerner, R.P.: PB 71  
 Domantovsky, Alexander: PA 52  
 Donchev, Alexander: PA 56  
 Donnelly, Stephen: O 25  
 Doriot, Sylvie: O 31  
 Dourdain, Sandrine: PC 15  
 Drazic, Goran: O 10  
 Du, Xin: PB 17  
 Dubey, Girjesh: PB 89  
 Dubreuil, Olivier: PB 49  
 Dugin, Sergey: PB 113  
 Duguay, Sebastien: O 44  
 Dupeyron, Danay: PA 112  
 Dzhumaev, Pavel: PA 59, PA 60  
 Díaz-hijar, Manuel: PC 115  
 Dürr, Michael: PB 89  
 Ehresmann, Arno: PB 76, PC 57  
 Eidelman, Kseniia: PB 88, PC 87  
 Elian, Rajaa: PA 85  
 Eller, Michael: PB 11  
 Elliman, Robert: INV 4, INV 7, O 13  
 Emelyanova, Olga: PA 60  
 Endrino, Jose L.: PC 6  
 England, Jonathan: O 13, O 23  
 Enikeev, Nariman: PA 60  
 Ensinger, Wolfgang: O 40, PA 1, PB 3  
 Esquinazi, Pablo: PB 77  
 Esteves, Christian Roberto Becker: PC 10  
 Fa, T.: PC 20  
 Facsko, Stefan: O 15, O 27, PA 107, PA 30, PB 44, PB 8, PC 6  
 Fairchild, Barbara: PB 106  
 Fan, Shiyu: PB 20  
 Fashen, Li: PC 61  
 Fassbender, Jürgen: O 15, PA 30  
 Faye, Djibril Nd.: PC 93  
 Fekete, Zoltan: PA 31  
 Fernandez Ballester, L.: PC 70  
 Fialho, Maria: PC 93

Fichtner, Paulo F. P.: O 22  
 Fidan, Mehmet: PC 62  
 Filintoglou, Kyriakos: PB 98  
 Filippousi, Maria: PA 105  
 Fisicaro, Giuseppe: O 21  
 Flege, Stefan: PB 3  
 Fleming, Robert: INV 8  
 Fleury-frenette, Karl: PB 49  
 Fortner, Jeffrey: PB 68  
 Fortuna, Franck: PB 59  
 Fortunato, Guglielmo: O 21  
 Franzen, Paulo: O 22  
 Fregnaux, Mathieu: O 44  
 Freund, Jonathan: O 2  
 Frey, Lothar: PA 25, PB 41  
 Fridmann, Joel: INV 7  
 Friedrich, Bárbara: PB 109, PC 10  
 Frost, Frank: O 7  
 Fu, E.: PC 20  
 Fujii, Makiko: O 28  
 Furjes, Peter: PA 31  
 Fuwa, Yasuhiro: PB 13  
 Gaca, Jaroslaw: PB 28  
 Gago, Raul: O 14  
 Gailly, Patrick: PB 49  
 Galetz, Mathias C.: PA 53  
 Galiana, Beatriz: O 14  
 Galindo-uribarri, Alfredo: PB 20  
 Galkin, Nikolay: PC 54  
 Ganchenkova, Maria: PA 60  
 Gao, Kun: PC 88  
 García, Gastón: PC 115  
 Garrido, Frederico: O 32  
 Garrido, Frédéric: O 4  
 Gaubas, Eugenijus: PA 82, PA 83  
 Gaul, Alexander: PB 76  
 Gawlik, Grzegorz: PA 5, PC 13  
 Gehrke, H.-G.: PC 111  
 Gemming, Sibylle: PC 6  
 Gennison, Michael: PC 16  
 Gentils, Aurélie: PB 59, PC 11  
 Geshev, Julian: PA 93  
 Giannakopoulos, Konstantinos: PA 110, PB 102  
 Giordano, Marina: O 8, PB 43  
 Giubertoni, Damiano: PA 7, PB 50, PC 7  
 Giuliani, Raquel: O 22  
 Glaser, M.: O 45  
 Gnaser, Hubert: PB 42  
 Goldhahn, Rüdiger: PA 80  
 Goncharov, Boris: PA 52  
 Goncharova, Darya: PA 52  
 Gorondy-novak, Sofia: PB 55  
 Goss, Jonathan: O 20  
 Gosset, Dominique: O 31, PC 2  
 Gotoh, Yasuhito: PC 39  
 Grande, Pedro: INV 4, O 13, PB 109, PC 10  
 Greaves, Graeme: O 25  
 Grigg, J.: PC 70  
 Gruber, Elisabeth: O 27, PA 98  
 Grundmann, Marius: PB 82, PC 63  
 Grygiel, Clara: O 43, PA 98, PC 113, PC 15  
 Guan, Jing: PA 48  
 Guan, Wei: PA 108  
 Guenette, Mathew C.: PB 65, PC 21  
 Guerra, Danieli: PC 116  
 Guerra, Danieli Born: PC 10  
 Guihard, Matthieu: INV 10  
 Guillous, Stéphane: PA 98  
 Gumenchuk, Galina: PC 48  
 Gupta, Srashti: PC 111  
 Gurovich, Boris: PA 52, PC 35  
 Gushenets, Vasily: PB 113  
 Gutierrez, Leandro Izê: PB 109, PC 10  
 Guttman, Andras: PA 31  
 Gwilliam, Russel: PC 47  
 Gwilliam, Russell: PA 108, PB 100  
 Güven, Olgun: PC 72  
 Ha, Yoosung: PC 29  
 Habler, Gerlinde: PB 64  
 Hajba, Laszlo: PA 31  
 Hakoda, Teruyuki: O 9  
 Hallén, Anders: PA 109, PA 41  
 Halsall, Matthew: PB 100, PC 47  
 Hanazono, Katsumi: PB 5  
 Hanif, Muhammad: O 29  
 Hankemeier, Sebastian: PB 76  
 Hardy, An: PC 63  
 Harnau, Ludger: INV 2  
 Hartwig, Alexander: PC 46  
 Hashimoto, Akihiro: PC 53  
 Hatada, Ruriko: PB 3

Havranek, Vladimir: PC 81  
 Hayashi, Masahiro: PB 2  
 Hebard, Arthur: INV 7  
 Heinig, Karl-heinz: O 6, PB 8  
 Heller, René: O 27, PA 107  
 Helm, M.: O 45  
 Helm, Manfred: O 15, PC 56, PC 58, PC 88  
 Heluani, Silvia P.: PB 77  
 Hershcovitch, Ady: PB 113  
 Hicks, Nathaniel: PB 9  
 Hijazi, Hussein: PB 18  
 Hinks, Jonathan: O 25  
 Hinrichs, Ruth: PA 40  
 Hlatshwayo, Thulani: PC 26  
 Hlawacek, Gregor: PA 9  
 Hnatowicz, Vladimir: PB 85  
 Hoefling, Marion: PB 3  
 Hoerold, Alexander: PA 96  
 Hofman, Gerard: PB 68  
 Hofsäss, H.: PC 111  
 Hofsäss, Hans: INV 6, PA 103, PB 93  
 Holland-moritz, Henry: PB 95  
 Holybee, Brandon: PB 44, PB 46  
 Hori, Fuminobu: PA 57, PC 53, PC 65  
 Hosemann, Peter: PB 57  
 Hoshino, Yasushi: PA 74  
 Hossain, Umme Habiba: PA 1  
 Hou, Chunfeng: PB 69  
 Houben, K.: PC 70  
 Houben, Kelly: PA 105  
 Hoummada, Khalid: PB 26  
 Houssiau, Laurent: PC 75  
 Hsieh, H.Y.: PC 91  
 Huckfeldt, Henning: PC 57  
 Huszank, Robert: PA 31  
 Hébert, Cécile: O 38  
 Hübler, Roberto: PA 45, PB 15  
 Hübner, Rene: O 15  
 Hübner, René: O 6  
 Hübner, René: PA 30  
 Iacob, Erica: PC 7  
 Ikeda, Shunsuke: PB 13  
 Ikenaga, Noriaki: PB 16, PB 19, PB 38  
 Ikeyama, Masami: PC 42  
 Imaeda, Norihiro: PA 91  
 Impellizzeri, Giuliana: O 21  
 Inkson, Beverley: PA 108  
 Intarasiri, Saweat: PB 30, PC 31, PC 32, PC 77  
 Ioannou-sougleridis, Vassilios: PA 110, PB 102  
 Ionescu, Mihail: PB 65, PC 21  
 Irvine, Kenneth: PA 84  
 Isabelle, Monnet: PC 16  
 Ishii, Koji: PA 57  
 Ishikawa, Norito: PA 104, PC 65  
 Ishimaru, Manabu: PB 27  
 Ishiyama, Taishi: PA 57  
 Ito, Hiroyuki: PB 38  
 Itoh, M.: PB 75  
 Iwase, Akihiro: O 35, PA 57, PC 53, PC 65  
 Izerrouken, Mahmoud: PB 23  
 Jachs, Bernhard: PB 64  
 Jagielski, Jacek: PA 5, PB 61, PC 13  
 Jaikuna, Tanwiwat: PA 68  
 Jaime, Danay Manzo: O 22  
 Jakiela, Rafal: PC 98  
 Jaksic, Milko: O 10, PB 116, PC 114  
 Janse Van Rensburg, Johan: PB 31  
 Japur, Rafael S.: O 22  
 Jarvas, Gabor: PA 31  
 Jaskóła, Marian: PC 76  
 Jede, Ralf: PA 24  
 Jelinek, Moriz: PB 41  
 Jenkins, Catherine A: PC 58  
 Jeynes, Chris: PA 108  
 Jianrong, Sun: PC 61  
 Jiao, Yang: PA 48, PA 72  
 Jiménez-rey, David: PC 14  
 Jin, Hyung-ha: PB 57, PB 58  
 Jin, Ke: O 5  
 Jiri, Ullschmied: PB 111  
 Johannes, Andreas: PB 94, PB 95  
 Johnson, Harley: O 2  
 Jose, Olivares: PC 16  
 Joshi, Shalik Ram: PC 40  
 Jozwik, Przemyslaw: PA 5, PB 28  
 Jozwik-biała, Iwona: PA 5, PB 61, PC 13  
 Jublot-leclerc, Stéphanie: PB 59  
 Just, William: O 22  
 Kaczmarek, Leonie: PC 102  
 Kadid, Soraya: PC 112  
 Kadyrzhanov, Kairat: PB 103

Kaida, Takuya: PC 84  
 Kajita, Shin: PB 105, PC 100  
 Kakiuchida, H.: PA 49, PB 75  
 Kalin, Boris: PA 59, PA 60  
 Kaliya Perumal Veerapandian, Savita: PA 25  
 Kamikawa, Tomohiro: PA 74  
 Kamioka, Kazuma: PC 84  
 Kaneno, Yasuyuki: PC 53  
 Kanesue, Takeshi: PB 13  
 Kanjilal, Dinakar: PC 38, PC 40  
 Karatas, Ozgun: PC 62  
 Karatchevtseva, Inna: PB 65, PC 21  
 Karl, Helmut: O 11, PC 46  
 Karlusic, Marko: O 10, PA 111, PB 116, PC 114  
 Kataoka, Izumi: PB 5  
 Kato, M.: PA 49, PB 75  
 Kato, Shigeki: PC 86  
 Katsikini, Maria: PB 98  
 Kawasaki, Tadahiro: PA 91  
 Kazmierczak, Urszula: PC 76  
 Kaitasov, Odile: PC 11  
 Kennedy, John: INV 9, PB 78  
 Kenzhaliev, B.: PA 76  
 Kern, Klaus: INV 2, PA 115, PB 89  
 Khalid, Muhammad: PC 56  
 Khein, Aung: PA 60  
 Khein, Aung Thurein: PA 59  
 Khelifi, Rim: O 44  
 Khyzhniy, Ivan: PC 48  
 Kim, Yeon Soo: PB 68  
 Kimura, Akihiko: PC 29  
 Kimura, Asahi: PB 2  
 Kimura, Takashi: PA 81, PB 6, PB 7  
 King, Donald: INV 8  
 King, Frederik: PA 53  
 Kinomura, Atsushi: PA 78, PC 84  
 Kirby, Brian J.: PA 93  
 Kirby, Nigel: PB 114  
 Kirnstotter, Stefan: PB 41  
 Kislitsyn, Sergey: PA 113  
 Klingner, Nico: PA 107  
 Kluth, Patrick: O 42, PB 114  
 Knights, Andy: PB 100  
 Ko, Eunsol: PB 58  
 Kobayashi, Hiroki: PB 1  
 Kobayashi, Tomohiro: O 9  
 Koide, Tetsuya: O 35, PC 53  
 Kojima, Hiroshi: PA 78, PC 53  
 Koka, Masashi: O 35  
 Kolodney, Eli: PA 44  
 Komarov, Fadei F.: PB 98  
 Komori, Katsuyuki: PB 105, PC 100  
 Korman, Andrzej: PC 76  
 Korolkov, Ilya: PC 72  
 Koshiba, Yusuke: PA 89  
 Koyn, Zachariah: PB 46  
 Kozlov, Alexander: PB 113  
 Kozlovskiy, Artem: PB 103  
 Kozubal, Maciej: PC 98  
 Kozubek, Roland: PB 116  
 Kral, Jaroslav: PB 45  
 Kramczynski, Detlef: PB 42  
 Krause, Matthias: PC 6  
 Krauser, J.: PC 111  
 Kremer, Felipe: INV 9  
 Krippendorf, Florian: PC 90  
 Kronast, Florian: PA 30  
 Kropachev, Gennady: PB 113  
 Kruszewski, Marcin: PC 76  
 Kuhudzai, Remeredzai Joseph: PC 26  
 Kuibeda, Rostislav: PB 113  
 Kukli, Kaupo: PB 102  
 Kuleshova, Evgenia: PA 52  
 Kulevoy, Timur: PB 113  
 Kumaki, Masafumi: PB 13  
 Kumar, Arvind: PC 59  
 Kun, Mo: PB 68  
 Kuriyama, Kazuo: PC 84  
 Kurpaska, Lukasz: PB 61  
 Kushida, Kazumasa: PC 84  
 Kusumori, Takeshi: PA 81, PB 6, PB 7  
 Kutza, Paul: PB 98  
 Kuznetsov, Andrej: PA 6  
 Kvashnina, K.: PC 70  
 Kwon, Junhyun: PB 57, PB 58  
 La Magna, Antonino: O 21  
 Laariedh, Farah: PB 29  
 Ladas, Spyridon: PA 110, PB 102  
 Lai, Chih-chung: PB 92  
 Lakshantha, Wickramaarachchige: PC 107  
 Lamhamdi, Mohamed: PA 75

Landru, Didier: INV 11  
 Lang, Maik: PB 114  
 Langlinay, Thomas: PB 18  
 Lankoff, Anna: PC 76  
 Laurence, Mechin: PC 16  
 Laven, Johannes: PB 41  
 Laverne, Jay: PA 38  
 Lavtentiev, Vasily: PC 81  
 Lazar, Mihai: PB 29  
 Lazenka, Vera: PB 82, PC 63  
 Le, Xiaoyun: PB 52, PC 105, PC 69  
 Lebius, Henning: PA 98, PB 116  
 Leclercq, Jean-louis: PB 29  
 Lee, Heun Tae: PB 60  
 Lefaix-jeuland, Helene: PB 55  
 Legris, Alexandre: PB 48  
 Legros, Corinne: O 43  
 Leino, Aleks: PB 114, PB 35  
 Lenz, Christoph: PB 64  
 Leontyeva-smirnova, Maria: PA 59, PA 60  
 Lepretre, Frederic: PB 55  
 Lescoat, Marie-laure: PB 59  
 Leskelä, Markku: PB 102  
 Levavasseur, Delphine: PA 98  
 Leveneur, Jérôme: INV 9, PB 78  
 Li, B.S.: PB 63  
 Li, Bingsheng: PC 18  
 Li, L.: PC 20  
 Li, Shuai: O 13  
 Li, Xiaoqiang: PB 59  
 Li, Xingji: PA 17, PA 18, PB 107, PB 69  
 Li, Y.H.: PC 28  
 Li, Yuanfei: PC 18  
 Liang, Hsin-te: PC 54  
 Liang, J.H.: PC 91  
 Liang, Jenq-horng: O 30  
 Liedke, Bartosz: O 3, O 6  
 Lilong, Pang: PC 61  
 Lim, S Q: O 19  
 Lima, Vincent: PA 1  
 Lin, C.M.: PC 91  
 Lin, Ko-wei: PC 54  
 Lindner, Jürgen: PA 30  
 Linnarsson, M. K: PA 41  
 Linnarsson, Margareta K.: O 1  
 Linnros, Jan: PA 109  
 Lisitsyn, Victor: PB 32  
 Lisitsyna, Liudmila: PB 72  
 Lisowska, Halina: PC 76  
 Liu, Chaoming: PA 17, PA 18, PB 107, PB 69  
 Liu, Peng: O 5  
 Liu, Ruiqin: PC 74  
 Liu, Tao: PC 30  
 Liu, Xinjun: O 13  
 Liu, Yu: PB 73  
 Liu, Yuan: PB 20  
 Lively, Michael: PB 46  
 Lopez-barbera, José Francisco: PA 93, PB 80  
 Lorenz, Katharina: PA 79, PA 80, PB 98, PC 93  
 Lorenz, Michael: PB 82, PC 63  
 Lorenz, Philipp: PB 98  
 Lorite, Israel: PB 77  
 Lou, Yu: PC 15  
 Loussouarn, Thomas: PB 55  
 Luca, Alfonz: PA 96  
 Lucas, Guillaume: O 38  
 Lugstein, A.: O 45  
 Lumpkin, Gregory L.: PB 65, PC 21  
 Ma, Guoliang: PA 17, PA 18, PB 69  
 Ma, Huan: PA 58  
 Maas, Diederik J.: PA 21, PA 22  
 Machida, Nobuya: PA 89  
 Mackova, A.: PA 62  
 Mackova, Anna: PA 63, PB 111, PB 85, PC 41  
 Madeira, Florence: INV 11  
 Magalhães, Sérgio: PC 93  
 Mailloa, J P: O 19  
 Majumder, Subrata: PC 40  
 Malherbe, Johan: PC 26  
 Malinowska, Aneta: PC 76  
 Malinsky, Petr: PA 63, PB 111, PB 85, PC 41  
 Manika, Ilze: PB 24  
 Maniks, Janis: PB 24  
 Manzano-santamaria, Javier: O 37  
 Mara, N.: PB 71  
 Marcel, Toulemonde: PC 16  
 Marchand, Benoit: PC 9  
 Marek, Swirkowicz: PC 13  
 Margutti, Giovanni: PA 7  
 Marika, Schleberger: PA 111  
 Marin Vargas, Andre Luis: PA 45, PB 15  
 Markwitz, Andreas: INV 9, PB 78



Martella, Christian: O 8, PB 43  
 Martin, Matthias: PA 8  
 Martinez, Rafael: PA 112, PB 18  
 Martinez-criado, Gema: PA 94  
 Martirani Paolillo, Diego: PA 7  
 Mashentseva, Anastassiya: PA 113, PC 72  
 Massy, Damien: INV 11  
 Mastromatteo, Massimo: O 21  
 Matej, Mayer: PC 67  
 Mathieu, Gilles: PC 97  
 Mathiot, Daniel: O 44  
 Matousek, Jindrich: PB 111  
 Matsui, Kei: PB 16  
 Matsui, Toshiyuki: O 35, PC 53  
 Matsunami, Noriaki: PA 49, PB 75  
 Matsuo, Jiro: O 28  
 Matsutani, Takaomi: PA 91  
 Mauchamp, Vincent: O 38  
 Mayr, Stefan: O 36  
 Mazarov, Paul: PA 24  
 Mazen, Frederic: INV 11  
 Maître, Alexandre: PC 2  
 Mcdaniel, Floyd: PC 107  
 Mcdonald, Kyle: INV 8  
 Mchargue, Carl: PB 27  
 Meersschaut, Johan: PC 49  
 Meftah, Ali: PC 112  
 Meisch, Tobias: PB 116  
 Mekterovic, Darko: PA 111  
 Mekterovic, Igor: PA 111  
 Mennucci, Carlo: PB 43  
 Menut, Denis: O 43  
 Menéndez Dalmau, Enric: PA 93, PB 80, PB 82, PC 63  
 Mercaldo, Lucia: PB 43  
 Merchant, Michael: INV 12  
 Metson, James: INV 9  
 Meutzner, Falk: PA 30  
 Meyer, Bruno K.: PB 4  
 Meyer, Walter: PB 31  
 Michely, Thomas: INV 1  
 Michler, Johann: PA 25  
 Migunova, Anastassiya: PA 113  
 Miksova, R.: PA 62  
 Miksova, Romana: PA 63, PC 41  
 Milazzo, Ruggero: O 21  
 Mills, Gerald: PB 20  
 Mine, Nicolas: PA 8  
 Ming, T.: PC 28  
 Mir, Anamul Haq Jeri: PC 16  
 Mirabella, Salvatore: O 20  
 Miro, Sandrine: O 31, O 33, O 4, O 43, PB 56, PC 2  
 Mishima, Tomoyoshi: PC 86  
 Mishra, Indrani: PC 40  
 Miyagawa, Go: PC 39  
 Mizohata, Kenichiro: PC 9  
 Mizutani, Tsuyoshi: PB 97  
 Modarresi, Hiwa: PB 82, PC 63  
 Moeller, Wolfhard: O 23, O 24  
 Mohamed, Walid: PB 68  
 Mohapatra, Satyabrata: PA 104  
 Moisy, Florent: PC 113  
 Moncoffre, Nathalie: PA 5, PC 13, PC 2  
 Monnet, Isabelle: O 43, PC 113  
 Monteiro, Teresa: PC 93  
 Moorkens, T.: PC 70  
 Morata, Stephane: PC 97  
 Mordkovich, Vladimir: PC 87  
 Moreno Barrado, Ana: O 14  
 Motta, Francis C.: INV 5  
 Motte, Vianney: O 31  
 Mousseau, Normand: INV 10  
 Mulders, Hans: PA 27  
 Muller, Dominique: O 44  
 Munoz Garcia, Javier: O 14  
 Muradoglu, Saliha: O 42  
 Murai, Takaaki: PB 97  
 Murmu, Peter: PB 78  
 Musumeci, Francesco: PA 33  
 Muñoz-martín, Ángel: PC 14  
 Mylonas, Stamatias: O 32  
 Möbus, Günter: PA 108  
 Möller, Wolfhard: PC 6  
 Nagy, Gyula: PA 31, PC 81  
 Nair, K G M: O 34  
 Naito, Muneyuki: PA 89  
 Nakamura, Tohru: PC 86  
 Nakao, Setsuo: PA 81, PB 7, PC 42  
 Nakao, Setuso: PB 6  
 Nakata, Jyoji: PA 74  
 Nameki, Hirofumi: PB 97

Nandi, Sanjoy: INV 4, O 13  
 Napolitani, Enrico: O 20, O 21  
 Naqvi, Syeda Rabab: PA 109, PA 41  
 Nasdala, Lutz: PB 64  
 Naumenko, Irina: PA 59  
 Nekvindova, Pavla: PC 41  
 Neudert, Andreas: PA 30  
 Neves, Armando J.: PC 93  
 Ngoepe, Phuti: PB 31  
 Nguyen, Tien Hien: O 32  
 Nietiadi, Maureen L.: O 24  
 Niimi, Satoshi: PC 44  
 Niinistö, Jaako: PB 102  
 Nikolaou, Nikolaos: PA 110, PB 102  
 Nishida, Kenji: PC 65  
 Nishimura, Ryotaro: PA 81  
 Nishimura, Tomoaki: PC 84  
 Nittler, Laurent: PA 64, PC 75  
 Noack, Stefan: PB 94, PB 95  
 Nogués, Josep: PA 93, PB 80  
 Nomaguchi, Tatsuhiro: PC 79  
 Nomoto, Toyokazu: PB 104, PB 105, PC 100, PC 44  
 Nordlund, Kai: O 26, O 29, PB 114, PB 35  
 Normand, Pascal: PA 110, PB 102  
 Norris, Scott: PB 44  
 Nowicki, Lech: O 32  
 Noël, Céline: PC 75  
 Nunes, Bruno: PC 108  
 Nussupov, K.: PA 76  
 Nuzhdin, V.I.: PA 62  
 O'hare, Edward: PB 68  
 Odeh, Ibrahim: PA 85  
 Oepen, Hans Peter: PB 76  
 Ogawa, Satoshi: PC 44  
 Ogawa, Satoshi: PB 97  
 Ohldag, H.: PB 77  
 Ohmura, Takahito: PC 65  
 Ohno, Noriyasu: PB 105, PC 100  
 Ohshima, Takeshi: PA 54  
 Ohya, Kaoru: PA 21, PA 22  
 Oikawa, Takuya: PC 86  
 Okamoto, Yoshihiro: PC 53  
 Okamura, Masahiro: PB 13  
 Okayasu, S.: PA 49, PB 75  
 Oks, Efim: PB 113  
 Okubo, Nariaki: PA 104  
 Olivares, Jose: PC 115  
 Olivares, José: O 37  
 Oliveira, Rogério: PB 12  
 Olivero, Paolo: PB 106  
 Oliviero, Erwan: O 38  
 Olshansky, Evgeni: PA 52  
 Omotoso, Ezekiel: PB 31  
 Orellovitch, Oleg: PC 80  
 Oswald, Jiri: PC 41  
 Ottaviani, Laurent: PC 97  
 Ou, Xin: O 15  
 Ozaki, Kimihiro: PA 81, PB 6, PB 7  
 Ozturk, Orhan: PC 62  
 Pacholski, Claudia: PB 95  
 Pailloux, Frédéric: O 38  
 Pakarinen, Olli: PB 114, PB 35  
 Paloura, Eleni: PB 98  
 Palumbo, Maria Elisabetta: PB 18  
 Panczer, Gerard: PA 5, PC 13  
 Pang, L.L.: PB 63  
 Pang, Lilong: PC 18  
 Panigrahi, Binay Kumar: O 34  
 Papaleo, Ricardo: PC 116  
 Papaléo, Ricardo Meurer: PB 109, PC 10, PC 78  
 Paradzah, Alexander: PB 31  
 Park, Sohyun: PC 67  
 Partoens, Bart: PA 105  
 Patel, M.: PC 28  
 Pathak, S.: PB 71  
 Patrick, Kluth: PC 16  
 Pauly, Matthias: INV 2  
 Pavlov, Jevgenij: PA 82, PA 83  
 Pavlovic, Nikolina: PC 63  
 Pazhin, Dmitriy: PC 87  
 Pecassou, Beatrice: PA 110, PB 102  
 Pecko, Stanislav: PC 71  
 Pedroli Renz, Renata: PA 45  
 Peeters, Francois: PA 105  
 Pelic, Bernadeta: PA 56, PC 64  
 Pellin, Michael: PB 68  
 Peng, Haibo: PB 17  
 Peng, Liu: PA 37  
 Peng, Nianhua: PA 108  
 Pereira, Lino: O 18, PA 93, PC 104

Perrin Toinin, Jacques: PB 26  
 Petriska, Martin: PB 67, PC 22  
 Petry, Winfried: PC 67  
 Peña-rodríguez, Ovidio: O 37  
 Peña-rodríguez, Ovidio: PC 115  
 Phanbunplook, Pongrawee: PC 77  
 Picot, T.: PC 70  
 Pillaca, Elver Juan De Dios: PB 12  
 Pillatsch, Lex: PA 25  
 Pilz, Wolfgang: PB 8  
 Pimblott, Simon: PA 38  
 Pípon, Yves: PC 2  
 Pireaux, Jean-jacques: PA 64, PC 75  
 Pizzagalli, Laurent: O 38  
 Planson, Dominique: PB 29  
 Plantevin, Olivier: PA 70, PC 95  
 Podgornii, Dmitriy: PC 87  
 Poelsema, Bene: PA 9  
 Pokor, Cédric: PB 59  
 Polity, Angelika: PB 4  
 Polsky, Valeriy: PA 59  
 Ponciano, Cassia R.: PB 18  
 Ponomaryov, Alexey: PC 48  
 Popok, V.N.: PA 62  
 Popok, Vladimir: O 29  
 Popov, Vladimir: O 29  
 Portavoce, Alain: PB 26  
 Portier, Stéphane: PA 8  
 Posselt, Matthias: O 3  
 Possnert, Göran: PA 109, PA 41  
 Potzger, Kay: PA 30  
 Prada, Alejandro: O 37  
 Pradeilles, Nicolas: PC 2  
 Prawer, Steven: PB 106  
 Preda, Iulian: PC 115  
 Prikhodko, Kirill: PA 52, PC 35  
 Primetzhofner, Daniel: O 1, PA 109, PA 41  
 Priolo, Francesco: O 21  
 Privezentsev, Vladimir: PB 88  
 Privitera, Vittorio: O 21  
 Prucnal, Sławomir: O 3, O 45, PC 88  
 Qiao, Mei: PC 30  
 Qu, Miao: PB 52, PC 105, PC 69  
 Radek, Manuel: O 3  
 Radic, Nikola: O 10, PA 111, PC 114  
 Rajta, Istvan: PA 31, PC 81  
 Rangamma, Jimmy: PA 98  
 Rao, Kalipatnam Vivek: PB 38  
 Rapaud, Olivier: PC 2  
 Ratajczak, Jacek: PC 98  
 Ratajczak, Renata: PA 5, PB 28, PC 13  
 Rauschenbach, Bernd: O 7  
 Rauschenbach, Stephan: INV 2, PA 115, PB 89  
 Reboh, Shay: INV 11  
 Recht, D: O 19  
 Redondo-cubero, A: PA 79  
 Rego, Ana: PC 108  
 Reinert, Tilo: PC 107  
 Ren, Fan: INV 7  
 Rensberg, Jura: PA 50  
 Repetto, Diego: O 8, PB 43  
 Rettenmayr, Markus: PC 102  
 Reuscher, Bernhard: PB 42  
 Rey, Cyrielle: PC 15  
 Ribeiro Da Silva, Manuel: O 18  
 Ribis, Joel: PB 48  
 Ribis, Joël: PC 11  
 Richter, Frank: PA 96  
 Ridgway, Mark: INV 9, O 42  
 Rieumont, Jacques: PA 112  
 Rieutord, François: INV 11  
 Riley, Daniel P.: PB 65  
 Rinke, Gordon: INV 2, PB 89  
 Ritala, Mikko: PB 102  
 Ritter, Robert: O 27  
 Rivera, Antonio: O 37  
 Rizza, Giancarlo: INV 3  
 Roca I Cabarrocas, Pere: PA 70, PC 95  
 Rodrigues, Joana: PC 93  
 Rodriguez, Matias: O 42, PB 114  
 Roelants, Sam: PA 105  
 Romero-romero, Elisa: PB 20  
 Rommel, Mathias: PA 25, PB 41  
 Ronning, Carsten: INV 13, PB 94, PB 95  
 Roorda, Sjoerd: O 39  
 Ropars, Frédéric: PB 18  
 Rothard, H.: PC 111  
 Rothard, Hermann: PB 18  
 Rout, Bibhudutta: PC 107  
 Roux, Laurent: PC 97  
 Rubanov, Sergey: PB 101, PB 106

Ruck, Ben: PB 78  
 Rudawski, Nick: INV 7  
 Rudzevich, Yauheni: PB 26  
 Rueb, Michael: PC 90  
 Rueffer, Rudolf: PA 105  
 Ruffell, Simon: O 13  
 Rui, Erming: PB 107  
 Rukade, Deepti: PB 84, PC 38  
 Rumler, Maxmilian: PA 25  
 Rusakov, Viacheslav: PB 103  
 Ruterana, P: PA 79  
 Ryuto, Hiromichi: PA 33, PB 1  
 Räisänen, Minna: PC 9  
 Räsiänen, Jyrki: PC 9  
 Sabelova, Veronika: PC 22  
 Sachan, Ritesh: O 5  
 Saerbeck, Thomas: PC 57  
 Saijo, Yusuke: PC 86  
 Saikrueng, Passakorn: PC 77  
 Saitoh, Yuichi: O 35, PC 53, PC 65  
 Sakamaki, Masako: O 35  
 Sakane, Hitoshi: O 35  
 Sakata, Akira: PA 33  
 Sakudo, Noriyuki: PB 16, PB 19, PB 38  
 Sakumoto, Naotake: PB 16, PB 38  
 Salazar, Josiane B.: O 22  
 Sall, Mamour: PC 113  
 Salou, Pierre: PA 98  
 Samela, Juha: O 29  
 Sandoval, Luis: O 24  
 Sansongsiri, Sakon: PC 77  
 Santic, Branko: PB 116, PC 114  
 Sarstedt, Margit: PA 96  
 Sartowska, Bozena: PC 80  
 Sataka, M.: PA 49, PB 75  
 Sattonnay, Gaël: O 43  
 Savchenko, Elena: PC 48  
 Sawamura, Naoya: PC 79  
 Schauries, Daniel: PB 114  
 Scheeler, Sebastian: PB 95  
 Schiettekatte, François: INV 10  
 Schleberger, Marika: PA 98, PB 116, PC 114  
 Schmid, Klaus: PC 67  
 Schmidt, Bernd: O 3  
 Schmidt, Emanuel: PA 50, PB 94  
 Schmidt, Matthias: PA 50  
 Schoffen, Julio R.: O 22  
 Schofield, Jennifer: PA 38  
 Scholz, Ferdinand: PB 116  
 Schuller, Ivan K.: PC 57  
 Schulze, Hans-joachim: PB 41  
 Schustereder, Werner: PB 41  
 Schwartz, Kurt: PB 24  
 Schwarz-selinger, Thomas: PB 60  
 Schweikert, Emile A.: PB 11  
 Schöppe, Philipp: PC 102  
 Schütze, Michael: PA 53, PA 56  
 Secchi, Maria: PB 50, PC 7  
 Seki, Toshio: O 28  
 Seleznev, Dmitry: PB 113  
 Sellami, Neila: O 43  
 Semboshi, Satoshi: PC 53, PC 65  
 Serge, Bouffard: PC 16  
 Serruys, Yves: O 4, PB 48, PB 55, PB 56  
 Setsuo, Nakao: PA 78  
 Severin, D.: PC 111  
 Shcherbachev, Kirill: PB 88, PC 87  
 Shen, Jie: PB 52, PC 105, PC 69  
 Shen, T.L.: PB 63  
 Shen, Tielong: PC 18  
 Shin, Chansun: PB 57  
 Shinada, Takahiro: PC 79  
 Shinya, Yagi: PB 105  
 Shipman, Patrick D.: INV 5  
 Shukla, Neeraj: O 34  
 Sickafus, K.E.: PC 28  
 Sickafus, Kurt: PB 27  
 Sidorowicz, Agata: PA 5  
 Siegel, Jakub: PB 85  
 Silva, Daniel: O 18  
 Simatos, Dimitrios: PA 110  
 Simdyankin, Sergei: O 20  
 Simeg Veternikova, Jana: PB 67, PC 22  
 Simon, Patrick: PC 113  
 Sina, Younes: PB 27  
 Singkarat, Somsorn: PA 11  
 Skarlatos, Dimitrios: PB 102  
 Skeren, Tomas: O 16, PB 45  
 Skorupa, W.: O 45  
 Skorupa, Wolfgang: PC 56, PC 58, PC 64, PC 88  
 Slepicka, Petr: PA 63

Slugen, Vladimir: PB 67, PC 22  
 Slugeň, Vladimír: PC 71  
 Smillie, L A: PB 25  
 Sobkowicz, Igor P.: PA 70, PC 95  
 Sojak, Stanislav: PB 67, PC 71  
 Solanki, Vanarajsinh: PC 40  
 Solorzano, Guillermo: PA 112  
 Song, Hong-lian: PC 30  
 Sonoda, Tsutomu: PA 81, PB 6, PB 7, PC 42  
 Sort, Jordi: PB 80  
 Sotelo, Daniela: PC 116  
 Southern-holland, Rachel: PB 100, PC 47  
 Souza, Cláudia Telles: PC 78  
 Spaggiari, Claudio: PA 7  
 Spolenak, Ralph: PA 58  
 Srivastava, P C: PC 59  
 Steitz, Roland: PA 93  
 Stepanov, A.L.: PA 62  
 Stephani, Kelly: PB 33  
 Stolyarov, Vladimir: PA 52  
 Stonert, Anna: PB 28  
 Stori, Elis Moura: PC 78  
 Straube, Benjamin: PB 77  
 Strazzulla, Giovanni: PB 18  
 Stumpf, Florian: PA 25  
 Stępkowski, Tomasz: PC 76  
 Su, Chiung-wu: PC 52  
 Sudfeld, Daniela: PA 27  
 Sugimura, Akira: PA 89  
 Sullivan, James: O 42  
 Sun, J.R.: PB 63  
 Sun, Jianrong: PC 18, PC 82  
 Sun, Wei: PB 73  
 Sun, Yiting: PC 49  
 Suvanam, Sethu Saveda: PA 109  
 Suvorov, Alexander: PA 84, PB 101, PC 103  
 Suvorova, Alexandra: PB 101, PB 106  
 Svensson, Bengt: PA 6  
 Svorcik, Vaclav: PB 85  
 Sychugov, Ilya: PA 109  
 Sylvain, Peugeot: PC 16  
 Szabo, Attila: PA 31  
 Szabo, Attila T.T.: PC 81  
 Szepliński, Zygmunt: PC 76  
 Szigeti, Marton: PA 31  
 Szilasi, Szabolcs: PA 31, PC 81  
 Tabachkova, Natalia: PC 87  
 Tabachkova, Nataliia: PB 88  
 Takahiro, Satoh: O 35  
 Takaoka, Gikan: PA 33, PB 1  
 Takeuchi, Mitsuki: PA 33, PB 1  
 Talla, Dominik: PB 64  
 Taltenov, Abzal: PC 72  
 Tan, Yang: O 12  
 Tanii, Takashi: PC 79  
 Tarkhov, Michael: PA 52, PC 35  
 Tekorius, Audrius: PA 82  
 Telles, Cláudia: PC 116  
 Templier, Claude: PB 80  
 Temst, K.: PC 70  
 Temst, Kristiaan: O 16, O 18, PA 105, PA 93, PB 80, PB 82, PC 104, PC 63, PC 85  
 Teramoto, T.: PA 49  
 Tesmer, J.: PB 71  
 Texier, Michael: PB 26  
 Thomas, Keith: PA 25  
 Thomaz, Raquel: PB 109, PC 10  
 Thome, Lionel: O 43, PC 13  
 Thompson, M O: PB 25  
 Thompson, Matthew: PB 65  
 Thomsen, Lars: PB 65, PC 21  
 Thomé, Lionel: O 32, O 4  
 Thopan, Prutchayawoot: PA 65, PB 112, PC 109  
 Tippawan, Udomrat: PB 30, PC 31, PC 32  
 Tokuhira, Shinnosuke: PA 54  
 Toquer, Guillaume: PC 15  
 Tormo-márquez, Victoria: PC 115  
 Torregrosa, Frank: PC 97  
 Torrisi, Lorenzo: PB 111  
 Toulemonde, Marcel: PA 50, PB 35  
 Toulhoat, Nelly: PC 2  
 Toyoda, Noriaki: PB 2  
 Tran, T T: O 19, PB 25  
 Tran, Tuan: PC 92  
 Trautmann, C.: PC 111  
 Trautmann, Christina: PB 114  
 Tribedi, Lokesh: PB 84  
 Tribollet, Jérôme: O 44  
 Troceller, Patrick: O 4  
 Trocellier, Patrick: O 33, PB 48, PB 55, PB 56  
 Tsai, Hsu-sheng: O 30, PB 92

Tsuji, Hiroshi: PC 39  
 Tsukada, Chie: PB 105, PC 100  
 Tupitsyna, Irina: PB 32  
 Turos, Andrzej: PB 28  
 Tynan, G.: PB 71  
 Uchida, Hirohisa: PA 54  
 Ueda, Mario: PB 12  
 Ueda, Osamu: PB 38  
 Ueyama, Daichi: PC 65  
 Umezu, Ikuro: PA 89  
 Undisz, Andreas: PC 102  
 Uno, Hiroyuki: O 35  
 Urbassek, Herbert M.: O 24, O 6  
 Usatii, Iure: PB 43  
 Usov, Igor: PA 84  
 Uyutnov, Serge: PC 48  
 Valdez, J.A.: PC 28  
 Valeev, V.F.: PA 62  
 Valencia, Sergio: PA 30  
 Valiev, Ruslan: PA 60  
 Van Bael, M.J.: PC 70  
 Van Bael, Margriet: PA 105  
 Van Bael, Margriet J.: PB 82, PC 63  
 Van Bael, Marlies K.: PC 63  
 Van Gastel, Raoul: PA 9  
 Van Haesendonck, C.: PC 70  
 Van Lierop, Johan: PC 54  
 Van Stiphout, Koen: PC 85  
 Vandervorst, Wilfried: O 16, PC 49  
 Vantomme, André: O 16, O 18, PA 105, PA 93, PB 80, PB 82, PC 104, PC 63, PC 85, PC 70  
 Vanzetti, Lia: PB 50  
 Varma, Shikha: PC 40  
 Vasconcellos, Marcos: PA 40  
 Vaubailion, Sylvain: O 33, PB 55, PB 56  
 Vazquez, Luis: O 14  
 Veldhoven, Emile Van: PA 21, PA 22  
 Veligura, Vasilisa: PA 9  
 Velisa, Gihan: O 4  
 Venkatachalam, Dinesh: INV 4, INV 7, O 13  
 Venäläinen, Annika: PC 9  
 Verdonck, Patrick: PC 49  
 Verkhoturov, Stanislav V.: PB 11  
 Ves, S.: PB 98  
 Vesely, Martin: PB 45  
 Victor, Guillaume: O 31, PC 2  
 Vizkelethy, George: INV 8  
 Von Borany, Johannes: PA 56, PC 90  
 Vos, Maarten: INV 4, O 13  
 Vosecek, Vaclav: PC 81  
 Vysniauskas, Juozas: PA 83  
 Wahl, Ulrich: O 18, PC 104  
 Wajler, Anna: PA 5  
 Wang, Gang: PB 73  
 Wang, H.: PC 70  
 Wang, Jing Jing: PA 108  
 Wang, Lei: PA 48, PA 72  
 Wang, Liqin: PB 107  
 Wang, Shunchong: PB 73  
 Wang, Tie-jun: PC 30  
 Wang, Tieshan: PB 17  
 Wang, Xiaotie: INV 7  
 Wang, Xue-lin: PC 30  
 Wang, Xuelin: PA 37, PB 22  
 Wang, Yongqiang: PB 71, PC 28  
 Wang, Yutian: PC 56, PC 58  
 Wang, Yuyu: PB 17  
 Wang, Z.G.: PB 63  
 Wang, Zhiguang: PC 18, PC 82  
 Washio, Masakazu: PB 13  
 Webb, Roger: PA 108  
 Weber, W. J.: PA 37  
 Weber, William: O 5, PB 114, PB 35  
 Wei, Binbin: PC 69  
 Wei, Kongfang: PC 18  
 Wen, J.: PC 28  
 Wendler, E: PA 79  
 Wendler, Elke: PA 50, PA 6, PA 80, PB 98, PC 102  
 Wendler, Lutz: PA 80  
 Wesch, Werner: PA 50  
 Weschke, Eugen: PC 56  
 Wiencek, Thomas: PB 68  
 Wierzbicka, Edyta: PB 28  
 Wijesundera, Dharshana: O 17  
 Wilhelm, Richard A.: PB 116  
 Wilhelm, Richard Arthur: O 27  
 Wilke, Martin: PB 76  
 Williams, G V M: PB 78  
 Williams, Grant: INV 9  
 Williams, Jim: O 19, PB 25, PC 92  
 Wintz, Sebastian: PA 30, PC 6

Wojcik, Marek: PB 28  
 Wojewódzka, Maria: PC 76  
 Wong-leung, Jennifer: PC 92  
 Wrocznskyj, Yaro: PC 54  
 Wu, C.W.: PC 91  
 Xiang, Bing-xi: PA 48, PA 72  
 Xiao, Liyi: PA 17, PA 18  
 Xue, Haizhou: O 5, PA 37  
 Yabin, Zhu: PC 61  
 Yachida, Gosuke: PA 74  
 Yacout, Abdellatif: PB 68  
 Yagi, Shinya: PB 104, PB 97, PC 100, PC 44  
 Yajima, Miyuki: PB 105, PC 100  
 Yakushin, Vladimir: PA 59, PA 60  
 Yamada, Isao: PB 2  
 Yamada, Ryo: PA 89  
 Yamaki, Tetsuya: O 9  
 Yamamoto, Muneaki: PB 104, PB 105, PC 100, PC 44  
 Yamamoto, Naoto: PB 104  
 Yamanaka, Takuya: PA 22  
 Yamasaki, Kayo: PA 91  
 Yamazaki, Yasunori: O 9  
 Yang, Jianqun: PA 17, PA 18, PB 107, PB 69  
 Yang, Wenjie: O 19  
 Yang, Zhangcan: PB 46  
 Yankov, Rossen: PA 56, PC 64  
 Yao, C.F.: PB 63  
 Yao, Cunfeng: PC 18, PC 82  
 Yao, S.D.: PC 20  
 Yaopromsiri, Chaitawat: PA 65  
 Yavirach, Piriya: PC 77  
 Ye, Bei: PB 68  
 Yokoyama, Yoshihiko: PA 57  
 Yoshida, Tomoko: PB 104, PB 105, PB 97, PC 100, PC 44  
 Yoshizaki, Hiroaki: PC 53  
 Yu, Liangdeng: PA 11, PB 112, PC 109  
 Yu, Xiao: PB 52, PC 105, PC 69  
 Yu, Xiao-fei: PC 30  
 Yuan, Ye: PC 56  
 Yun, Di: PB 68  
 Yuyu, Wang: PC 61  
 Yvon, A.: PA 75  
 Zabels, Robert: PB 24  
 Zandelazini, Carlos: PB 77  
 Zandvliet, Harold J. W.: PA 9  
 Zarkadoula, Eva: O 5  
 Zdorovets, Maxim: PA 113  
 Zhanbotin, Arman: PB 103  
 Zhang, Gaolong: PB 52, PC 105, PC 69  
 Zhang, Jie: PB 52, PC 105, PC 69  
 Zhang, Kun: PA 103, PB 93  
 Zhang, Lian: PC 30  
 Zhang, Xiaodong: PC 106  
 Zhang, Xiaofu: PB 52, PC 105, PC 69  
 Zhang, Yanwen: O 5, PA 37, PB 35  
 Zhang, Yanyan: PB 52, PC 105, PC 69  
 Zhao, Jin-hua: PB 22, PC 30  
 Zhao, Yongtao: PB 17  
 Zharikov, S.: PA 76  
 Zheng, Ce: PC 11  
 Zhiguang, Wang: PC 61  
 Zhong, Haowen: PB 52, PC 105, PC 69  
 Zhou, S.: O 45  
 Zhou, Shengqiang: O 12, PB 72, PB 73, PC 55, PC 56, PC 58, PC 88  
 Zhou, Yu-fan: PC 30  
 Zhu, Huiping: PC 18  
 Zhu, Y.B.: PB 63  
 Zhu, Yabin: PC 18, PC 82  
 Zink, Mareike: O 36  
 Zirour, Hamza: PB 23  
 Zou, Yu: PA 58  
 Zschau, Hans-eberhard: PA 53, PA 55  
 Zschornak, Matthias: PC 6  
 Zu, Jianhua: PC 74  
 Ünal, Ahmet Akin: PA 30